August 2016

Cognitive Radio Systems: Performance Analysis and Optimal Resource Allocation

Gozde Ozcan
Syracuse University

Abstract

Rapid growth in the use of wireless services coupled with inefficient utilization of scarce spectrum resources has led to the analysis and development of cognitive radio systems. Cognitive radio systems provide dynamic and more efficient utilization of the available spectrum by allowing unlicensed users (i.e., cognitive or secondary users) to access the frequency bands allocated to the licensed users (i.e., primary users) without causing harmful interference to the primary user transmissions. The central goal of this thesis is to conduct a performance analysis and obtain throughput- and energy-efficient optimal resource allocation strategies for cognitive radio systems. Cognitive radio systems, which employ spectrum sensing mechanisms to learn the channel occupancy by primary users, generally operate under sensing uncertainty arising due to false alarms and miss-detections. This thesis analyzes the performance of cognitive radio systems in a practical setting with imperfect spectrum sensing.

In the first part of the thesis, optimal power adaptation schemes that maximize the achievable rates of cognitive users with arbitrary input distributions in underlay cognitive radio systems subject to transmit and interference power constraints are studied. Simpler approximations of optimal power control policies in the low-power regime are determined. Low-complexity optimal power control algorithms are proposed.

Next, energy efficiency is considered as the performance metric and power allocation strategies that maximize the energy efficiency of cognitive users in the presence of time-slotted primary users are identified. The impact of different levels of channel knowledge regarding the transmission link between the secondary transmitter and secondary receiver,

and the interference link between the secondary transmitter and primary receiver on the optimal power allocation is addressed. In practice, the primary user may change its status during the transmission phase of the secondary users. In such cases, the assumption of time-slotted primary user transmission no longer holds. With this motivation, the spectral and energy efficiency in cognitive radio systems with unslotted primary users are analyzed and the optimal frame duration and energy-efficient optimal power control schemes subject to a collision constraint are jointly determined.

The second line of research in this thesis focuses on symbol error rate performance of cognitive radio transmissions in the presence of imperfect sensing decisions. General formulations for the optimal decision rule and error probabilities for arbitrary modulation schemes are provided. The optimal decision rule for rectangular quadrature amplitude modulation (QAM) is characterized, and closed-form expressions for the average symbol error probability attained with the optimal detector under both transmit power and interference constraints are derived.

Furthermore, throughput of cognitive radio systems for both fixed-rate and variable-rate transmissions in the finite-blocklength regime is studied. The maximum constant arrival rates that the cognitive radio channel can support with finite blocklength codes while satisfying statistical quality of service (QoS) constraints imposed as limitations on the buffer violation probability are characterized.

In the final part of the thesis, performance analysis in the presence of QoS requirements is extended to general wireless systems, and energy efficiency and throughput optimization with arbitrary input signaling are studied when statistical QoS constraints are imposed as limitations on the buffer violation probability. Effective capacity is chosen as the performance metric to characterize the maximum throughput subject to such buffer constraints by capturing the asymptotic decay-rate of buffer occupancy. Initially, constant-rate source is considered and subsequently random arrivals are taken into account.

COGNITIVE RADIO SYSTEMS: PERFORMANCE ANALYSIS AND OPTIMAL RESOURCE ALLOCATION

By

Gozde Ozcan

B.S., Bilkent University, Ankara, Turkey, 2011

DISSERTATION

Submitted in partial fulfillment of the requirements for the degree of

Doctor of Philosophy in Electrical and Computer Engineering

Syracuse University

August 2016

Acknowledgement

First and foremost, I would like to express my sincere and deepest gratitude to my advisor, Prof. Mustafa Cenk Gursoy, for his invaluable guidance throughout my doctoral study. His immense knowledge and creative thinking have been the source of inspiration for me. I am truly fortunate to have had the opportunity to work under his guidance.

I would like to thank all my Ph.D. defense committee members Prof. Carlos E. Caicedo Bastidas, Prof. Jian Tang, Prof. Pramod Varshney, Prof. Senem Velipasalar, and Prof. Yingbin Liang for carefully reading my thesis.

I am grateful to my fellow labmates, Chuang, Esma, Yi, Teddy for their friendship, cheerful cooperation and the discussions in the lab. I am very glad to have such a peaceful work environment. I have learned a lot through their research during weekly group meetings.

Most importantly, this thesis would not have been possible without the love and support of my parents and my family members. Especially, I am indebted to my dearest mother, Saadet Ozcan, without her continuous encouragement I never would have been able to reach my goals. I admire her enthusiasm, vision and dedication to everything she does. I also extend my heartfelt gratitude to my sister, Hande Ozcan, for always finding a way to cheer me up and being there for me as my best friend. I am always amazed and inspired by her passion about science and her determination to continue experimenting regardless of number of failed experiments like Thomas Edison's process in inventing the light bulb. I want to express my deepest love and special thanks to my husband, Zafer Sahinoglu, who has been my pillar of strength and has stood beside me through all the good times and the bad.

Finally, this thesis is especially dedicated to the memory of my beloved grandfather, Satilmis Demirdizen, who was a skilled communicator with a depth of knowledge and a great storyteller, encouraged me to be good listener, to build my imagination and to think beyond the possible, and to my dearest grandmother, Muserref Demirdizen who has loved me unconditionally and has been a role model to me for kindness and caring.

I would also like to acknowledge the financial support from NSF grants CNS - 0834753, CCF-0917265 and CNS-1443966.

Table of Contents

List of Figures

List of Tables

Chapter 1

Introduction

1.1 Cognitive Radio Systems

It has been predicted that the number of wireless devices will reach around 100 billion by 2025 [1]. This explosive growth in wireless devices and new wireless applications prompts unprecedented demand on the radio spectrum. Indeed, the radio spectrum is a finite natural resource and the prime portion of the RF spectrum (e.g., between 30 MHz to 3 GHz) has already been allocated to specific applications or services. On the other hand, the Spectrum-Policy Task Force of the Federal Communications Commission (FCC) [2] reported that several portions of the spectrum are inefficiently used and hence are underutilized.

In light of this fact, cognitive radio has been proposed as an innovative technology to improve the efficiency in the use of limited, temporally and spatially underutilized licensed radio frequency spectrum. Cognitive radio was first introduced by Mitola in [3] as a smart wireless device that senses the environment, learns and automatically adapts its transmission parameters without changing any hardware structure. Through such cognition and the reconfigurability features, cognitive radio systems enable the unlicensed users (i.e., cognitive or secondary users) to access the licensed spectrum without causing harmful interference to the licensed users (i.e., primary users). Hence, this technology provides bright prospects

for implementing flexible spectrum allocation strategies and opening up bandwidth for new wireless services.

The cognitive radio technology has become more mature for commercial use over the years. In this regard, standardization activities, such as by IEEE 802.22 [4] for unlicensed access in VHF/UHF TV broadcast bands between 54 MHz and 790 MHz, IEEE 802.11af (also referred to as White-Fi) [5] for WiFi technology over unused TV bands and IEEE SCC41 [6], and regulations such as by the FCC [7] in the US and other regulatory bodies in different countries, facilitate widespread operational adoption of this promising technology. Beyond TV white spaces, cognitive radio systems find applications to improve the spectrum utilization in cellular systems, wireless LANs, machine-to-machine communications, vehicle-to-vehicle networks, wireless e-health services, and public safety services [8], [9].

Three communication models for cognitive radio have been proposed depending on how a cognitive user accesses the licensed channel: (i) underlay transmission scheme [10], (ii) opportunistic spectrum access (OSA) scheme [11] and sensing-based spectrum sharing (SSS) scheme [12]. Specifically, in the underlay transmission scheme, cognitive users transmit only if the interference at the primary receivers is kept below a certain threshold. In the SSS scheme, cognitive users initially perform channel sensing to detect primary user activity and then start transmission in the channel as long as they control the interference inflicted on the primary user by adapting the transmission power according to the channel sensing results. In particular, secondary users transmit at two different power levels depending on whether the channel is detected to be occupied and not occupied by the primary users. In the OSA scheme, cognitive users are allowed to transmit data only if no primary user activity is detected, and hence secondary users exploit only the silent periods in the transmissions of primary users, called as spectrum opportunities.

1.2 State of the Art and Gap in the Literature

1.2.1 Power allocation strategies in underlay cognitive radio systems

Power adaptation strategies have been extensively studied in order to enhance the performance of underlay cognitive radio systems while providing sufficient protection for the primary users. In this regard, the authors in [13] considered power allocation policies for truncated channel inversion with fixed rate (TIFR) and truncated optimum rate allocation (ORA) transmission schemes to maximize the ergodic capacity of the secondary user subject to average or peak transmit power constraints together with interference power constraints in such a way that the minimum rate requirement for the primary receiver is satisfied with a certain probability. The authors in [14] obtained optimal power allocation strategies that maximize the ergodic capacity of the secondary user under either peak or average transmit power constraints together with a constraint on the outage capacity of the primary user. In addition, the work in [15] mainly focused on the optimal power control strategies that maximize the ergodic capacity of the secondary user subject to peak/average transmit power constraints together with an upper bound on the outage capacity loss of the primary user due to secondary user transmission. In [16], optimal power allocation schemes that maximize the achievable rates of an orthogonal frequency-division multiplexing (OFDM)-based cognitive radio system were determined. In addition to ergodic capacity, the work in [17] considered the TIFR scheme to maximize the outage capacity of the secondary user subject to both peak and average interference power constraints. Also, the authors in [18] obtained the optimal power allocation strategies for the ergodic capacity, delay-limited capacity and the outage capacity of cognitive radio channels subject to peak/average transmit and peak/average interference constraints.

In all of the aforementioned studies, the implicit assumption was that the input signal follows a Gaussian distribution, leading to elegant closed-form expressions for the optimal

power allocation schemes. However, it may not be easy to realize Gaussian inputs in practice, and correspondingly inputs chosen from discrete constellations such as pulse amplitude modulation (PAM), quadrature amplitude modulation (QAM) and phase shift keying (PSK) are frequently employed in practical applications. Therefore, it is of great importance to obtain the power allocation strategies achieved with finite discrete constellations in cognitive radio systems.

1.2.2 Energy efficiency in cognitive radio sytems

Energy efficiency in cognitive radio systems has been recently addressed. For instance, the study in [19] mainly focused on spectral efficiency and energy efficiency of cognitive cellular networks in 5G mobile communication systems. The authors in [20] studied the optimal power allocation and power splitting at the secondary transmitter that maximize the energy efficiency of the secondary user as long as a minimum secrecy rate for the primary user is satisfied. Also, the authors in [21] designed energy-efficient optimal sensing strategies and optimal sequential sensing order in multichannel cognitive radio networks. In addition, the sensing time and transmission duration were jointly optimized in [22]. Several recent studies investigated power allocation/control to maximize the energy efficiency in different settings. The authors in [23] studied the optimal subcarrier assignment and power allocation to maximize either minimum energy efficiency among all secondary users or average energy efficiency in an OFDM-based cognitive radio network. Moreover, an optimal power loading algorithm was proposed in [24] to maximize the energy efficiency of an OFDM-based cognitive radio system in the presence of imperfect channel side information (CSI) of transmission link between secondary transmitter and secondary receiver. In the energy efficiency analysis of aforementioned works, secondary users are assumed to transmit only when the channel is sensed as idle. The work in [25] mainly focused on optimal power allocation to achieve the maximum energy efficiency of OFDM-based cognitive radio networks. Also, energy-efficient optimal power allocation in cognitive multiple input and multiple output (MIMO) broadcast

channel was studied in [26]. The authors in [27] proposed iterative algorithms to find the power allocation maximizing the sum energy efficiency of secondary users in heterogeneous cognitive two-tier networks. In these works, secondary users always share the spectrum with primary users without performing channel sensing.

The work in [28] mainly focused on the design of the optimal sensing duration and sensing decision threshold to maximize the weighted sum of the energy efficiency and spectral efficiency. The authors in [29] analyzed the optimal sensing duration that maximizes the energy efficiency of secondary user subject to a constraint on the detection probability. The work in [30] studied the optimal power control scheme that maximizes sum of energy efficiencies of the cognitive femto users for 5G communications. In these works, it is assumed that primary users transmit in a time-slotted fashion, i.e., the activity of the primary users (e.g., active or inactive) remains the same during the entire frame duration. In practice, primary and secondary user transmissions may not necessarily be synchronized. In this case, it is of significant interest to consider unslotted primary user in the analysis of energy efficiency of cognitive radio systems.

1.2.3 Error rate performance of cognitive radio transmissions

Several recent studies incorporate error rates in cognitive radio analysis. For instance, the authors in [31] characterized the optimal constellation size of M-QAM and the optimal power allocation scheme that maximize the channel capacity of secondary users for a given target bit error rate (BER), interference and peak power constraints. In [32], the opportunistic scheduling in multiuser underlay cognitive radio systems was studied in terms of link reliability. The work in [33] mainly focused on the power allocation scheme minimizing the upper bound on the symbol error probability of phase shift keying (PSK) in multiple antenna transmissions of secondary users. The authors in [34] proposed a channel switching algorithm for secondary users by exploiting the multichannel diversity to maximize the received SNR at the secondary receiver and evaluated the transmission performance in terms of average

symbol error probability. The optimal antenna selection that minimizes the symbol error probability in underlay cognitive radio systems was investigated in [35]. Moreover, the recent work in [36] analyzed the minimum BER of a cognitive transmission subject to both average transmit power and interference power constraints. In their model, the secondary transmitter is equipped with multiple antennas among which only one antenna that maximizes the weighted difference between the channel gains of transmission link from the secondary transmitter to the secondary receiver and interference link from the secondary transmitter to the primary receiver is selected for transmission. The authors in [37] obtained a closed-form BER expression under the assumption that the interference limit of the primary receiver is very high. Also, the work in [38] focused on the optimal power allocation that minimizes the average BER subject to peak/average transmit power and peak/average interference power constraints while the interference on the secondary users caused by primary users is omitted.

In the error rate analysis of these studies, channel sensing errors are not taken into consideration. Practical cognitive radio systems, which employ spectrum sensing mechanisms to learn the channel occupancy by primary users, generally operate under sensing uncertainty arising due to false alarms and miss-detections.

1.2.4 The performance of cognitive radio sytems under QoS constraints

One of the most important consideration for cognitive radio systems especially supporting streaming and interactive multimedia applications is to satisfy quality-of-service (QoS) requirements of secondary users in terms of buffer or delay constraints. In this respect, by incorporating the notion of the effective capacity, the authors in [39] obtained the optimal rate and power allocation strategy for secondary users in Nakagami fading channels under statistical delay QoS constraints. Moreover, the recent work in [40] mainly focused on the impact of adaptive M-QAM modulation on the effective capacity of secondary users under interference power and delay-QoS constraints. Notably, in most studies, it is implicitly as-

sumed that channel codes with arbitrarily long codewords can be used for transmission and consequently the well-known logarithmic channel capacity expressions of Gaussian channels are employed for analysis. On the other hand, the performance of cognitive radio systems operating under QoS constraints in the flinite-blocklength regime has not been sufficiently addressed.

1.2.5 Throughput- and energy-efficient transmission strategies under QoS constraints

The analysis and application of effective capacity in wireless systems have attracted growing interest in recent years. For instance, the authors in [41] first proposed the optimal power and rate adaptation schemes that maximize the effective capacity of a point-to-point wireless communication link. Then, they considered multichannel communications and derived the optimal power control policy for multicarrier and MIMO systems in [42]. In [43], the energy efficiency was formulated as the ratio of effective capacity to the total power consumption including circuit power and the optimal power allocation for multicarrier systems over a frequency-selective fading channel was determined. The work in [44] mainly focused on an energy-efficient power allocation scheme for delay-sensitive multimedia traffic in both low- and high-signal-to-noise ratio (SNR) regimes. Recently, the authors in [45] determined the QoS-driven optimal power control policy in closed-form to maximize the effective capacity subject to a minimum required energy efficiency level. The authors in [46] employed the notion of effective capacity and analyzed the energy efficiency under QoS constraints in the low-power and wideband regimes by characterizing the minimum energy per bit and wideband slope. Also, in [47], the minimum energy per bit and the wideband slope region for the dirty paper coding (DPC) and time division multiple access (TDMA) schemes under heterogeneous QoS constraints were characterized. Additionally, the authors in [48] obtained the effective capacity of correlated multiple input single output (MISO) channels and further analyzed the performance in low- and high-SNR regimes. Moreover, the asymptotic expres-

sion of the effective capacity in the low power regime for a Nakagami-m fading channel was derived in [49].

The resource allocation schemes of these studies are determined under the assumption of Gaussian input. Rather, practical applications often resort to simple discrete constellations. Hence, it is important and practically appealing to derive more general QoS-driven power allocation schemes for achieving the maximum energy efficiency when the input does not necessarily follow a Gaussian distribution.

1.3 Main Contributions

We summarize the main contributions of the thesis below:

- In Chapter 3, we identify the optimal power control policies that maximize the achievable rates of secondary users with arbitrary input signaling in underlay cognitive radio systems subject to peak/average transmit power constraints along with peak/average interference power constraints. We propose low-complexity optimal power control algorithms which do not impose any restrictions on the input distribution. Therefore, the proposed algorithms are applicable to more realistic and practical settings and are not restricted to the Gaussian input. We analyze the optimal power control policies in the low-power regime.

- In Chapter 4, we obtain the optimal power allocation strategies that maximize the energy efficiency of secondary users under the assumption that primary and secondary transmissions are synchronized. We assume different levels of CSI regarding the transmission and interference links, namely perfect CSI of both transmission and interference links, perfect CSI of the transmission link and imperfect CSI of the interference link, imperfect CSI of both links, or statistical CSI of both links. We develop a low-complexity algorithm based on Dinkelbach's method to iteratively solve the power allocation problem.

- In Chapter 5, we consider the case in which the primary changes its status during the transmission phase of the secondary users, and hence primary and secondary transmissions are not synchronized. Under this assumption, we derive, in closed-form, the optimal power control policy that maximizes the energy efficiency of the secondary users subject to transmit power, interference power and collision constraints in the presence of sensing errors. We do not impose any limitations on the number of transitions of the primary user activity. In order to consider the energy efficiency and spectral efficiency requirements of the secondary users jointly, we obtain the optimal power control scheme that maximizes the average throughput of the secondary users while satisfying the minimum required energy efficiency. We propose low-complexity algorithms for jointly finding the optimal power control policy and frame duration.

- In Chapter 6, we investigate the error rate performance of cognitive radio transmissions in the presence of imperfect sensing results and primary users interference, which is modeled to have a Gaussian mixture probability density function (which includes pure Gaussian distribution as a special case). We derive, for both sensing-based spectrum sensing and opportunistic spectrum access schemes, the optimal detector structure, and then we present a closed-form expression of the average symbol error probability under constraints on the transmit power and interference.

- In Chapter 7, we characterize the throughput of cognitive radio systems under buffer constraints in the finite blocklength regime by making use of the effective capacity. We assume that finite blocklength codes are used by the cognitive secondary users for sending messages. Hence, in our setup, transmission rates are possibly less than the channel capacity and errors can occur leading to retransmission requests. We consider the availability of channel side information at only the secondary transmitter, and at both the secondary transmitter and secondary receiver.

- In Chapter 8, we analyze the effective capacity achieved with arbitrarily distributed

signals under statistical QoS constraints (imposed as limitations on buffer overflow probabilities) in the presence of constant-rate sources. We derive the optimal power adaptation scheme that maximizes the effective capacity with arbitrary input signaling subject to an average transmit power constraint. We analyze the proposed optimal power policy under extremely stringent QoS constraints and also looser QoS constraints. Also, we analyze the energy efficiency performance with arbitrary input signaling in the low power regime. We analyze the tradeoff between the effective capacity and energy efficiency achieved with arbitrarily distributed signals. Then, we consider random sources and incorporate more general random arrival models, assuming arbitrary distributions for the transmitted signals, and analyze the optimal power control policies accordingly.

1.4 Outline of Thesis

Thesis mainly focuses on performance analysis of cognitive radio systems and throughput- and energy-efficient resource allocation schemes. The remainder of the thesis is organized as follows: Chapter 2 provides the necessary preliminary background on topics studied in the subsequent chapters of the thesis. Chapter 3 presents the optimal power control policies for underlay cognitive radio systems with arbitrary input distributions. Chapter 4 mainly characterizes energy efficient transmission strategies for cognitive users in the presence of imperfect sensing results under the assumption that the primary user adopts a time-slotted transmission scheme. In Chapter 5, the optimal power control policies that maximize the energy efficiency or average throughput of secondary users operating with unslotted primary users are derived. In Chapter 6, error rate performance of cognitive radio systems with channel sensing errors is analyzed. In Chapter 7, throughput of cognitive users with finite blocklength codes under QoS constraints is characterized. In Chapter 8, throughput- and energy- efficient power allocation schemes with arbitrary input signaling for general wire-

less systems operating subject to QoS constraints are identified for both constant-rate and random arrivals. Chapter 9 concludes this thesis and discusses future research directions.

1.4.1 Bibliographic Note

- The results in Chapter 3 appeared in the journal paper:
  - G. Ozcan and M. C. Gursoy, "Optimal power control for underlay cognitive radio systems with arbitrary input distributions," *IEEE Trans. Wireless Commun.*, vol. 14, no. 8, pp. 4219-4233, Mar. 2015

  and in the conference paper:
  - G. Ozcan and M. C. Gursoy, "Optimal power control for underlay cognitive radio systems with arbitrary input distributions," in *Proc. of the IEEE Global Commun. Conf. (Globecom)*, pp. 3453-3458, Austin, TX, Dec. 2014.
- The results in Chapter 4 appeared in part in the conference paper:
  - G. Ozcan and M. C. Gursoy, "Energy-efficient power adaptation for cognitive radio systems under imperfect channel sensing," in *Proc. of the 33rd Annual IEEE Inter. Conf. on Computer Commun. (INFOCOM) Workshop on Green Cognitive Commun. and Computer Networking (GCCCN)*, pp. 706-711, Toronto, ON, May 2014.
- The results in Chapter 5 appeared in part in the conference paper:
  - G. Ozcan, M. C. Gursoy, and J. Tang, "Power control for cognitive radio systems with unslotted primary users under sensing uncertainty," in *Proc. of the IEEE Inter. Conf. on Commun. (ICC)*, pp. 1428-1433, London, June 2015.
- The results in Chapter 6 appeared in the journal paper:

  - G. Ozcan, M. C. Gursoy, and S. Gezici, "Error rate analysis of cognitive radio transmissions with imperfect channel sensing," *IEEE Trans. Wireless Commun.*, vol. 13, no. 3, pp. 1642-1655, Feb. 2014

  and in the conference paper:

  - G. Ozcan, M. C. Gursoy, and S. Gezici, "Error rate analysis of cognitive radio transmissions with imperfect channel sensing," in *Proc. of the IEEE Veh. Tech. Conf. (VTC Fall)*, pp. 1-5, Vegas, NV, Sept. 2013.

- The results in Chapter 7 appeared in the journal paper:

  - G. Ozcan and M. C. Gursoy, "Throughput of cognitive radio systems with finite blocklength codes," *IEEE J. Sel. Areas Commun.*, vol. 31, no. 11, pp. 2541-2554, Nov. 2013

  and in the conference paper:

  - G. Ozcan and M. C. Gursoy, "Throughput of cognitive radio systems with finite blocklength codes," in *Proc. of the 46th Annual Conf. on Inf. Sciences and Systems (CISS)*, pp. 1-6, Princeton, NJ, Mar. 2012.

- The results in Chapter 8 appeared in part in the conference papers:

  - G. Ozcan and M. C. Gursoy, "QoS-driven power control for fading channels with arbitrary input distributions," in *Proc. of the IEEE Int. Symp. on Inf. Theory (ISIT)*, pp. 1381-1385, Honolulu, HI, July 2014
  - G. Ozcan and M. C. Gursoy, "Energy-efficient power control under QoS constraints with arbitrary input signaling," to appear in *Proc. of the 50th Annual Conf. on Inf. Sciences and Systems (CISS)*, Princeton, NJ, Mar. 2016
  - G. Ozcan, M. Ozmen, and M. C. Gursoy, "QoS-driven energy-efficient power control with random arrivals and arbitrary input distributions," to be presented

in *Proc. of the IEEE Int. Symp. on Inf. Theory (ISIT)*, Barcelona, Spain, July 2016.

Chapter 2

Background and Preliminary Concepts

2.1 Spectrum Sensing

Cognitive radio systems employ spectrum sensing mechanisms to learn the channel occupancy by primary users. In particular, spectrum sensing can be formulated as a hypothesis testing problem in which there are two hypotheses based on whether primary users are active or inactive over the channel, denoted by $\mathcal{H}_0$ and $\mathcal{H}_1$, respectively. Many spectrum sensing methods have been studied in the literature (see e.g., [50], [51] and references therein) including matched filter detection, energy detection and cyclostationary feature detection. Each method has its own advantages and disadvantages. However, all sensing methods are inevitably subject to errors in the form of false alarms and miss detections due to possibly low signal-to-noise ratio (SNR) levels of primary users, noise uncertainty, multipath fading and shadowing in wireless channels. Spectrum sensing is performed imperfectly with possible errors, and sensing performance depends on the sensing method only through detection and false alarm probabilities. As a result, any sensing method can be employed in the rest of the analysis in this thesis. Let $\hat{\mathcal{H}}_1$ and $\hat{\mathcal{H}}_0$ denote the sensing decisions that the channel is

occupied and not occupied by the primary users, respectively. Hence, by conditioning on the true hypotheses, the detection and false-alarm probabilities are defined, respectively, as follows:

$$\mathscr{P}_{\mathrm{d}} = \Pr\{\hat{\mathcal{H}}_1|\mathcal{H}_1\}, \tag{2.1}$$

$$\mathscr{P}_{\mathrm{f}} = \Pr\{\hat{\mathcal{H}}_1|\mathcal{H}_0\}. \tag{2.2}$$

Then, the conditional probabilities of idle sensing decision given the true hypotheses can be expressed as

$$\Pr\{\hat{\mathcal{H}}_0|\mathcal{H}_1\} = 1 - \mathscr{P}_{\mathrm{d}}, \tag{2.3}$$

$$Pr\{\hat{\mathcal{H}}_0|\mathcal{H}_0\} = 1 - \mathscr{P}_{\mathrm{f}}. \tag{2.4}$$

2.2 Relation between Minimum Mean Square Error and Mutual Information

The input-output relation over a flat-fading channel is expressed as

$$y[i] = h[i]x[i] + n[i] \quad i = 1, 2, \ldots \tag{2.5}$$

where $x[i]$ and $y[i]$ denote the transmitted and received signals, respectively, and $n[i]$ is a zero-mean, circularly symmetric, complex Gaussian random variable with variance N_0. It is assumed that noise samples $\{n[i]\}$ form an independent and identically distributed (i.i.d) sequence. Also, $h[i]$ represents the channel fading coefficient. We omit the time index i for notational brevity and we express the transmitted signal x in terms of a normalized unit-power arbitrarily distributed input signal s. Now, the received signal can be expressed

as

$$y = \sqrt{\rho}s + w, \tag{2.6}$$

where $\rho = Pz$, where P denotes the transmission power and z represents the channel power gain between the transmitter and receiver (i.e., $z = |h|^2$), and w is the normalized Gaussian noise with unit variance. Let us define the input-output mutual information $\mathcal{I}(\rho)$ as

$$\mathcal{I}\big(\rho\big) = \mathcal{I}\Big(s; \sqrt{\rho}s + w\Big). \tag{2.7}$$

In the case of Gaussian-distributed s, $\mathcal{I}(\rho) = \log_2(1+\rho)$. On the other hand, for any arbitrarily distributed equiprobable signal s with a constellation $\mathcal{X}$, we have [52]

$$\mathcal{I}(\rho) = \log_2|\mathcal{X}| - \frac{1}{\pi|\mathcal{X}|}\sum_{s\in\mathcal{X}}\int \log_2\left(\sum_{s'\in\mathcal{X}} \mathrm{e}^{-\rho|s-s'|^2 - 2\sqrt{\rho}\mathcal{R}\{(s-s')^* w\}}\right)\mathrm{e}^{-|w|^2}dw \tag{2.8}$$

where $|\mathcal{X}|$ denotes the size of the constellation $\mathcal{X}$, and the integration is carried out on the complex plane. The relation between the mutual information and the minimum mean-square error (MMSE) is given by [53]

$$\dot{\mathcal{I}}(\rho) = \mathrm{MMSE}(\rho)\log_2\mathrm{e} \tag{2.9}$$

where $\dot{\mathcal{I}}(\cdot)$ denotes the first derivative of the mutual information, $\mathcal{I}(\rho)$, with respect to ρ. The above relation is a key factor in deriving the power control policy in independent and parallel channels [52]. The MMSE estimate of s is expressed as

$$\hat{s}(y,\rho) = \mathbb{E}\{s \mid \sqrt{\rho}s + w\}. \tag{2.10}$$

Then, the corresponding MMSE is

$$\mathrm{MMSE}(\rho) = \mathbb{E}\{|s - \hat{s}(y,\rho)|^2\}. \tag{2.11}$$

It should be noted that $\mathrm{MMSE}(\cdot) \in [0,1]$. When the input signal s is Gaussian, $\mathrm{MMSE}(\rho) = \frac{1}{1+\rho}$. On the other hand, for any equiprobable input signal s belonging to the constellation $\mathcal{X}$, we have [52]

$$\mathrm{MMSE}(\rho) = 1 - \frac{1}{\pi|\mathcal{X}|}\int \frac{\left|\sum_{s\in\mathcal{X}} s\mathrm{e}^{2\sqrt{\rho}\mathcal{R}\{ys^*\}-\rho|s|^2}\right|^2}{\sum_{s\in\mathcal{X}} \mathrm{e}^{2\sqrt{\rho}\mathcal{R}\{ys^*\}-\rho|s|^2}}\mathrm{e}^{-|y|^2}dy. \tag{2.12}$$

The above MMSE expression can be explicitly determined for specific constellations such as binary phase-shift keying (BPSK), quadrature phase-shift keying (QPSK) as follows: [52]

$$\mathrm{MMSE}^{\mathrm{BPSK}}(\rho) = 1 - \int_{-\infty}^{\infty} \tanh(2\sqrt{\rho}\phi)\frac{\mathrm{e}^{-(\phi-\sqrt{\rho})^2}}{\sqrt{\pi}}d\phi, \tag{2.13}$$

$$\mathrm{MMSE}^{\mathrm{QPSK}}(\rho) = \mathrm{MMSE}^{\mathrm{BPSK}}\Big(\frac{\rho}{2}\Big). \tag{2.14}$$

In addition, MMSE for 4-pulse amplitude modulation (4-PAM) is given by

$$\mathrm{MMSE}^{\text{4-PAM}}(\rho) = 1 - \int_{-\infty}^{\infty} \frac{\left(\mathrm{e}^{-8\rho/5}\sinh\left(6\sqrt{\frac{\rho}{5}}\phi\right) + \sinh\left(2\sqrt{\frac{\rho}{5}}\phi\right)\right)^2}{\mathrm{e}^{-8\rho/5}\cosh\left(6\sqrt{\frac{\rho}{5}}\phi\right) + \cosh\left(2\sqrt{\frac{\rho}{5}}\phi\right)}\frac{\mathrm{e}^{-\phi^2-\rho/5}}{10\sqrt{\pi}}d\phi \tag{2.15}$$

Exploiting the MMSE expression of 4-PAM in (2.15), we can easily find the MMSE for 16-quadrature amplitude modulation (16-QAM) can easily follows:

$$\mathrm{MMSE}^{\text{16-QAM}}(\rho) = \mathrm{MMSE}^{\text{4-PAM}}\Big(\frac{\rho}{2}\Big). \tag{2.16}$$

For other constellations, the MMSE expression in (2.12) and the mutual information in (2.8) can easily be computed by first expressing them as double integrals and then applying the Gauss-Hermite quadrature rules [54].

2.3 Throughput under Statistical Queueing Limitations

Many important wireless applications (e.g. mobile streaming/interactive video, voice over IP (VoIP), interactive gaming and mobile TV) require certain QoS guarantees for acceptable performance levels at the end-user. In [55], a link-layer channel model called the effective capacity, is proposed to serve as a suitable metric to quantify the performance of wireless systems under statistical QoS constraints. In particular, Wu and Negi in [55] defined the effective capacity as the maximum constant arrival rate that a given service process can support in order to guarantee a statistical QoS requirement characterized by the QoS exponent θ. If we define Q as the stationary queue length, then θ is the decay rate of the tail of the distribution of the queue length Q:

$$\lim_{q\to\infty} \frac{\log P(Q \geq q)}{q} = -\theta. \tag{2.17}$$

Therefore, for large q_{max}, the buffer overflow probability can be approximated as exponentially decaying at the rate θ:

$$P(Q \geq q_{\max}) \approx e^{-\theta q_{\max}}. \tag{2.18}$$

It should be also noted that larger values of θ impose faster decay rate, hence implying stricter queueing or QoS constraints. On the other hand, smaller θ values indicate looser constraints. The effective capacity, which quantifies the throughput under a buffer constraint in the form of (2.18), is given by ([55], [56])

$$R_E = -\lim_{t\to\infty} \frac{1}{\theta t} \log_e \mathbb{E}\{e^{-\theta S[t]}\} \triangleq -\frac{\Lambda(-\theta)}{\theta} \tag{2.19}$$

where $\Lambda(\theta) = \lim_{t\to\infty} \frac{1}{t} \log_e \mathbb{E}\{e^{\theta S[t]}\}$, $S[t] = \sum_{i=1}^{t} r_i$ is the time-accumulated service process and $\{r_i, i = 1, 2, \ldots\}$ denotes the discrete-time stationary and ergodic stochastic service process.

Chapter 3

Optimal Power Control for Underlay Cognitive Radio Systems with Arbitrary Input Distributions

This chapter studies optimal power control policies that maximize the achievable rates of underlay cognitive radio systems with arbitrary input distributions under both peak/average transmit power and peak/average interference power constraints for general fading distributions. Low-complexity optimal power control algorithms are proposed. Simpler approximations of optimal power control policies in the low-power regime are determined. The impact of the fading severity of both interference and transmission links and transmit power and interference power constraints on the maximum achievable rate of the cognitive user for different practical constellations and Gaussian signals are investigated.

The remainder of the chapter is organized as follows: Section 3.1 introduces the system model. In Section 3.2, optimal power control policies that maximize the achievable rate of the secondary user with arbitrary input distributions subject to different combinations of transmit power and interference power constraints are determined and the optimal power control algorithms are provided. Subsequently, the low-power analysis is conducted in Sec-

tion 3.3, where approximations to the optimal power control policies and the corresponding closed-form second-order achievable rate expressions are obtained. Numerical results are presented and discussed in Section 3.4.

3.1 System Model

We consider an underlay cognitive radio system in which the secondary users coexist with the licensed primary users while satisfying certain interference constraints. The instantaneous channel power gains of the transmission link between the secondary transmitter and the secondary receiver and of the interference link between the secondary transmitter and the primary receiver are denoted by z_s and z_{sp}, respectively as illustrated in Figure 3.1. The secondary transmitter is assumed to have perfect knowledge of z_s and z_{sp}. In particular, the secondary receiver can estimate z_s and then send it back to the secondary transmitter through an error-free feedback link. Also, the knowledge of interference channel power gain z_{sp} can be obtained by several methods: direct channel feedback from the primary receiver to the secondary transmitter [57], indirect feedback from a third party such as band manager [58], or periodic sensing of a pilot symbol sent from the primary receiver by assuming channel reciprocity [59].

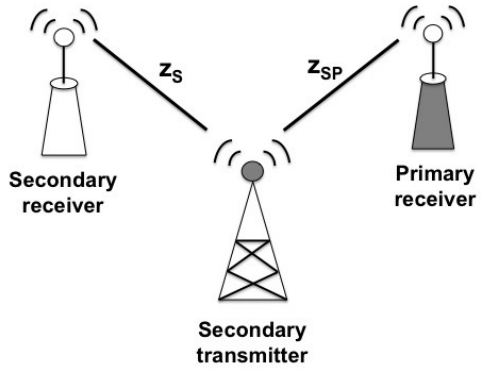

Figure 3.1: Underlay cognitive radio system model.

The channel between the secondary transmitter and the secondary receiver is assumed to be flat-fading. Hence, under these assumptions, the discrete-time channel input-output

relation is given by

$$y[i] = h_s[i]x[i] + n_w[i] + n_p[i] \qquad i = 1, 2, \ldots \tag{3.1}$$

where i represents the time index, $x[i]$ and $y[i]$ denote the transmitted and received signals, respectively, $n_w[i]$ is a zero-mean, circularly symmetric, additive complex Gaussian noise at secondary receiver, i.e., $n_w \sim \mathcal{CN}(0, \sigma_w^2)$ and $n_p[i]$ is the interference at secondary receiver due to primary user transmission. It is further assumed that $n_p[i]$ follows a Gaussian distribution, i.e., $n_w \sim \mathcal{CN}(0, \sigma_p^2)$. Thus, $n_w+n_p \sim \mathcal{CN}(0, \sigma_w^2+\sigma_p^2)$. Without loss of generality, the variance $\sigma_w^2+\sigma_p^2$ is assumed to be 1. Also, $\{n_w[i]\}$ and $\{n_p[i]\}$ are assumed to form an independent and identically distributed (i.i.d) sequence. In the above expression, $h_s[i]$ represents the channel fading coefficient between the secondary transmitter and the secondary receiver, and hence the channel power gain is $z_s[i] = |h_s[i]|^2$.

Hereafter, time index i is omitted for brevity of notation. We express the transmitted signal x as

$$x = \sqrt{P(z_s, z_{sp})}s \tag{3.2}$$

where s is a unit-power arbitrarily-distributed input signal and $P(z_s, z_{sp})$ denotes the instantaneous transmission power, which is a function of the channel gains z_s and z_{sp}. Then, by also assuming that the channel phase rotations are offset at the receiver with the knowledge of the phase of the fading coefficient h_s, the received signal in (3.1) can be rewritten as

$$y = \sqrt{P(z_s, z_{sp})z_s}s + w. \tag{3.3}$$

3.2 Optimal Power Control

In this section, we derive the optimal power control policies that maximize the achievable rates of the secondary user with arbitrary input distributions subject to transmit power and interference power constraints. For a given power control policy $P(z_s, z_{sp})$, the achievable rate of the secondary user is expressed as

$$\mathbb{E}\{\mathcal{I}(P(z_s, z_{sp})z_s)\} = \int_{z_s>0} \int_{z_{sp}>0} \mathcal{I}(P(z_s, z_{sp})z_s) f_{z_s}(z_s) f_{z_{sp}}(z_{sp}) dz_s dz_{sp} \tag{3.4}$$

where $\mathcal{I}(.)$ denotes the input-output mutual information, $f_{z_s}(\cdot)$ and $f_{z_{sp}}(\cdot)$ represent the probability density functions (PDFs) of the channel gains of the transmission link between the secondary transmitter and the secondary receiver and of the interference link between the secondary transmitter and the primary receiver, respectively. With this characterization, the optimal power adaptation problem can be formulated as

$$P^*(z_s, z_{sp}) = \underset{P(z_s,z_{sp})\in\mathcal{P}}{\arg\max}\ \mathbb{E}\{\mathcal{I}(P(z_s, z_{sp})z_s)\} \tag{3.5}$$

where $P^*(z_s, z_{sp})$ denotes the optimal power control strategy and $\mathcal{P}$ is the set of feasible power control schemes with which the transmit power and interference power constraints are satisfied. In the following subsections, the optimization problem in (3.5) is studied under four scenarios, where different combinations of peak/average transmit power and peak/average interference power constraints are imposed.

3.2.1 Peak transmit power and peak interference power constraints

In this case, peak constraints are imposed on the transmission and interference powers, and hence the optimization problem in (3.5) is subject to

$$P(z_s, z_{sp}) \leq P_{\text{pk}}, \tag{3.6}$$

$$P(z_s, z_{sp}) z_{sp} \leq Q_{\text{pk}}, \tag{3.7}$$

where P_{pk} denotes the peak transmit power limit of the secondary transmitter due to hardware and battery constraints, and Q_{pk} represents the peak limit on the received interference power at the primary receiver, which is imposed to satisfy short-term QoS requirements of the primary users. The above constraints can be more concisely expressed as $P(z_s, z_{sp}) \leq \min\left(P_{\text{pk}}, \frac{Q_{\text{pk}}}{z_{sp}}\right)$. Moreover, the objective function in (3.5) is strictly concave [52]. Hence, the maximum rate is achieved when the secondary user transmits at the maximum available instantaneous power. Therefore, the optimal power control is given by

$$P^*(z_{sp}) = \min\left(P_{\text{pk}}, \frac{Q_{\text{pk}}}{z_{sp}}\right) \tag{3.8}$$

which can further be written as

$$P^*(z_{sp}) = \begin{cases} \frac{Q_{\text{pk}}}{z_{sp}}, & z_{sp} \geq \frac{Q_{\text{pk}}}{P_{\text{pk}}} \\ P_{\text{pk}}, & z_{sp} < \frac{Q_{\text{pk}}}{P_{\text{pk}}} \end{cases}. \tag{3.9}$$

It should be noted that $P^*(z_{sp})$ becomes independent of the channel power gain of the transmission link z_s and the input distribution, and depends only on the channel power gain of the interference link, z_{sp}.

3.2.2 Peak transmit power and average interference power constraints

In this case, the constraints are given by

$$P(z_s, z_{sp}) \leq P_{\text{pk}}, \tag{3.10}$$

$$\mathbb{E}\{P(z_s, z_{sp}) z_{sp}\} \leq Q_{\text{avg}}, \tag{3.11}$$

where Q_{avg} represents the average received interference power limit at the primary receiver, which is imposed to satisfy the long-term QoS requirements of the primary users. In the following result, we identify the optimal power adaptation strategy for this case.

Theorem 3.2.1 *The optimal power control policy under the constraints in (3.10) and (3.11) is given by*

$$P^*(z_s, z_{sp}) = \min\left\{\frac{1}{z_s} MMSE^{-1}\Big(\min\left\{1, \frac{\lambda z_{sp}}{\log_2 \text{e}\ z_s}\right\}\Big), P_{\text{pk}}\right\} \tag{3.12}$$

where $MMSE^{-1}(\cdot) \in [0, \infty)$ denotes inverse MMSE function and λ is the Lagrange multiplier, which can be determined by satisfying the average interference power constraint in (3.11) with equality.

Proof: See Appendix A.

The projected subgradient method is employed to numerically find the value of λ. In this method, λ is updated iteratively in the direction of a negative subgradient of the Lagrangian $L(P(z_s, z_{sp})$ given in (A.1) in Appendix A until convergence as follows:

$$\lambda^{(n+1)} = \Big(\lambda^{(n)} - t\big(Q_{\text{avg}} - \mathbb{E}\{P^*(z_s, z_{sp}) z_{sp}\}\big)\Big)^+ \tag{3.13}$$

where $(x)^+ = \max\{0, x\}$, n is the iteration index and t is the step size. For a constant t, it was shown that convergence to the optimal λ value is guaranteed within a small range [60].

From (3.12), it is observed that the optimal power control policy depends on the input distribution through the inverse MMSE function. In real-time systems, $\text{MMSE}^{-1}(.)$ can be precomputed and stored in memory for the constellation of interest. Alternatively, by using the fact that MMSE is a monotonically decreasing function, $P^*(z_s, z_{sp})$ can be efficiently determined by first computing the MMSE in (2.12) for the corresponding input constellation and then solving for the condition in (A.5) in Appendix A with numerical root finding methods, e.g., bisection method. The optimal power control algorithm for this scenario is given in Table 3.1.

The authors in [52] proposed the optimal power allocation scheme called *mercury/waterfilling* for parallel channels with arbitrary input distributions subject to an average power constraint in a non-cognitive context. Different from [52], [61], the proposed optimal power control policy in (3.12) is a function of the channel power gains of both transmission and interference links, z_s and z_{sp}, respectively. Therefore, we call this power control scheme as *two-dimensional truncated mercury/waterfilling.*

Remark 3.2.1 *When the input signal is Gaussian, we have* $MMSE^{-1}(\rho) = \frac{1}{\rho} - 1$. *Substituting this expression into (3.12), we can see that the optimal power control policy becomes*

$$P^*(z_s, z_{sp}) = \min\left\{\left(\frac{\log_2 \mathrm{e}}{\lambda z_{sp}} - \frac{1}{z_s}\right)^+, P_{\text{pk}}\right\} \tag{3.14}$$

which is in agreement with the result obtained in [18]. It is also seen that the above power adaptation is in the form of truncated waterfilling *with water level* $\frac{\log_2 \mathrm{e}}{\lambda z_{sp}}$, *which depends on the channel power gain of the interference link,* z_{sp}.

Table 3.1: The optimal power control algorithm that maximizes the achievable rate of the secondary user under peak transmit power and average interference power constraints

Algorithm 1

Initialize $P_h(z_s, z_{sp}) = P_{h,\text{init}}$, $P_l(z_s, z_{sp}) = P_{l,\text{init}}$, $\epsilon > 0$, $\delta > 0$, $t > 0$, $\lambda^{(0)} = \lambda_{\text{init}}$, $\mu^{(0)} = \mu_{\text{init}}$
$n \leftarrow 0$
If the average interference constraint in (3.11) is satisfied when $P^*(z_s, z_{sp}) = P_{\text{pk}}$, then stop.
repeat
  if $\frac{\log_2 \mathrm{e}\ z_s}{z_{sp}} \leq \lambda^{(n)}$ **then**
    $P^*(z_s, z_{sp}) = 0$
  else
    repeat
      update $P^*(z_s, z_{sp}) = \frac{1}{2}\big(P_h(z_s, z_{sp}) + P_l(z_s, z_{sp})\big)$
      if $g(P^*(z_s, z_{sp}))g(P_h(z_s, z_{sp})) < 0$ (where $g(.)$ is defined in (A.5)), then
        $P_l(z_s, z_{sp}) \leftarrow P^*(z_s, z_{sp})$
      else if $g(P^*(z_s, z_{sp}))g(P_l(z_s, z_{sp})) < 0$, then
        $P_h(z_s, z_{sp}) \leftarrow P^*(z_s, z_{sp})$
      end if
    until $|g(P^*(z_s, z_{sp}))| < \epsilon$
  end if
  $P^*(z_s, z_{sp}) = \min\big(P_{\text{pk}}, P^*(z_s, z_{sp})\big)$
  update λ using the projected subgradient method as follows
  $\lambda^{(n+1)} = \big(\lambda^{(n)} - t(Q_{\text{avg}} - \mathbb{E}\{P^*(z_s, z_{sp})z_{sp}\})\big)^+$
  $n \leftarrow n + 1$
until $|\lambda^{(n)}(Q_{\text{avg}} - \mathbb{E}\{P^*(z_s, z_{sp})z_{sp}\})| \leq \delta$

Table 3.2: The optimal power control algorithm that maximizes the achievable rate of the secondary user under average transmit power and peak interference power constraints

Algorithm 2

Initialize $P_h(z_s, z_{sp}) = P_{h,\text{init}}$, $P_l(z_s, z_{sp}) = P_{l,\text{init}}$, $\epsilon > 0$, $\delta > 0$, $t > 0$, $\lambda^{(0)} = \lambda_{\text{init}}$, $\mu^{(0)} = \mu_{\text{init}}$
$n \leftarrow 0$
If the average transmit power constraint in (3.15) is satisfied when $P^*(z_s, z_{sp}) = \frac{Q_{\text{pk}}}{z_{sp}}$, then stop.
repeat
  if $\log_2 \mathrm{e}\ z_s \leq \mu^{(n)}$ **then**
    $P^*(z_s, z_{sp}) = 0$
  else
    Find $P^*(z_s, z_{sp})$ by bisection method as done in Algorithm 1 where $g(.)$ is replaced by $h(.)$ given in (B.2).
  end if
  $P^*(z_s, z_{sp}) = \min\left(\frac{Q_{\text{pk}}}{z_{sp}}, P^*(z_s, z_{sp})\right)$
  update μ using the projected subgradient method as follows
  $\mu^{(n+1)} = \left(\mu^{(n)} - t(P_{\text{avg}} - \mathbb{E}\{P^*(z_s, z_{sp})\})\right)^+$
  $n \leftarrow n + 1$
until $|\mu^{(n)}(P_{\text{avg}} - \mathbb{E}\{P^*(z_s, z_{sp})\})| \leq \delta$

Table 3.3: The optimal power control algorithm that maximizes the achievable rate of the secondary user under average transmit power and average interference power constraints

Algorithm 3

Initialize $P_h(z_s, z_{sp}) = P_{h,\text{init}}$, $P_l(z_s, z_{sp}) = P_{l,\text{init}}$, $\epsilon > 0$, $\delta > 0$, $t > 0$, $\lambda^{(0)} = \lambda_{\text{init}}$, $\mu^{(0)} = \mu_{\text{init}}$
$n \leftarrow 0$
repeat
  if $\log_2 \mathrm{e}\ z_s - \lambda^{(n)} z_{sp} \leq \mu^{(n)}$ **then**
    $P^*(z_s, z_{sp}) = 0$
  else
    Find $P^*(z_s, z_{sp})$ by bisection method as done in Algorithm 1 where $g(.)$ is replaced by $\eta(.)$ given in (C.2).
  end if
  update μ and λ using the projected subgradient method as follows
  $\mu^{(n+1)} = \left(\mu^{(n)} - t(P_{\text{avg}} - \mathbb{E}\{P^*(z_s, z_{sp})\})\right)^+$
  $\lambda^{(n+1)} = \left(\lambda^{(n)} - t(Q_{\text{avg}} - \mathbb{E}\{P^*(z_s, z_{sp}) z_{sp}\})\right)^+$
  $n \leftarrow n + 1$
until $|\mu^{(n)}(P_{\text{avg}} - \mathbb{E}\{P^*(z_s, z_{sp})\})| \leq \delta$ and $|\lambda^{(n)}(Q_{\text{avg}} - \mathbb{E}\{P^*(z_s, z_{sp}) z_{sp}\})| \leq \delta$

3.2.3 Average transmit power and peak interference power constraints

In this case, we have the following two constraints for the optimization problem given in (3.5):

$$\mathbb{E}\{P(z_s, z_{sp})\} \leq P_{\text{avg}}, \tag{3.15}$$

$$P(z_s, z_{sp}) z_{sp} \leq Q_{\text{pk}}, \tag{3.16}$$

where P_{avg} denotes the average transmit power limit at the secondary transmitter. Under these constraints, the optimal power control scheme is determined as in the following result.

Theorem 3.2.2 *The optimal power control policy subject to the constraints in (3.15) and*

(3.16) is obtained as

$$P^*(z_s, z_{sp}) = \min\left\{\frac{1}{z_s} MMSE^{-1}\Big(\min\Big\{1, \frac{\mu}{\log_2 \mathrm{e}\ z_s}\Big\}\Big), \frac{Q_{\mathrm{pk}}}{z_{sp}}\right\} \tag{3.17}$$

Above, the Lagrange multiplier μ is chosen such that the average transmit power constraint in (3.15) is satisfied with equality.

Proof: See Appendix B.

Again, the power control algorithm for this case is detailed in Table 3.2.

Remark 3.2.2 *Inserting $MMSE^{-1}(\rho) = \frac{1}{\rho} - 1$ into (3.17), the optimal power control policy becomes the* truncated waterfilling *scheme for Gaussian inputs as follows*

$$P^*(z_s, z_{sp}) = \min\left\{\left(\frac{\log_2 \mathrm{e}}{\mu} - \frac{1}{z_s}\right)^+, \frac{Q_{\mathrm{pk}}}{z_{sp}}\right\} \tag{3.18}$$

which has the same structure as given in [18].

3.2.4 Average transmit power and average interference power constraints

Finally, we consider the case in which the secondary transmitter operates under both average transmit and average interference power constraints expressed as

$$\mathbb{E}\{P(z_s, z_{sp})\} \leq P_{\mathrm{avg}}, \tag{3.19}$$

$$\mathbb{E}\{P(z_s, z_{sp}) z_{sp}\} \leq Q_{\mathrm{avg}}. \tag{3.20}$$

The main characterization is as follows with the power control algorithm provided in Table 3.3:

Theorem 3.2.3 *The optimal power control policy under the constraints in (3.19) and (3.20)*

is determined as

$$P^*(z_s, z_{sp}) = \frac{1}{z_s} MMSE^{-1}\Big(\min\Big\{1, \frac{\mu + \lambda z_{sp}}{\log_2 \mathrm{e}\ z_s}\Big\}\Big) \tag{3.21}$$

where μ and λ are the Lagrange multipliers, which can be jointly obtained by inserting the above optimal power expression into the constraints given in (3.19) and (3.20).

Proof: See Appendix C.

Remark 3.2.3 *When the input signal is Gaussian, we have*

$$P^*(z_s, z_{sp}) = \left(\frac{\log_2 \mathrm{e}}{\mu + \lambda z_{sp}} - \frac{1}{z_s}\right)^+ \tag{3.22}$$

which is again consistent with the power allocation scheme given in [18].

Overall, our results throughout this section can be regarded as the generalization of the optimal power control strategies characterized for only Gaussian inputs to arbitrarily distributed inputs, including frequently-used finite constellations such as BPSK, QPSK, and QAM.

3.3 Low-Power Regime Analysis

In this section, we characterize the optimal power control policies that maximize the achievable rates of the secondary user with arbitrary input distributions in the low-power regime. We note that operating at low power levels is of interest in cognitive radio systems due to the facts that less interference is inflicted on the primary users and energy efficiency of cognitive secondary users is generally improved in this regime.

Similarly as in the previous section, the proposed optimal power expressions are derived for general fading distributions. In special cases, we further provide closed-form approximations of the maximum achievable rates in the low-power regime. In determining these

expressions, we consider unit-mean Nakagami-m fading, which is analytically tractable and widely used to model urban and indoor multipath propagation. By changing the parameter $m \in [0.5, \infty)$, the Nakagami-m fading covers different models describing the statistical behavior of the radio propagation environment. More specifically, in the case of $m = 0.5$, the Nakagami-m distribution specializes to the one-sided Gaussian distribution, which corresponds to the most severe fading. For $m = 1$, the Nakagami-m distribution becomes the Rayleigh fading, which is used to model multipath fading with no direct line-of-sight (LOS) component. As m goes to infinity, the Nakagami-m fading channel converges to a nonfading additive white Gaussian noise (AWGN) channel. Under the assumption of the Nakagami-m fading, the channel power gains of the transmission link, z_s, and interference link, z_{sp}, follow gamma distributions with PDFs given, respectively, as

$$f_{z_s}(z_s; m_s) = \frac{m_s^{m_s} z_s^{m_s-1}}{\Gamma(m_s)} \mathrm{e}^{-m_s z_s} \qquad z_s \geq 0, m_s \geq 0.5, \tag{3.23}$$

$$f_{z_{sp}}(z_{sp}; m_{sp}) = \frac{m_{sp}^{m_{sp}} z_{sp}^{m_{sp}-1}}{\Gamma(m_{sp})} \mathrm{e}^{-m_{sp} z_{sp}} \quad z_{sp} \geq 0, m_{sp} \geq 0.5 \tag{3.24}$$

where $\Gamma(.)$ is the gamma function [62, eq. 6.1.1] and m_s and m_{sp} control the severity of the amplitude fading of the transmission link and the interference link, respectively.

3.3.1 Peak transmit power and peak interference power constraints

The optimal power policy in the low power regime subject to the constraints in (3.6) and (3.7) is the same as in (3.8). Next, we find a closed-form expression for the maximum achievable rate of the secondary user attained with the optimal power control policy in (3.8).

We first express the mutual information achieved with arbitrary input distributions in the low-power regime as follows:

$$\mathcal{I}(\rho) = \dot{\mathcal{I}}(0)\rho \log_2 \mathrm{e} + \frac{\ddot{\mathcal{I}}(0)}{2}\rho^2 \log_2 \mathrm{e} + o(\rho^2) \tag{3.25}$$

where $\rho = P(z_s, z_{sp})z_s$ and $\dot{\mathcal{I}}(0) = 1$ [52]. Substituting the optimal power control policy in (3.8) into the above mutual information expression and taking the expectation with respect to fading, the maximum achievable rate can be found as

$$\begin{aligned} R_{\text{opt}}(P_{\text{pk}}, Q_{\text{pk}}) = &\int_0^{\frac{Q_{\text{pk}}}{P_{\text{pk}}}} \int_0^{\infty} \left(P_{\text{pk}} z_s + \frac{\ddot{\mathcal{I}}(0) P_{\text{pk}}^2 z_s^2}{2} \right) \log_2 \text{e} \; f_{z_s}(z_s) f_{z_{sp}}(z_{sp}) dz_s dz_{sp} \\ &+ \int_{\frac{Q_{\text{pk}}}{P_{\text{pk}}}}^{\infty} \int_0^{\infty} \left(\frac{Q_{\text{pk}} z_s}{z_{sp}} + \frac{\ddot{\mathcal{I}}(0) Q_{\text{pk}}^2}{2} \frac{z_s^2}{z_{sp}^2} \right) \log_2 \text{e} \; f_{z_s}(z_s) f_{z_{sp}}(z_{sp}) dz_s dz_{sp}. \end{aligned} \tag{3.26}$$

Evaluating the integrals in (3.26) gives the closed-form expression for the maximum achievable rate as follows:

$$\begin{aligned} R_{\text{opt}}(P_{\text{pk}}, Q_{\text{pk}}) = &\left(P_{\text{pk}} \frac{\Gamma(m_s+1)}{\Gamma(m_s) m_s} + \ddot{\mathcal{I}}(0) \frac{P_{\text{pk}}^2}{2} \frac{\Gamma(m_s+2)}{\Gamma(m_s) m_s^2} \right) \left(1 - \frac{\Gamma(m_{sp}, \frac{m_{sp} Q_{\text{pk}}}{P_{\text{pk}}})}{\Gamma(m_{sp})} \right) \log_2 \text{e} \\ &+ Q_{\text{pk}} \frac{m_{sp}}{m_s} \frac{\Gamma(m_s+1)}{\Gamma(m_s)} \frac{\Gamma(m_{sp}-1, \frac{m_{sp} Q_{\text{pk}}}{P_{\text{pk}}})}{\Gamma(m_{sp})} \log_2 \text{e} + \ddot{\mathcal{I}}(0) \frac{Q_{\text{pk}}^2}{2} \left(\frac{m_{sp}}{m_s} \right)^2 \frac{\Gamma(m_s+2)}{\Gamma(m_s)} \\ &\times \frac{\Gamma(m_{sp}-2, \frac{m_{sp} Q_{\text{pk}}}{P_{\text{pk}}})}{\Gamma(m_{sp})} \log_2 \text{e} \text{ for } m_{sp} > 2, \end{aligned} \tag{3.27}$$

where $\Gamma(a, b)$ is the incomplete gamma function [62, eq. 6.5.3].

In addition, if the power allocation problem is only constrained by peak transmit power constraint P_{pk}, the achievable rate can be computed as

$$R_{\text{opt}}(P_{\text{pk}}) = \int_0^{\infty} \int_0^{\infty} \left(P_{\text{pk}} z_s + \frac{\ddot{\mathcal{I}}(0) P_{\text{pk}}^2 z_s^2}{2} \right) \log_2 \text{e} \; f_{z_s}(z_s) f_{z_{sp}}(z_{sp}) dz_s dz_{sp}. \tag{3.28}$$

Evaluating the above integral yields the closed-form achievable rate expression under only P_{pk} constraint in the following:

$$R_{\text{opt}}(P_{\text{pk}}) = \left(P_{\text{pk}} \frac{\Gamma(m_s+1)}{\Gamma(m_s) m_s} + \ddot{\mathcal{I}}(0) \frac{P_{pk}^2}{2} \frac{\Gamma(m_s+2)}{\Gamma(m_s) m_s^2} \right) \log_2 \text{e}. \tag{3.29}$$

Moreover, if the power allocation problem is only constrained by peak interference power

constraint $Q_{\rm pk}$, the achievable rate can be expressed as

$$R_{\rm opt}(Q_{\rm pk}) = \int_0^\infty \int_0^\infty \left(\frac{Q_{\rm pk} z_s}{z_{sp}} + \frac{\ddot{\mathcal{I}}(0) Q_{\rm pk}^2}{2} \frac{z_s^2}{z_{sp}^2} \right) \log_2 \mathrm{e}\ f_{z_s}(z_s) f_{z_{sp}}(z_{sp}) dz_s dz_{sp}. \tag{3.30}$$

By performing above integration, a closed-form achievable rate expression subject to only $Q_{\rm pk}$ constraint can be found as

$$R_{\rm opt}(Q_{\rm pk}) = Q_{\rm pk} \Big(\frac{m_{sp}}{m_s} \Big) \frac{\Gamma(m_s+1)\Gamma(m_{sp}-1)}{\Gamma(m_{sp})\Gamma(m_s)} \log_2 \mathrm{e} + \frac{Q_{\rm pk}^2}{2} \ddot{\mathcal{I}}(0) \Big(\frac{m_{sp}}{m_s} \Big)^2 \frac{\Gamma(m_s+2)\Gamma(m_{sp}-2)}{\Gamma(m_{sp})\Gamma(m_s)} \log_2 \mathrm{e}. \tag{3.31}$$

3.3.2 Peak transmit power and average interference power constraints

In this case, by using the low-power expansion of MMSE in terms of the first and second derivatives of the mutual information, we can simplify the optimal power control policy in the low power regime as in the following result.

Theorem 3.3.1 *The optimal power control policy that maximizes the achievable rate of the secondary user in the low-power regime, i.e., as $P_{\rm pk} \to 0$ and $Q_{avg} \to 0$, with arbitrary input distributions belonging to discrete constellations under the constraints in (3.10) and (3.11) can be approximated as*

$$P^*(z_s, z_{sp}) = \min \left\{ \left(\frac{\frac{\lambda z_{sp}}{\log_2 \mathrm{e}} - z_s}{\ddot{\mathcal{I}}(0) z_s^2} \right)^+, P_{\rm pk} \right\} \tag{3.32}$$

where $\ddot{\mathcal{I}}(0)$ denotes the second derivative of mutual information evaluated at $SNR = 0$ and λ is the Lagrange multiplier associated with the average interference power constraint in (3.11).

Proof: See Appendix D.

We immediately see that the resulting optimal power control policy in (3.32) is simpler and depends on the input distribution through $\ddot{\mathcal{I}}(0)$ rather than $\mathrm{MMSE}^{-1}(\cdot)$. In particular,

for quadrature symmetric constellations such as QPSK, 8-PSK or 16-QAM, we have $\ddot{\mathcal{I}}(0) = -1$ while real valued constellations such as BPSK and m-PAM have $\ddot{\mathcal{I}}(0) = -2$ [52]. It should also be noted that we can obtain the low power behavior of MMSE for the Gaussian input by setting $\ddot{\mathcal{I}}(0) = -1$ in (D.1). Hence, inserting $\ddot{\mathcal{I}}(0) = -1$ in (3.32), the optimal power expressions for Gaussian input can readily be obtained.

3.3.3 Average transmit power and peak interference power constraints

Similarly as in the previous subsection, we first identify the optimal power adaptation strategy in the low-power regime.

Theorem 3.3.2 *In the low-power regime, the optimal power control policy subject to the constraints in (3.15) and (3.16) is approximated by*

$$P^*(z_s, z_{sp}) = \min\left\{\left(\frac{\frac{\mu}{\log_2 \mathrm{e}} - z_s}{\ddot{\mathcal{I}}(0) z_s^2}\right)^+, \frac{Q_{\mathrm{pk}}}{z_{sp}}\right\}. \tag{3.33}$$

Since similar procedures as in the proof of Theorem 3.3.1 are employed, the proof is omitted. Inserting the above optimal power policy into (3.25) and taking the expectation with respect to channel power gains z_s and z_{sp} do not yield a closed-form maximum achievable rate expression. Hence, we provide closed-form expressions under only an average transmit power constraint.

If only an average power constraint is imposed (or if the interference constraint is loose), the optimal power control has the same formulation as in (3.33) with $\frac{Q_{\mathrm{pk}}}{z_{sp}}$ eliminated. Hence, in this setting, the maximum achievable rate can be found as

$$R_{\mathrm{opt}}(P_{\mathrm{avg}}) = \int_{\frac{\mu}{\log_2 \mathrm{e}}}^{\infty} \frac{1}{2\ddot{\mathcal{I}}(0)} \left(\left(\frac{\mu}{\log_2 \mathrm{e}\ z_s}\right)^2 - 1\right) \log_2 \mathrm{e}\ f_{z_s}(z_s) dz_s \tag{3.34}$$

and the above integration yields the following closed-form maximum achievable rate expres-

sion:

$$R_{\text{opt}}(P_{\text{avg}}) = \frac{\mu^2 m_s^2}{2\ddot{\mathcal{I}}(0)\log_2 \mathrm{e}}\left(\frac{\Gamma(m_s-2,\frac{m_s\mu}{\log_2 \mathrm{e}})}{\Gamma(m_s)}\right) - \frac{\log_2 \mathrm{e}}{2\ddot{\mathcal{I}}(0)}\left(\frac{\Gamma(m_s,\frac{m_s\mu}{\log_2 \mathrm{e}})}{\Gamma(m_s)}\right). \tag{3.35}$$

If the average transmit power constraint in (3.15) is satisfied with strict inequality, then μ is zero. Otherwise, μ is determined by satisfying the constraint in (3.15) with equality or equivalently by solving

$$\frac{\mu m_s^2}{\ddot{\mathcal{I}}(0)\log_2 \mathrm{e}}\left(\frac{\Gamma(m_s-2,\frac{m_s\mu}{\log_2 \mathrm{e}})}{\Gamma(m_s)}\right) - \frac{m_s}{\ddot{\mathcal{I}}(0)}\left(\frac{\Gamma(m_s-1,\frac{m_s\mu}{\log_2 \mathrm{e}})}{\Gamma(m_s)}\right) = P_{\text{avg}}. \tag{3.36}$$

It should be noted that the expressions in (3.35) and (3.36) are in terms of the incomplete gamma function, which can easily be computed via numerical tools. In order to obtain further simplified achievable rate expressions free of the Lagrange multiplier μ, we further approximate and simplify the formulations in (3.35) and (3.36) at asymptotically low power levels by using the fact that

$$\lim_{P_{\text{avg}}\to 0} \mu(P_{\text{avg}}) = \infty \tag{3.37}$$

which can be shown by following the approach below. Let us first define the function $H(x)$ for $x \in (0,\infty)$ as follows:

$$H(x) = \mathbb{E}\left[\frac{1}{z_s}\text{MMSE}^{-1}\Big(\min\Big\{1, \frac{x}{\log_2 \mathrm{e}\ z_s}\Big\}\Big)\right] \tag{3.38}$$

which is continuous, takes nonnegative values by definition, and strictly monotonically decreasing since it is the inverse of the MMSE function, which is also strictly monotonically decreasing in its argument. Hence, the function $H(x)$ is invertible by construction. The Lagrange multiplier $\mu(P_{\text{avg}})$ is a function of P_{avg} and can be found by setting $H(\mu(P_{\text{avg}})) = P_{\text{avg}}$. Taking the limits of both sides as P_{avg} goes to zero and using the above-mentioned properties

of the function $H(x)$, the relation in (3.37) is obtained.

Consequently, we perform series expansion for expressions in (3.35) and (3.36) as $\mu(P_{\text{avg}}) \to \infty$ as follows:

$$R_{\text{opt}}(P_{\text{avg}}) = \frac{2^{-m_s\mu}\mu^{m_s}}{2\ddot{\mathcal{I}}(0)\Gamma(m_s)}\left(-\frac{2m_s^{m_s-2}\log(2)^{m_s-3}}{\mu^2} + o\left(\frac{1}{\mu}\right)^3\right) \tag{3.39}$$

$$P_{\text{avg}} = \frac{2^{-m_s\mu}\mu^{m_s}}{\ddot{\mathcal{I}}(0)\Gamma(m_s)}\left(-\frac{m_s^{m_s-2}\log(2)^{m_s-3}}{\mu^3} + o\left(\frac{1}{\mu}\right)^4\right). \tag{3.40}$$

By combining the above expressions, we can rewrite $R_{\text{opt}}(P_{\text{avg}})$ in terms of P_{avg} as

$$R_{\text{opt}}(P_{\text{avg}}) = P_{\text{avg}}\mu(P_{\text{avg}}). \tag{3.41}$$

By solving the expression in (3.40), $\mu(P_{\text{avg}})$ can be found as

$$\mu(P_{\text{avg}}) = \frac{3-m_s}{m_s\log(2)}W_{-1}\left(\beta\left(\frac{1}{P_{\text{avg}}}\right)^{\frac{1}{3-m_s}}\right) \tag{3.42}$$

where $m_s > 3$, $\beta = \frac{1}{3-m_s}\left(\frac{m_s}{-\ddot{\mathcal{I}}(0)\Gamma(m_s)}\right)^{\frac{1}{3-m_s}}$, which depends on the input distribution through $\ddot{\mathcal{I}}(0)$, and $W_{-1}(.)$ represents the lower branch of the Lambert function [63]. Hence, inserting $\mu(P_{\text{avg}})$ in (3.42) into (3.41) gives

$$R_{\text{opt}}(P_{\text{avg}}) = \frac{3-m_s}{m_s\log(2)}P_{\text{avg}}W_{-1}\left(\beta\left(\frac{1}{P_{\text{avg}}}\right)^{\frac{1}{3-m_s}}\right). \tag{3.43}$$

By substituting $\ddot{\mathcal{I}}(0) = -1$ into the above rate expression, the result can readily be specialized to the Gaussian input, which is obtained in [64], where the unit of the achievable rate is chosen as nats per channel use.

3.3.4 Average transmit power and average interference power constraints

Finally, we address the case in which average constraints are imposed on the transmission and interference powers, and obtain the following result on the low-power approximation of the optimal power control strategy. Again the proof is omitted for brevity.

Theorem 3.3.3 *In the low-power regime, the optimal power control policy subject to the constraints in (3.19) and (3.20) is approximated by*

$$P^*(z_s, z_{sp}) = \left(\frac{\frac{\mu+\lambda z_{sp}}{\log_2 \mathrm{e}} - z_s}{\ddot{\mathcal{I}}(0) z_s^2} \right)^+, \tag{3.44}$$

where μ and λ are the Lagrange multipliers corresponding to the constraints given in (3.19) and (3.20), respectively.

3.4 Numerical Results

In this section, we first provide numerical results to identify the impact of transmit power and interference power constraints, input distributions, and fading severity on the achievable rates attained with optimal power control. Subsequently, we analyze the optimal power control in the low-power regime. In the optimization algorithm, unless mentioned explicitly, we set $\epsilon = 0.00001$, $\delta = 0.0001$, $t = 0.01$ in the iterations. In the numerical results, we consider Nakagami-m fading.

3.4.1 Optimal Power Control

In Fig. 3.2, we plot the instantaneous power levels as a function of the channel power gains of the transmission link z_s and of the interference link z_{sp}, respectively, for the Gaussian signal (left subfigure) and BPSK signal (right subfigure). Peak transmit power and average interference power constraints are imposed with $P_{\mathrm{pk}} = 10$ dB and $Q_{\mathrm{avg}} = 6$ dB.

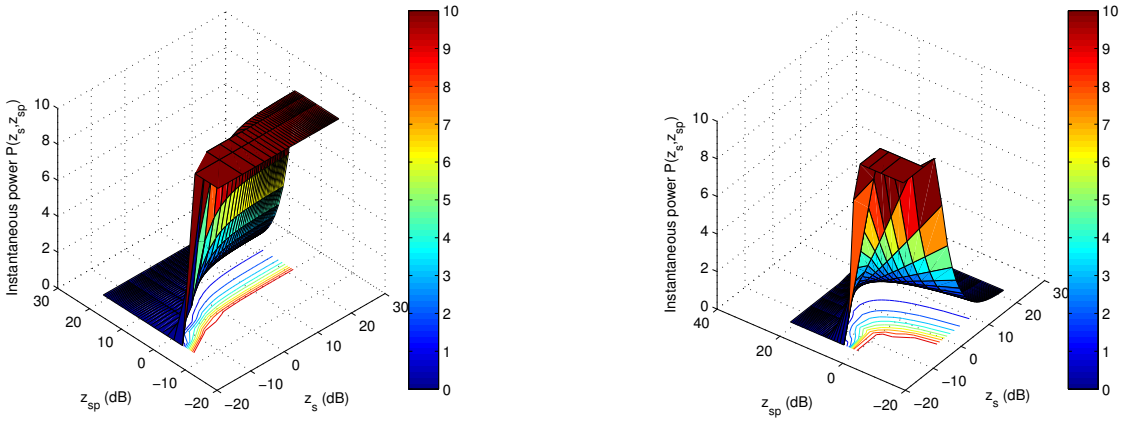

Figure 3.2: Instantaneous power level vs. channel power gains z_s and z_{sp} under peak transmit and average interference power constraints. $P_{\text{pk}} = 10$ dB and $Q_{\text{avg}} = 6$ dB. Left and right subfigures are for the Gaussian and BPSK inputs, respectively.

When the input is Gaussian, it is seen that more power is assigned to the stronger channel (i.e., higher values of z_s) opportunistically while the power level generally diminishes as the fading power of the interference link, z_{sp}, increases. In contrast to the power adaptation scheme for the Gaussian input, it is observed that instantaneous power for BPSK signal first increases and then decreases with the channel power gain of the transmission link, z_s. In other words, when the channel gain is higher than a threshold, the transmission power is lowered with increasing channel gain. This is due to the fact that increasing the power beyond a certain level is not very beneficial because BPSK mutual information is upper bounded by 2 bits/symbol and gets saturated eventually. Hence, the strategy of performing channel inversion at very high channel gains and allocating more power to the weaker channel conditions turns out to be the optimal one. Note that this strategy has implications on interference management, highlighting the importance of addressing power control for practical input distributions in cognitive radio settings.

In Fig. 3.3, we plot the maximum achievable rates in bits per channel use as a function of the peak transmit power constraint P_{pk} for Gaussian, BPSK and QPSK inputs and for different values of m_s and m_{sp} (i.e., different fading severity) in the transmission and interference links. In this figure, we consider that a peak interference constraint is also imposed

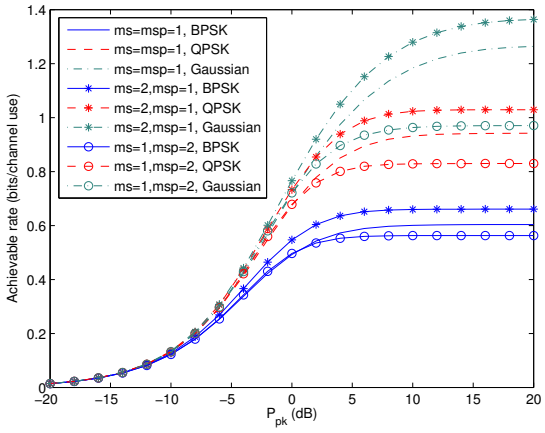

Figure 3.3: Maximum achievable rate vs. peak transmit power constraint, P_{pk}, for BPSK, QPSK, and Gaussian inputs under different fading severity. $Q_{\text{pk}} = -1$ dB.

and Q_{pk} is chosen as -1 dB. It is seen that as P_{pk} increases, maximum achievable rates initially increase and then stay constant for all inputs because the transmission power is eventually limited by the interference power constraint, Q_{pk}. It is observed that Gaussian inputs always achieve higher rates compared to QPSK and BPSK inputs in the high power regime while the performances of Gaussian, QPSK and BPSK inputs approach each other in the low power regime. Another observation is that if the transmission link experiences less severe fading or the fading in the interference link is more severe, the achievable rates become higher. We also note that as the fading in the interference link becomes more severe, the increase in the maximum achievable rate of Gaussian inputs is higher than the increase in the maximum achievable rates of QPSK and BPSK inputs.

In Fig 3.4, we again display the maximum achievable rates as a function of the peak transmit power limit, P_{pk} for Gaussian, BPSK and QPSK inputs. It is assumed that $Q_{\text{pk}} = -1$ dB. In this figure, we consider two cases regarding the availability of the channel side information (CSI). When the CSI of the interference link z_{sp} is available at the transmitter, optimal transmission power is given in (3.9). On the other hand, in the lack of the knowledge of z_{sp}, it is assumed that the interference outage constraint $\Pr(P\, z_{sp} > Q_{\text{pk}}) \leq \epsilon$ is imposed, i.e., the probability that the received power exceeds the peak interference level is limited by

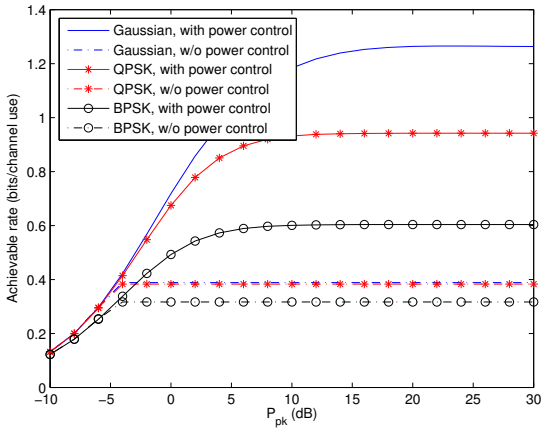

Figure 3.4: Maximum achievable rate vs. peak transmit power constraint, P_{pk}, for BPSK, QPSK, and Gaussian inputs with or without the CSI of the interference link. $Q_{\text{pk}} = -1$ dB.

ϵ. Hence, under this setting, the transmit power is given by $P = \min\left\{P_{\text{pk}}, \frac{Q_{\text{pk}}}{F^{-1}_{z_{sp}}(1-\epsilon)}\right\}$ where $F^{-1}_{z_{sp}}$ denotes the inverse cumulative distribution function (CDF) of z_{sp}. It is assumed that $\epsilon = 0.1$. It is seen that small gains are possible at low values of P_{pk} in the absence of the CSI of the interference link. This is due to allowing the violation of the peak interference level with some small probability. Note that violations are not tolerated when z_{sp} is perfectly known. The possible gains diminish if stricter outage constraints are imposed. On the other hand, when P_{pk} is relatively large, we notice that having CSI and adapting the power level benefits the secondary users. This is also beneficial to the primary users as their interference constraints are satisfied all the time. In the figure, it is also interesting to note that the throughput gains due to the availability of CSI of interference link z_{sp} is the highest for the Gaussian input, and throughput gain increases as the modulation size increases.

In Fig. 3.5, we plot the maximum achievable rates as a function of the average interference power constraint, Q_{avg} for Gaussian, 16-QAM, QPSK and BPSK inputs. In the left subfigure, peak transmit power constraint is not imposed whereas P_{pk} is set to 6 dB in the right subfigure. It is assumed that $m_s = m_{sp} = 1$. We both consider the achievable rates of non-Gaussian inputs (i.e.,16-QAM, QPSK and BPSK inputs) achieved with optimal power control assuming Gaussian input signaling and with the proposed power control considering

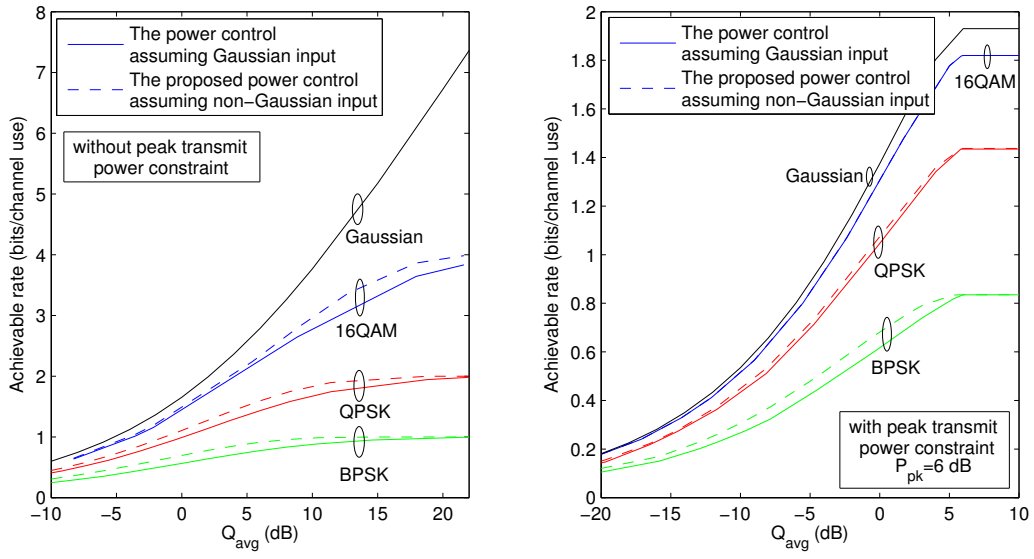

Figure 3.5: Maximum achievable rate vs. average interference power constraint, Q_{avg}, for BPSK, QPSK, 16-QAM and Gaussian inputs. While only an average interference power constraint is considered in the left subfigure, an additional peak transmit constraint with $P_{\text{pk}} = 6$ dB is imposed in the right subfigure.

the non-Gaussian signaling. When there is no peak transmit power constraint, maximum achievable rate with Gaussian input increases as Q_{avg} increases while maximum achievable rates of 16-QAM, QPSK and BPSK inputs increase first and then saturate at 4, 2 and 1 bit per channel use, respectively, due to being finite constellations. When the peak transmit power constraint is imposed, maximum achievable rates for all inputs increase initially with increasing Q_{avg} and then start saturating due to the presence of P_{pk} as seen in the right subfigure. It is also observed that the achievable rates of 16-QAM, QPSK and BPSK inputs obtained with the power control assuming Gaussian input signaling are lower than that obtained under the proposed optimal power control considering non-Gaussian signaling since the power control under the assumption of Gaussian input signaling is suboptimal for these non-Gaussian inputs. Therefore, it is concluded that if the actual signal input distribution is not taken into account, considerable performance loss occurs for systems optimized under the Gaussian input assumption.

In Fig. 3.6, we plot the maximum achievable rates as a function of the average transmit

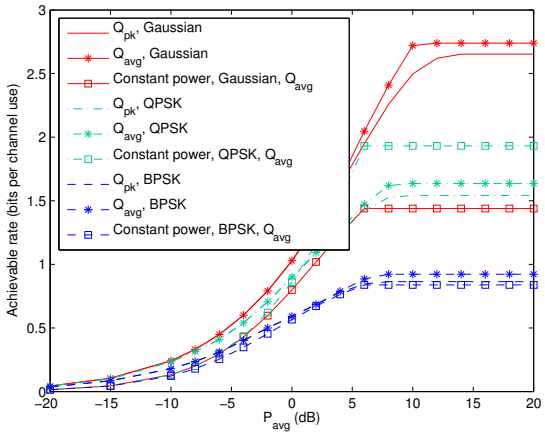

Figure 3.6: Maximum achievable rate vs. average transmit power constraint, P_{avg}, for BPSK, QPSK, and Gaussian inputs under either average or peak interference constraints, and constant power scheme.

power constraint, P_{avg} for Gaussian, QPSK and BPSK inputs under either peak interference power constraint Q_{pk} or average interference power constraint, Q_{avg}. It is assumed that $Q_{\text{pk}} = Q_{\text{avg}} = 6$ dB. In order to highlight the gains achieved with power control, we also plot the rates attained with constant power transmissions when Q_{avg} is imposed. Expectedly, higher achievable rates are observed under average interference constraints compared to that attained under peak interference constraints for all inputs since power adaptation under average interference power constraints is more flexible than that under peak interference power constraints. It is observed that the highest rate is achieved with the Gaussian input and there is substantial throughput difference between Gaussian input and BPSK, QPSK inputs. Hence if the system performance is predicted under the assumption of Gaussian input and the inputs are chosen from discrete constellations in actual applications, it is seen that there would be considerable performance loss in terms of achievable rates. It is also observed that optimal power control policy always outperforms constant power scheme for all inputs, but the highest throughput gain is achieved with Gaussian input.

3.4.2 Low-Power Analysis

Fig. 3.7 shows the maximum achievable rates vs. peak transmit power constraint, P_{pk} for Gaussian, BPSK and QPSK inputs. It is assumed that $m_s = 1, m_{sp} = 3$. In this figure, a low-power scenario is considered. As before, it is again observed that the maximum achievable rates increase with increasing P_{pk} and then become limited by peak interference power constraint, Q_{pk}. It is seen that low-power approximation in (3.27) matches well with the exact rates, confirming the accuracy of the approximation at low power levels. It is also seen that Gaussian and QPSK inputs exhibit nearly the same performance in the low power regime. Therefore, QPSK input can be efficiently used in practical systems rather than the Gaussian input which is difficult to implement.

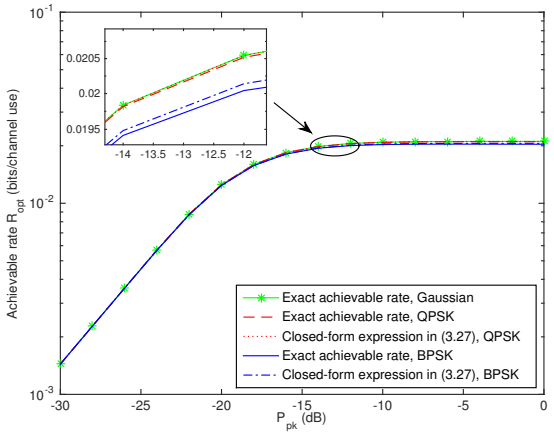

Figure 3.7: Maximum achievable rate vs. peak transmit power constraint, P_{pk}. $Q_{\text{pk}} = -20$ dB.

In Fig. 3.8, we display the maximum achievable rates vs. peak interference power constraint, Q_{pk} for Gaussian, BPSK and QPSK inputs in the low-power regime. It is again assumed that $m_s = 1, m_{sp} = 3$. The maximum achievable rates increase with increasing Q_{pk} for all inputs. The gap between the closed-form maximum achievable rate expression in (3.31) and the exact maximum achievable rate evaluated by inserting the corresponding optimal transmission power into (2.8) is relatively small in the low-power regime.

Fig. 3.9 depicts the maximum achievable rates as a function of average interference

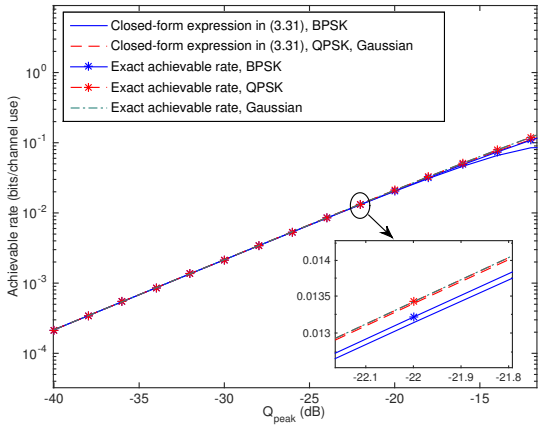

Figure 3.8: Maximum achievable rate vs. peak interference power constraint, Q_{pk}.

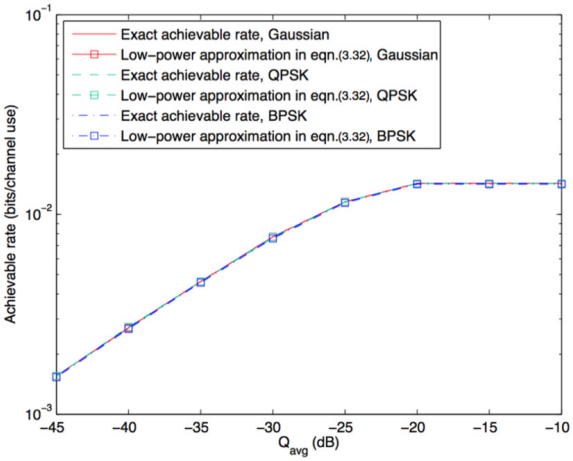

Figure 3.9: Maximum achievable rate vs. average interference power constraint, Q_{avg}. $P_{\text{pk}} = -20$ dB.

power constraint, Q_{avg} for Gaussian, BPSK and QPSK inputs. Again, a low-power scenario is addressed. We consider peak constraint on the transmit power, i.e., $P_{\text{pk}} = -20$ dB. It is assumed that $m_s = m_{sp} = 1$. As Q_{avg} increases, the maximum achievable rates increase and get saturated for all inputs due to limitations on the peak transmit power, P_{pk}. It is seen that the low-power approximation (3.32) of the optimal power control leads to similar performance in terms of the achievable rates compared with the optimal power control scheme, demonstrating the accuracy of (3.32).

In Fig. 3.10, we illustrate the maximum achievable rates vs. average transmit power

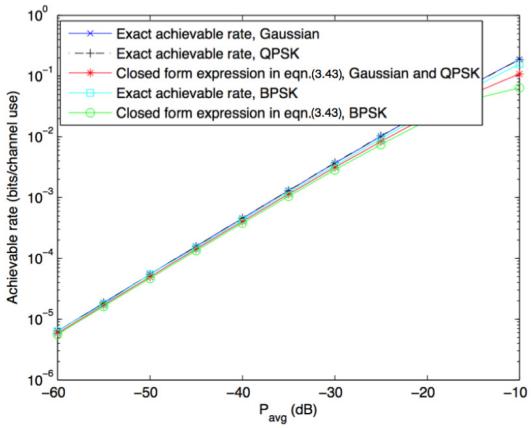

Figure 3.10: Maximum achievable rate vs. average transmit power constraint, P_{avg}.

constraint, P_{avg} for Gaussian, BPSK and QPSK inputs. We consider that $m_s = 4$, $m_{sp} = 1$. As P_{avg} increases, maximum achievable rates increase. It is seen that for low power values, the closed-form maximum achievable rate expression in (3.43) matches well with the exact maximum achievable rate achieved with the corresponding optimal transmission power in (3.33) without a constraint on the peak interference power. This is in agreement with our analysis in Section 3.3.3.

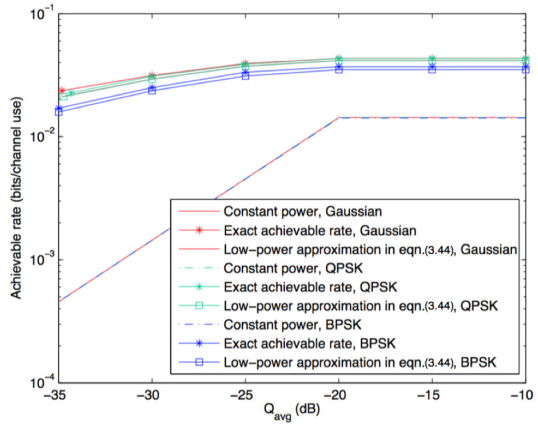

Figure 3.11: Maximum achievable rate vs. average interference power constraint, Q_{avg}. $P_{\text{avg}} = -20$ dB

In Fig. 3.11, we display the maximum achievable rates vs. average interference power constraint, Q_{avg} for Gaussian, BPSK and QPSK inputs under optimal power control and constant power schemes. We set $m_s = m_{sp}$ to 1 and $P_{\text{avg}} = -20$ dB. The maximum achievable

rates increase with increasing Q_{avg} and then capped due to the presence of P_{avg}. It is seen that substantially higher rates are achieved with optimal power control policy compared to constant power scheme. It is observed from the figure that QPSK and Gaussian inputs show nearly the same throughput gain whereas BPSK has the smallest throughput gain when the optimal power control is applied.

Chapter 4

Energy Efficiency in Cognitive Radio Systems with Channel Sensing Errors – Time-slotted Primary Users

This chapter presents energy-efficient power allocation schemes for secondary users in sensing-based spectrum sharing cognitive radio systems with time-slotted primary users. The optimal power levels are identified in the presence of different levels of CSI regarding the transmission and interference links at the secondary transmitter, namely perfect CSI of both transmission and interference links, perfect CSI of the transmission link and imperfect CSI of the interference link, imperfect CSI of both links or only statistical CSI of both links.

Section 4.1 introduces the system model and defines the energy efficiency of secondary users in the presence of imperfect sensing results. In Section 4.2, energy efficiency maximization problems subject to peak/average transmit power constraints and average interference constraint in the presence of imperfect sensing results and different levels of CSI regarding the transmission and interference links are formulated and the corresponding optimal power allocation schemes are derived. Subsequently, numerical results are presented and discussed in Section 4.3.

4.1 System Model

We consider a sensing-based spectrum sharing cognitive radio system in which a secondary transmitter-receiver pair utilizes the spectrum holes in the licensed bands of the primary users. The term "spectrum holes" denotes underutilized frequency intervals at a particular time and certain location. In order to detect the spectrum holes, secondary users initially perform channel sensing over a duration of τ symbols. It is assumed that secondary users employ frames of T symbols. Hence, data transmission is performed in the remaining duration of $T - \tau$ symbols.

The channel is considered to be block flat-fading channel in which the fading coefficients stay the same in one frame duration and vary independently from one frame to another. Secondary users are assumed to transmit under both idle and busy sensing decisions. Therefore, by considering the true nature of the primary user activity together with the channel sensing decisions, the four possible channel input-output relations betw energy efficiencyn the secondary transmitter-receiver pair can be expressed as follows:

$$y_i = \begin{cases} hx_{0,i} + n_i & \text{if } (\mathcal{H}_0, \hat{\mathcal{H}}_0) \\ hx_{1,i} + n_i & \text{if } (\mathcal{H}_0, \hat{\mathcal{H}}_1) \\ hx_{0,i} + n_i + s_i & \text{if } (\mathcal{H}_1, \hat{\mathcal{H}}_0) \\ hx_{1,i} + n_i + s_i & \text{if } (\mathcal{H}_1, \hat{\mathcal{H}}_1), \end{cases} \tag{4.1}$$

where $i = 1, \ldots, T - \tau$. Above, x and y are the transmitted and received signals, respectively and h is the channel fading coefficient of the transmission link between the secondary transmitter and the secondary receiver, which is assumed to be Gaussian distributed with mean zero and variance σ_h^2. In addition, n_i and s_i denote the additive noise and the primary users' received faded signal. Both $\{n_i\}$ and $\{s_i\}$ are assumed to be independent and identically distributed circularly-symmetric, zero-mean Gaussian sequences with variances N_0 and σ_s^2, respectively. Moreover, the subscripts 0 and 1 in the transmitted signal indicate the

transmission power levels of the secondary users. More specifically, the average power level is $P_0(g,h)$ if the channel is detected to be idle while it is $P_1(g,h)$ if the channel is detected to be busy. Also, g denotes the channel fading coefficient of the interference link between the secondary transmitter and the primary receiver. System model is depicted in Fig. 4.1.

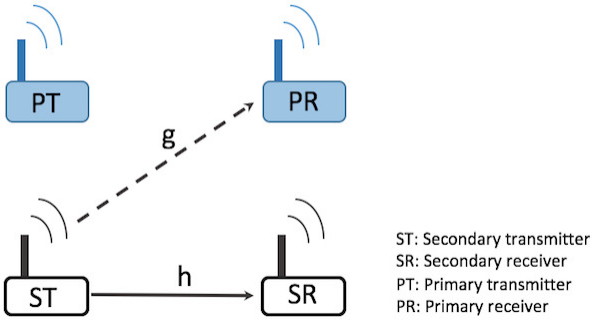

Figure 4.1: System model.

Based on the input-output relation in (4.1), the additive disturbance is given by

$$w_i = \begin{cases} n_i & \text{if } \mathcal{H}_0 \text{ is true} \\ n_i + s_i & \text{if } \mathcal{H}_1 \text{ is true} \end{cases}. \tag{4.2}$$

The achievable rate of secondary users is given by

$$\begin{aligned} R_G &= \frac{T-\tau}{T}\Pr(\hat{\mathcal{H}}_0)\big[h(y|h,\hat{\mathcal{H}}_0) - h(y|x_0,h,\hat{\mathcal{H}}_0)\big] + \frac{T-\tau}{T}\Pr(\hat{\mathcal{H}}_1)(h(y|h,\hat{\mathcal{H}}_1) - h(y|x_1,h,\hat{\mathcal{H}}_1)), \\ &= \frac{T-\tau}{T}\Pr(\hat{\mathcal{H}}_0)\big[h(y|h,\hat{\mathcal{H}}_0) - h(w|h,\hat{\mathcal{H}}_0)\big] + \frac{T-\tau}{T}\Pr(\hat{\mathcal{H}}_1)\big[h(y|h,\hat{\mathcal{H}}_1) - h(w|h,\hat{\mathcal{H}}_1)\big], \end{aligned}$$

where $h(.)$ denotes the differential entropy. Due to imperfect sensing results, the additive disturbance, w follows Gaussian mixture distribution and the differential entropy of Gaussian mixture density does not admit closed-form expression. However, a closed-form lower bound on the achievable rate expression of secondary users can be obtained in the following result.

Proposition 4.1.1 *The lower bound on the achievable rate of secondary users in the pres-*

ence of imperfect sensing decisions is given by

$$R_a = \mathbb{E}_{g,h}\big\{R\big(P_0(g,h), P_1(g,h)\big)\big\} = \frac{T-\tau}{T}\sum_{k=0}^{1}\Pr(\hat{\mathcal{H}}_k)\mathbb{E}_{g,h}\left\{\log\left(1+\frac{P_k(g,h)|h|^2}{N_0+\Pr(\mathcal{H}_1|\hat{\mathcal{H}}_k)\sigma_s^2}\right)\right\}, \tag{4.3}$$

where $k \in \{0,1\}$ *and* $\mathbb{E}\{.\}$ *denotes expectation operation. Also,* $\Pr\{\hat{\mathcal{H}}_1\}$ *and* $\Pr\{\hat{\mathcal{H}}_0\}$ *denote the probabilities of channel being detected as busy and idle, respectively, and can be expressed as*

$$\Pr\{\hat{\mathcal{H}}_1\} = \Pr\{\mathcal{H}_0\}\mathscr{P}_{\rm f} + \Pr\{\mathcal{H}_1\}\mathscr{P}_{\rm d}, \tag{4.4}$$

$$\Pr\{\hat{\mathcal{H}}_0\} = \Pr\{\mathcal{H}_0\}(1-\mathscr{P}_{\rm f}) + \Pr\{\mathcal{H}_1\}(1-\mathscr{P}_{\rm d}). \tag{4.5}$$

Proof: See Appendix E.

Theorem 4.1.1 *The difference between* $(R_G - R_a)$ *is upper bounded by*

$$\begin{aligned} R_G - R_a \leq \Big(\frac{T-\tau}{T}\Big)\Bigg[\mathbb{E}_{g,h}\Bigg\{\sum_{k=1}^{2}\log\left(\frac{\sum_{i=1}^{2}\frac{\Pr(\mathcal{H}_i|\hat{\mathcal{H}}_k)}{c_i}}{\left(1+\frac{P_k(g,h)|h|^2}{N_0+\Pr(H_1|\hat{\mathcal{H}}_k)\sigma_s^2}\right)\sum_{i=1}^{2}\frac{\Pr(\mathcal{H}_i|\hat{\mathcal{H}}_k)}{c_i+|h|^2P_k(g,h)}}\right)\Bigg\} \\ -\sum_{k=1}^{2}\Pr(\hat{\mathcal{H}}_k)\left(\frac{N_0+\Pr(H_1|\hat{\mathcal{H}}_k)\sigma_s^2}{N_0+\sigma_s^2}\right)+\sum_{k=1}^{2}\Pr(\hat{\mathcal{H}}_k)\mathbb{E}_{g,h}\left\{1+\frac{\Pr(\mathcal{H}_i|\hat{\mathcal{H}}_k)\sigma_s^2}{N_0+|h|^2P_k(g,h)}\right\}\Bigg] \end{aligned} \tag{4.6}$$

where $c_1 = N_0 + \sigma_s^2$ *and* $c_2 = N_0$.

Proof: See Appendix F.

In Fig. 4.2, we plot the difference between $(R_G - R_a)$ as a function of noise variance, N_0. We assume that $\mathscr{P}_{\rm d} = 0.8, \mathscr{P}_{\rm f} = 0.1$ and $\sigma_s^2 = 1$. It is seen that as noise variance, N_0, increases, the difference approaches zero, hence the lower bound on the achievable rate expression becomes tighter.

With the characterization of the achievable rate in (4.3), we now define the energy effi-

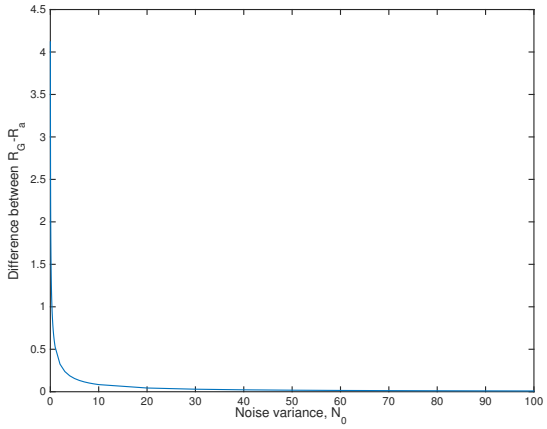

Figure 4.2: Achievable energy efficiency η_{EE} vs. achievable rate R_a.

ciency as the ratio of the achievable rate to the total power consumption in the following:

$$\eta_{\text{EE}} = \frac{\mathbb{E}_{g,h}\big\{R\big(P_0(g,h), P_1(g,h)\big)\big\}}{\mathbb{E}_{g,h}\{\Pr\{\hat{\mathcal{H}}_0\}P_0(g,h) + \Pr\{\hat{\mathcal{H}}_1\}P_1(g,h)\} + P_{\text{c}}}. \tag{4.7}$$

Above, the total power consists of average transmission power and circuit power, denoted by P_{c}. In practical systems, the circuit power accounts for a part of the total power consumption. Accurate circuit power consumption formulation of the transceiver was given in [65], [66], where the circuit power includes power consumption of signal processing and active circuit blocks such as mixers, frequency synthesizers, active filters and digital-to-analog converter. This portion of power consumption excludes that of the power amplifier and is independent of the transmission rate. Practical cognitive radio transceivers are built on similar circuit blocks [67]. Considering these facts, we assume that the transmit power is used for reliable data transmission while circuit power represents the average power consumed by the electronic circuits, and is independent of the transmission state.

The achievable energy efficiency expression in (4.7) can serve as a lower bound since the lower bound on achievable rate R_a in (4.3) is employed. The usefulness of this energy efficiency expression is due to its being an explicit function of sensing performance.

In Fig. 4.3, we plot the energy efficiency expression in (4.7) (indicated as the lower bound)

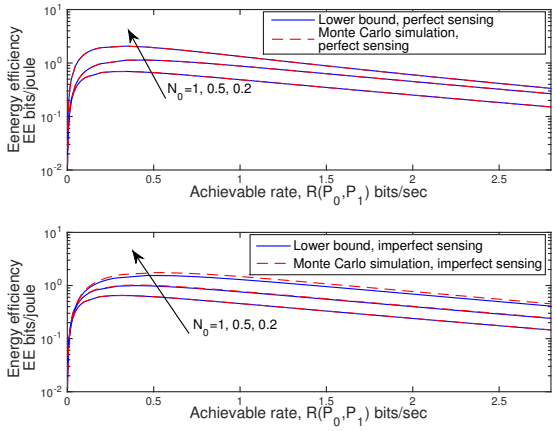

Figure 4.3: Achievable energy efficiency η_{EE} vs. achievable rate R_a.

and the exact energy efficiency, in which we use Gaussian input and consider Gaussian mixture noise in the mutual information, as a function of achievable rate for both perfect sensing (i.e., $\mathscr{P}_{\mathrm{d}} = 1$ and $\mathscr{P}_{\mathrm{f}} = 0$) and imperfect sensing (i.e., $\mathscr{P}_{\mathrm{d}} = 0.8$ and $\mathscr{P}_{\mathrm{f}} = 0.2$). The graph is displayed in logarithmic scale to highlight the difference between the exact energy efficiency and the lower bound on energy efficiency. In order to evaluate the exact energy efficiency achieved with Gaussian input, we performed Monte Carlo simulations with 2×10^6 samples. In the case of perfect sensing, the lower bound and simulation result perfectly match as expected since in this case additive disturbance has Gaussian distribution rather than a Gaussian mixture. In the case of imperfect sensing, it is seen that the gap between the lower bound and exact energy efficiency decreases as N_0 increases, which matches with Theorem 4.1.1. Additionally, since circuit power is taken into consideration with value $P_c = 0.1$, energy efficiency vs. achievable rate curve is bell-shaped and is also quasiconcave [68]. It is observed that maximum energy efficiency is achieved at nearly the same achievable rate for both lower bound and exact energy efficiency expressions.

In the following section, we derive power allocation schemes that maximize the energy efficiency of the secondary users in the presence of sensing errors, different combinations of transmit power and average interference power constraints, and different levels of CSI regarding the transmission and interference links.

4.2 Optimal Power Allocation

4.2.1 Average Transmit Power Constraint and Average Interference Power Constraint

Now, we obtain the optimal power allocation strategies to maximize the energy efficiency of secondary users under average transmit power and average interference power constraints in the presence of different levels of CSI regarding the transmission and interference links, namely perfect CSI of both transmission and interference links, perfect CSI of the transmission link and imperfect CSI of the interference link, imperfect CSI of both links, or statistical CSI of both links.

4.2.1.1 Perfect CSI of both transmission and interference links

In this case, it is assumed that CSI of both transmission and interference links is perfectly known by the secondary transmitter. In this setting, the maximum energy efficiency under both average transmit power and interference power constraints can be found by solving the following optimization problem:

$$\max_{\substack{P_0(g,h)\\P_1(g,h)}} \eta_{\mathrm{EE}} = \frac{\mathbb{E}_{g,h}\big\{R\big(P_0(g,h),P_1(g,h)\big)\big\}}{\mathbb{E}_{g,h}\{\Pr\{\hat{\mathcal{H}}_0\}P_0(g,h)+\Pr\{\hat{\mathcal{H}}_1\}P_1(g,h)\}+P_{\mathrm{c}}} \tag{4.8}$$

$$\text{subject to} \quad \mathbb{E}_{g,h}\{\Pr\{\hat{\mathcal{H}}_0\}\,P_0(g,h)+\Pr\{\hat{\mathcal{H}}_1\}\,P_1(g,h)\} \le P_{\mathrm{avg}} \tag{4.9}$$

$$\mathbb{E}_{g,h}\{\big[(1-\mathscr{P}_{\mathrm{d}})\,P_0(g,h)+\mathscr{P}_{\mathrm{d}}\,P_1(g,h)\big]|g|^2\} \le Q_{\mathrm{avg}} \tag{4.10}$$

$$P_0(g,h)\ge 0, P_1(g,h)\ge 0, \tag{4.11}$$

where P_{avg} denotes the maximum average transmission power of the secondary transmitter and Q_{avg} represents the maximum allowed average interference power at the primary receiver. In particular, average transmit power constraint in (4.9) is chosen to satisfy the long-term power budget of the secondary users and average interference power constraint in (4.10) is

imposed to limit the interference, and hence to protect the primary user transmission. In this setting, the optimal power allocation strategy that maximizes the energy efficiency of secondary users is determined in the following result.

Theorem 4.2.1 *The optimal power allocation under the constraints in (4.9) and (4.10) is given by*

$$P_0^*(g,h) = \left[\frac{\frac{T-\tau}{T}\Pr\{\hat{\mathcal{H}}_0\}\log_2 e}{(\lambda_1+\alpha)\Pr\{\hat{\mathcal{H}}_0\}+\nu_1|g|^2(1-\mathscr{P}_{\rm d})} - \frac{N_0+\Pr(\mathcal{H}_1|\hat{\mathcal{H}}_0)\sigma_s^2}{|h|^2}\right]^+ \tag{4.12}$$

$$P_1^*(g,h) = \left[\frac{\frac{T-\tau}{T}\Pr\{\hat{\mathcal{H}}_1\}\log_2 e}{(\lambda_1+\alpha)\Pr\{\hat{\mathcal{H}}_1\}+\nu_1|g|^2\mathscr{P}_{\rm d}} - \frac{N_0+\Pr(\mathcal{H}_1|\hat{\mathcal{H}}_1)\sigma_s^2}{|h|^2}\right]^+, \tag{4.13}$$

where $[x]^+$ *denotes* $\max(x,0)$*,* α *is a nonnegative parameter, and* λ_1 *and* ν_1 *are nonnegative Lagrange multipliers.*

Proof: See Appendix G.

Above, the Lagrange multipliers λ_1 and ν_1 can be jointly obtained by inserting the optimal power allocation schemes (4.12) and (4.13) into the constraints (4.9) and (4.10). However, solving these constraints does not give closed-form expressions for λ_1 and ν_1. Therefore, we employ the subgradient method, i.e., λ_1 and ν_1 are updated iteratively according to the subgradient direction until convergence as follows:

$$\lambda_1^{(n+1)} = \Big[\lambda_1^{(n)} - t\big(P_{\rm avg} - \mathbb{E}_{g,h}\{\Pr\{\hat{\mathcal{H}}_0\}\,P_0^{(n)}(g,h) + \Pr\{\hat{\mathcal{H}}_1\}\,P_1^{(n)}(g,h)\}\big)\Big]^+ \tag{4.14}$$

$$\nu_1^{(n+1)} = \Big[\nu_1^{(n)} - t\big(Q_{\rm avg} - \mathbb{E}_{g,h}\{\big[(1-\mathscr{P}_{\rm d})\,P_0^{(n)}(g,h) + \mathscr{P}_{\rm d}\,P_1^{(n)}(g,h)\big]|g|^2\}\big)\Big]^+, \tag{4.15}$$

where n and t denote the iteration index and the step size, respectively. When the step size is chosen to be constant, it was shown that the subgradient method is guaranteed to converge to the optimal value within a small range [60].

For a given value of α, the optimal power levels in (4.12), (4.13) can be found until $F(\alpha) \leq \epsilon$ is satisfied. Dinkelbach's method converges to the optimal solution at a superlinear

convergence rate. The detailed proof of convergence can be found in [69]. In the case of $F(\alpha) = 0$ in (G.5), the solution is optimal otherwise ϵ-optimal solution is obtained. In the following table, Dinkelbach method-based iterative power allocation algorithm for energy efficiency maximization under imperfect sensing is summarized.

Algorithm 4 Dinkelbach method-based power allocation that maximizes energy efficiency of cognitive radio systems under both average transmit power and interference constraints

Initialization: $\mathscr{P}_{\rm d} = \mathscr{P}_{\rm d,init}$, $\mathscr{P}_{\rm f} = \mathscr{P}_{\rm f,init}$, $\epsilon > 0$, $\delta > 0$, $t > 0$, $\alpha^{(0)} = \alpha_{\rm init}$, $\lambda_1^{(0)} = \lambda_{1,\rm init}$, $\nu_1^{(0)} = \nu_{1,\rm init}$
$n \leftarrow 0$
repeat
  calculate $P_0^*(g,h)$ and $P_1^*(g,h)$ using (4.12) and (4.13), respectively;
  update λ_1 and ν_1 using subgradient method as follows:
  $k \leftarrow 0$
  repeat
    $\lambda_1^{(k+1)} = \Big[\lambda_1^{(k)} - t\big(P_{\rm avg} - \mathbb{E}_{g,h}\{\Pr\{\hat{\mathcal{H}}_0\}P_0^{(k)}(g,h) + \Pr\{\hat{\mathcal{H}}_1\}\, P_1^{(k)}(g,h)\}\big)\Big]^+$
    $\nu_1^{(k+1)} = \Big[\nu_1^{(k)} - t\big(Q_{\rm avg} - \mathbb{E}_{g,h}\{[(1-\mathscr{P}_{\rm d})\, P_0^{(k)}(g,h) + \mathscr{P}_{\rm d}P_1^{(k)}(g,h)]|g|^2\}\big)\Big]^+$
    $k \leftarrow k+1$
  until $|\nu_1^{(k)}\big(Q_{\rm avg} - \mathbb{E}_{g,h}\{[(1-\mathscr{P}_{\rm d})\, P_0^{(k)}(g,h) + \mathscr{P}_{\rm d}P_1^{(k)}(g,h)]|g|^2\}\big)| \leq \delta$ and $|\lambda_1^{(k)}\big(P_{\rm avg} - \mathbb{E}\{\Pr\{\hat{\mathcal{H}}_0\}\, P_0^{(k)}(g,h) + \Pr\{\hat{\mathcal{H}}_1\}\, P_1^{(k)}(g,h)\}\big)| \leq \delta$
  $\alpha^{(n+1)} = \frac{\mathbb{E}_{g,h}\left\{R\left(P_0^*(g,h),P_1^*(g,h)\right)\right\}}{\mathbb{E}_{g,h}\{\Pr\{\hat{\mathcal{H}}_0\}P_0^*(g,h)+\Pr\{\hat{\mathcal{H}}_1\}P_1^*(g,h)\}+P_{\rm c}}$
  $n \leftarrow n+1$
until $|F(\alpha^{(n)})| \leq \epsilon$

Note that in the case of $\alpha = 0$, energy efficiency maximization problem is equivalent to spectral efficiency maximization. Therefore, setting $\alpha = 0$ in (4.12) and (4.13) provides the optimal power allocation strategies that maximize the average achievable rate of secondary users. In addition, if the circuit power in the total power consumption model is assumed to be rate-dependent rather than constant, the optimization problem is shown to be quasiconcave [70]. Hence, similar technique as in the proof of Theorem 4.2.1 can be used to derive the optimal power control strategy in the case of rate-dependent circuit power.

Remark 4.2.1 *The power allocation schemes in (4.12) and (4.13) have the structure of water-filling policy with respect to channel power gain $|h|^2$ between the secondary transmitter*

and secondary receiver, but average transmit and average interference power constraints are not necessarily satisfied with equality in constrast to to the case of throughput maximization. In addition, the water level in this policy depends on the interference channel power gain $|g|^2$ *between the secondary transmitter and the primary receiver, i.e., less power is allocated when the interference link has a higher channel gain.*

Remark 4.2.2 *The proposed power allocation schemes in (4.12) and (4.13) depend on the sensing performance through detection and false alarm probabilities,* $\mathscr{P}_{\mathrm{d}}$ *and* $\mathscr{P}_{\mathrm{f}}$*, respectively. When both perfect sensing, i.e.,* $\mathscr{P}_{\mathrm{d}} = 1$ *and* $\mathscr{P}_{\mathrm{f}} = 0$*, and spectral efficiency maximization are considered, i.e.,* α *is set to* 0*, the power allocation schemes become similar to that given in [18]. However, in our analysis the secondary users have two power allocation schemes depending on the presence or absence of active primary users.*

4.2.1.2 Perfect CSI of transmission link and imperfect CSI of interference link

In practice, it may be difficult to obtain perfect CSI of the interference link due to the lack of cooperation between secondary and primary users. In this case, the channel fading coefficient of the interference link can be expressed as

$$g = \hat{g} + \tilde{g}, \tag{4.16}$$

where $\hat{g}$ denotes the estimate of the channel fading coefficient and $\tilde{g}$ represents the corresponding estimate error. It is assumed that $\hat{g}$ and $\tilde{g}$ follow independent, circularly symmetric complex Gaussian distributions with mean zero and variances $1 - \sigma_g^2$ and σ_g^2, respectively, i.e., $\hat{g} \sim \mathcal{N}(0, 1 - \sigma_g^2)$ and $\tilde{g} \sim \mathcal{N}(0, \sigma_g^2)$. Under this assumption, the average interference

constraint can be written as

$$\begin{aligned} Q_{\text{avg}} &\geq \mathbb{E}_{g,\hat{g},h}\{\big[(1-\mathscr{P}_{\text{d}})P_0(\hat{g},h)+\mathscr{P}_{\text{d}}P_1(\hat{g},h)\big]|g|^2\} \\ &= \mathbb{E}_{\hat{g},h}\{\big[(1-\mathscr{P}_{\text{d}})P_0(\hat{g},h)+\mathscr{P}_{\text{d}}P_1(\hat{g},h)\big](|\hat{g}|^2+|\tilde{g}|^2)\} \\ &= \mathbb{E}_{\hat{g},h}\{\big[(1-\mathscr{P}_{\text{d}})P_0(\hat{g},h)+\mathscr{P}_{\text{d}}P_1(\hat{g},h)\big](|\hat{g}|^2+\sigma_g^2)\}, \end{aligned} \tag{4.17}$$

where the power levels P_0 and P_1 are now expressed as functions of the estimate $\hat{g}$. Now, the optimal power allocation problem under the assumptions of perfect instantaneous CSI of the transmission link and imperfect instantaneous CSI of the interfence link can be formulated as follows:

$$\max_{\substack{P_0(\hat{g},h)\\P_1(\hat{g},h)}} \eta_{\text{EE}} = \frac{\mathbb{E}_{\hat{g},h}\big\{R\big(P_0(\hat{g},h),P_1(\hat{g},h)\big)\big\}}{\mathbb{E}_{\hat{g},h}\{\Pr\{\hat{\mathcal{H}}_0\}P_0(\hat{g},h)+\Pr\{\hat{\mathcal{H}}_1\}P_1(\hat{g},h)\}+P_{\text{c}}} \tag{4.18}$$

$$\text{subject to } \mathbb{E}_{\hat{g},h}\{\Pr\{\hat{\mathcal{H}}_0\}\,P_0(\hat{g},h)+\Pr\{\hat{\mathcal{H}}_1\}\,P_1(\hat{g},h)\} \leq P_{\text{avg}} \tag{4.19}$$

$$\mathbb{E}_{\hat{g},h}\{\big[(1-\mathscr{P}_{\text{d}})\,P_0(\hat{g},h)+\mathscr{P}_{\text{d}}\,P_1(\hat{g},h)\big](|\hat{g}|^2+\sigma_g^2)\} \leq Q_{\text{avg}} \tag{4.20}$$

$$P_0(\hat{g},h)\geq 0, P_1(\hat{g},h)\geq 0 \tag{4.21}$$

In the following result, we determine the optimal power allocation strategy in closed-form for this case.

Theorem 4.2.2 *The optimal power allocation subject to the constraints in (4.19) and (4.20) is obtained as*

$$P_0^*(\hat{g},h) = \left[\frac{\frac{T-\tau}{T}\Pr\{\hat{\mathcal{H}}_0\}\log_2 e}{(\lambda_2+\alpha)\Pr\{\hat{\mathcal{H}}_0\}+\nu_2(1-\mathscr{P}_{\text{d}})(|\hat{g}|^2+\sigma_g^2)}-\frac{N_0+\Pr(\mathcal{H}_1|\hat{\mathcal{H}}_0)\sigma_s^2}{|h|^2}\right]^+ \tag{4.22}$$

$$P_1^*(\hat{g},h) = \left[\frac{\frac{T-\tau}{T}\Pr\{\hat{\mathcal{H}}_1\}\log_2 e}{(\lambda_2+\alpha)\Pr\{\hat{\mathcal{H}}_1\}+\nu_2\mathscr{P}_{\text{d}}(|\hat{g}|^2+\sigma_g^2)}-\frac{N_0+\Pr(\mathcal{H}_1|\hat{\mathcal{H}}_1)\sigma_s^2}{|h|^2}\right]^+, \tag{4.23}$$

where λ_2 and ν_2 are nonnegative Lagrange multipliers associated with the average transmit power in (4.19) and average interference power constraints in (4.20), respectively.

Proof: We mainly follow the same steps as in the proof of Theorem 4.2.1, but with several modifications due to imperfect knowledge of the interference link. More specifically, the KKT conditions now become

$$\frac{\frac{T-\tau}{T}\Pr\{\hat{\mathcal{H}}_0\}|h|^2\log_2 e}{N_0+\Pr(\mathcal{H}_1|\hat{\mathcal{H}}_0)\sigma_s^2+P_0^*(\hat{g},h)|h|^2}-(\lambda_2+\alpha)\Pr\{\hat{\mathcal{H}}_0\}-\nu_2(|\hat{g}|^2+\sigma_g^2)(1-\mathscr{P}_{\rm d})=0 \quad (4.24)$$

$$\frac{\frac{T-\tau}{T}\Pr\{\hat{\mathcal{H}}_1\}|h|^2\log_2 e}{N_0+\Pr(\mathcal{H}_1|\hat{\mathcal{H}}_1)\sigma_s^2+P_1^*(g,h)|h|^2}-(\lambda_2+\alpha)\Pr\{\hat{\mathcal{H}}_1\}-\nu_2(|\hat{g}|^2+\sigma_g^2)\mathscr{P}_{\rm d}=0 \quad (4.25)$$

$$\lambda_2(\mathbb{E}_{\hat{g},h}\{\Pr\{\hat{\mathcal{H}}_0\}\,P_0^*(\hat{g},h)+\Pr\{\hat{\mathcal{H}}_1\}\,P_1^*(\hat{g},h)\}-P_{\rm avg})=0 \quad (4.26)$$

$$\nu_2(\mathbb{E}_{\hat{g},h}\{\big[(1-\mathscr{P}_{\rm d})\,P_0^*(\hat{g},h)+\mathscr{P}_{\rm d}\,P_1^*(\hat{g},h)\big](|\hat{g}|^2+\sigma_g^2)\}-Q_{\rm avg})=0 \quad (4.27)$$

$$\lambda_2\geq 0,\nu_2\geq 0. \quad (4.28)$$

Solving for $P_0^*(\hat{g},h)$ in (4.24) and $P_1^*(\hat{g},h)$ in (4.25) lead to the optimal power values in (4.22) and (4.23), respectively. □

Remark 4.2.3 *We note that the optimal power levels in (4.22) and (4.23) now depend on the channel estimation error of the interference link, σ_g^2. More specifically, the water level is also determined by σ_g^2, i.e., inaccurate estimation with higher channel estimation error results in lower water levels, hence lower transmission powers.*

Remark 4.2.4 *We can readily obtain the power allocation schemes under perfect sensing by setting $\mathscr{P}_{\rm d}=1$ and $\mathscr{P}_{\rm f}=0$ in (4.22) and (4.23). In addition, the proposed power schemes capture the power levels under perfect CSI of the interference link as a special case when $\sigma_g^2=0$.*

4.2.1.3 Imperfect CSI of both transmission and interference links

In this case, we assume that in addition to the imperfect knowledge of the interference link, the secondary transmitter has imperfect CSI of the transmission link. The channel fading

coefficient of the transmission link is written as

$$h = \hat{h} + \tilde{h}. \tag{4.29}$$

Above, $\hat{h}$ is the estimate of the channel fading coefficient of the transmission link and $\tilde{h}$ is the corresponding estimation error. It is assumed that $\hat{h}$ and $\tilde{h}$ are independent, circularly symmetric complex Gaussian distributed with zero mean and variances $1-\sigma_h^2$ and σ_h^2, respectively, i.e., $\hat{h} \sim \mathcal{N}(0, 1-\sigma_h^2)$ and $\tilde{h} \sim \mathcal{N}(0, \sigma_h^2)$. In this case, by taking into account imperfect CSI of both links, the achievable rate of secondary users is given by

$$\begin{aligned} R_a &= \mathbb{E}_{\hat{g},\hat{h},h}\big\{R\big(P_0(\hat{g},\hat{h}), P_1(\hat{g},\hat{h})\big)\big\} \\ &= \frac{T-\tau}{T}\sum_{k=0}^{1}\Pr(\hat{\mathcal{H}}_k)\int_{\hat{g}}\left(\int_{\hat{h}}\left(\int_{|h|^2}\log\left(1+\frac{P_k(\eta,\zeta)\gamma}{N_0+\Pr(\mathcal{H}_1|\hat{\mathcal{H}}_k)\sigma_s^2}\right)f_{|h|^2|\hat{h}}(\gamma \mid \hat{h})d\gamma\right)f_{\hat{h}}(\zeta)d\zeta\right)f_{\hat{g}}(\eta)d\eta, \end{aligned} \tag{4.30}$$

where $f_{|h|^2|\hat{h}}(\gamma \mid \hat{h})$ denotes the probability density function (pdf) of $|h|^2$ conditioned on $\hat{h}$, and in the case of Rayleigh fading, the corresponding pdf is given by

$$f_{|h|^2|\hat{h}}(\gamma \mid \hat{h}) = \frac{1}{\alpha_h^2}\mathrm{e}^{-\frac{\gamma+|\hat{h}|^2}{\alpha_h^2}} I_0\left(\frac{2}{\alpha_h^2}\sqrt{|\hat{h}|^2\gamma}\right), \tag{4.31}$$

where $I_0(.)$ represents the modified Bessel function of the first kind [62]. Consequently, the optimal power allocation problem can be expressed as

$$\max_{\substack{P_0(\hat{g},\hat{h})\\P_1(\hat{g},\hat{h})}} \eta_{\mathrm{EE}} = \frac{\mathbb{E}_{\hat{g},\hat{h},h}\big\{R\big(P_0(\hat{g},\hat{h}), P_1(\hat{g},\hat{h})\big)\big\}}{\mathbb{E}_{\hat{g},\hat{h},h}\{\Pr\{\hat{\mathcal{H}}_0\}P_0(\hat{g},\hat{h})+\Pr\{\hat{\mathcal{H}}_1\}P_1(\hat{g},\hat{h})\}+P_{\mathrm{c}}} \tag{4.32}$$

$$\text{subject to } \mathbb{E}_{\hat{g},\hat{h},h}\{\Pr\{\hat{\mathcal{H}}_0\}\,P_0(\hat{g},\hat{h}) + \Pr\{\hat{\mathcal{H}}_1\}\,P_1(\hat{g},\hat{h})\} \le P_{\mathrm{avg}} \tag{4.33}$$

$$\mathbb{E}_{\hat{g},\hat{h},h}\{\big[(1-\mathscr{P}_{\mathrm{d}})\,P_0(\hat{g},\hat{h}) + \mathscr{P}_{\mathrm{d}}\,P_1(\hat{g},\hat{h})\big](|\hat{g}|^2+\sigma_g^2)\} \le Q_{\mathrm{avg}} \tag{4.34}$$

$$P_0(\hat{g},\hat{h}) \ge 0, P_1(\hat{g},\hat{h}) \ge 0 \tag{4.35}$$

We obtain the following result for the optimal power allocation scheme.

Theorem 4.2.3 *The optimal power allocation subject to the constraints in (4.33) and (4.34) is obtained as*

$$P_0^*(\hat{g},\hat{h}) = \bar{P}_0(\hat{g},\hat{h}) \tag{4.36}$$

$$P_1^*(\hat{g},\hat{h}) = \bar{P}_1(\hat{g},\hat{h}), \tag{4.37}$$

where $\bar{P}_0(\hat{g},\hat{h})$ *and* $\bar{P}_1(\hat{g},\hat{h})$ *are the solutions to the following equations, respectively*

$$\int_0^\infty \frac{\left(\frac{T-\tau}{T}\right)\Pr\{\hat{\mathcal{H}}_0\}\log_2 e\gamma}{N_0+\Pr\{\hat{\mathcal{H}}_0\}\sigma_s^2+\bar{P}_0(\hat{g},\hat{h})\gamma} f_{|h|^2|\hat{h}}(\gamma,\hat{h})d\gamma = (\lambda_3+\alpha)\Pr\{\hat{\mathcal{H}}_0\} + \nu_3(1-\mathscr{P}_{\rm d})(|\hat{g}|^2+\sigma_g^2) \tag{4.38}$$

$$\int_0^\infty \frac{\left(\frac{T-\tau}{T}\right)\Pr\{\hat{\mathcal{H}}_1\}\log_2 e\gamma}{N_0+\Pr\{\hat{\mathcal{H}}_1\}\sigma_s^2+\bar{P}_1(\hat{g},\hat{h})\gamma} f_{|h|^2|\hat{h}}(\gamma,\hat{h})d\gamma = (\lambda_3+\alpha)\Pr\{\hat{\mathcal{H}}_1\} + \nu_3\mathscr{P}_{\rm d}(|\hat{g}|^2+\sigma_g^2). \tag{4.39}$$

If there are no positive solutions for (4.38) and (4.39) given the values of $\hat{g}$ *and* $\hat{h}$*, the instantaneous power levels are set to zero, i.e.,* $P_0^*(\hat{g},\hat{h})=0$ *and* $P_1^*(\hat{g},\hat{h})=0$*.*

Proof: Similar to the proof of Theorem 4.2.1, we first express the optimization problem in a subtractive form, which is a concave function of transmission power levels, and then define the Lagrangian as

$$\begin{aligned} L(P_0,P_1,\lambda_3,\nu_3,\alpha) = {} & \mathbb{E}_{\hat{g},\hat{h},h}\big\{R\big(P_0(\hat{g},\hat{h}),P_1(\hat{g},\hat{h})\big)\big\} - \alpha(\mathbb{E}_{\hat{g},\hat{h},h}\{\Pr\{\hat{\mathcal{H}}_0\}P_0(\hat{g},\hat{h})+\Pr\{\hat{\mathcal{H}}_1\}P_1(\hat{g},\hat{h})\}+P_{\rm c}) \\ & - \lambda_3(\mathbb{E}_{\hat{g},\hat{h},h}\{\Pr\{\hat{\mathcal{H}}_0\}\,P_0(\hat{g},\hat{h})+\Pr\{\hat{\mathcal{H}}_1\}\,P_1(\hat{g},\hat{h})\}-P_{\rm avg}) - \nu_3(\mathbb{E}_{\hat{g},\hat{h},h}\{\big[(1-\mathscr{P}_{\rm d})\,P_0(\hat{g},\hat{h})+\mathscr{P}_{\rm d}\,P_1(\hat{g},\hat{h})\big] \\ & \times(|\hat{g}|^2+\sigma_g^2)\}-Q_{\rm avg}). \end{aligned} \tag{4.40}$$

Setting the derivatives of the Lagrangian in (4.40) with respect to $P_0^*(\hat{g},\hat{h})$ and $P_1^*(\hat{g},\hat{h})$ to zero and arranging the terms yield the desired results in (4.38) and (4.39), respectively. □

Remark 4.2.5 *Let* $f_0(P_0(\hat{g},\hat{h}))$ *and* $f_1(P_1(\hat{g},\hat{h}))$ *denote the left-hand sides of (4.38) and*

(4.39), respectively, as a function of the transmission powers and let ω_0 *and* ω_1 *denote the right-hand sides of (4.38) and (4.39), respectively. For given values of* $\hat{g}$ *and* $\hat{h}$, $f_0(P_0(\hat{g},\hat{h}))$ *and* $f_1(P_1(\hat{g},\hat{h}))$ *are positive decreasing functions of transmission powers with their maximum values* $f_0(0)$ *and* $f_1(0)$ *obtained at* $P_0(\hat{g},\hat{h}) = 0$ *and* $P_1(\hat{g},\hat{h}) = 0$, *respectively. Hence, the optimal solutions* P_0^* *and* P_1^* *can be characterized as*

$$P_0^* = \begin{cases} f_0^{-1}(\omega_0) & 0 < \omega_0 < f_0(0) \\ 0 & \omega_0 \geq f_0(0) \end{cases} \tag{4.41}$$

$$P_1^* = \begin{cases} f_1^{-1}(\omega_1) & 0 < \omega_1 < f_1(0) \\ 0 & \omega_1 \geq f_1(0). \end{cases} \tag{4.42}$$

It is seen from the above expressions that we allocate power only when $f_0(0) > \omega_0$ *and* $f_1(0) > \omega_1$, *otherwise power levels are zero. Also, the average transmission powers attained with the proposed above optimal power levels are decreasing functions of* ω_1 *and* ω_2, *respectively since* $f_0^{-1}(\omega_0)$ *and* $f_1^{-1}(\omega_1)$ *are decreasing in* ω_0 *and* ω_1, *respectively. Hence, in that sense, the optimal power allocation can be interpreted again as water-filling policy.*

Remark 4.2.6 *The proposed power levels in (4.36) and (4.37) are functions of the variance of the estimation error of the transmission link,* σ_h^2 *and interference link,* σ_g^2. *Hence, Theorem 4.2.3 can be seen as a generalization of the power allocation schemes attained under perfect CSI of transmission link and interference links, i.e., this case can be recovered by setting* $\sigma_h^2 = 0$ *and* $\sigma_g^2 = 0$.

4.2.1.4 Statistical CSI of both transmission and interference links

In this case, the secondary transmitter has only statistical CSI of both transmission and interference links, i.e., knows only the fading distribution of both transmission and interference

links. Under this assumption, the power allocation problem is formulated as follows:

$$\max_{P_0,P_1} \eta_{\mathrm{EE}} = \frac{R(P_0,P_1)}{\mathbb{E}\{\Pr\{\hat{\mathcal{H}}_0\}P_0+\Pr\{\hat{\mathcal{H}}_1\}P_1\}+P_{\mathrm{c}}} \tag{4.43}$$

$$\text{subject to} \quad \mathbb{E}\{\Pr\{\hat{\mathcal{H}}_0\}\,P_0 + \Pr\{\hat{\mathcal{H}}_1\}\,P_1\} \leq P_{\mathrm{avg}} \tag{4.44}$$

$$\mathbb{E}\{\left[(1-\mathscr{P}_{\mathrm{d}})\,P_0 + \mathscr{P}_{\mathrm{d}}\,P_1\right]|g|^2\} \leq Q_{\mathrm{avg}} \tag{4.45}$$

$$P_0 \geq 0, P_1 \geq 0 \tag{4.46}$$

Note that transmission power levels P_0 and P_1 are no longer functions of g and h. There are no closed-form expressions for the optimal power levels P_0^* and P_1^*. However, we can solve (4.43) numerically by transforming the optimization problem into an equivalent parametrized concave form and using convex optimization tools.

4.2.2 Peak Transmit Power Constraint and Average Interference Power Constraint

Next, we assume that peak transmit power constraints are imposed rather than average power constraints. Interference is still controlled via average interference constraints. Peak transmit power constraint is imposed to limit the instantaneous transmit power of the secondary users, and hence corresponds to a stricter constraint compared to the average transmit power constraint.

4.2.2.1 Perfect CSI of both transmission and interference links

Energy-efficient power allocation under the assumption of perfect CSI of both transmission and interference links can be obtained by solving the following problem:

$$\max_{\substack{P_0(g,h)\\P_1(g,h)}} \eta_{\mathrm{EE}} = \frac{\mathbb{E}_{g,h}\big\{R\big(P_0(g,h),P_1(g,h)\big)\big\}}{\mathbb{E}_{g,h}\{\Pr\{\hat{\mathcal{H}}_0\}P_0(g,h)+\Pr\{\hat{\mathcal{H}}_1\}P_1(g,h)\}+P_{\mathrm{c}}} \tag{4.47}$$

$$\text{subject to} \quad P_0(g,h) \le P_{\mathrm{pk},0} \tag{4.48}$$

$$P_1(g,h) \le P_{\mathrm{pk},1} \tag{4.49}$$

$$\mathbb{E}_{g,h}\big\{\big[(1-\mathscr{P}_{\mathrm{d}})\,P_0(g,h)+\mathscr{P}_{\mathrm{d}}\,P_1(g,h)\big]|g|^2\big\} \le Q_{\mathrm{avg}} \tag{4.50}$$

$$P_0(g,h)\ge 0, P_1(g,h)\ge 0, \tag{4.51}$$

where $P_{\mathrm{pk},0}$ and $P_{\mathrm{pk},1}$ denote the peak transmit power limits when the channel is detected as idle and busy, respectively. Under the above constraints, the optimal power allocation strategy is determined in the following result.

Theorem 4.2.4 *The optimal power allocation scheme that maximizes the EE of the secondary users subject to the constraints in (4.48), (4.49) and (4.50) is given by*

$$P_0^*(g,h)=\begin{cases} 0, & |g|^2 \ge \breve{g}_{1,0} \\ \frac{\frac{T-\tau}{T}\Pr\{\hat{\mathcal{H}}_0\}\log_2 e}{\nu_4|g|^2(1-\mathscr{P}_{\mathrm{d}})+\alpha\Pr\{\hat{\mathcal{H}}_0\}} - \frac{N_0+\Pr(\mathcal{H}_1|\hat{\mathcal{H}}_0)\sigma_s^2}{|h|^2}, & \breve{g}_{1,0} > |g|^2 > \breve{g}_{2,0} \\ P_{\mathrm{pk},0}, & |g|^2 \le \breve{g}_{2,0} \end{cases} \tag{4.52}$$

$$P_1^*(g,h)=\begin{cases} 0, & |g|^2 \ge \breve{g}_{1,1} \\ \frac{\frac{T-\tau}{T}\Pr\{\hat{\mathcal{H}}_1\}\log_2 e}{\nu_4|g|^2\mathscr{P}_{\mathrm{d}}+\alpha\Pr\{\hat{\mathcal{H}}_1\}} - \frac{N_0+\Pr(\mathcal{H}_1|\hat{\mathcal{H}}_1)\sigma_s^2}{|h|^2}, & \breve{g}_{1,1} > |g|^2 > \breve{g}_{2,1} \\ P_{\mathrm{pk},1}, & |g|^2 \le \breve{g}_{2,1} \end{cases} \tag{4.53}$$

where

$$\check{g}_{1,j} = \frac{1}{\nu_4 \rho_j}\left(\frac{\frac{T-\tau}{T}\Pr\{\hat{\mathcal{H}}_j\}\log_2 e|h|^2}{N_0 + \Pr(\mathcal{H}_1|\hat{\mathcal{H}}_j)\sigma_s^2} - \alpha \Pr\{\hat{\mathcal{H}}_j\}\right), \tag{4.54}$$

$$\check{g}_{2,j} = \frac{1}{\nu_4 \rho_j}\left(\frac{\frac{T-\tau}{T}\Pr\{\hat{\mathcal{H}}_j\}\log_2 e|h|^2}{P_{\mathrm{pk,j}}|h|^2 + N_0 + \Pr(\mathcal{H}_1|\hat{\mathcal{H}}_j)\sigma_s^2} - \alpha \Pr\{\hat{\mathcal{H}}_j\}\right). \tag{4.55}$$

In the above expressions, $j \in \{0,1\}$, $\rho_0 = 1 - \mathscr{P}_{\mathrm{d}}$ *and* $\rho_1 = \mathscr{P}_{\mathrm{d}}$.

Proof: By transforming the above optimization problem into an equivalent parametrized concave form and following the same steps as in the proof of Theorem 4.2.1 with peak transmit power constraints instead of average transmit power constraint, we can readily obtain the optimal power allocation schemes as in (4.52) and (4.53), respectively.

Remark 4.2.7 *Different from Theorem 4.2.1, the optimal power levels are limited by* $P_{pk,0}$ *and* $P_{pk,1}$*, respectively, when the channel fading coefficient of the interference link is less than a certain threshold, which is mainly determined by the sensing performance through the detection and false-alarm probabilities.*

Remark 4.2.8 *By setting* $\alpha = 0$, $\mathscr{P}_{\mathrm{d}} = 1$ *and* $\mathscr{P}_{\mathrm{f}} = 0$ *in (4.52) and (4.53), we can see that the power allocation schemes in (4.52) and (4.53) have similar structures as those in [18] in the case of throughput maximization where average interference power constraint is satisfied with equality. However, this constraint is not necessarily satistifed with equality in energy efficiency maximization.*

Algorithm 1 can be modified to maximize the energy efficiency subject to peak power constraints and average interference constraint in such a way that $P_0^*(g,h)$ and $P_1^*(g,h)$ are computed using (4.52) and (4.53), respectively and only Lagrange multiplier ν_4 is updated according to (4.15).

4.2.2.2 Perfect CSI of the transmission link and imperfect CSI of the interference link

In the presence of perfect CSI of the transmission link and imperfect CSI of the interference link, the optimization problem in (4.18) is subject to

$$P_0(\hat{g},h) \leq P_{\text{pk},0} \tag{4.56}$$

$$P_1(\hat{g},h) \leq P_{\text{pk},1} \tag{4.57}$$

$$\mathbb{E}_{\hat{g},h}\{\left[(1-\mathscr{P}_{\text{d}})\,P_0(\hat{g},h)+\mathscr{P}_{\text{d}}\,P_1(\hat{g},h)\right](|\hat{g}|^2+\sigma_g^2)\} \leq Q_{\text{avg}} \tag{4.58}$$

The main characterization for the optimal power allocation is as follows:

Theorem 4.2.5 *The optimal power allocation scheme under the constraints in (4.56), (4.57) and (4.58) is obtained as*

$$P_0^*(\hat{g},h)=\begin{cases} 0, & |\hat{g}|^2 \geq \hat{g}_{1,0} \\ \frac{\frac{T-\tau}{T}\Pr\{\hat{\mathcal{H}}_0\}\log_2 e}{\nu_5(|\hat{g}|^2+\sigma_g^2)(1-\mathscr{P}_{\text{d}})+\alpha\Pr\{\hat{\mathcal{H}}_0\}}-\frac{N_0+\Pr(\mathcal{H}_1|\hat{\mathcal{H}}_0)\sigma_s^2}{|h|^2}, & \hat{g}_{1,0}>|\hat{g}|^2>\hat{g}_{2,0} \\ P_{\text{pk},0}, & |\hat{g}|^2 \leq \hat{g}_{2,0} \end{cases} \tag{4.59}$$

$$P_1^*(\hat{g},h)=\begin{cases} 0, & |\hat{g}|^2 \geq \hat{g}_{1,1} \\ \frac{\frac{T-\tau}{T}\Pr\{\hat{\mathcal{H}}_1\}\log_2 e}{\nu_5(|\hat{g}|^2+\sigma_g^2)\mathscr{P}_{\text{d}}+\alpha\Pr\{\hat{\mathcal{H}}_1\}}-\frac{N_0+\Pr(\mathcal{H}_1|\hat{\mathcal{H}}_1)\sigma_s^2}{|h|^2}, & \hat{g}_{1,1}>|\hat{g}|^2>\hat{g}_{2,1} \\ P_{\text{pk},1}, & |\hat{g}|^2 \leq \hat{g}_{2,1}. \end{cases} \tag{4.60}$$

Above,

$$\hat{g}_{1,j} = \frac{1}{\nu_5\rho_j}\left(\frac{\frac{T-\tau}{T}\Pr\{\hat{\mathcal{H}}_j\}\log_2 e|h|^2}{N_0+\Pr(\mathcal{H}_1|\hat{\mathcal{H}}_j)\sigma_s^2}-\alpha\Pr\{\hat{\mathcal{H}}_j\}\right)-\sigma_g^2, \tag{4.61}$$

$$\hat{g}_{2,j} = \frac{1}{\nu_5\rho_j}\left(\frac{\frac{T-\tau}{T}\Pr\{\hat{\mathcal{H}}_j\}\log_2 e|h|^2}{P_{\text{pk,j}}|h|^2+N_0+\Pr(\mathcal{H}_1|\hat{\mathcal{H}}_j)\sigma_s^2}-\alpha\Pr\{\hat{\mathcal{H}}_j\}\right)-\sigma_g^2. \tag{4.62}$$

Since similar steps as in the proof of Theorem 4.2.1 are followed, the proof is omitted.

Remark 4.2.9 *In the optimal power allocation schemes given in (4.59) and (4.60), the cut-off values, $\hat{g}_{1,j}$ and $\hat{g}_{2,j}$ for the estimated channel power gain of the interference link depend on the channel estimation error variance of the interference link as different from the results in Theorem* 4.2.4.

4.2.2.3 Imperfect CSI of both transmission and interference links

We again have peak transmit power and average interference power constraints. However, different from the previous cases, the transmission link is imperfectly known at the secondary transmitter. Therefore, the power levels are functions of $\hat{g}$ and $\hat{h}$. We derive the following result for the optimal power allocation schemes that maximize the energy efficiency of the secondary users. Again the proof is omitted for brevity.

Theorem 4.2.6 *The optimal power allocation under peak transmit power and average interference power constraints is given by*

$$P_0^*(\hat{g},\hat{h}) = \min\left(P_{\mathrm{pk},0}, \bar{P}_0(\hat{g},\hat{h})\right) \tag{4.63}$$

$$P_1^*(\hat{g},\hat{h}) = \min\left(P_{\mathrm{pk},1}, \bar{P}_1(\hat{g},\hat{h})\right), \tag{4.64}$$

where $\bar{P}_0(\hat{g},\hat{h})$ is solution to

$$\int_0^\infty \frac{\left(\frac{T-\tau}{T}\right)\Pr\{\hat{\mathcal{H}}_0\}\log_2 e\gamma}{N_0 + \Pr\{\hat{\mathcal{H}}_0\}\sigma_s^2 + \bar{P}_0(\hat{g},\hat{h})\gamma} f_{|h|^2|\hat{h}}(\gamma,\hat{h})d\gamma = \alpha\Pr\{\hat{\mathcal{H}}_0\} + \nu_6(1-\mathscr{P}_{\mathrm{d}})(|\hat{g}|^2+\sigma_g^2) \tag{4.65}$$

and $\bar{P}_1(\hat{g},\hat{h})$ is solution to

$$\int_0^\infty \frac{\left(\frac{T-\tau}{T}\right)\Pr\{\hat{\mathcal{H}}_1\}\log_2 e\gamma}{N_0 + \Pr\{\hat{\mathcal{H}}_1\}\sigma_s^2 + \bar{P}_1(\hat{g},\hat{h})\gamma} f_{|h|^2|\hat{h}}(\gamma,\hat{h})d\gamma = \alpha\Pr\{\hat{\mathcal{H}}_1\} + \nu_6\mathscr{P}_{\mathrm{d}}(|\hat{g}|^2+\sigma_g^2). \tag{4.66}$$

4.2.2.4 Statistical CSI of both transmission and interference links

In this case, the optimal power allocation problem is subject to peak transmit and average interference power constraints under the assumption of the availability of only statistical CSI of both transmission and interference links. The optimal values of P_0^* and P_1^* can be found numerically by converting the optimization problem into an equivalent parametrized concave form and employing convex optimization tools.

4.2.3 Average Transmit Power Constraint and Peak Interference Power Constraint

Finally, we consider the case in which the secondary transmitter operates under average transmit power constraint and peak interference power constraints, which are imposed to satisfy short-term QoS requirements of the primary users.

4.2.3.1 Perfect CSI of both transmission and interference links

In this case, the objective function in (4.8) is subject to the following constraints:

$$\mathbb{E}_{g,h}\{\Pr\{\hat{\mathcal{H}}_0\}\, P_0(g,h) + \Pr\{\hat{\mathcal{H}}_1\}\, P_1(g,h)\} \leq P_{\text{avg}} \tag{4.67}$$

$$P_0(g,h)|g|^2 \leq Q_{\text{pk},0} \tag{4.68}$$

$$P_1(g,h)|g|^2 \leq Q_{\text{pk},1} \tag{4.69}$$

where $Q_{\text{pk,k}}$ for $k \in \{0,1\}$ represents the peak limit on the received interference power at the primary receiver. Under these constraints, we derive the optimal power allocation scheme as follows:

Theorem 4.2.7 *The optimal power allocation strategy under average transmit power in*

(4.67) and peak interference power constraints in (4.68) and (4.69) is obtained as

$$P_0^*(g,h) = \min\left(\left[\frac{\frac{T-\tau}{T}\log_2 e}{(\lambda_4+\alpha)} - \frac{N_0+\Pr(\mathcal{H}_1|\hat{\mathcal{H}}_0)\sigma_s^2}{|h|^2}\right]^+, \frac{Q_{pk,0}}{|g|^2}\right) \tag{4.70}$$

$$P_1^*(g,h) = \min\left(\left[\frac{\frac{T-\tau}{T}\log_2 e}{(\lambda_4+\alpha)} - \frac{N_0+\Pr(\mathcal{H}_1|\hat{\mathcal{H}}_1)\sigma_s^2}{|h|^2}\right]^+, \frac{Q_{pk,1}}{|g|^2}\right) \tag{4.71}$$

Above, λ_4 is the Lagrange multiplier associated with the average transmit power in (4.67).

Proof: The optimization problem is first expressed in terms of an equivalent concave form. Then, the similar steps as in the proof of Theorem 4.2.1 are followed. However, peak interference power constraints are imposed instead of average interference power constraint. Therefore, in this case the optimal powers are limited by peak interference power constraints, $Q_{\mathrm{pk,k}}$ for $k \in \{0,1\}$.

4.2.3.2 Perfect CSI of the transmission link and imperfect CSI of the interference link

We have the following constraints for the optimization problem in (4.18) given as

$$\mathbb{E}_{g,h}\{\Pr\{\hat{\mathcal{H}}_0\}\, P_0(g,h) + \Pr\{\hat{\mathcal{H}}_1\}\, P_1(g,h)\} \leq P_{\mathrm{avg}} \tag{4.72}$$

$$\Pr(P_0(g,h)|g|^2 \geq Q_{\mathrm{pk},0}|\hat{g}) \leq \xi_0 \tag{4.73}$$

$$\Pr(P_1(g,h)|g|^2 \geq Q_{\mathrm{pk},1}|\hat{g}) \leq \xi_1 \tag{4.74}$$

where ξ_k for $k \in \{0,1\}$ denotes the outage threshold. The constraints in (4.73) and (4.74) can be further expressed as [71]

$$P_0(g,h) \leq \frac{Q_{\mathrm{pk},0}}{F^{-1}_{|g|^2|\hat{g}}(1-\xi_0,\hat{g})} \tag{4.75}$$

$$P_1(g,h) \leq \frac{Q_{\mathrm{pk},1}}{F^{-1}_{|g|^2|\hat{g}}(1-\xi_1,\hat{g})}. \tag{4.76}$$

Above, $F^{-1}_{|g|^2|\hat{g}}(.,\hat{g})$ represents the inverse cumulative density function of $|g|^2$ given $\hat{g}$. In this setting, the main characterization is given as follows:

Theorem 4.2.8 *The optimal power allocation strategy under the constraints in (4.73) and (4.74) is given by*

$$P_0^*(\hat{g},h) = \min\left(\left[\frac{\frac{T-\tau}{T}\log_2 e}{(\lambda_5+\alpha)} - \frac{N_0+\Pr(\mathcal{H}_1|\hat{\mathcal{H}}_0)\sigma_s^2}{|h|^2}\right]^+, \frac{Q_{\text{pk},0}}{F^{-1}_{|g|^2|\hat{g}}(1-\xi_0,\hat{g})}\right) \tag{4.77}$$

$$P_1^*(\hat{g},h) = \min\left(\left[\frac{\frac{T-\tau}{T}\log_2 e}{(\lambda_5+\alpha)} - \frac{N_0+\Pr(\mathcal{H}_1|\hat{\mathcal{H}}_1)\sigma_s^2}{|h|^2}\right]^+, \frac{Q_{\text{pk},1}}{F^{-1}_{|g|^2|\hat{g}}(1-\xi_1,\hat{g})}\right) \tag{4.78}$$

Above, λ_5 is the Lagrange multiplier.

The proof is omitted for brevity.

4.2.3.3 Imperfect CSI of both transmission and interference links

It is assumed that the secondary users operate under the constraints below:

$$\mathbb{E}_{g,h}\{\Pr\{\hat{\mathcal{H}}_0\}\, P_0(g,h) + \Pr\{\hat{\mathcal{H}}_1\}\, P_1(g,h)\} \leq P_{\text{avg}} \tag{4.79}$$

$$P_0(g,h) \leq \frac{Q_{\text{pk},0}}{F^{-1}_{|g|^2|\hat{g}}(1-\xi_0,\hat{g})} \tag{4.80}$$

$$P_1(g,h) \leq \frac{Q_{\text{pk},1}}{F^{-1}_{|g|^2|\hat{g}}(1-\xi_1,\hat{g})}. \tag{4.81}$$

In the following result, we derive the optimal power allocation scheme for this case.

Theorem 4.2.9 *The optimal power allocation strategy under average transmit power in (4.79) and peak interference power constraints in (4.80) and (4.81) is obtained as*

$$P_0^*(\hat{g},\hat{h}) = \min\left(\frac{Q_{\text{pk},0}}{F^{-1}_{|g|^2|\hat{g}}(1-\xi_0,\hat{g})}, \bar{P}_0(\hat{g},\hat{h})\right), \tag{4.82}$$

$$P_1^*(\hat{g},\hat{h}) = \min\left(\frac{Q_{\text{pk},1}}{F^{-1}_{|g|^2|\hat{g}}(1-\xi_1,\hat{g})}, \bar{P}_1(\hat{g},\hat{h})\right) \tag{4.83}$$

where $\bar{P}_0(\hat{g},\hat{h})$ *is solution to*

$$\int_0^{\infty} \frac{\left(\frac{T-\tau}{T}\right)\Pr\{\hat{\mathcal{H}}_0\}\log_2 e\gamma}{N_0+\Pr\{\hat{\mathcal{H}}_0\}\sigma_s^2+\bar{P}_0(\hat{g},\hat{h})\gamma} f_{|h|^2|\hat{h}}(\gamma,\hat{h})d\gamma = (\lambda_6+\alpha)\Pr\{\hat{\mathcal{H}}_0\} \tag{4.84}$$

and $\bar{P}_1(\hat{g},\hat{h})$ *is solution to*

$$\int_0^{\infty} \frac{\left(\frac{T-\tau}{T}\right)\Pr\{\hat{\mathcal{H}}_1\}\log_2 e\gamma}{N_0+\Pr\{\hat{\mathcal{H}}_1\}\sigma_s^2+\bar{P}_1(\hat{g},\hat{h})\gamma} f_{|h|^2|\hat{h}}(\gamma,\hat{h})d\gamma = (\lambda_6+\alpha)\Pr\{\hat{\mathcal{H}}_1\}. \tag{4.85}$$

Again, the proof is omitted for the sake of brevity.

4.3 Numerical Results

In this section, we present numerical results to illustrate the energy efficiency of secondary users attained with the proposed energy efficiency maximizing power allocation methods in the presence of imperfect sensing results and different levels of CSI regarding the transmission and interference links. Unless mentioned explicitly, it is assumed that noise variance is $N_0 = 0.1$, the variance of primary user signal is $\sigma_s^2 = 1$. Also, the prior probabilities are $\Pr\{\mathcal{H}_0\} = 0.4$ and $\Pr\{\mathcal{H}_1\} = 0.6$. The frame duration T and sensing duration τ are set to 100 and 10, respectively. The circuit power is $P_c = 0.1$. The step sizes λ and ν are set to 0.1 and tolerance ϵ is chosen as 10^{-6}.

In Fig. 4.4, we display maximum energy efficiency as a function of peak/average transmit power constraints for perfect sensing (i.e., $\mathscr{P}_{\rm d} = 1$ and $\mathscr{P}_{\rm f} = 0$) and imperfect sensing (i.e., $\mathscr{P}_{\rm d} = 0.8$ and $\mathscr{P}_{\rm f} = 0.1$). It is assumed that $Q_{\rm avg} = -8$ dB. Optimal power allocation is performed by assuming perfect instantaneous CSI at the secondary transmitter. It is seen that perfect detection of the primary user activity results in higher energy efficiency compared to the case with imperfect sensing decisions. In particular, the probabilities $\Pr(\mathcal{H}_1|\hat{\mathcal{H}}_0)$ and $\Pr(\mathcal{H}_0|\hat{\mathcal{H}}_1)$ are zero due to perfect spectrum sensing and hence, the secondary users do not experience additive disturbance from primary users, which leads to higher achievable

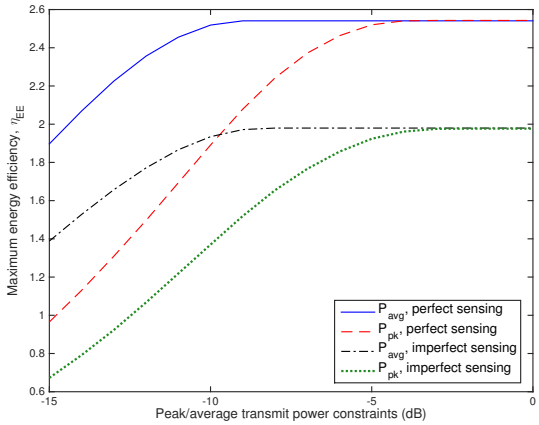

Figure 4.4: Maximum energy efficiency η_{EE} vs. peak/average transmit power constraints.

rates, and hence higher energy efficiency compared to imperfect sensing case. It is also observed that maximum energy efficiency increases with increasing peak/average transmit power constraints. When peak/average transmit power constraints become sufficiently large compared to Q_{avg}, maximum energy efficiency stays constant since the power is determined by average interference constraint, Q_{avg} rather than peak/average transmit power constraints. Moreover, higher energy efficiency is obtained under average transmit power constraint since the optimal power allocation under average transmit power constraint is more flexible than that under peak transmit power constraint.

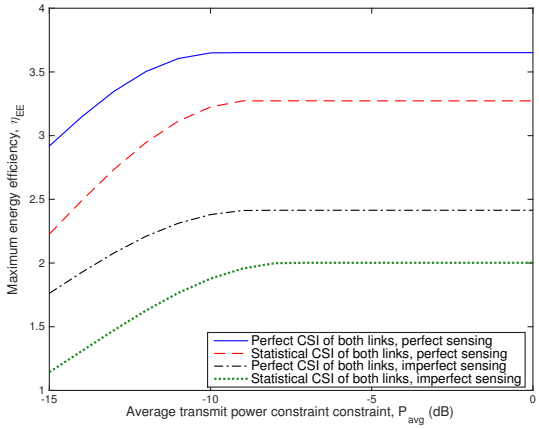

Figure 4.5: Maximum energy efficiency η_{EE} vs. average transmit power constraint.

In Fig. 4.5, we plot maximum energy efficiency attained with the proposed optimal power

allocation schemes as a function of the average transmit power constraint under perfect sensing with $\mathscr{P}_{\rm d} = 1$ and $\mathscr{P}_{\rm f} = 0$) and imperfect sensing with $\mathscr{P}_{\rm d} = 0.8$ and $\mathscr{P}_{\rm f} = 0.1$. We assume the availability of either perfect instantaneous CSI or statistical CSI of both transmission and interference links at the secondary transmitter. $Q_{\rm avg}$ is set to -25 dB. It is observed from the figure that when the optimal power allocation with perfect instantaneous CSI is applied, higher energy efficiency is achieved compared to the optimal power allocation with statistical CSI. More specifically, the power allocation scheme assuming perfect instantaneous CSI can exploit favorable channel conditions and higher transmission power is allocated to better channel, and hence a secondary user's power budget is more efficiently utilized compared to the power allocation scheme assuming statistical CSI in which the power levels do not change according to channel conditions. It is also seen that imperfect sensing decisions significantly affect the performance of secondary users, resulting in lower energy efficiency under both optimal power allocation strategies.

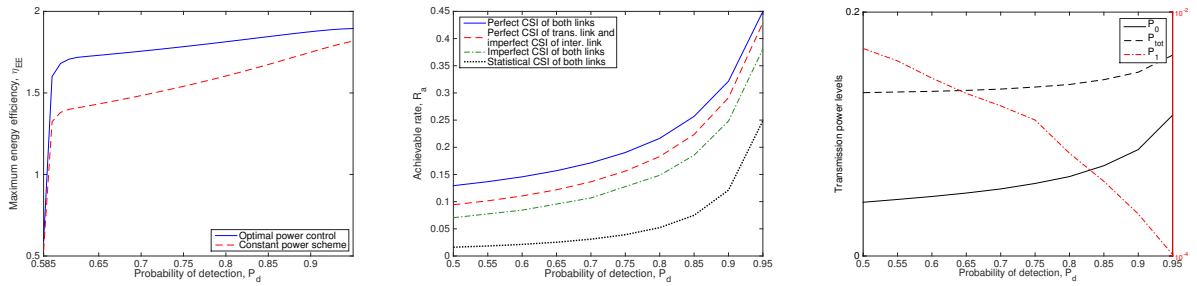

(a) $\eta_{\rm EE}$ vs. $\mathscr{P}_{\rm d}$ (b) R_a vs. $\mathscr{P}_{\rm d}$ (c) $P_{\rm tot}$, P_0 and P_1 vs. $\mathscr{P}_{\rm d}$

Figure 4.6: (a) Maximum achievable energy efficiency, $\eta_{\rm EE}$ vs. probability of detection, $\mathscr{P}_{\rm d}$; (b) achievable rate maximizing energy efficiency, R_a vs. $\mathscr{P}_{\rm d}$; (c) optimal total transmission power, $P_{\rm tot}$ and P_0, P_1 vs. $\mathscr{P}_{\rm d}$.

In Fig. 4.6, we display maximum energy efficiency, achievable rate R_a, and optimal powers, $P_{\rm tot}$, P_0 and P_1 as a function of detection probability, $\mathscr{P}_{\rm d}$. It is assumed that peak transmit power constraints are $P_{{\rm pk},0} = P_{{\rm pk},1} = -4$ dB and average interference power constraint is $Q_{\rm avg} = -25$ dB. In addition, probability of false alarm, $\mathscr{P}_{\rm f}$ is set to 0.1. We consider the power allocation schemes for the following four cases: (1) perfect CSI of both transmission and interference links; (2) perfect CSI of the transmission link and imperfect

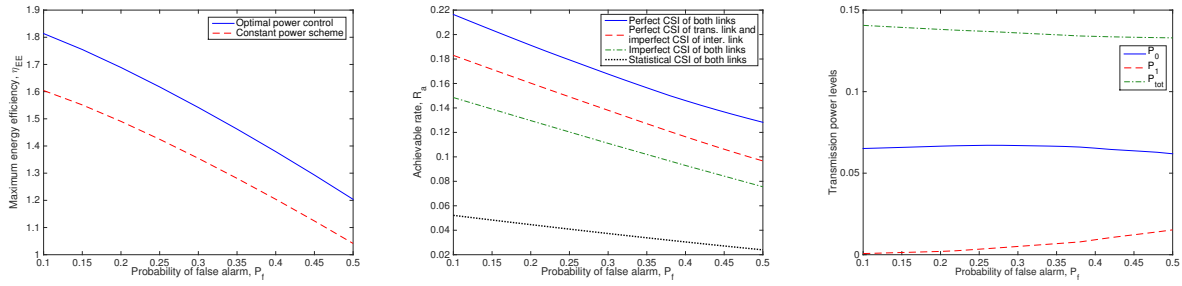

(a) η_{EE} vs. $\mathscr{P}_{\text{f}}$ (b) R_a vs. $\mathscr{P}_{\text{f}}$ (c) P_{tot}, P_0 and P_1 vs. $\mathscr{P}_{\text{f}}$

Figure 4.7: (a) Maximum energy efficiency, η_{EE} vs. probability of false alarm, $\mathscr{P}_{\text{f}}$; (b) achievable rate maximizing energy efficiency, R_a vs. $\mathscr{P}_{\text{f}}$; (c) optimal total transmission power, P_{tot} and P_0, P_1 vs. $\mathscr{P}_{\text{f}}$.

CSI of the interference link; (3) imperfect CSI of both transmission and interference links; and (4) only statistical CSI of both transmission and interference links. We only plot optimal powers, P_{tot}, P_0 and P_1 for the optimal power allocation with perfect instantaneous CSI of both links since the same trend is observed under the assumption of other CSI levels. As $\mathscr{P}_{\text{d}}$ increases, secondary users have more reliable sensing performance. Hence, secondary users experience miss detection events less frequently, which results in increased achievable rate. The transmission power under idle sensing decision, P_0 increases with increasing $\mathscr{P}_{\text{d}}$ while transmission power under busy sensing decision, P_1 decreases with increasing $\mathscr{P}_{\text{d}}$. Since achievable rate increases and total transmission power slightly increases, maximum energy efficiency of secondary users increases as sensing performance improves. It is also seen that the power allocation scheme with perfect instantaneous CSI of both links outperforms the other proposed power allocation strategies. Moreover, the performance of secondary users in terms of throughput and energy efficiency degrades gradually as we have less and less information regarding the transmission and interference links at the secondary transmitter.

Fig. 4.7 shows maximum energy efficiency, achievable rate, R_a and optimal powers, P_{tot}, P_0 and P_1 as a function of false alarm probability, $\mathscr{P}_{\text{f}}$. We consider the same setting as in the previous figure. It is again assumed that $P_{pk,0} = P_{\text{pk},1} = -4$ dB and $Q_{\text{avg}} = -8$ dB. Since optimal powers maximizing energy efficiency show similiar trends as a function of $\mathscr{P}_{\text{f}}$, we only plot the optimal power levels under the assumption of perfect instantaneous CSI of both

transmission and interference links in Fig. 4.7 (c). Probability of detection, $\mathscr{P}_{\mathrm{d}}$ is chosen as 0.8. As $\mathscr{P}_{\mathrm{f}}$ increases, channel sensing performance deteriorates. In this case, secondary users detect the channel as busy more frequently even if the channel is idle. Total transmission power maximizing energy efficiency slightly decreases with increasing $\mathscr{P}_{\mathrm{f}}$. In addition, since the available channel is not utilized efficiently, secondary users have smaller achievable rate, which leads to lower achievable energy efficiency. Again, the power allocation scheme with perfect instantaneous CSI of both links gives the best performance in terms of throughput and energy efficiency.

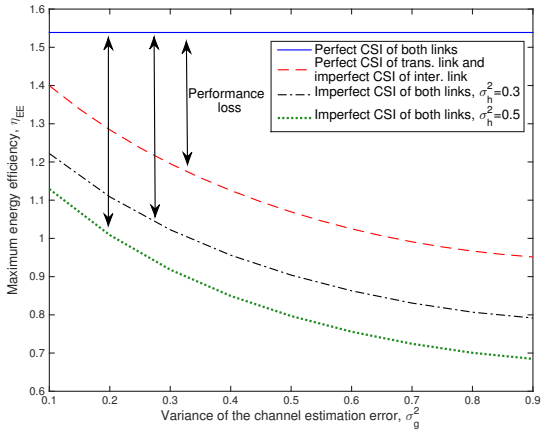

Figure 4.8: Maximum energy efficiency η_{EE} vs. channel estimation error variance of the interference link, $\sigma)g^2$.

In Fig. 4.8, we display maximum energy efficiency as a function of channel estimation error variance of the interference link. Power allocation is employed by perfect CSI of transmission link and imperfect CSI of interference link, and imperfect CSI of both links with $\sigma_h^2 = 0.3$ and $\sigma_h^2 = 0.5$. We assume that $P_{pk,0} = P_{\mathrm{pk},1} = -4$ dB and $Q_{\mathrm{avg}} = -25$ dB, and sensing is imperfect with $\mathscr{P}_{\mathrm{d}} = 0.8$ and $\mathscr{P}_{\mathrm{f}} = 0.1$. The energy efficiency attained with the optimal power allocation assuming perfect CSI of both links is displayed as a baseline to compare the performance loss due to imperfect CSI of either interference link or of both transmission and interference links at the secondary transmitter. It is observed that energy efficiency of secondary users decreases as the variance of the channel estimation error in the

interference link, σ_g^2, increases and hence the channel estimate becomes less accurate. The secondary users even have lower energy efficiency when CSI of both links are imperfectly known. Therefore, accurate estimation of both transmission and interference links is crucial in order to achieve better energy efficiency.

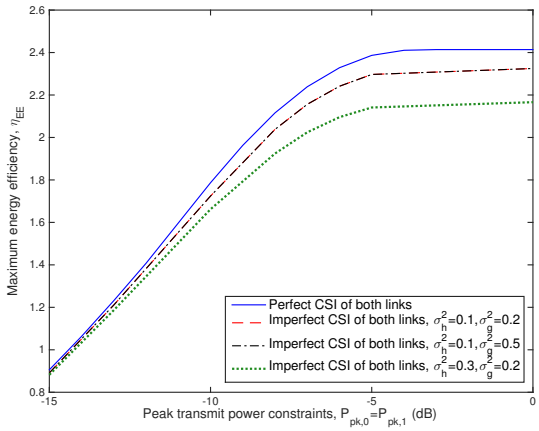

Figure 4.9: Maximum energy efficiency η_{EE} vs. peak transmit power constraints, $P_{\text{pk},0} = P_{\text{pk},1}$.

Fig. 4.9 shows maximum energy efficiency as a function of the peak transmit power constraints, $P_{\text{pk},0} = P_{\text{pk},1}$ under imperfect sensing result (i.e., when $\mathscr{P}_{\text{d}} = 0.8$ and $\mathscr{P}_{\text{f}} = 0.1$). We consider the optimal power allocation schemes assuming either perfect CSI of both links or imperfect CSI of both links with $\sigma_h^2 = 0.1$ and $\sigma_g^2 = 0.2$, $\sigma_h^2 = 0.1$ and $\sigma_g^2 = 0.5$, and $\sigma_h^2 = 0.3$ and $\sigma_g^2 = 0.2$. Average interference constraint, Q_{avg} is set to -10 dB. When channel estimation error of the transmission link increases from 0.1 and 0.3 keeping $\sigma_g^2 = 0.2$, energy efficiency of secondary users decreases more compared to the case when the channel estimation error of the interference link increases from 0.2 to 0.5 while $\sigma_h^2 = 0.1$ since the average interference constraint is loose, and imperfect CSI of the interference link only slightly affects the performance. Also, as P_{pk} increases, energy efficiency of secondary users first increases and then stays constant since average transmission power reaches to the value that maximizes energy efficiency. Therefore, further increasing P_{pk} does not provide any energy efficiency improvement.

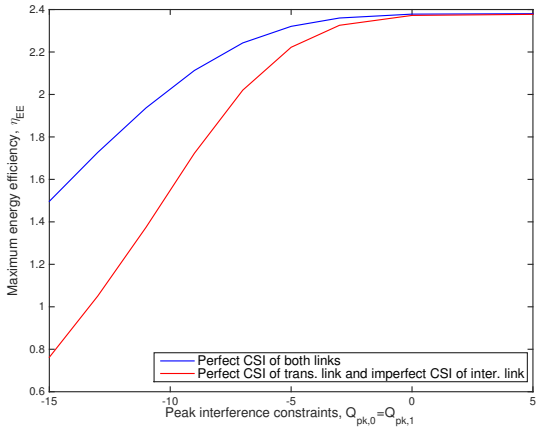

Figure 4.10: Maximum energy efficiency η_{EE} vs. peak interference power constraints, $Q_{\mathrm{pk},0} = Q_{\mathrm{pk},1}$.

In Fig. 4.10, we plot maximum energy efficiency as a function of the peak interference power constraints, $Q_{\mathrm{pk},0} = Q_{\mathrm{pk},1}$. It is assumed that $\mathscr{P}_{\mathrm{d}} = 0.8$ and $\mathscr{P}_{\mathrm{f}} = 0.1$. We consider that either perfect instantaneous CSI of both links or perfect CSI of transmission link and imperfect CSI of interference link is available at the secondary transmitter. We set P_{avg} to -10 dB, outage thresholds $\xi_0 = \xi_1$ to 0.1 and $\sigma_g^2 = 0.1$. It is seen that energy efficiency under both cases first increases with increasing interference power constraints, and then get constant and approach the same value due to average transmit power constraint. Also, the availability of imperfect CSI of interference link deterioates the system performance and leads to lower energy efficiency compared to that of perfect CSI of interference link.

Chapter 5

Energy Efficiency in Cognitive Radio Systems with Channel Sensing Errors – Unslotted Primary Users

In the previous chapter, we consider the primary and secondary transmission are synchronized in which the primary user activity does not change during the transmission duration of the secondary users. In this chapter, we assume that the primary user transmits in an unslotted fashion, i.e., the activity of the primary users can change during the frame duration of the secondary users, and we do not impose any limitations on the number of transitions of the primary user activity. This chapter mainly focuses on energy efficiency and average throughput maximization for cognitive radio systems in the presence of unslotted primary users. The optimal power control policy which maximizes the energy efficiency of the secondary users or maximizes the average throughput while satisfying a minimum required energy efficiency under average/peak transmit power and average interference power constraints are derived.

Section 5.1 introduces the primary user activity model, opportunistic spectrum access scheme and collision constraint. In Section 5.2 and Section 5.3, the optimal power control schemes that maximize the energy efficiency of the secondary users and the average through-

put under a minimum energy efficiency constraint are derived, respectively. The algorithms for jointly determining the optimal power control and frame duration are also developed. Numerical results are provided and discussed in Section 5.4.

5.1 System Model

We consider a cognitive radio system consisting of a pair of primary transmitter and receiver, and a pair of secondary transmitter and receiver. Secondary users opportunistically access the channel licensed to the primary users. In the following subsections, we describe the primary user activity model, opportunistic spectrum access policy of the secondary users, and the formulation of the collision constraint imposed for the protection of the primary users.

5.1.1 Primary User Activity Model

Differing from the majority of the studies (which assume that the primary users adopt a time-slotted transmission scheme), we consider a continuous, i.e., unslotted transmission structure

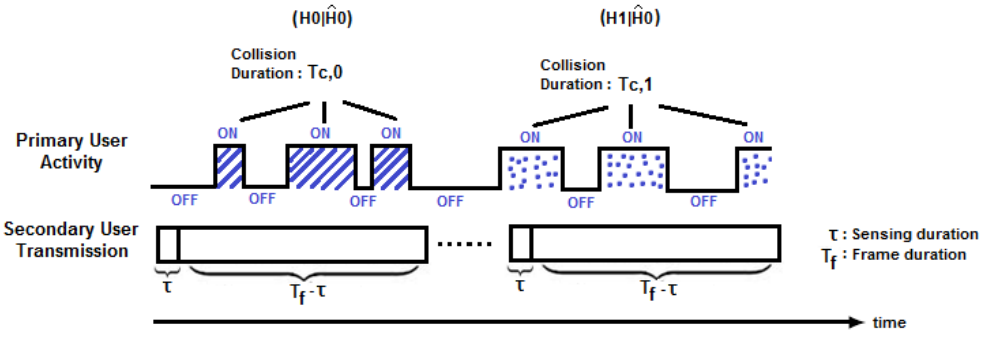

Figure 5.1: Frame structure of the primary and secondary users.

We assume that the primary user activity follows a semi-Markov process with ON and OFF states, which is shown to be a good model for primary user traffic based on measurements and simulations [72], [73]. In this model, the ON state indicates that the primary user is transmitting while the OFF state represents that the channel is not occupied by the primary user. Such a process is also known as an alternating renewal process. The durations

of ON and OFF periods are independent of each other and are exponentially distributed with means λ_0 and λ_1, respectively, and therefore have probability density functions

$$f_{\mathrm{ON}}(t) = \frac{1}{\lambda_0}\mathrm{e}^{-\frac{t}{\lambda_0}}, \text{ and } f_{\mathrm{OFF}}(t) = \frac{1}{\lambda_1}\mathrm{e}^{-\frac{t}{\lambda_1}}. \tag{5.1}$$

Hence, the prior probabilities of channel being vacant or occupied by the primary user can be expressed, respectively, as

$$\Pr\{\mathcal{H}_0\} = \frac{\lambda_0}{\lambda_0+\lambda_1}, \quad \Pr\{\mathcal{H}_1\} = \frac{\lambda_1}{\lambda_0+\lambda_1}. \tag{5.2}$$

5.1.2 Opportunistic Spectrum Access by the Secondary Users

Secondary users employ frames of duration T_{f}. In the initial duration of τ seconds, secondary users perform channel sensing and monitor the primary user activity. Subsequently, data transmission starts in the remaining frame duration of $T_{\mathrm{f}}-\tau$ seconds only if the primary user activity is not detected, the event of which is denoted by $\hat{\mathcal{H}}_0$. Spectrum sensing is modeled as a simple binary hypothesis testing problem with two hypotheses $\mathcal{H}_0$ and $\mathcal{H}_1$ corresponding to the absence and presence of the primary user signal, respectively. Many spectrum sensing methods have been proposed [51], and the corresponding sensing performance is characterized by two parameters, namely the probabilities of detection and false alarm, which are defined as

$$P_{\mathrm{d}} = \Pr\{\hat{\mathcal{H}}_1|\mathcal{H}_1\}, \quad P_{\mathrm{f}} = \Pr\{\hat{\mathcal{H}}_1|\mathcal{H}_0\}, \tag{5.3}$$

where $\hat{\mathcal{H}}_1$ denotes the event that the primary user activity is detected. We note that any sensing method can be employed in the rest of the analysis since the results depend on the sensing performance only through the probabilities of detection and false alarm, and the sensing duration.

5.1.3 Collision Constraints

We first describe the secondary users' collisions with the primary users, which can lead to considerable performance degradation in the primary user communication. Subsequently, we impose a constraint on the ratio of the average collision duration to the transmission duration in order to protect the primary users. Depending on the true nature of the primary user activity at the beginning of the frame, collisions between the primary and secondary users can occur in the following two cases:

- *Case* 1: The channel is not occupied by the primary user and is correctly detected as idle at the beginning of the frame. Even if the primary user is not actually transmitting initially, it is possible for the primary user to start data transmission at any time during the current frame, which results in a collision event. By conditioning on the correct detection of the initial absence of the primary user, the ratio of the average collision duration to data transmission duration, which is called the collision duration ratio, can be expressed as

$$\mathscr{P}_{c,0} = \frac{\mathbb{E}\{T_{c|\mathcal{H}_0,\hat{\mathcal{H}}_0}\}}{T_{\mathrm{f}} - \tau}, \tag{5.4}$$

  where $\mathbb{E}\{\cdot\}$ denotes the expectation, and $T_{c|\mathcal{H}_0,\hat{\mathcal{H}}_0}$ is a random variable representing the collision duration between the secondary and primary users given that the primary user is inactive initially at the beginning of the frame (event $\mathcal{H}_0$) and the sensing decision is idle (event $\hat{\mathcal{H}}_0$). Assuming that the primary user is in the OFF state at first and taking into account the possible multiple transitions between ON and OFF states, $\mathbb{E}\{T_{c|\mathcal{H}_0,\hat{\mathcal{H}}_0}\}$ can be found by following a similar analysis as in [74, Theorem 2]. Hence, $P_{c,0}$ is given by

$$\mathscr{P}_{c,0} = \Pr\{\mathcal{H}_1\} - \frac{\lambda_0 \Pr\{\mathcal{H}_1\}^2}{T_{\mathrm{f}} - \tau}\left(1 - \mathrm{e}^{-\frac{T_{\mathrm{f}}-\tau}{\lambda_0 \Pr\{\mathcal{H}_1\}}}\right). \tag{5.5}$$

- *Case* 2: The primary user is actually present in the channel at the beginning of the frame, however the secondary user miss-detects the primary user activity, resulting in a collision right away due to sensing error. Multiple collisions can also occur if the primary user turns OFF and then back ON in a single frame once or multiple times. Similar to the first case, by conditioning on the miss detection event, the collision duration ratio can be found as

$$\mathscr{P}_{c,1} = \frac{\mathbb{E}\{T_{c|\mathcal{H}_1,\hat{\mathcal{H}}_0}\}}{T_{\mathrm{f}} - \tau} \tag{5.6}$$

$$= \Pr\{\mathcal{H}_1\} + \frac{\lambda_1 \Pr\{\mathcal{H}_0\}^2}{T_{\mathrm{f}} - \tau}\left(1 - \mathrm{e}^{-\frac{T_{\mathrm{f}}-\tau}{\lambda_0 \Pr\{\mathcal{H}_1\}}}\right) \tag{5.7}$$

  where $T_{c|\mathcal{H}_1,\hat{\mathcal{H}}_0}$ is a random variable describing the collision duration between the secondary and primary users given that the primary user is active at the beginning of the frame but sensing decision is incorrectly an idle channel.

Based on the above two cases, the collision duration ratio averaged over the true nature of the primary user activity given the idle sensing decision $\hat{\mathcal{H}}_0$ can be expressed as

$$\mathscr{P}_c = \Pr\{\mathcal{H}_0|\hat{\mathcal{H}}_0\}\mathscr{P}_{c,0} + \Pr\{\mathcal{H}_1|\hat{\mathcal{H}}_0\}\mathscr{P}_{c,1} \tag{5.8}$$

where $\Pr\{\mathcal{H}_0|\hat{\mathcal{H}}_0\}$ and $\Pr\{\mathcal{H}_1|\hat{\mathcal{H}}_0\}$ denote the conditional probabilities of the primary user being active or inactive given the idle sensing decision, respectively, which can be written in terms of P_{d} and P_{f} as

$$\Pr\{\mathcal{H}_0|\hat{\mathcal{H}}_0\} = \frac{\Pr\{\mathcal{H}_0\}(1-P_{\mathrm{f}})}{\Pr\{\mathcal{H}_0\}(1-P_{\mathrm{f}}) + \Pr\{\mathcal{H}_1\}(1-P_{\mathrm{d}})}, \tag{5.9}$$

$$\Pr\{\mathcal{H}_1|\hat{\mathcal{H}}_0\} = \frac{\Pr\{\mathcal{H}_1\}(1-P_{\mathrm{d}})}{\Pr\{\mathcal{H}_0\}(1-P_{\mathrm{f}}) + \Pr\{\mathcal{H}_1\}(1-P_{\mathrm{d}})}. \tag{5.10}$$

In the following, we provide two key properties of $\mathscr{P}_c$.

Proposition 5.1.1 *The average collision duration ratio $\mathscr{P}_c$ under idle sensing decision has*

the following properties:

- *It is an increasing function of the frame duration* T_{f} *for* $P_{\mathrm{f}} < P_{\mathrm{d}}$ *and a decreasing function for* $P_{\mathrm{f}} > P_{\mathrm{d}}$.
- *It takes values between* $\Pr\{\mathcal{H}_1|\hat{\mathcal{H}}_0\}$ *and* $\Pr\{\mathcal{H}_1\}$.

Proof: See Appendix H.

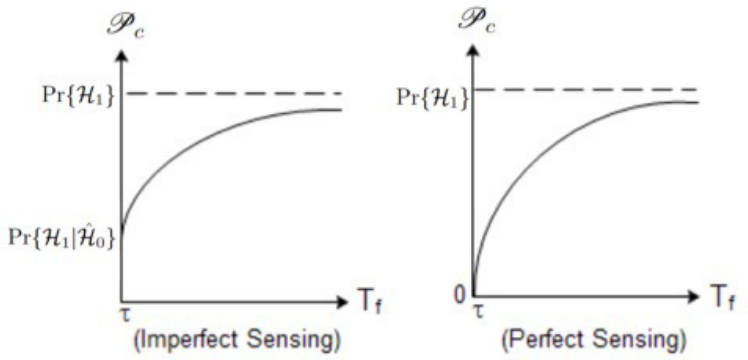

Figure 5.2: Average collision duration vs. frame duration T_{f} in the cases of imperfect sensing and perfect sensing.

In Fig. 5.2, we illustrate $\mathscr{P}_c$ as a function of the frame duration T_{f} when $P_{\mathrm{f}} < P_{\mathrm{d}}$, i.e., correct detection probability is greater than the false alarm probability. Note that this is generally the desired case in practice in which the probability of detection is expected to be greater than 0.5 and the probability of false alarm be less than 0.5 for reliable sensing performance. In the figure, both imperfect sensing and perfect sensing are considered. For the case of imperfect sensing, $\mathscr{P}_c$ takes values between $\Pr\{\mathcal{H}_1|\hat{\mathcal{H}}_0\}$ and $\Pr\{\mathcal{H}_1\}$. For perfect sensing, $\mathscr{P}_c$ is first 0 since $\Pr\{\mathcal{H}_1|\hat{\mathcal{H}}_0\} = 0$, which corresponds to no collision event initially, as expected, and then $\mathscr{P}_c$ starts to increase with increasing T_{f} as it becomes more likely that the primary user initiates a transmission and secondary users collide with the primary users.

5.2 Energy-Efficient Optimal Power Control and Frame Duration

5.2.1 Average Transmit Power and Average Interference Power Constraints

In this subsection, we determine the optimal power control policy and frame duration that maximize the EE of the secondary users operating subject to average transmit power, average interference power and collision constraints in the presence of sensing uncertainty and unslotted primary users. The optimization problem can be formulated as

$$\max_{T_{\mathrm{f}},P(g,h)} \eta_{EE} = \frac{R_{\mathrm{avg}}}{\left(\frac{T_{\mathrm{f}}-\tau}{T_{\mathrm{f}}}\right)P(\hat{\mathcal{H}}_0)\mathbb{E}\{P(g,h)\}+P_{c_r}} \tag{5.11}$$

$$\text{subject to} \quad \mathscr{P}_c \leq \mathscr{P}_{c,max} \tag{5.12}$$

$$\left(\frac{T_{\mathrm{f}}-\tau}{T_{\mathrm{f}}}\right)\Pr\{\hat{\mathcal{H}}_0\}\mathbb{E}\big\{P(g,h)\big\} \leq P_{\mathrm{avg}} \tag{5.13}$$

$$\left(\frac{T_{\mathrm{f}}-\tau}{T_{\mathrm{f}}}\right)\mathscr{P}_c\Pr\{\hat{\mathcal{H}}_0\}\mathbb{E}\big\{P(g,h)|g|^2\big\} \leq Q_{\mathrm{avg}} \tag{5.14}$$

$$P(g,h) \geq 0 \tag{5.15}$$

$$T_{\mathrm{f}} \geq \tau, \tag{5.16}$$

where the EE in the objective function is defined as the ratio of average throughput of the secondary users to the total power consumption, including average transmission power and circuit power, denoted by P_{c_r}. Above, $P(g,h)$ denotes the instantaneous transmission power as a function of the channel fading coefficient g of the interference link between the secondary transmitter and the primary receiver, and the channel fading coefficient h of the transmission link between the secondary transmitter and the secondary receiver. The average transmission

rate expression, R_{avg} is given by

$$R_{\text{avg}} = \Big(\frac{T_{\text{f}}-\tau}{T_{\text{f}}}\Big)\mathbb{E}\Big\{ \Pr\{\mathcal{H}_0\}(1-P_{\text{f}})\Big[\log_2\Big(1+\frac{P(g,h)|h|^2}{N_0}\Big)(1-\mathscr{P}_{c,0})+\log_2\Big(1+\frac{P(g,h)|h|^2}{N_0+\sigma_s^2}\Big)\mathscr{P}_{c,0}\Big] + \Pr\{\mathcal{H}_1\}(1-P_{\text{d}})\Big[\log_2\Big(1+\frac{P(g,h)|h|^2}{N_0}\Big)(1-\mathscr{P}_{c,1})+\log_2\Big(1+\frac{P(g,h)|h|^2}{N_0+\sigma_s^2}\Big)\mathscr{P}_{c,1}\Big]\Big\}, \tag{5.17}$$

where N_0 and σ_s^2 represent the variances of the additive Gaussian noise and primary user's received faded signal, respectively. It is assumed that the secondary transmitter has perfect channel side information (CSI), i.e., perfectly knows the values of g and h. While the assumption of perfect CSI is idealistic, channel knowledge can be obtained rather accurately if the mobility in the environment and channel variations are relatively slow. More specifically, secondary transmitter can acquire channel knowledge once the secondary receiver learns the channel and sends this information via an error-free feedback link. Also, the knowledge of the interference link, g, can be obtained through direct feedback from the primary receiver [57], indirect feedback from a third party such as a band manager [58] or by periodically sensing the pilot symbols sent by the primary receiver under the assumption of channel reciprocity [59].

In (5.12), $\mathscr{P}_{c,max}$ denotes the maximum tolerable collision duration ratio, which needs to be greater than $P(\mathcal{H}_1|\hat{\mathcal{H}}_0)$ based on Proposition 5.1.1 because, otherwise, the constraint cannot be satisfied. Since $\mathscr{P}_c$ is an increasing function of T_{f} when $P_{\text{f}} < P_{\text{d}}$, the collision constraint in (5.12) provides an upper bound on the frame duration T_{f} as follows:

$$T_{\text{f}} \leq \mathscr{P}_c^{-1}(\mathscr{P}_{c,max}). \tag{5.18}$$

Above, $\mathscr{P}_c^{-1}(.)$ is the inverse function of $\mathscr{P}_c$. In addition to the collision constraint in (5.12), we consider an average transmit power constraint in (5.13), where P_{avg} denotes the maximum average transmit power of the secondary transmitter. Also, in order to satisfy the long-term QoS requirements of the primary users, we further impose an interference power constraint in (5.14), where Q_{avg} represents the average received interference power limit at the primary

receiver.

As the frame duration increases, the secondary users have more time for data transmission, which leads to higher throughput, consequently higher EE. On the other hand, the primary user is more likely to become active with increasing transmission duration. In this case, the secondary users may collide with the primary transmission more frequently, which reduces the throughput, and hence EE. Therefore, there indeed exists an optimal frame duration that achieves the best tradeoff between the EE of the secondary users and collisions with the primary users. It can be easily verified that the EE is not a concave function of the frame duration T_{f} since the second derivative of the EE with respect T_{f} is less than, greater than or equal to zero depending on the values of the sensing parameters and prior probabilities of primary user being active and idle. However, the optimal frame duration which maximizes the EE can easily be obtained using a one-dimensional exhaustive search within the interval $(\tau, \mathscr{P}_c^{-1}(\mathscr{P}_{c,max})]$. For a given frame duration, we derive the optimal power control policy in the following result.

Theorem 5.2.1 *The optimal power control that maximizes the EE of the secondary users operating subject to the average transmit power constraint in (5.13) and average interference power constraint in (5.14) in the presence of sensing errors and unslotted primary users is given by*

$$P_{opt}(g,h) = \left[\frac{A_0 + \sqrt{\Delta_0}}{2}\right]^+ \tag{5.19}$$

$$\text{where } A_0 = \frac{\log_2(e)}{(\alpha+\lambda)+\nu\mathscr{P}_c|g|^2} - \frac{2N_0+\sigma_s^2}{|h|^2} \tag{5.20}$$

$$\Delta_0 = A_0^2 - \frac{4}{|h|^2}\left(\frac{N_0(N_0+\sigma_s^2)}{|h|^2} - \frac{\log_2(e)(N_0+(1-\mathscr{P}_c)\sigma_s^2)}{(\alpha+\lambda)+\nu\mathscr{P}_c|g|^2}\right). \tag{5.21}$$

Above, $(x)^+ = \max\{0, x\}$ *and* α *is a nonnegative parameter. Morever,* λ *and* ν *are the Lagrange multipliers which can be jointly obtained by inserting the above optimal power control into the constraints in (5.13) and (5.14), respectively.*

Table 5.1

Algorithm 5 The optimal power control and frame duration algorithm that maximizes the EE of the secondary users under the average transmit power, average interference power, and collision constraints

Initialize $P_{\mathrm{d}} = \mathscr{P}_{\mathrm{d,init}}$, $P_{\mathrm{f}} = \mathscr{P}_{\mathrm{f,init}}$, $\epsilon > 0$, $\delta > 0$, $t > 0$, $\alpha^{(0)} = \alpha_{\mathrm{init}}$, $\lambda^{(0)} = \lambda_{\mathrm{init}}$, $\nu^{(0)} = \nu_{\mathrm{init}}$, $\mathscr{P}_{c,max} = \mathscr{P}_{c,max,\mathrm{init}}$
if $\mathscr{P}_{c,max} < \Pr\{\mathcal{H}_1|\hat{\mathcal{H}}_0\}$ **then**
  $T_{\mathrm{f,opt}} = 0, P_{\mathrm{opt}}(g,h) = 0$
else
  $k \leftarrow 0$
  repeat
    $n \leftarrow 0$
    repeat
      calculate $P_{\mathrm{opt}}(g,h)$ using (8.31);
      update λ and ν using subgradient method as follows:
      $\lambda^{(n+1)} = \Big(\lambda^{(n)} - t\Big(P_{\mathrm{avg}} - \Big(\frac{T_{\mathrm{f}}-\tau}{T_{\mathrm{f}}}\Big)\Pr\{\hat{\mathcal{H}}_0\}\mathbb{E}\big\{P_{\mathrm{opt}}(g,h)\big\}\Big)\Big)^{+}$
      $\nu^{(n+1)} = \Big(\nu^{(n)} - t\Big(Q_{\mathrm{avg}} - \Big(\frac{T_{\mathrm{f}}-\tau}{T_{\mathrm{f}}}\Big)\mathscr{P}_c\Pr\{\hat{\mathcal{H}}_0\}\mathbb{E}\big\{P_{\mathrm{opt}}(g,h)|g|^2\big\}\Big)\Big)^{+}$
      $n \leftarrow n+1$
    until $\Big|\lambda^{(n)}\Big(P_{\mathrm{avg}} - \Big(\frac{T_{\mathrm{f}}-\tau}{T_{\mathrm{f}}}\Big)\Pr\{\hat{\mathcal{H}}_0\}\mathbb{E}\big\{P_{\mathrm{opt}}(g,h)\big\}\Big)\Big| \le \delta$ and $\Big|\nu^{(n)}\Big(Q_{\mathrm{avg}} - \Big(\frac{T_{\mathrm{f}}-\tau}{T_{\mathrm{f}}}\Big)\mathscr{P}_c\Pr\{\hat{\mathcal{H}}_0\}\mathbb{E}\big\{P_{\mathrm{opt}}(g,h)|g|^2\big\}\Big)\Big| \le \delta$
    $\alpha^{(k+1)} = \frac{R_{\mathrm{avg}}}{\Big(\frac{T_{\mathrm{f}}-\tau}{T_{\mathrm{f}}}\Big)\Pr\{\hat{\mathcal{H}}_0\}\mathbb{E}\{P_{\mathrm{opt}}(g,h)\}+P_{c_r}}$
    $k \leftarrow k+1$
  until $|F(\alpha^{(k)})| \le \epsilon$
  $\eta_{EE} = \alpha^{(k)}$
  $T_{\mathrm{f,opt}} = \arg\max \eta_{EE}$ by bisection search
  $P^{*}_{\mathrm{opt}}(g,h) = [P_{\mathrm{opt}}(g,h)]_{T_{\mathrm{f}}=T_{\mathrm{f,opt}}}$
end if

Proof: See Appendix I.

The values of λ and ν can be obtained numerically via the projected subgradient method. In this method, λ and ν are updated iteratively in the direction of a negative subgradient of the Lagrangian function $\mathcal{L}(P(g,h),\lambda,\nu,\alpha)$ (given in (I.5) in Appendix I) until convergence

as follows:

$$\lambda^{(n+1)} = \Big(\lambda^{(n)} - t\Big(P_{\text{avg}} - \Big(\frac{T_{\text{f}} - \tau}{T_{\text{f}}}\Big) \Pr\{\hat{\mathcal{H}}_0\}\mathbb{E}\big\{P(g,h)\big\}\Big)\Big)^{+} \tag{5.22}$$

$$\nu^{(n+1)} = \Big(\nu^{(n)} - t\Big(Q_{\text{avg}} - \Big(\frac{T_{\text{f}} - \tau}{T_{\text{f}}}\Big) \mathscr{P}_c \Pr\{\hat{\mathcal{H}}_0\}\mathbb{E}\big\{P(g,h)|g|^2\big\}\Big)\Big)^{+}, \tag{5.23}$$

where n is the iteration index and t is the step size. For a constant t, λ and ν are shown to converge to the optimal values within a small range [60].

In Table 5.1, we provide our low-complexity algorithm for jointly finding the optimal power control policy and frame duration, which maximize the EE of the secondary users in the presence of unslotted primary users and imperfect sensing decisions. In the table, for a given value of α and frame duration T_{f}, the optimal power control is obtained when $F(\alpha) \leq \epsilon$ is satisfied, where $F(\alpha)$ is defined in (I.4) in Appendix I and α is a nonnegative parameter. The solution is optimal if $F(\alpha) = 0$, otherwise ϵ-optimal solution is obtained.

Remark 5.2.1 *The optimal power control policy in (8.31) is a decreasing function of average collision duration ratio, $\mathscr{P}_c$. In particular, when the secondary users have higher $\mathscr{P}_c$, less power is allocated in order to limit the interference inflicted on the primary user transmission. Also, the proposed power control policy depends on sensing performance through $\mathscr{P}_c$, which is a function of detection and false alarm probabilities, P_{d} and P_{f}, respectively.*

Remark 5.2.2 *By setting $\alpha = 0$ in (I.1) in Appendix I, the optimization problem becomes*

$$\max_{P(g,h)\geq 0} R_{avg} \tag{5.24}$$

which corresponds to the throughput maximization problem. Therefore, solving the above optimization problem or equivalently inserting $\alpha = 0$ into the proposed scheme in (8.31), we can readily obtain the optimal power control strategy that maximizes the average throughput of secondary users in the presence of unslotted primary users.

Remark 5.2.3 *By inserting $\alpha = 0$, $\mathscr{P}_{c,0} = 0$ and $\mathscr{P}_{c,1} = 1$ into (8.31), we can see that*

the optimal power control scheme has a similar structure to the scheme that maximizes the throughput of secondary users operating over a single frequency band given in [75, eq. (36)], where it is assumed that the primary users do not change their activity during the entire frame duration of the secondary users, i.e., a time-slotted transmission scheme. Hence, our results can be specialized to the time-slotted case by setting $\mathscr{P}_{c,0}$ and $\mathscr{P}_{c,1}$ equal to 0 and 1, respectively.

5.2.2 Peak Transmit Power and Average Interference Power Constraints

In this subsection, we consider that the secondary user transmission is subject to peak transmit power and average interference power constraints. Under these assumptions, the optimization problem can be expressed as

$$\max_{T_{\mathrm{f}},P(g,h)} \eta_{EE} = \frac{R_{\mathrm{avg}}}{\left(\frac{T_{\mathrm{f}}-\tau}{T_{\mathrm{f}}}\right)\Pr\{\hat{\mathcal{H}}_0\}\mathbb{E}\{P(g,h)\} + P_{c_r}} \tag{5.25}$$

$$\text{subject to } \mathscr{P}_c \leq \mathscr{P}_{c,max} \tag{5.26}$$

$$P(g,h) \leq P_{\mathrm{pk}} \tag{5.27}$$

$$\left(\frac{T_{\mathrm{f}}-\tau}{T_{\mathrm{f}}}\right)\mathscr{P}_c \Pr\{\hat{\mathcal{H}}_0\}\mathbb{E}\left\{P(g,h)|g|^2\right\} \leq Q_{\mathrm{avg}} \tag{5.28}$$

$$P(g,h) \geq 0 \tag{5.29}$$

$$T_{\mathrm{f}} \geq \tau, \tag{5.30}$$

where P_{pk} represents the peak transmit power limit at the secondary transmitter. Subsequently, the optimal power control policy is determined in the following result.

Theorem 5.2.2 *For a given frame duration T_{f}, the optimal power control scheme subject to*

the constraints in (5.27) – (5.30) is obtained as

$$P_{opt}(g,h) = \min\left\{\left[\frac{A_1+\sqrt{\Delta_1}}{2}\right]^+, P_{\rm pk}\right\} \tag{5.31}$$

$$\textit{where } A_1 = \frac{\log_2(e)}{\alpha+\mu\mathscr{P}_c|g|^2} - \frac{2N_0+\sigma_s^2}{|h|^2} \tag{5.32}$$

$$\Delta_1 = A_1^2 - \frac{4}{|h|^2}\left(\frac{N_0(N_0+\sigma_s^2)}{|h|^2} - \frac{\log_2(e)(N_0+(1-\mathscr{P}_c)\sigma_s^2)}{\alpha+\mu\mathscr{P}_c|g|^2}\right). \tag{5.33}$$

Above, μ is the Lagrange multiplier associated with the average interference power constraint in (5.28).

Since we follow similar steps as in the proof of Theorem 5.2.1, the proof is omitted for the sake of brevity.

Remark 5.2.4 *Different from the optimal power control strategy in Theorem 5.2.1, the instantaneous transmission power level in (5.31) is limited by $P_{\rm pk}$ due to the peak transmit power constraint, which imposes stricter limitations than the average transmit power constraint.*

Remark 5.2.5 *Setting $\alpha = 0$ in (5.31), we obtain the optimal power control strategy which maximizes the throughput of secondary users with unslotted primary users, which is in agreement with the result derived in [76].*

Algorithm 1 can be easily modified to maximize the EE of the secondary users under peak transmit power and average interference constraints by calculating the power level, $P_{\rm opt}(g,h)$ through the expression in (5.31) and updating the Lagrange multiplier μ similarly as in (5.23).

5.3 Spectrally-Efficient Optimal Power Control and Frame Duration with a Minimum EE Constraint

5.3.1 Average Transmit Power and Average Interference Power Constraints

In this subsection, we analyze the EE-SE tradeoff by formulating the optimal power control problem to maximize the average throughput of the secondary users subject to a minimum EE constraint, and average transmit power, average interference power and collision constraints. The optimization problem is formulated as follows:

$$\max_{T_{\rm f}\geq\tau, P(g,h)\geq 0} R_{\rm avg} \tag{5.34}$$

$$\text{subject to } \mathscr{P}_c \leq \mathscr{P}_{c,max} \tag{5.35}$$

$$\frac{R_{\rm avg}}{\left(\frac{T_{\rm f}-\tau}{T_{\rm f}}\right)\Pr\{\hat{\mathcal{H}}_0\}\mathbb{E}\{P(g,h)\}+P_{c_r}} \geq \mathrm{EE}_{\min} \tag{5.36}$$

$$\left(\frac{T_{\rm f}-\tau}{T_{\rm f}}\right)\mathscr{P}_c\Pr\{\hat{\mathcal{H}}_0\}\mathbb{E}\big\{P(g,h)|g|^2\big\} \leq Q_{\rm avg} \tag{5.37}$$

$$\left(\frac{T_{\rm f}-\tau}{T_{\rm f}}\right)\Pr\{\hat{\mathcal{H}}_0\}\mathbb{E}\big\{P(g,h)\big\} \leq P_{\rm avg}, \tag{5.38}$$

where $\mathrm{EE}_{\min}$ denotes the minimum required EE. The optimal power control is determined in two steps. In the first step, we determine the average power level at which the required minimum EE is achieved. In the second step, we optimally allocate the transmission power in order to maximize the average throughput of the secondary users by combining the power level obtained in the first step under average transmit power and average interference power constraints. In this regard, we first provide the following result.

Proposition 5.3.1 *For a given frame duration $T_{\rm f}$, the average power level that satisfies the*

minimum required EE can be obtained as

$$P^*_{avg} = \Big(\frac{T_{\rm f}-\tau}{T_{\rm f}}\Big)\Pr\{\hat{\mathcal{H}}_0\}\mathbb{E}\big\{P^*(g,h)\big\} \tag{5.39}$$

and $P^*(g,h)$ *is given by*

$$P^*(g,h) = \left[\frac{A_3+\sqrt{\Delta_3}}{2}\right]^+, \tag{5.40}$$

$$\textit{where } A_3 = \frac{(1+\eta)\log_2(e)}{\eta EE_{min}} - \frac{2N_0+\sigma_s^2}{|h|^2} \tag{5.41}$$

$$\Delta_3 = A_3^2 - \frac{4}{|h|^2}\left(\frac{N_0(N_0+\sigma_s^2)}{|h|^2} - \frac{(1+\eta)\log_2(e)(N_0+(1-\Pr\{\hat{\mathcal{H}}_0\}\mathscr{P}_c)\sigma_s^2)}{\eta EE_{min}}\right). \tag{5.42}$$

The optimal value of η *can be found by solving the equation below:*

$$R_{avg} + \eta\left(\Big(\frac{T_{\rm f}-\tau}{T_{\rm f}}\Big)\Pr\{\hat{\mathcal{H}}_0\}\mathbb{E}\big\{P^*(g,h)\big\}\right) = 0. \tag{5.43}$$

Proof: See Appendix J.

Using the results in Proposition 5.3.1, the throughput optimization problem subject to the minimum EE constraint is equivalent to the throughput maximization under an average power constraint with the power limit, $P^*_{\rm avg}$, which achieves the minimum required EE. By combining this power limit with the average transmit power constraint in (5.38), we define the operating average transmission power as follows:

$$P_{op} = \begin{cases} P^*_{\rm avg} & \text{if } P_{\rm avg} \geq P^*_{\rm avg} \\ P_{\rm avg} & \text{if } P_{\rm avg} < P^*_{\rm avg} \\ & \text{and } \eta_{EE}\big|_{\text{s.t.(5.13) and (5.14)}} \geq \text{EE}_{\min} \\ 0 & \text{if } P_{\rm avg} < P^*_{\rm avg} \\ & \text{and } \eta_{EE}\big|_{\text{s.t.(5.13) and (5.14)}} < \text{EE}_{\min} \end{cases} \tag{5.44}$$

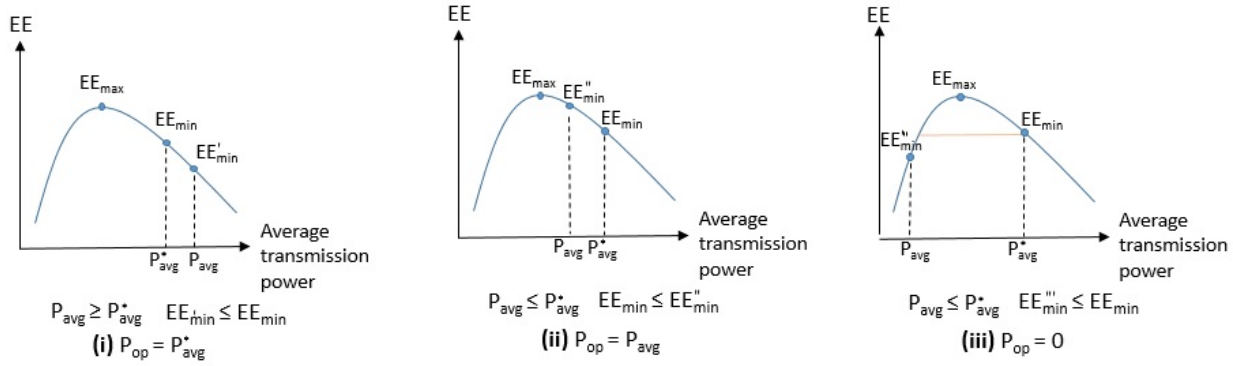

Figure 5.3: The operating average transmission power for three cases.

The operating average transmission power is determined according to three cases as illustrated in Fig. 5.3.

Case (i): When P_{avg} is larger than P^*_{avg}, average transmit power constraint P_{avg} is loose. Since operating at average transmission power level greater than P^*_{avg} violates the minimum required EE constraint, we set $P_{op} = P^*_{\text{avg}}$ and the optimal transmission power control policy is obtained by satisfying P^*_{avg} with equality. This case is illustrated in Fig. 5.3.(i).

Case (ii): As shown in Fig. 5.3.(ii), when P_{avg} is less than P^*_{avg} and the EE achieved at P_{avg} is greater than EE_{min}, average transmit power constraint P_{avg} is dominant. Since average transmission power is limited by P_{avg}, we set $P_{op} = P_{\text{avg}}$ and the optimal transmission power control policy is found when P_{avg} is satisfied with equality.

Case (iii): As demonstrated in Fig. 5.3.(iii), when $P_{\text{avg}} < P^*_{\text{avg}}$ and the EE achieved at P_{avg} is less than EE_{min}, there is no feasible solution, and hence we set $P_{op} = 0$

In the following result, we identify the optimal power control strategy.

Theorem 5.3.1 *For a given frame duration T_{f}, if $P_{avg} < P^*_{avg}$ and the maximum EE subject to the constraints in (5.13) and (5.14) is less than EE_{min}, the power level is set to zero, i.e., $P^*_0(g,h) = 0$, otherwise we allocate the power according to*

$$P_{opt}(g,h) = \left[\frac{A_4 + \sqrt{\Delta_4}}{2}\right]^+ \tag{5.45}$$

Table 5.2

Algorithm 6 The optimal power control and frame duration algorithm that maximizes the average throughput of the secondary users under the minimum EE, average transmit power, average interference power, and collision constraints

For a given P_{d}, P_{f}, $\mathscr{P}_{c,max}$, $\mathrm{EE}_{\min}$, initialize $\eta^{(0)} = \eta_{\mathrm{init}}$, $\vartheta^{(0)} = \vartheta_{\mathrm{init}}$, $\varphi^{(0)} = \varphi_{\mathrm{init}}$
if $\mathscr{P}_{c,max} < \Pr\{\mathcal{H}_1|\hat{\mathcal{H}}_0\}$ **then**
  $T_{\mathrm{f,opt}} = 0, P_{\mathrm{opt}}(g,h) = 0$
else
  Find the optimal value of η that solves (5.43) by using a root-finding function.
  Calculate $P^*_{\mathrm{avg}} = \left(\frac{T_{\mathrm{f}}-\tau}{T_{\mathrm{f}}}\right) P(\hat{\mathcal{H}}_0)\mathbb{E}\{P^*(g,h)\}$ where $P^*(g,h)$ is given in (5.40).
  if $P_{\mathrm{avg}} < P^*_{\mathrm{avg}}$ and $\eta_{EE}|_{\text{s.t.(5.13) and (5.14)}} < \mathrm{EE}_{\min}$ **then**
    $P_{\mathrm{opt}}(g,h) = 0$
  else
    $P_{op} = \min(P_{\mathrm{avg}}, P^*_{\mathrm{avg}})$ and calculate $P_{\mathrm{opt}}(g,h)$ using (5.45)
    Update ϑ and φ using subgradient method
  end if
  Calculate R_{avg} using (5.17)
  $T_{\mathrm{f,opt}} = \arg\max R_{\mathrm{avg}}$ by bisection search
  $P^*_{\mathrm{opt}}(g,h) = [P_{\mathrm{opt}}(g,h)]_{T_{\mathrm{f}}=T_{\mathrm{f,opt}}}$
end if

$$\textit{where } A_4 = \frac{\log_2(e)}{\vartheta + \varphi\mathscr{P}_c|g|^2} - \frac{2N_0 + \sigma_s^2}{|h|^2} \tag{5.46}$$

$$\Delta_4 = A_4^2 - \frac{4}{|h|^2}\left(\frac{N_0(N_0+\sigma_s^2)}{|h|^2} - \frac{\log_2(e)(N_0 + (1-\mathscr{P}_c)\sigma_s^2)}{\vartheta + \varphi\mathscr{P}_c|g|^2}\right). \tag{5.47}$$

Above, ϑ and φ are the Lagrange multipliers associated with the average transmit power constraint, $\min(P_{avg}, P^*_{avg})$ *and interference power constraint in (5.37), respectively.*

Proof: See Appendix K.

In Table 5.2, we provide the details of an algorithm for jointly finding the optimal power control policy and frame duration that maximize the average throughput of the secondary users subject to constraints on collision duration ratio, the minimum required EE, average transmit power and interference power in the presence of unslotted primary users.

5.3.2 Peak Transmit Power and Average Interference Power Constraints

In this subsection, we consider that the objective function in (5.34) is subject to the constraints in (5.35)- (5.37) and the peak transmit power constraint $P(g,h) < P_{pk}$ instead of the average transmit power constraint. In this case, we derive the optimal power control as follows:

Theorem 5.3.2 *The average power level at which the minimum required EE is achieved can be determined by inserting the power control given below in (5.48) into (8.50):*

$$P^*(g,h) = \left\{ \left[\frac{A_3 + \sqrt{\Delta_3}}{2} \right]^+, P_{\text{pk}} \right\}, \tag{5.48}$$

where A_3 and Δ_3 are given in (5.41) and (5.42), respectively. If the maximum EE at P_{pk} is less than EE_{min}, the power level is set to zero, i.e., $P_{opt}(g,h) = 0$, otherwise the optimal power control can be found as

$$P_{opt}(g,h) = \min \left\{ \left[\frac{A_4 + \sqrt{\Delta_4}}{2} \right]^+, P_{\text{pk}} \right\} \tag{5.49}$$

Above, A_4 and Δ_4 are given in (5.46) and (5.47), respectively.

Proof: We follow similar steps as in the proof of Proposition 5.3.1 and Theorem 4.2.3 with peak transmit power constraint in consideration. Therefore, the power levels are limited by P_{pk} in this case. □

5.4 Numerical Results

In this section, we present and discuss the numerical results for the optimal power control and frame duration, which maximize the EE or throughput of the secondary users, and analyze the resulting collisions with the unslotted primary users. Unless mentioned explicitly, the

noise variance is $N_0 = 0.01$ and the variance of primary user's received signal is $\sigma_s^2 = 0.1$. Also, the mean values of the durations of ON and OFF periods, denoted by λ_0 and λ_1, are set to 650 ms and 352 ms, respectively so that $\Pr\{\mathcal{H}_0\} \approx 0.65$, corresponding to the setting in the voice over Internet protocol (VoIP) traffic [77], [78]. The step size t and tolerance ϵ are chosen as 0.1 and 10^{-5}, respectively. The circuit power P_{c_r} is set to 1. We consider a Rayleigh fading environment, and hence the channel power gains of the transmission link and interference link are exponentially distributed with unit mean.

It is assumed that the secondary users employ energy detection scheme for spectrum sensing, and hence the probabilities of detection and false alarm are expressed, respectively as [79]

$$P_{\rm d} = \mathcal{Q}\bigg(\Big(\frac{\varepsilon}{N_0} - \sigma_s^2 - 1\Big)\sqrt{\frac{\tau f_s}{2\sigma^2 + 1}}\bigg) \tag{5.50}$$

$$P_{\rm f} = \mathcal{Q}\bigg(\Big(\frac{\varepsilon}{N_0} - 1\Big)\sqrt{\tau f_s}\bigg), \tag{5.51}$$

where $\mathcal{Q}(x) = \int_x^\infty \frac{1}{\sqrt{2\pi}} \mathrm{e}^{-t^2/2} dt$ is the Gaussian Q-function, ε represents the decision threshold and f_s denotes the sampling frequency. The decision threshold ε can be chosen to satisfy the target detection and false alarm probabilities, denoted by $\bar{P}_{\rm d}$ and $\bar{P}_{\rm f}$, respectively and the resulting sensing duration τ is expressed as

$$\tau = \frac{1}{f_s}\left(\frac{\mathcal{Q}^{-1}(\bar{P}_{\rm f}) - \sqrt{2\sigma_s^2 + 1}\mathcal{Q}^{-1}(\bar{P}_{\rm d})}{\sigma_s^2}\right)^2. \tag{5.52}$$

In the numerical computations, f_s is set to 100 kHz.

In Fig. 5.4, we plot the average throughput of the secondary users, $R_{\rm avg}$, as a function of the frame duration $T_{\rm f}$ for $P_{\rm pk} = 10$ dB and different average power constraints, namely $Q_{\rm avg} = -15$ dB, $Q_{\rm avg} = -10$ dB and $Q_{\rm avg} = 0$ dB. We consider target detection probability $\bar{P}_{\rm d} = 0.9$ and false alarm probability $\bar{P}_{\rm f} = 0.1$, and hence τ becomes 7.21 ms. Transmission power level is chosen according to $\min\left\{P_{\rm pk}, \left(\frac{T_{\rm f}}{T_{\rm f}-\tau}\right)\frac{Q_{\rm avg}}{\Pr\{\mathcal{H}_0,\hat{\mathcal{H}}_0\}\mathscr{P}_{c,0}+\Pr\{\mathcal{H}_1,\hat{\mathcal{H}}_0\}\mathscr{P}_{c,1}}\right\}$. In this

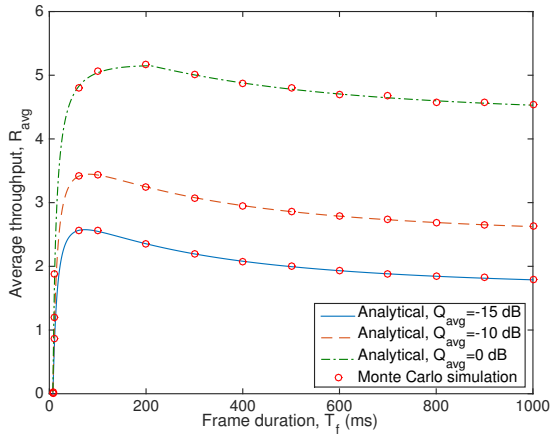

Figure 5.4: Average throughput of the secondary users, R_{avg} vs. frame duration, T_{f}.

setting, average throughput formulation in (5.17) is also verified through Monte Carlo simulations with 100000 runs. It is seen that R_{avg} initially increases with increasing transmission duration. After reaching a peak value, R_{avg} begins to diminish as the secondary user starts colliding with primary user transmissions more frequently, degrading the performance. It is also observed that as the interference power constraint gets looser, i.e., as Q_{avg} changes from -15 to 0 dB, higher throughput is achieved since secondary user transmits at higher power levels. As illustrated in the figure, R_{avg} is not a concave function of T_{f}. However, R_{avg} curves are seen to exhibit a quasiconcave property and there exists an optimal frame duration that maximizes the throughput.

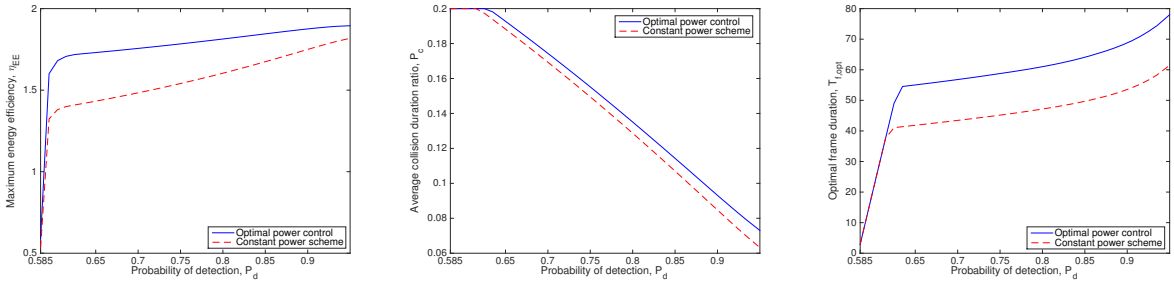

(a) (b) (c)

Figure 5.5: (a) Maximum EE of the secondary users vs. the probability of detection, P_{d} (b) Average collision duration ratio, $\mathscr{P}_c$ vs. P_{d} (c) Optimal frame duration, $T_{\text{f,opt}}$ vs. P_{d}.

In Fig. 5.5, we display the maximum EE η_{EE}, average collision duration ratio $\mathscr{P}_c$, and

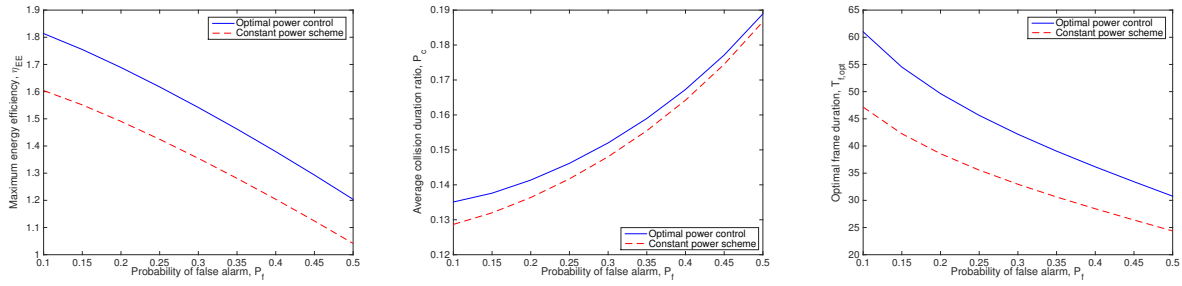

(a) (b) (c)

Figure 5.6: (a) Maximum EE of the secondary users vs. the probability of false alarm, $P_{\rm f}$ (b) Average collision duration ratio, $\mathscr{P}_c$ vs. $P_{\rm f}$ (c) Optimal frame duration, $T_{\rm f,opt}$ vs. $P_{\rm f}$.

the optimal frame duration $T_{\rm f,opt}$ as functions of the probability of detection $P_{\rm d}$. We set the maximum collision limit as $\mathscr{P}_{c,max} = 0.2$. It is assumed that the average transmit power constraint is $P_{\rm avg} = 10$ dB and average interference power constraint is $Q_{\rm avg} = -20$ dB. We consider both the transmission with the optimal power control policy and constant-power transmission. For the constant power case, power is not adaptively varied with respect to the channel power gains of the transmission link and interference link. On the other hand, optimal power control derived in (8.31) is a function of both h and g. As $\bar{P}_{\rm d}$ increases while keeping $\bar{P}_{\rm f}$ fixed at 0.1 and hence sensing performance improves, secondary user has a higher EE and lower collision duration ratio. For $P_{\rm d}$ values less than 0.585, collision constraint is not satisfied for any value of the frame duration $T_{\rm f}$, and therefore the secondary user throughput is 0. When $P_{\rm d}$ takes values between 0.585 and 0.6, maximum EE is achieved at the maximum collision limit, i.e, when $\mathscr{P}_c = 0.2$. It is also observed that the optimal power control leads transmissons with a larger frame duration while satisfying the maximum allowed collision limit and achieving a higher EE compared to constant-power transmissions.

In Fig. 5.6, we plot the maximum EE η_{EE}, average collision duration ratio $\mathscr{P}_c$, and the optimal frame duration $T_{\rm f,opt}$ as functions of the probability of false alarm $P_{\rm f}$. We consider the same setting as in the previous figure. It is seen that as $P_{\rm f}$ increases while keeping $P_{\rm d}$ fixed at 0.9, sensing performance degrades and secondary users experience more false alarm events, which leads to more collisions with the primary user transmission. Therefore,

secondary user has a lower EE in both cases of optimal power control and constant power. We also notice in Fig. 5.6(a) that the optimal power control outperforms constant-power transmissions.

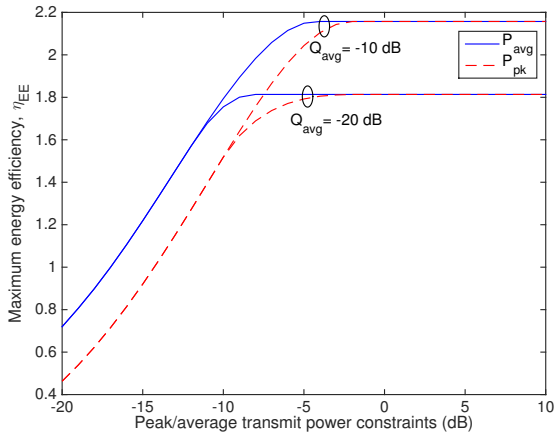

Figure 5.7: Maximum EE of the secondary users, η_{EE} vs. peak/average transmit power constraints.

The maximum EE, η_{EE}, as a function of peak/average transmit power constraints is illustrated in Fig. 5.7. Regarding the average interference constraint, we consider two scenarios: $Q_{\text{avg}} = -10$ dB and $Q_{\text{avg}} = -20$ dB. Target probabilities of detection and false alarm are set to 0.8 and 0.1, respectively, for which the corresponding sensing duration is 4.85 ms. In addition, the frame duration is selected to maximize the EE. It can be seen from the figure that for low values of P_{avg} and P_{pk}, average interference power constraints are loose, and hence the power is determined by either the average or peak transmit power constraint, which results in the same EE regardless of whether $Q_{\text{avg}} = -10$ dB or $Q_{\text{avg}} = -20$ dB. The EE of the secondary users increases with increasing peak/average transmit power levels. As expected, peak transmit power constraint yields lower EE compared to that achieved under the average transmit power constraint since the instantaneous transmission power is limited by P_{pk} under the peak transmit power constraint, which imposes stricter limitations than the average transmit power constraint. As the constraints become less stringent and the peak and average transmit power levels are further increased, the maximum EE levels off and becomes the same under peak/average transmit power constraints since the power

starts being allocated according to only the average interference constraint, Q_{avg}, due to this constraint being the dominant one.

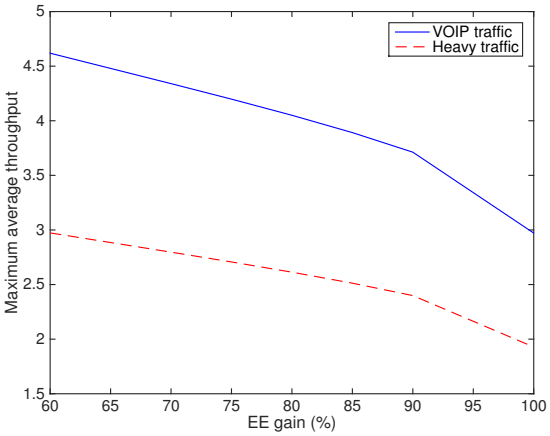

Figure 5.8: Maximum average throughput vs. EE gain.

In Fig. 5.8, we display the maximum average throughput as a function of the EE gain in percentage for different levels of primary traffic. More specifically, we consider a normal traffic load, i.e., VOIP traffic with $\lambda_0 = 650$ ms and $\lambda_1 = 352$ ms as assumed before, and also heavy traffic load with $\lambda_0 = 350$ ms and $\lambda_1 = 650$ ms so that $\Pr\{\mathcal{H}_0\} \approx 0.37$. It is assumed that $\mathscr{P}_{c,max} = 0.3$, average transmit power constraint is $P_{\text{avg}} = 0$ dB and average interference power constraint is $Q_{\text{avg}} = 10$ dB, and $\bar{P}_{\text{d}} = 0.8$, $\bar{P}_{\text{f}} = 0.1$, and hence $\tau = 4.85$ ms. The frame duration for normal traffic and heavy traffic are chosen optimally as $T_{\text{f}} = 125$ ms and $T_{\text{f}} = 36$ ms, respectively, in order to maximize the EE in each traffic model. The EE gain is calculated as the ratio of the minimum required EE, EE_{min}, to the maximum EE achieved with the proposed power control in (8.31). It is seen that a tradeoff between the EE and SE indeed exists, i.e., as the EE gain increases, the maximum average throughput of the secondary users decreases. We also note that the primary user with a heavy traffic load occupies the channel more often, and hence the secondary users have less opportunity to access the channel. In this heavy-load scenario, secondary users experience more frequent collisions with the primary user transmission. As a result, secondary users have lower throughput in the presence of heavy primary-user traffic compared to the case

with a normal primary-user traffic.

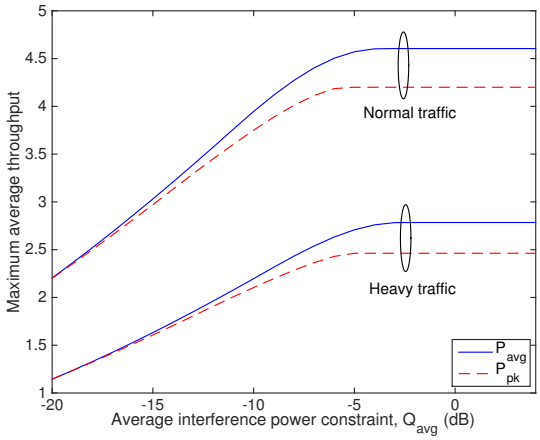

Figure 5.9: Maximum average throughput vs. average interference power constraint, Q_{avg} under a minimum EE constraint.

In Fig. 5.9, we display the maximum average throughput as a function of the average interference power constraint, Q_{avg}, under a minimum EE constraint, namely $\text{EE}_{\text{min}} = 1$ bit/joule in the presence of primary users with normal and heavy traffic loads. The frame duration is selected to maximize the system performance for each case. We assume imperfect spectrum sensing with $P_{\text{d}} = 0.8$ and set $P_{\text{f}} = 0.1$ and $P_{\text{avg}} = P_{\text{pk}} = 4$ dB, $\mathscr{P}_{c,max} = 0.3$. As Q_{avg} increases, the secondary users transmit with higher power levels, resulting in higher throughput. However, increasing Q_{avg} further than a certain threshold does not provide performance improvements since the power starts being limited by either P_{avg} or P_{pk}. In addition, secondary users have higher throughput with longer transmission duration when the primary user has a normal traffic load rather than a heavy one.

Chapter 6

Error Rate Analysis of Cognitive Radio Transmissions with Imperfect Channel Sensing

In this chapter, we analyze the symbol error rate performance of cognitive radio transmissions with channel sensing errors in the presence of Gaussian mixture distributed primary user's interference (which includes pure Gaussian as a special case). Two different transmission schemes, namely sensing-based spectrum sharing (SSS) and opportunistic spectrum access (OSA), are considered. Initially, for both transmission schemes, general formulations for the optimal decision rule and error probabilities are provided for arbitrary modulation schemes under the assumptions that the receiver is equipped with the sensing decision and perfect knowledge of the channel fading, and the primary user's received faded signals at the secondary receiver has a Gaussian mixture distribution. Subsequently, the general approach is specialized to rectangular quadrature amplitude modulation (QAM).

Section 6.1 introduces the system model. In Section 6.2, general formulations for the optimal detection rule and average symbol error probability in the presence of channel sensing errors are provided for SSS and OSA schemes. In Section 6.3, closed-form average symbol

error probability expressions for specific modulation types, i.e., arbitrary rectangular QAM and PAM are derived subject to both transmit power and interference constraints under the assumptions of Gaussian-mixture-distributed primary user faded signal and imperfect channel sensing decisions. Numerical results are provided and discussed in Section 6.4.

6.1 System Model

We consider a cognitive radio system consisting of a pair of secondary transmitter-receiver and a pair of primary transmitter-receiver[1]. The secondary user initially performs channel sensing to detect the primary user activity.

6.1.1 Power and Interference Constraints

Following channel sensing, the secondary transmitter performs data transmission over a flat-fading channel. In the SSS scheme, the average transmission power is selected depending on the channel sensing decision. More specifically, the average transmission power is P_1 if primary user activity is detected in the channel (denoted by the event $\hat{\mathcal{H}}_1$) whereas the average power is P_0 if no primary user transmissions are sensed (denoted by the event $\hat{\mathcal{H}}_0$). We assume that there is a peak constraint on these average power levels, i.e., we have

$$P_0 \leq P_{\text{pk}} \quad \text{and} \quad P_1 \leq P_{\text{pk}}, \tag{6.1}$$

where P_{pk} denotes the peak transmit power limit. We further impose an average interference constraint in the following form:

$$(1 - \mathscr{P}_{\text{d}})\, P_0\, \mathbb{E}\{|g|^2\} + \mathscr{P}_{\text{d}}\, P_1\, \mathbb{E}\{|g|^2\} \leq Q_{\text{avg}} \tag{6.2}$$

[1]The analysis in the this work can be extended to account for more than one primary transmitter-receiver pair by 1) slightly modifying the interference constraints to limit the worst-case interference on multiple primary receivers and 2) selecting a Gaussian mixture density that reflects the distribution of the received faded sum signal of multiple primary transmitters.

where $\mathscr{P}_{\rm d}$ is the detection probability and g is the channel fading coefficient between the secondary transmitter and the primary receiver. Note that with probability $\mathscr{P}_{\rm d}$, primary user activity is correctly detected and primary receiver experiences average interference proportional to $P_1\mathbb{E}\{|g|^2\}$. On the other hand, with probability $(1-\mathscr{P}_{\rm d})$, miss-detections occur, secondary user transmits with power P_0, and primary receiver experiences average interference proportional to $P_0\mathbb{E}\{|g|^2\}$. Therefore, $Q_{\rm avg}$ can be regarded as a constraint on the average interference inflicted on the primary user[2].

In the OSA scheme, no transmission is allowed when the channel is detected as busy and hence, we set $P_1 = 0$. Now with the peak power and average interference constraints, we have

$$P_0 \leq P_{\rm pk} \quad \text{and} \quad (1-\mathscr{P}_{\rm d})\, P_0\, \mathbb{E}\{|g|^2\} \leq Q_{\rm avg} \tag{6.3}$$

which can be combined to write

$$P_0 \leq \min\left\{P_{\rm pk}, \frac{Q_{\rm avg}}{(1-\mathscr{P}_{\rm d})\mathbb{E}\{|g|^2\}}\right\}. \tag{6.4}$$

Above, we have introduced the average interference constraint. However, if the instantaneous value of the fading coefficient g is known at the secondary transmitter, then a peak interference constraint in the form

$$P_i|g|^2 \leq Q_{\rm pk} \tag{6.5}$$

for $i = 0, 1$ can be imposed. Note that transmission power P_0 in an idle-sensed channel is also required to satisfy the interference constraint due to sensing uncertainty (i.e., due to the consideration of miss-detection events). Hence, a rather strict form of interference control is

[2]Note that the rest of the analysis can easily be extended to the case of M primary receivers by replacing the constraint in (6.2) with $(1-\mathscr{P}_{\rm d})P_0 \max_{1\leq i\leq M}\mathbb{E}\{|g_i|^2\} + \mathscr{P}_{\rm d}P_1 \max_{1\leq i\leq M}\mathbb{E}\{|g_i|^2\} \leq Q_{\rm avg}$, where g_i is the channel fading coefficient between the secondary transmitter and the $i^{\rm th}$ primary receiver. In this setting, $Q_{\rm avg}$ effectively becomes a constraint on the worst-case average interference.

being addressed under these limitations. Now, including the peak power constraint, we have

$$P_i \leq \min\left\{P_{\text{pk}}, \frac{Q_{\text{pk}}}{|g|^2}\right\} \tag{6.6}$$

for $i = 0, 1$ (while keeping $P_1 = 0$ in the OSA scheme). Above, Q_{pk} denotes the peak received power limit at the primary receiver.

6.1.2 Cognitive Channel Model

As a result of channel sensing decisions and the true nature of primary user activity, we have four possible cases which are described below together with corresponding input-output relationships:

- *Case (I)*: A busy channel is sensed as busy, denoted by the joint event $(\mathcal{H}_1, \hat{\mathcal{H}}_1)$.

$$\text{(Correct detection)} \qquad y = hs + n + w. \tag{6.7}$$

- *Case (II)*: A busy channel is sensed as idle, denoted by the joint event $(\mathcal{H}_1, \hat{\mathcal{H}}_0)$.

$$\text{(Miss-detection)} \qquad y = hs + n + w. \tag{6.8}$$

- *Case (III)*: An idle channel is sensed as busy, denoted by the joint event $(\mathcal{H}_0, \hat{\mathcal{H}}_1)$.

$$\text{(False alarm)} \qquad y = hs + n. \tag{6.9}$$

- *Case (IV)*: An idle channel is sensed as idle, denoted by the joint event $(\mathcal{H}_0, \hat{\mathcal{H}}_0)$.

$$\text{(Correct detection)} \qquad y = hs + n. \tag{6.10}$$

In the above expressions, s is the transmitted signal, y is the received signal, and h denotes zero-mean, circularly-symmetric complex fading coefficient between the secondary transmitter and the secondary receiver with variance σ_h^2. n is the circularly-symmetric complex Gaussian noise with mean zero and variance $\mathbb{E}\{|n|^2\} = \sigma_n^2$, and hence has the pdf

$$f_n(n) = \frac{1}{2\pi\sigma_n^2} \mathrm{e}^{-\frac{|n|^2}{2\sigma_n^2}} = \frac{1}{2\pi\sigma_n^2} \mathrm{e}^{-\frac{n_r^2+n_i^2}{2\sigma_n^2}}. \tag{6.11}$$

The active primary user's received faded signal at the secondary receiver is denoted by w. Notice that if the primary users are active and hence the hypothesis $\mathcal{H}_1$ is true as in cases (I) and (II), the secondary receiver experiences interference from the primary user's transmission in the form of w. We assume that w has a Gaussian mixture distribution, i.e., its pdf is a weighted sum of p complex Gaussian distributions with zero mean and variance σ_l^2 for $1 \leq l \leq p$:

$$f_w(w) = \sum_{l=1}^{p} \frac{\lambda_l}{2\pi\sigma_l^2} \mathrm{e}^{-\frac{|w|^2}{2\sigma_l^2}} \tag{6.12}$$

where the weights λ_l satisfy $\sum_{l=1}^{p} \lambda_l = 1$ with $\lambda_l \geq 0$ for all l.

Remark 6.1.1 *Primary user's received faded signal has a Gaussian mixture distribution, if we, for instance, have*

$$w = h_{ps} u \tag{6.13}$$

where h_{ps}, which is the channel fading coefficient between the primary transmitter and the secondary receiver, is a circularly symmetric, complex, zero-mean, Gaussian random variable, and u is the primary user's modulated digital signal. Note that w is conditionally Gaussian given u. Now, assuming that the modulated signal u can take p different values with prior probabilities given by λ_l for $1 \leq l \leq p$, w has a Gaussian mixture distribution as

in (6.12). In the case of multiple primary transmitters for which we have

$$w = \sum_i h_{ps,i} u_i, \tag{6.14}$$

the above argument can easily be extended if all channel fading coefficients $\{h_{ps,i}\}$ *are zero-mean Gaussian distributed.*

Remark 6.1.2 *Gaussian mixture model is generally rich enough to accurately approximate a wide variety of density functions [80, Section 3.2]. This fact indicates that the applicability of our results can be extended to various other settings in which* w *has a distribution included in this class of densities. Additionally, in the special case of* $p = 1$*, the Gaussian mixture distribution becomes the pure complex Gaussian distribution. Hence, the results obtained for the Gaussian mixture distribution can readily be specialized to derive those for the Gaussian distributed* w *as well.*

As observed from the input-output relationships in (6.7)–(6.10), when the true state of the primary users is idle, corresponding to the cases (III) and (IV), the additive disturbance is simply the background noise n. On the other hand, in cases (I) and (II) in which the channel is actually busy, the additive disturbance becomes

$$z = n + w \qquad \text{if } \mathcal{H}_1 \text{ is true} \tag{6.15}$$

whose distribution can be obtained through the convolution of density functions of the background Gaussian noise n and the primary user's received faded signal w. Using the result of Gaussian convolution of Gaussian mixture given by [81], the distribution of z can be obtained as

$$f_z(z) = \sum_{l=1}^{p} \frac{\lambda_l}{2\pi(\sigma_l^2 + \sigma_n^2)} \mathrm{e}^{-\frac{|z|^2}{2(\sigma_l^2+\sigma_n^2)}}. \tag{6.16}$$

Note that z also has a Gaussian mixture distribution. Note further that the pdf of z can be expressed in terms of its real and imaginary components as

$$f_{z_r,z_i}(z_r,z_i)=\sum_{l=1}^{p}\frac{\lambda_l}{2\pi(\sigma_l^2+\sigma_n^2)}\mathrm{e}^{-\frac{(z_r+z_i)^2}{2(\sigma_l^2+\sigma_n^2)}}. \tag{6.17}$$

Moreover, the marginal distributions of each component are given by

$$f_{z_r}(z_r)=\sum_{l=1}^{p}\frac{\lambda_l}{\sqrt{2\pi(\sigma_l^2+\sigma_n^2)}}\mathrm{e}^{-\frac{z_r^2}{2(\sigma_l^2+\sigma_n^2)}}, \tag{6.18}$$

$$f_{z_i}(z_i)=\sum_{l=1}^{p}\frac{\lambda_l}{\sqrt{2\pi(\sigma_l^2+\sigma_n^2)}}\mathrm{e}^{-\frac{z_i^2}{2(\sigma_l^2+\sigma_n^2)}}. \tag{6.19}$$

It is easily seen that the pdf of z in (6.17) cannot be factorized into the product of the marginal pdf's of its real and imaginary parts $f_{z_r}(z_r)f_{z_i}(z_i)$, given in (6.18) and (6.19), respectively. Therefore, the real and imaginary parts of the additive disturbance z are dependent. When $p=1$, i.e., in the case of a pure Gaussian distribution, the joint distribution can written as a product of its real and imaginary components since they are independent.

6.2 General Formulations for the Optimal Decision Rule and Error Probabilities

In this section, we present the optimal decision rule and the average symbol error probability for the cognitive radio system in the presence of channel sensing errors. We provide general formulations applicable to any modulation type under SSS and OSA schemes. More specific analysis for arbitrary rectangular QAM and PAM is conducted in Section 6.3.

6.2.1 The Optimal Decision Rule

In the cognitive radio setting considered in this work, the optimal maximum *a posteriori* probability (MAP) decision rule given the sensing decision $\hat{\mathcal{H}}_k$ and the channel fading coef-

ficient h can be formulated for any arbitrary M-ary digital modulation as follows:

$$\hat{s} = \underset{0\le m\le M-1}{\arg\max}\ \Pr\{s_m|y,h,\hat{\mathcal{H}}_k\} \tag{6.20}$$

$$= \underset{0\le m\le M-1}{\arg\max}\ p_m f(y|s_m,h,\hat{\mathcal{H}}_k) \tag{6.21}$$

$$= \underset{0\le m\le M-1}{\arg\max}\ p_m\big(\Pr\{\mathcal{H}_0|\hat{\mathcal{H}}_k\}f(y|s_m,h,\hat{\mathcal{H}}_k,\mathcal{H}_0) + \Pr\{\mathcal{H}_1|\hat{\mathcal{H}}_k\}f(y|s_m,h,\hat{\mathcal{H}}_k,\mathcal{H}_1)\big), \tag{6.22}$$

where p_m is the prior probability of signal constellation point s_m and $k \in \{0,1\}$. Above, (6.21) follows from Bayes' rule and (6.22) is obtained by conditioning the density function on the hypotheses $\mathcal{H}_0$ and $\mathcal{H}_1$. Note that $f(y|s_m,h,\hat{\mathcal{H}}_k,\mathcal{H}_j)$ in (6.22) is the conditional distribution of the received real signal y given the transmitted signal s_m, channel fading coefficient h, channel sensing decision $\hat{\mathcal{H}}_k$, and true state of the channel $\mathcal{H}_j$, and can be expressed as

$$f(y|s_m,h,\hat{\mathcal{H}}_k,\mathcal{H}_j) = \begin{cases} \frac{1}{2\pi\sigma_n^2}\mathrm{e}^{-\frac{|y-s_m h|^2}{2\sigma_n^2}}, & j=0 \\ \sum_{l=1}^{p}\frac{\lambda_l}{2\pi(\sigma_l^2+\sigma_n^2)}\mathrm{e}^{-\frac{|y-s_m h|^2}{2(\sigma_l^2+\sigma_n^2)}}, & j=1 \end{cases} \tag{6.23}$$

for $m = 0,\ldots,M-1$. Note that the sensing decision $\hat{\mathcal{H}}_k$ affects the density function through the power of the transmitted signal s_m. Moreover, the conditional probabilities in (6.22) can be expressed as

$$\Pr\{\mathcal{H}_j|\hat{\mathcal{H}}_k\} = \frac{\Pr\{\mathcal{H}_j\}\Pr\{\hat{\mathcal{H}}_k|\mathcal{H}_j\}}{\sum_{j=0}^{1}\Pr\{\mathcal{H}_j\}\Pr\{\hat{\mathcal{H}}_k|\mathcal{H}_j\}} \quad j,k\in\{0,1\},$$

where $\Pr\{\mathcal{H}_0\}$ and $\Pr\{\mathcal{H}_1\}$ are the prior probabilities of the channel being idle and busy, respectively, and the conditional probabilities in the form $\Pr\{\hat{\mathcal{H}}_k|\mathcal{H}_j\}$ depend on the channel sensing performance, $\mathscr{P}_\mathrm{d} = \Pr\{\hat{\mathcal{H}}_1|\mathcal{H}_1\}$ is the detection probability and $\mathscr{P}_\mathrm{f} = \Pr\{\hat{\mathcal{H}}_1|\mathcal{H}_0\}$ is the false alarm probability. From these formulations, we see that the optimal decision rule

in general depends on the sensing reliability.

6.2.2 Average Symbol Error Probability

The average symbol error probability (SEP) for the MAP decision rule in (6.20) in the SSS scheme can be computed as

$$\begin{aligned}
\text{SEP} &= 1 - \sum_{m=0}^{M-1} p_m \Pr\{\hat{s} = s_m | s_m\} \\
&= 1 - \sum_{m=0}^{M-1} \sum_{k=0}^{1} p_m \Pr\{\hat{\mathcal{H}}_k\} \Pr\{\hat{s} = s_m | s_m, \hat{\mathcal{H}}_k\} \\
&= 1 - \sum_{m=0}^{M-1} \sum_{j,k=0}^{1} p_m \Pr\{\hat{\mathcal{H}}_k\} \Pr\{\mathcal{H}_j | \hat{\mathcal{H}}_k\} \Pr\{\hat{s} = s_m | s_m, \hat{\mathcal{H}}_k, \mathcal{H}_j\}.
\end{aligned} \tag{6.24}$$

The above average symbol error probability can further be expressed as

$$\begin{aligned}
\text{SEP} = 1 - \sum_{m=0}^{M-1} p_m \Bigg[& \Pr\{\hat{\mathcal{H}}_0\} \Bigg(\Pr\{\mathcal{H}_1 | \hat{\mathcal{H}}_0\} \int_{D_{m,0}} f(y | s_m, h, \hat{\mathcal{H}}_0, \mathcal{H}_1)\, dy \\
& \qquad + \Pr\{\mathcal{H}_0 | \hat{\mathcal{H}}_0\} \int_{D_{m,0}} f(y | s_m, h, \hat{\mathcal{H}}_0, \mathcal{H}_0)\, dy \Bigg) \\
& + \Pr\{\hat{\mathcal{H}}_1\} \Bigg(\Pr\{\mathcal{H}_1 | \hat{\mathcal{H}}_1\} \int_{D_{m,1}} f(y | s_m, h, \hat{\mathcal{H}}_1, \mathcal{H}_1)\, dy \\
& \qquad + \Pr\{\mathcal{H}_0 | \hat{\mathcal{H}}_1\} \int_{D_{m,1}} f(y | s_m, h, \hat{\mathcal{H}}_1, \mathcal{H}_0)\, dy \Bigg) \Bigg],
\end{aligned} \tag{6.25}$$

where $D_{m,0}$ and $D_{m,1}$ are the decision regions of each signal constellation point s_m for $0 \leq m \leq M-1$ when the channel is sensed to be idle and busy, respectively.

If cognitive user transmission is not allowed in the case of the channel being sensed as occupied by the primary users, we have the OSA scheme for which the average probability

of error can be expressed as

$$\begin{aligned}\text{SEP} &= 1 - \sum_{m=0}^{M-1}\sum_{j=0}^{1} p_m \Big(\Pr\{\mathcal{H}_j|\hat{\mathcal{H}}_0\} \Pr\{\hat{s} = s_m | s_m, \hat{\mathcal{H}}_0, \mathcal{H}_j\} \Big) \\ &= 1 - \sum_{m=0}^{M-1}\sum_{j=0}^{1} p_m \Big(\Pr\{\mathcal{H}_j|\hat{\mathcal{H}}_0\} \int_{D_{m,0}} f(y|s_m, h, \hat{\mathcal{H}}_0, \mathcal{H}_j) \Big).\end{aligned} \tag{6.26}$$

6.3 Error Rate Analysis for M-ary Rectangular QAM

In this section, we conduct a more detailed analysis by considering rectangular QAM transmissions to demonstrate the key tradeoffs in a lucid setting. Correspondingly, we determine the optimal decision regions by taking channel sensing errors into consideration and identify the error rates for SSS and OSA schemes. We derive closed-form minimum average symbol error probability expressions under the transmit power and interference constraints. Note that the results for QAM can readily be specialized for PAM, QPSK, and BPSK transmissions.

6.3.1 Optimal decision regions under channel sensing uncertainty

The signal constellation point $s_{n,q}$ in $M_I \times M_Q$ rectangular QAM signaling can be expressed in terms of its real and imaginary parts, respectively, as

$$s_{n,q} = s_n + j s_q, \tag{6.27}$$

where the amplitude level of each component is given by

$$s_n = (2n + 1 - M_I)\frac{d_{min,k}}{2} \quad \text{for} \quad n = 0, \ldots, M_I - 1, \tag{6.28}$$

$$s_q = (2q + 1 - M_Q)\frac{d_{min,k}}{2} \quad \text{for} \quad q = 0, \ldots, M_Q - 1. \tag{6.29}$$

Above, M_I and M_Q are the modulation size on the in-phase and quadrature components, respectively, and $d_{min,k}$ denotes the minimum distance between the signal constellation points and is given by

$$d_{min,k} = \sqrt{\frac{12P_k}{M_I^2 + M_Q^2 - 2}} \qquad k \in \{0, 1\} \tag{6.30}$$

where P_k is the transmission power under sensing decision $\hat{\mathcal{H}}_k$.

It is assumed that the fading realizations are perfectly known at the receiver. In this case, phase rotations caused by the fading can be offset by multiplying the channel output y with $\mathrm{e}^{-j\theta_h}$ where θ_h is the phase of the fading coefficient h. Hence, the modified received signal can be written in terms of its real and imaginary parts as follows:

$$\bar{y} = \bar{y}_r + j\bar{y}_i = y\mathrm{e}^{-j\theta_h} = \begin{cases} s_n|h| + \bar{n}_r + j(s_q|h| + \bar{n}_i), & \text{under } \mathcal{H}_0 \\ s_n|h| + \bar{n}_r + \bar{w}_r + j(s_q|h| + \bar{n}_i + \bar{w}_i), & \text{under } \mathcal{H}_1 \end{cases}$$

where the subscripts r and i are used to denote the real and imaginary components of the signal, respectively. Note that $\bar{n} = \bar{n}_r + j\bar{n}_i$ and $\bar{w} = \bar{w}_r + j\bar{w}_i$ have the same statistics as n and w, respectively, due to their property of being circularly symmetric. Hence, given the transmitted signal constellation point $s_{n,q}$, the distribution of the modified received signal $\bar{y}$ is given by

$$f_{\bar{y}_r,\bar{y}_i}(\bar{y}_r, \bar{y}_i | s_{n,q}, h, \hat{\mathcal{H}}_k, \mathcal{H}_j) = \begin{cases} \frac{1}{2\pi\sigma_n^2}\mathrm{e}^{-\frac{(\bar{y}_r - s_n|h|)^2 + (\bar{y}_i - s_q|h|)^2}{2\sigma_n^2}}, & j = 0 \\ \sum_{l=1}^{p} \frac{\lambda_l}{2\pi(\sigma_l^2 + \sigma_n^2)}\mathrm{e}^{-\frac{(\bar{y}_r - s_n|h|)^2 + (\bar{y}_i - s_q|h|)^2}{2(\sigma_l^2 + \sigma_n^2)}}, & j = 1 \end{cases}. \tag{6.31}$$

Moreover, the real and imaginary parts of noise, i.e., $\bar{n}_r$ and $\bar{n}_i$ are independent zero-mean Gaussian random variables, and the real and imaginary parts of primary users' faded signal, i.e., $\bar{w}_r$ and $\bar{w}_i$, are Gaussian mixture distributed random variables.

In the following, we characterize the decision regions of the optimal detection rule for

equiprobable QAM signaling in the presence of sensing uncertainty.

Proposition 6.3.1 *For cognitive radio transmissions with* equiprobable *rectangular M-QAM modulation (with constellation points expressed as in (6.27)–(6.29)) under channel sensing uncertainty in both SSS and OSA schemes, the optimal detection thresholds under any channel sensing decision are located midway between the received signal points. Hence, the optimal detector structure does not depend on the sensing decision.*

Proof: See Appendix L.

6.3.2 The average symbol error probability under channel sensing uncertainty

We present closed-form average symbol error probability expressions under both transmit power and interference constraints for SSS and OSA schemes. Initially, we express the error probabilities for a given value of the fading coefficient h. Subsequently, we address averaging over fading and also incorporate power and interference constraints. We note that in the presence of peak interference constraints, the transmitted power level depends on the fading coefficient g experienced in the channel between the secondary and primary users as seen in (6.6). Therefore, we in this case consider an additional averaging of the error rates with respect to g.

6.3.2.1 Sensing-based spectrum sharing (SSS) scheme

Under the optimal decision rule given in the previous subsection, the average symbol error probability of *equiprobable* signals for a given fading coefficient h can be expressed as

$$\mathrm{SEP}(P,h)=\sum_{m=1}^{M}\sum_{j,k=0}^{1}\frac{\Pr\{\hat{\mathcal{H}}_k\}}{M}\Pr\{\mathcal{H}_j|\hat{\mathcal{H}}_k\}\Pr\{e|s_{n,q},h,\hat{\mathcal{H}}_k,\mathcal{H}_j\}, \tag{6.32}$$

where $\Pr\{e|s_{n,q}, h, \mathcal{H}_j, \hat{\mathcal{H}}_k\}$ denotes the conditional error probability given the transmitted signal $s_{n,q}$, channel fading h, sensing decision $\hat{\mathcal{H}}_k$, and true state of the channel $\mathcal{H}_j$.

We can group the error patterns of rectangular M-QAM modulation into three categories. Specifically, the probability of error for the signal constellation points on the corners is equal due to the symmetry in signaling and detection. The same is also true for the points on the sides and the inner points.

The symbol error probability for the four corner points is given by

$$\begin{aligned}\mathrm{SEP}_{1,k}(P,h) = 1 - \int_{a_1}^{\infty}\int_{a_1}^{\infty} \big(&\Pr\{\mathcal{H}_0|\hat{\mathcal{H}}_k\} f_{n_r,n_i}(n_r,n_i) dn_r dn_i \\ &+ \Pr\{\mathcal{H}_1|\hat{\mathcal{H}}_k\} f_{z_r,z_i}(z_r,z_i) dz_r dz_i\big)\end{aligned} \tag{6.33}$$

where $a_1 = -\frac{d_{min,k}|h|}{2}$ and $k \in \{0,1\}$. The distributions of the Gaussian noise $f_{n_r,n_i}(n_r,n_i)$ and the primary user's interference signal plus noise $f_{z_r,z_i}(z_r,z_i)$ are given in (6.11) and (6.17), respectively. After evaluating the integrals, the above expression becomes

$$\begin{aligned}\mathrm{SEP}_{1,k}(P,h) =& \Pr\{\mathcal{H}_0|\hat{\mathcal{H}}_k\}\left\{2Q\left(\sqrt{\frac{d_{min,k}^2|h|^2}{4\sigma_n^2}}\right) - Q^2\left(\sqrt{\frac{d_{min,k}^2|h|^2}{4\sigma_n^2}}\right)\right\} \\ &+ \Pr\{\mathcal{H}_1|\hat{\mathcal{H}}_k\}\sum_{l=1}^{p}\lambda_l\left\{2Q\left(\sqrt{\frac{d_{min,k}^2|h|^2}{4(\sigma_l^2+\sigma_n^2)}}\right) - Q^2\left(\sqrt{\frac{d_{min,k}^2|h|^2}{4(\sigma_l^2+\sigma_n^2)}}\right)\right\}\end{aligned} \tag{6.34}$$

where $Q(x) = \int_x^{\infty}\frac{1}{\sqrt{2\pi}}e^{-t^2/2}dt$ is the Gaussian Q-function. For the $2(M_I + M_Q - 4)$ points on the sides, except the corner points, the symbol error probability is

$$\begin{aligned}\mathrm{SEP}_{2,k}(P,h) = 1 - \int_{a_1}^{\infty}\int_{a_1}^{a_2} \big(&\Pr\{\mathcal{H}_0|\hat{\mathcal{H}}_k\} f_{n_r,n_i}(n_r,n_i) dn_r dn_i \\ &+ \Pr\{\mathcal{H}_1|\hat{\mathcal{H}}_k\} f_{z_r,z_i}(z_r,z_i) dz_r dz_i\big)\end{aligned} \tag{6.35}$$

where $a_2 = \frac{d_{min,k}|h|}{2}$. After performing the integrations, we can express $\mathrm{SEP}_{2,k}(P,h)$ as

$$\begin{aligned}\mathrm{SEP}_{2,k}(P,h) =& \Pr\{\mathcal{H}_0|\hat{\mathcal{H}}_k\}\left\{3Q\left(\sqrt{\frac{d_{min,k}^2|h|^2}{4\sigma_n^2}}\right) - 2Q^2\left(\sqrt{\frac{d_{min,k}^2|h|^2}{4\sigma_n^2}}\right)\right\} \\ &+ \Pr\{\mathcal{H}_1|\hat{\mathcal{H}}_k\}\sum_{l=1}^{p}\lambda_l\left\{3Q\left(\sqrt{\frac{d_{min,k}^2|h|^2}{4(\sigma_l^2+\sigma_n^2)}}\right) - 2Q^2\left(\sqrt{\frac{d_{min,k}^2|h|^2}{4(\sigma_l^2+\sigma_n^2)}}\right)\right\}.\end{aligned} \tag{6.36}$$

Finally, the symbol error probability for $M-2(M_I+M_Q)+4$ inner points is obtained from

$$\begin{aligned}\mathrm{SEP}_{3,k}(P,h) = 1 - \int_{a_1}^{a_2}\int_{a_1}^{a_2} \big(&\Pr\{\mathcal{H}_0|\hat{\mathcal{H}}_k\} f_{n_r,n_i}(n_r,n_i) dn_r dn_i \\ &+ \Pr\{\mathcal{H}_1|\hat{\mathcal{H}}_k\} f_{z_r,z_i}(z_r,z_i) dz_r dz_i \big)\end{aligned} \tag{6.37}$$

which can be evaluated to obtain

$$\begin{aligned}\mathrm{SEP}_{3,k}(P,h) =& \Pr\{\mathcal{H}_0|\hat{\mathcal{H}}_k\}\left\{4Q\left(\sqrt{\frac{d^2_{min,k}|h|^2}{4\sigma_n^2}}\right) - 4Q^2\left(\sqrt{\frac{d^2_{min,k}|h|^2}{4\sigma_n^2}}\right)\right\} \\ &+ \Pr\{\mathcal{H}_1|\hat{\mathcal{H}}_k\}\sum_{l=1}^{p}\lambda_l\left\{4Q\left(\sqrt{\frac{d^2_{min,k}|h|^2}{4(\sigma_l^2+\sigma_n^2)}}\right) - 4Q^2\left(\sqrt{\frac{d^2_{min,k}|h|^2}{4(\sigma_l^2+\sigma_n^2)}}\right)\right\}.\end{aligned} \tag{6.38}$$

Overall, we can express $\mathrm{SEP}(P,h)$ in (6.32) by combining $\mathrm{SEP}_{1,k}(P,h)$, $\mathrm{SEP}_{2,k}(P,h)$ and $\mathrm{SEP}_{3,k}(P,h)$ as follows

$$\begin{aligned}\mathrm{SEP}(P,h) = \sum_{k=0}^{1}\frac{\Pr\{\hat{\mathcal{H}}_k\}}{M}\Big(&4\,\mathrm{SEP}_{1,k}(P,h) + 2(M_I+M_Q-4)\mathrm{SEP}_{2,k}(P,h) \\ &+ (M-2(M_I+M_Q)+4)\mathrm{SEP}_{3,k}(P,h)\Big).\end{aligned} \tag{6.39}$$

After rearranging the terms, the final expression for the average symbol error probability $\mathrm{SEP}(P,h)$ is given by

$$\begin{aligned}\mathrm{SEP}(P,h) = \sum_{k=0}^{1}\Pr\{\hat{\mathcal{H}}_k\}\Bigg\{ &\Pr\{\mathcal{H}_0|\hat{\mathcal{H}}_k\}\left[2\left(2-\frac{1}{M_I}-\frac{1}{M_Q}\right)Q\left(\sqrt{\frac{d^2_{min,k}|h|^2}{4\sigma_n^2}}\right)\right. \\ &\left. - 4\left(1-\frac{1}{M_I}\right)\left(1-\frac{1}{M_Q}\right)Q^2\left(\sqrt{\frac{d^2_{min,k}|h|^2}{4\sigma_n^2}}\right)\right] \\ &+ \Pr\{\mathcal{H}_1|\hat{\mathcal{H}}_k\}\left[2\left(2-\frac{1}{M_I}-\frac{1}{M_Q}\right)\sum_{l=1}^{p}\lambda_l Q\left(\sqrt{\frac{d^2_{min,k}|h|^2}{4(\sigma_l^2+\sigma_n^2)}}\right)\right. \\ &\left. - 4\left(1-\frac{1}{M_I}\right)\left(1-\frac{1}{M_Q}\right)\sum_{l=1}^{p}\lambda_l Q^2\left(\sqrt{\frac{d^2_{min,k}|h|^2}{4(\sigma_l^2+\sigma_n^2)}}\right)\right]\Bigg\}.\end{aligned} \tag{6.40}$$

This expression can be specialized to square QAM signaling by setting $M_I = M_Q = \sqrt{M}$.

We observe above that while the optimal decision rule does not depend on the sensing decisions, the error rates are functions of detection and false alarm probabilities. Note also

that the expressions above are for a given value of fading. The unconditional symbol error probability averaged over fading can be evaluated from

$$\mathrm{SEP}(P) = \int_0^\infty \mathrm{SEP}(P,x) f_{|h|^2}(x) dx. \tag{6.41}$$

In the special case of a Rayleigh fading model for which the fading power has an exponential distribution with unit mean, i.e., $f_{|h|^2}(x) = \mathrm{e}^{-x}$, the above integral can be evaluated by adopting the same approach as in [82] and using the indefinite integral form of the Gaussian Q-function [83] and square of the Gaussian Q-function [84], given, respectively, by

$$Q(x) = \frac{1}{\pi}\int_0^{\frac{\pi}{2}} \mathrm{e}^{\left(-\frac{x^2}{2sin^2\phi}\right)} d\phi, \tag{6.42}$$

$$Q^2(x) = \frac{1}{\pi}\int_0^{\frac{\pi}{4}} \mathrm{e}^{\left(-\frac{x^2}{2sin^2\phi}\right)} d\phi \quad \text{for} \quad x \geq 0. \tag{6.43}$$

The resulting unconditional average symbol error probability over Rayleigh fading is given by

$$\begin{aligned}
\mathrm{SEP}(P) = \sum_{k=0}^{1} \Pr\{\hat{\mathcal{H}}_k\} \Bigg\{ & \Pr\{\mathcal{H}_0|\hat{\mathcal{H}}_k\} \Bigg[\left(2 - \frac{1}{M_I} - \frac{1}{M_Q}\right)\left(1 - \frac{1}{\beta_{0,k}}\right) \\
& - 2\left(1 - \frac{1}{M_I}\right)\left(1 - \frac{1}{M_Q}\right)\left(\frac{2}{\pi}\frac{1}{\beta_{0,k}} \tan^{-1}\left(\frac{1}{\beta_{0,k}}\right) - \frac{1}{\beta_{0,k}} + \frac{1}{2}\right)\Bigg] \\
& + \Pr\{\mathcal{H}_1|\hat{\mathcal{H}}_k\} \Bigg[\left(2 - \frac{1}{M_I} - \frac{1}{M_Q}\right) \sum_{l=1}^{p} \lambda_l \left(1 - \frac{1}{\beta_{1,k}}\right) \\
& - 2\left(1 - \frac{1}{M_I}\right)\left(1 - \frac{1}{M_Q}\right) \sum_{l=1}^{p} \lambda_l \left(\frac{2}{\pi}\frac{1}{\beta_{1,k}} \tan^{-1}\left(\frac{1}{\beta_{1,k}}\right) - \frac{1}{\beta_{1,k}} + \frac{1}{2}\right)\Bigg]\Bigg\}.
\end{aligned} \tag{6.44}$$

Above, $\beta_{0,k} = \sqrt{1 + \frac{2}{3P_k}({M_I}^2 + {M_Q}^2 - 2)\sigma_n^2}$ and $\beta_{1,k} = \sqrt{1 + \frac{2}{3P_k}({M_I}^2 + {M_Q}^2 - 2)(\sigma_l^2 + \sigma_n^2)}$ for $1 \leq l \leq p$. The average symbol error probability for rectangular QAM signaling in the presence of Gaussian-distributed w can readily be obtained by letting $l = 1$ in (6.44). Although the SEP expression in (6.44) seems complicated, it is in fact very simple to evaluate.

Furthermore, this SEP(P) can be upper bounded as

$$\mathrm{SEP}(P) \leq \left(2 - \frac{1}{M_I} - \frac{1}{M_Q}\right) \sum_{k=0}^{1} \Pr\{\hat{\mathcal{H}}_k\} \left\{ \Pr\{\mathcal{H}_0|\hat{\mathcal{H}}_k\} \left(1 - \frac{1}{\beta_{0,k}}\right) + \Pr\{\mathcal{H}_1|\hat{\mathcal{H}}_k\} \sum_{l=1}^{p} \lambda_l \left(1 - \frac{1}{\beta_{1,k}}\right) \right\}. \tag{6.45}$$

This upper bound follows by removing the negative terms that include $Q^2(\cdot)$ on the right-hand side of (6.40) and then integrating with respect to fading distribution. Note also that the upper bound in (6.45) with $M_Q = 1$ is the exact symbol error probability for PAM modulation.

Note further that the SEP expression in (6.44) is a function of the transmission powers P_0 and P_1. The optimal choice of the power levels under peak power and average interference constraints given in (6.1) and (6.2) and the resulting error rates can be determined by solving

$$\mathrm{SEP}(P_{\mathrm{pk}}, Q_{\mathrm{avg}}) = \min_{\substack{P_0 \leq P_{\mathrm{pk}},\, P_1 \leq P_{\mathrm{pk}} \\ (1-\mathscr{P}_{\mathrm{d}})\, P_0\, \mathbb{E}\{|g|^2\} + \mathscr{P}_{\mathrm{d}}\, P_1\, \mathbb{E}\{|g|^2\} \leq Q_{\mathrm{avg}}}} \mathrm{SEP}(P_0, P_1). \tag{6.46}$$

If the fading coefficient g between the secondary transmitter and the primary receiver is known and peak interference constraints are imposed, then the maximum transmission power is given by

$$P_i^* = \min\left\{P_{\mathrm{pk}}, \frac{Q_{\mathrm{pk}}}{|g|^2}\right\} \quad \text{for } i = 0, 1. \tag{6.47}$$

After inserting these P_0^* and P_1^* into the SEP upper bound in (6.45) and evaluating the expectation over the fading coefficient g, we obtain

$$\mathrm{SEP} \leq \int_0^{b_1} \mathrm{SEP}_u(P_{peak}) f_{|g|^2}(y) dy + \int_{b_1}^{\infty} \mathrm{SEP}_u\left(\frac{Q_{\mathrm{pk}}}{y}\right) f_{|g|^2}(y) dy \tag{6.48}$$

where $b_1 = \frac{Q_{\mathrm{pk}}}{P_{\mathrm{pk}}}$ and SEP_u denotes the upper bound in (6.45). If $|g|^2$ is exponentially distributed with unit mean, then by using the identity in [85, eq. 3.362.2], we can evaluate

the second integral on the right-hand side of (6.48) and express the upper bound as

$$\begin{aligned}\mathrm{SEP} \leq (1-\mathrm{e}^{-b_1})\mathrm{SEP}(P_{\mathrm{pk}}) + \left(2-\frac{1}{M_I}-\frac{1}{M_Q}\right)\sum_{k=0}^{1}\Pr\{\hat{\mathcal{H}}_k\} \\ \times\left\{\Pr\{\mathcal{H}_0|\hat{\mathcal{H}}_k\}\left[\mathrm{e}^{b_1}-2\sqrt{\gamma_0\pi}\mathrm{e}^{\gamma_0}Q\big(\sqrt{2}(b_1+\gamma_0)\big)\right]\right. \\ \left.+\Pr\{\mathcal{H}_1|\hat{\mathcal{H}}_k\}\sum_{l=1}^{p}\lambda_l\left[\mathrm{e}^{b_1}-2\sqrt{\gamma_1\pi}\mathrm{e}^{\gamma_1}Q\big(\sqrt{2}(b_1+\gamma_1)\big)\right]\right\},\end{aligned} \tag{6.49}$$

where $\gamma_0 = \frac{3b_1P_{\mathrm{pk}}}{2(M_I^2+M_Q^2-2)\sigma_n^2}$, $\gamma_1 = \frac{3b_1P_{\mathrm{pk}}}{2(M_I^2+M_Q^2-2)(\sigma_l^2+\sigma_n^2)}$.

It should be noted that we can easily obtain the *exact* symbol error probability expressions for PAM modulation by replacing $M_I = M$ and $M_Q = 1$ in (6.40), (6.44), (6.49).

6.3.2.2 Opportunistic spectrum access (OSA) scheme

In the OSA scheme, secondary users are not allowed to transmit when the primary user activity is sensed in the channel. Therefore, we only consider error patterns under $\hat{\mathcal{H}}_0$ given in (6.34), (6.36), (6.38). Hence, following the same approach adopted in SSS scheme, the average symbol error probability under the OSA scheme is obtained as

$$\begin{aligned}\mathrm{SEP}(P_0) = \Pr\{\mathcal{H}_0|\hat{\mathcal{H}}_0\}\left[\left(2-\frac{1}{M_I}-\frac{1}{M_Q}\right)\left(1-\frac{1}{\beta_{0,0}}\right)\right. \\ \left.-2\left(1-\frac{1}{M_I}\right)\left(1-\frac{1}{M_Q}\right)\left(\frac{2}{\pi}\frac{1}{\beta_{0,0}}\tan^{-1}\left(\frac{1}{\beta_{0,0}}\right)-\frac{1}{\beta_{0,0}}+\frac{1}{2}\right)\right] \\ +\Pr\{\mathcal{H}_1|\hat{\mathcal{H}}_0\}\left[\left(2-\frac{1}{M_I}-\frac{1}{M_Q}\right)\sum_{l=1}^{p}\lambda_l\left(1-\frac{1}{\beta_{1,0}}\right)\right. \\ \left.-2\left(1-\frac{1}{M_I}\right)\left(1-\frac{1}{M_Q}\right)\sum_{l=1}^{p}\lambda_l\left(\frac{2}{\pi}\frac{1}{\beta_{1,0}}\tan^{-1}\left(\frac{1}{\beta_{1,0}}\right)-\frac{1}{\beta_{1,0}}+\frac{1}{2}\right)\right].\end{aligned} \tag{6.50}$$

Similarly, the SEP upper bound becomes

$$\mathrm{SEP}(P) \leq \left(2-\frac{1}{M_I}-\frac{1}{M_Q}\right)\left\{\Pr\{\mathcal{H}_0|\hat{\mathcal{H}}_0\}\left(1-\frac{1}{\beta_{0,0}}\right)+\Pr\{\mathcal{H}_1|\hat{\mathcal{H}}_0\}\sum_{l=1}^{p}\lambda_l\left(1-\frac{1}{\beta_{1,0}}\right)\right\}. \tag{6.51}$$

Note that under average interference constraints, the maximum allowed transmission power in an idle-sensed channel is given by

$$P_0^* = \min\left\{P_{\mathrm{pk}}, \frac{Q_{\mathrm{avg}}}{(1-\mathscr{P}_{\mathrm{d}})\mathbb{E}\{|g|^2\}}\right\}. \tag{6.52}$$

On the other hand, if the peak interference power constraint is imposed, the maximum allowed transmission power is

$$P_0^* = \min\left\{P_{\rm pk}, \frac{Q_{\rm pk}}{|g|^2}\right\}. \tag{6.53}$$

After inserting this P_0^* into (6.51), assuming again that $|g|^2$ is exponentially distributed with unit mean, and evaluating the integration in a similar fashion as in SSS scheme, an upper bound on the average symbol error probability can be obtained as

$$\begin{aligned}\text{SEP} \leq \left(1 - \mathrm{e}^{\frac{Q_{\rm pk}}{P_{\rm pk}}}\right)\text{SEP}(P_{\rm pk}) + \left(2 - \frac{1}{M_I} - \frac{1}{M_Q}\right) \\ \times \left\{ \Pr\{\mathcal{H}_0|\hat{\mathcal{H}}_0\}\left[\mathrm{e}^{\frac{Q_{\rm pk}}{P_{\rm pk}}} - 2\sqrt{\psi_0\pi}\mathrm{e}^{\psi_0}Q\left(\sqrt{2}\left(\frac{Q_{\rm pk}}{P_{\rm pk}} + \psi_0\right)\right)\right] \right. \\ \left. + \Pr\{\mathcal{H}_1|\hat{\mathcal{H}}_0\}\sum_{l=1}^{p}\lambda_l\left[\mathrm{e}^{\frac{Q_{\rm pk}}{P_{\rm pk}}} - 2\sqrt{\psi_1\pi}\mathrm{e}^{\psi_1}Q\left(\sqrt{2}\left(\frac{Q_{\rm pk}}{P_{\rm pk}} + \psi_1\right)\right)\right]\right\},\end{aligned} \tag{6.54}$$

where $\psi_0 = \frac{3Q_{pk}}{2(M_I^2+M_Q^2-2)\sigma_n^2}$ and $\psi_1 = \frac{3Q_{pk}}{2(M_I^2+M_Q^2-2)(\sigma_l^2+\sigma_n^2)}$.

6.4 Numerical Results

In this section, we present numerical results to demonstrate the error performance of a cognitive radio system in the presence of channel sensing uncertainty for both SSS and OSA schemes. More specifically, we numerically investigate the impact of sensing performance (e.g., detection and false-alarm probabilities), different levels of peak transmission power and average and peak interference constraints on cognitive transmissions in terms of symbol error probability. Theoretical results are validated through Monte Carlo simulations. Unless mentioned explicitly, the following parameters are employed in the numerical computations. It is assumed that the variance of the background noise is $\sigma_n^2 = 0.01$. When the primary user signal is assumed to be Gaussian, its variance, σ_w^2 is set to 0.5. On the other hand, in the case of primary user's received signal w distributed according to the Gaussian mixture model, we assume that $p = 4$, i.e., there are four components in the mixture, $\lambda_l = 0.25$ for all $1 \leq l \leq 4$,

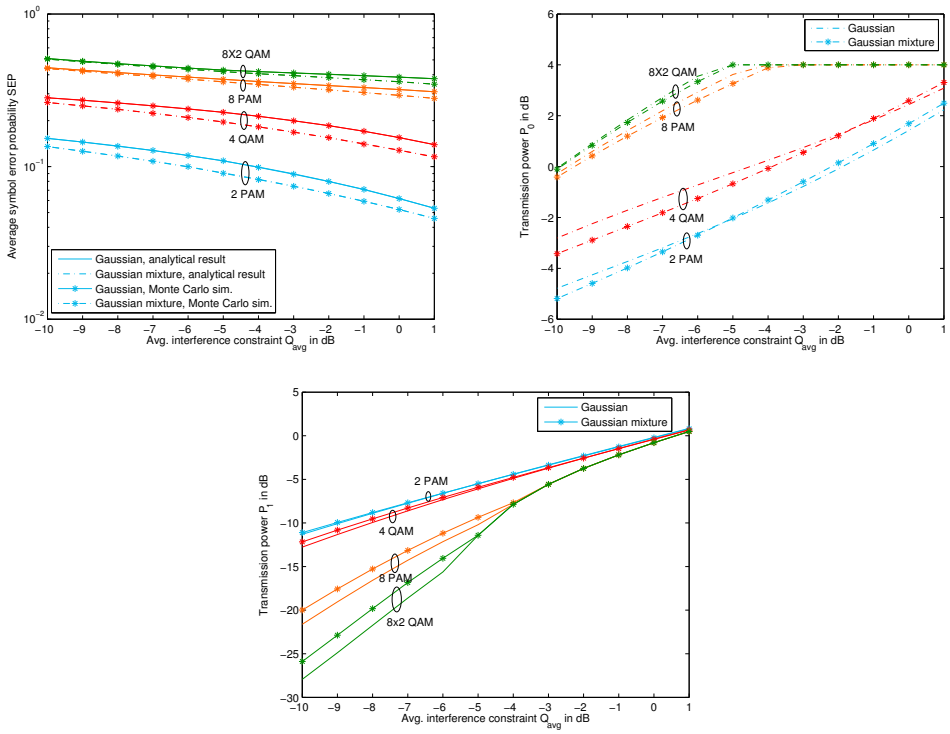

Figure 6.1: Average symbol error probability SEP, and transmission powers P_0 and P_1 vs. average interference constraint, Q_{avg} in SSS scheme.

and the variance is still $\sigma_w^2 = 0.5$. Also, the primary user is active over the channel with a probability of 0.4, hence $\Pr\{\mathcal{H}_1\} = 0.4$ and $\Pr\{\mathcal{H}_0\} = 0.6$. Finally, we consider a Rayleigh fading channel between the secondary users with fading power pdf given by $f_{|h|^2}(x) = \mathrm{e}^{-x}$ for $x \geq 0$, and also assume that the fading power $|g|^2$ in the channel between the secondary transmitter and primary receiver is exponentially distributed with $\mathbb{E}\{|g|^2\} = 1$.

6.4.1 SEP under Average Interference Constraints

We initially consider peak transmit and average interference constraints as given in (6.1) and (6.2), respectively. In the following numerical results, for the SSS scheme, we plot the error probabilities and optimal transmission power levels obtained by solving (6.46). In the case of OSA, we plot the average error probability expressed in (6.50) with maximum allowed power P_0^* given in (6.52).

In Fig. 6.1, we display the average symbol error probability (SEP) and optimal trans-

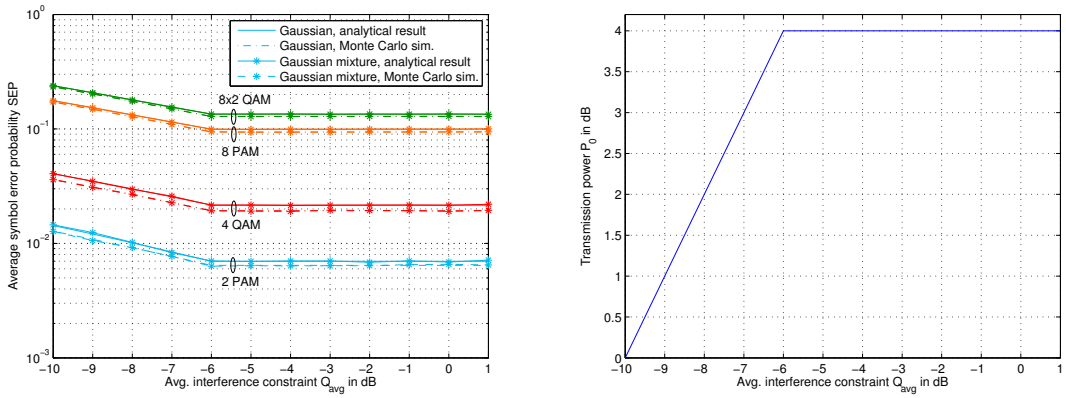

Figure 6.2: Average symbol error probability SEP and transmission powers P_0 vs. average interference constraint, Q_{avg} in OSA scheme.

mission powers P_0 and P_1 as a function of the average interference constraint, Q_{avg}, in the SSS scheme. $\mathscr{P}_{\text{d}}$ and $\mathscr{P}_{\text{f}}$ are set to 0.9 and 0.05, respectively. The peak transmission power is $P_{\text{pk}} = 4$ dB. We assume that the secondary users employ 2-PAM, 4-QAM, 8-PAM and 8×2-QAM modulation schemes for data transmission. We have considered both Gaussian and Gaussian-mixture distributed w. In addition to the analytical results obtained by using (6.44) and solving (6.46), we performed Monte Carlo simulations to determine the SEP. We notice in the figure that analytical and simulation results agree perfectly. Additionally, it is seen that for all modulation types, error rate performance of secondary users improves as average interference constraint becomes looser (i.e., as Q_{avg} increases), allowing transmission power levels P_0 and P_1 to become higher as illustrated in the lower subfigures. Saturation seen in the plot of P_0 is due to the peak constraint P_{pk}. Other observations are as follows. As the modulation size increases, SEP increases as expected. It is also interesting to note that lower SEP is attained in the presence of Gaussian-mixture distributed w when compared with the performance when w has a pure Gaussian density with the same variance.

In Fig. 6.2, average SEP and transmission power P_0 are plotted as a function of the average interference constraint, Q_{avg}, for the OSA scheme. We again set $P_{\text{pk}} = 4$ dB, $\mathscr{P}_{\text{d}} = 0.9$ and $\mathscr{P}_{\text{f}} = 0.05$, and consider 2-PAM, 4-QAM, 8-PAM and 8×2-QAM schemes. It is observed from the figure that as Q_{avg} increases, error probabilities initially decrease and

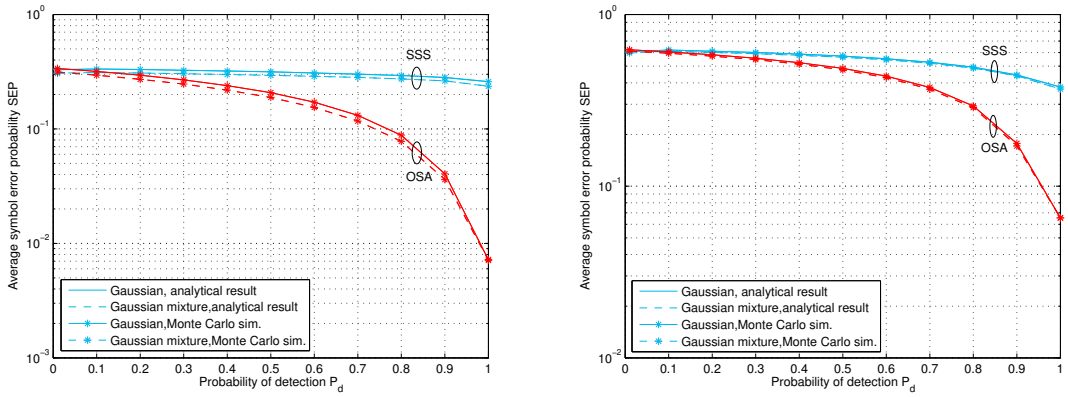

Figure 6.3: Average symbol error probability SEP of 4-QAM (left subfigure) and 8-PAM (right subfigure) signaling vs. detection probability $\mathscr{P}_{\rm d}$ for SSS and OSA schemes.

then remain constant due to the fact that the secondary users can initially afford to transmit with higher transmission power P_0 as the interference constraint becomes less strict, but then get limited by the peak transmission power constraint and send data at the fixed power level of $P_{\rm pk}$. Again, we observe that lower error probabilities are attained when the primary user's received signal w follows a Gaussian mixture distribution.

In Fig. 6.3, the average SEPs of 4-QAM (in the left subfigure) and 8-PAM signaling (in the lower subfigure) are plotted as a function of the detection probability $\mathscr{P}_{\rm d}$. $\mathscr{P}_{\rm f}$ is set to 0.05. We consider both SSS and OSA schemes. It is assumed that $P_{\rm pk} = 4$ dB and $Q_{\rm avg} = -10$ dB. We observe that SEP for both modulation types in both SSS and OSA schemes decreases as $\mathscr{P}_{\rm d}$ increases. Hence, performance improves with more reliable sensing. In this case, the primary reason is that more reliable detection enables the secondary users transmit with higher power in an idle-sensed channel. For instance, if $\mathscr{P}_{\rm d} = 1$, then the transmission power P_0 is only limited by $P_{\rm pk}$ in both SSS and OSA. In the figure, we also notice that lower SEP is achieved in the OSA scheme, when compared with the SSS scheme, due to the fact that OSA avoids transmission over a busy-channel in which interference from the primary user's transmission results in a more noisy channel and consequently higher error rates are experienced. At the same time, it is important to note that not transmitting in a busy-sensed channel as in OSA potentially reduces data rates.

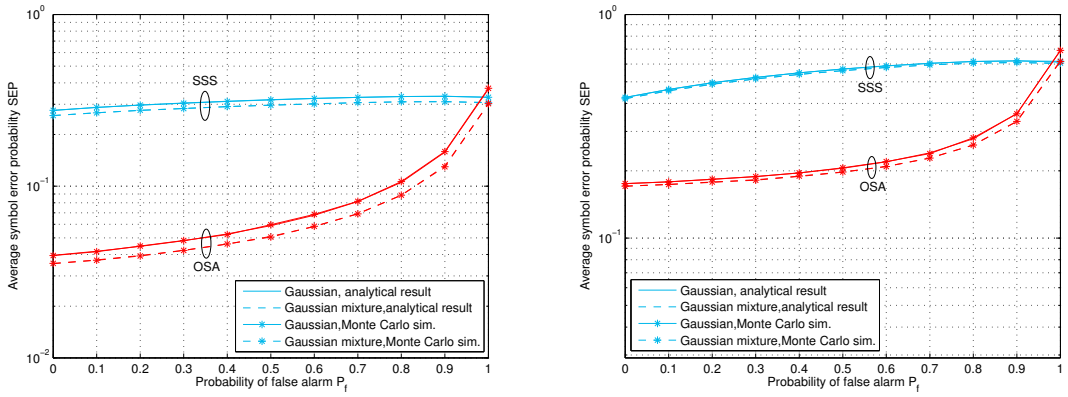

Figure 6.4: Average symbol error probability SEP of 4-QAM (left subfigure) and 8-PAM (right subfigure) signaling vs. probability of false alarm $\mathscr{P}_{\mathrm{f}}$ for SSS and OSA schemes.

In Fig. 6.4, the average SEPs of 4-QAM and 8-PAM signaling are plotted as a function of the false alarm probability $\mathscr{P}_{\mathrm{f}}$ for both SSS and OSA. It is assumed that $\mathscr{P}_{\mathrm{d}} = 0.9$. It is further assumed that $P_{\mathrm{pk}} = 4$ dB and $Q_{\mathrm{avg}} = -10$ dB, again corresponding to the case in which average interference power constraint is dominant compared to the peak transmit power constraint. In both schemes, SEP increases with increasing false alarm probability $\mathscr{P}_{\mathrm{f}}$. Hence, degradation in sensing reliability leads to performance loss in terms of error probabilities. In OSA, the transmission power $P_0 = \min\left\{P_{\mathrm{pk}}, \frac{Q_{\mathrm{avg}}}{(1-\mathscr{P}_{\mathrm{d}})\mathbb{E}\{|g|^2\}}\right\}$ does not depend on $\mathscr{P}_{\mathrm{f}}$ and hence is fixed in the figure. The increase in the error rates can be attributed to the fact that secondary users more frequently experience interference from primary user's transmissions due to sensing uncertainty. For instance, in the extreme case in which $\mathscr{P}_{\mathrm{f}} = 1$, the probability terms in (6.50) become $\Pr\{\mathcal{H}_0|\hat{\mathcal{H}}_0\} = 0$ and $\Pr\{\mathcal{H}_1|\hat{\mathcal{H}}_0\} = 1$, indicating that although the channel is sensed as idle, it is actually busy with probability one and the additive disturbance in OSA transmissions always includes w. In the SSS scheme, higher $\mathscr{P}_{\mathrm{f}}$ leads to more frequent transmissions with power P_1 which is generally smaller than P_0 in order to limit the interference on the primary users. Transmission with smaller power expectedly increases the error probabilities. On the other hand, we interestingly note that as $\mathscr{P}_{\mathrm{f}}$ approaches 1, P_1 becomes higher than P_0 when (6.46) is solved, resulting in a slight decrease in SEP when $\mathscr{P}_{\mathrm{f}}$ exceeds around 0.9.

6.4.2 SEP under Peak Interference Constraints

We now address the peak interference constraints by assuming that the transmission powers are limited as in (6.6). In this subsection, analytical error probability curves are plotted using the upper bounds in (6.49) in the case of SSS and in (6.54) in the case of OSA since we only have closed-form expressions for the error probability upper bounds when we need to evaluate an additional expectation with respect to $|g|^2$. Note that these upper bounds provide exact error probabilities when PAM is considered. Additionally, the discrepancy in QAM is generally small as demonstrated through comparisons with Monte Carlo simulations which provide the exact error rates in the figures.

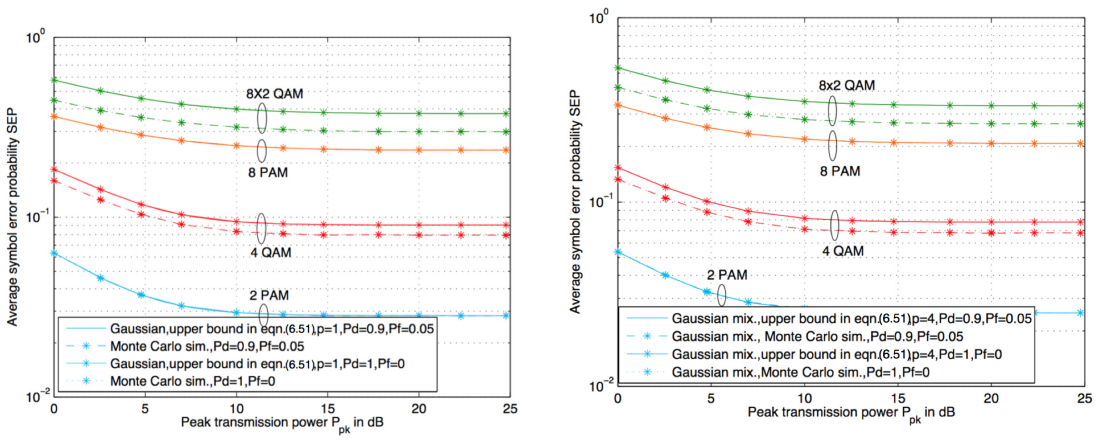

Figure 6.5: Average symbol error probability SEP vs. peak transmission power P_{pk} in dB for SSS scheme when the primary user signal is modeled by Gaussian distribution (left subfigure) and Gaussian mixture distribution (right subfigure).

In Fig. 6.5, we plot the average SEP as a function of the peak transmission power, P_{pk}, for the SSS scheme in the presence of Gaussian distributed and Gaussian-mixture distributed primary user's received faded signal w in the left and right subfigures, respectively. The secondary users again employ 2-PAM, 4-QAM, 8-PAM and 8×2-QAM schemes. The peak interference power constraint, Q_{pk} is set to 4 dB. It is seen that Monte Carlo simulations match with the analytical results for PAM and are slightly lower than the analytical upper bounds for QAM. As expected, the average SEP initially decreases with increasing P_{pk} and a higher modulation size leads to higher error rates at the same transmission power level.

We again observe that lower error rates are experienced when w has a Gaussian mixture distribution rather than a Gaussian distribution with the same variance. It is also seen that as P_{pk} increases, the SEP curves in all cases approach some error floor at which point interference constraints become the limiting factor.

Another interesting observation is the following. In Fig. 6.5, SEPs are plotted for two different pairs of detection and false alarm probabilities. In the first scenario, channel sensing is perfect, i.e., $\mathscr{P}_{\text{d}} = 1$ and $\mathscr{P}_{\text{f}} = 0$. In the second scenario, we have $\mathscr{P}_{\text{d}} = 0.9$ and $\mathscr{P}_{\text{f}} = 0.05$. In both scenarios, we observe the same error rate performance. This is because the same transmission power is used regardless of whether the channel is detected as idle or busy, i.e., $P_i^* = \min\left\{P_{\text{pk}}, \frac{Q_{\text{pk}}}{|g|^2}\right\}$ for both $i = 0, 1$. The interference constraints are very strict. Hence, averaging over channel sensing decisions becomes averaging over the prior probabilities of channel occupancy, which does not depend on the probabilities of detection and false alarm. Indeed, spectrum sensing can be altogether omitted under these constraints.

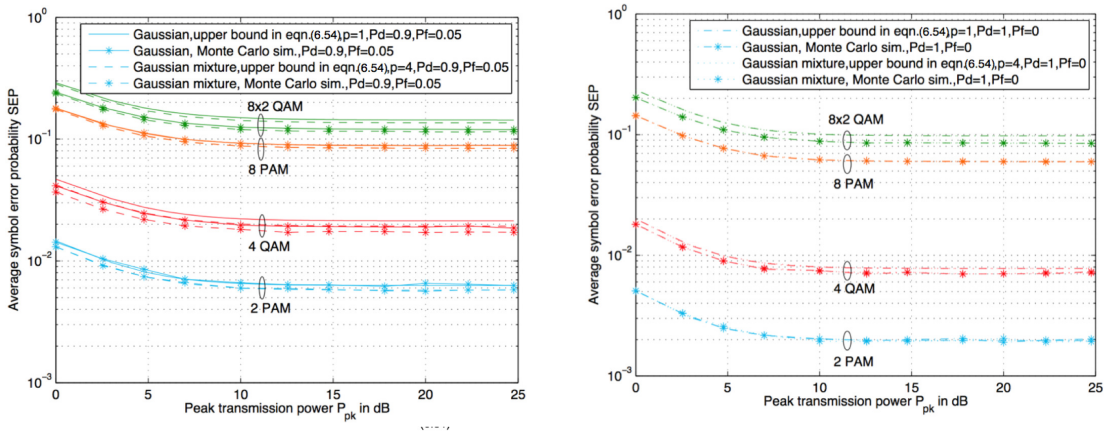

Figure 6.6: Average symbol error probability SEP vs. peak transmission power P_{pk} in dB for OSA scheme in the presence of Gaussian and Gaussian mixture primary user's interference signal under imperfect sensing result (left subfigure) and perfect sensing result (right subfigure).

In Fig. 6.6, we plot the average SEP as a function of P_{pk} for the OSA scheme. As before, 2-PAM, 4-QAM, 8-PAM and 8×2-QAM are considered. Imperfect sensing with $\mathscr{P}_{\text{d}} = 0.9$ and $\mathscr{P}_{\text{f}} = 0.05$ is considered in the left subfigure whereas perfect sensing (i.e., $\mathscr{P}_{\text{d}} = 1$ and $\mathscr{P}_{\text{f}} = 0$) is assumed in the lower subfigure. In both subfigures, it is seen

that increasing P_{pk} initially reduces SEP which then hits an error floor as the interference constraints start to dominate. It is also observed that perfect channel sensing improves the error rate performance of cognitive users. Note that if sensing is perfect, secondary users transmit only if the channel is actually idle and experience only the background noise n. On the other hand, under imperfect sensing, secondary users transmit in miss-detection scenarios as well, in which they are affected by both the background noise and primary user interference w, leading to higher error rates. Cognitive radio transmission impaired by Gaussian mixture distributed w again results in lower SEP compared to Gaussian distributed w. But, of course, this distinction disappears with perfect sensing in the lower subfigure since the secondary users experience only the Gaussian background noise n as noted above. Finally, the gap between the analytical and simulation results for QAM is due to the use of upper bounds in the analytical error curves as discussed before.

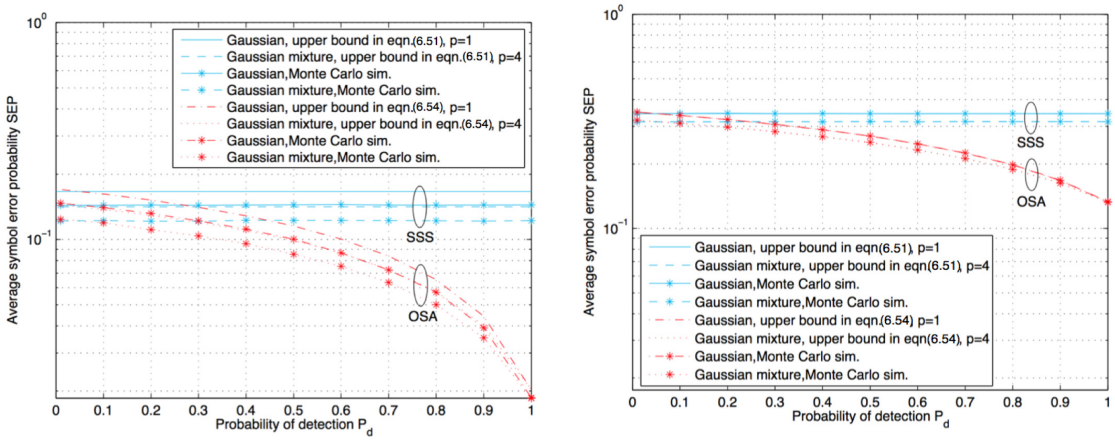

Figure 6.7: Average symbol error probability SEP of 4-QAM (left subfigure) and 8-PAM (right subfigure) signaling vs. detection probability $\mathscr{P}_{\text{d}}$ for SSS and OSA schemes.

In Fig. 6.7, we display the average SEP of 4-QAM and 8-PAM signaling as a function of the detection probability $\mathscr{P}_{\text{d}}$. $\mathscr{P}_{\text{f}}$ is set to 0.05. Both SSS and OSA schemes are considered. Here, we also assume that $P_{\text{pk}} = 4$ dB, $Q_{\text{pk}} = 0$ dB. It is seen that error rate performances for SSS scheme for both modulation types do not depend on detection probability because of the same reasoning explained in the discussion of Fig. 6.5. On the other hand, the error rate performance for the OSA scheme improves with increasing detection probability since

the secondary user experiences less interference from the primary user activity. It is also seen that OSA scheme outperforms SSS scheme.

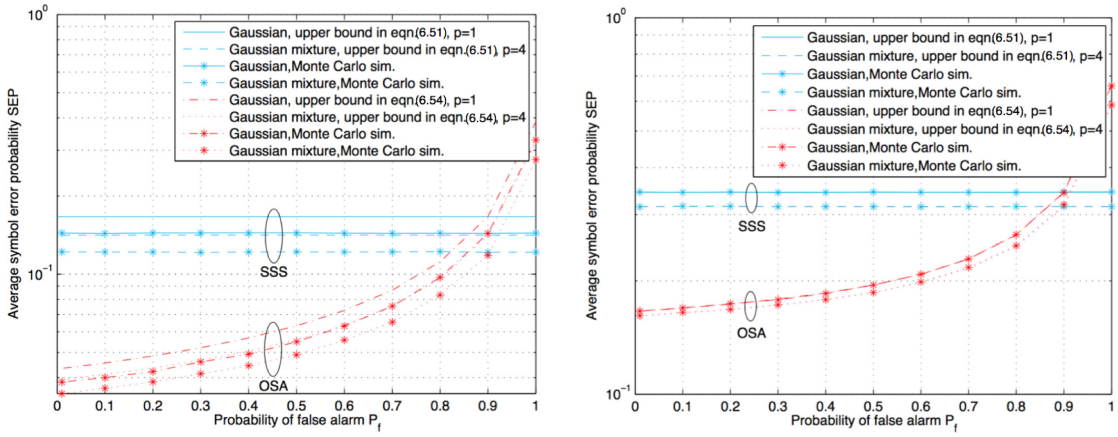

Figure 6.8: Average symbol error probability SEP of 4-QAM (left subfigure) and 8-PAM (right subfigure) signaling vs. probability of false alarm $\mathscr{P}_{\mathrm{f}}$ for SSS and OSA schemes.

In Fig. 6.8, we analyze the average SEP of 4-QAM and 8-PAM signaling as a function of the false alarm probability $\mathscr{P}_{\mathrm{f}}$. Detection probability is $\mathscr{P}_{\mathrm{d}} = 0.9$. Similarly as before, $P_{\mathrm{pk}} = 4$ dB and $Q_{\mathrm{pk}} = 0$ dB. Again, error rate performance does not depend on $\mathscr{P}_{\mathrm{f}}$ in the SSS scheme. It is observed that SEP in OSA scheme increases with increasing false alarm probability. Hence, degradation in the sensing performance in terms of increased false alarm probabilities leads to degradation in the error performance. Deterioration in the performance is due to more frequent exposure to interference from primary user's transmissions in the form of w.

Chapter 7

Throughput of Cognitive Radio Systems with Finite Blocklength Codes and QoS Constraints

In this chapter, throughput achieved in cognitive radio channels with finite blocklength codes under buffer limitations is studied. It is assumed that finite blocklength codes are employed in the data transmission phase. Hence, errors can occur in reception and retransmissions can be required. In the absence of CSI at the transmitter, fixed-rate transmission is performed whereas under perfect CSI knowledge, for a given target error probability, the transmitter varies the rate according to the channel conditions. Under these assumptions, throughput in the presence of buffer constraints is determined by characterizing the maximum constant arrival rates that can be supported by the cognitive radio channel while satisfying certain limits on buffer violation probabilities.

We introduce the system model in Section 7.1. Section 7.2 gives an overview of the channel capacity with finite blocklength codes. In Section 7.3, we study effective throughput under the following two assumptions: CSI is known perfectly by either the receiver only or both the transmitter and receiver. The numerical results are illustrated in Section 7.4.

7.1 System Model

In the cognitive radio model we consider, secondary users first determine the channel status (i.e., idle or busy) through spectrum sensing and then enter into data transmission phase with rate and power that depend on the sensing decision. Secondary users are allowed to coexist with primary users in the channel as long as their interference level does not deteriorate the performance of primary users. We also assume that channel sensing and data transmission are performed in frames of T seconds. Duration of first N seconds is allocated to channel sensing in which the secondary users observe either primary users' faded sum signal plus Gaussian background noise or just Gaussian background noise, and make a decision on primary user activity. In the remaining $T - N$ seconds, data transmission is performed over a flat-fading channel with additive Gaussian background noise and possibly additive interference arising due to transmissions from active primary users.

7.1.1 Markov Model for Primary User Activity

It is assumed that the primary users' activity in the channel remains the same during the frame duration of T seconds. On the other hand, activity from one frame to another or equivalently the channel being busy or idle is modeled as a two-state Markov chain depicted in Figure 7.1. The busy state indicates that primary users are active in the channel whereas idle state represents no primary user activity. In Fig. 7.1, $P_{i,j}$, with $i, j \in \{I, B\}$, denotes the transition probability from state i to state j, satisfying $\sum_j P_{i,j} = 1$. Note that we set $P_{B,I} = s$ and $P_{I,B} = q$.

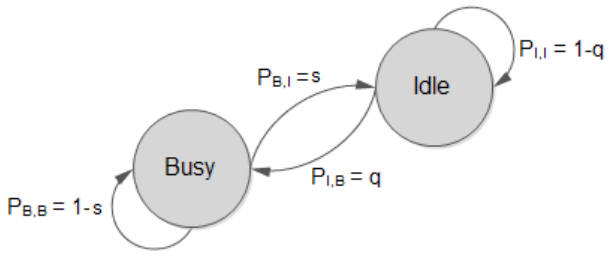

Figure 7.1: Two-state Markov chain to model the primary user activity.

Given the above two-state Markov chain, we can easily determine the prior probabilities that the channel is busy and idle, denoted by $\Pr(\mathcal{H}_1)$ and $\Pr(\mathcal{H}_0)$, respectively, as follows:

$$\Pr(\mathcal{H}_1) = \frac{P_{I,B}}{P_{I,B} + P_{B,B}} = \frac{q}{q+s},\ \Pr(\mathcal{H}_0) = \frac{P_{B,I}}{P_{B,I} + P_{I,I}} = \frac{s}{s+q} \tag{7.1}$$

with notations $\mathcal{H}_0$ and $\mathcal{H}_1$ described below.

7.1.2 Channel Sensing

Channel sensing is performed in the first N seconds. The remaining duration of $T - N$ seconds is reserved for data transmission. As in [86], we formulate channel sensing as a binary hypothesis testing problem:

$$\begin{aligned} \mathcal{H}_0 &: y_i = n_i \qquad i = 1, 2, \ldots, NB \\ \mathcal{H}_1 &: y_i = s_i + n_i \quad i = 1, 2, \ldots, NB \end{aligned} \tag{7.2}$$

where n_i denotes complex circularly symmetric background Gaussian noise samples with mean zero and variance $\mathbb{E}\{|n_i|^2\} = \sigma_n^2$, i.e., $n \sim \mathcal{CN}(0, \sigma_n^2)$. s_i denotes the primary users' faded sum signal at the cognitive secondary receiver and can, for instance, be expressed as

$$s_i = \sum_{j=1}^{K} g_{ps,j}\, u_j \tag{7.3}$$

where K is the number of active primary transmitters, u_j is the j^{th} primary user's transmitted signal and $g_{ps,j}$ denotes the fading coefficient between the j^{th} primary transmitter and the secondary receiver. Therefore, hypothesis $\mathcal{H}_0$ above corresponds to the case in which primary users are inactive in the channel whereas hypothesis $\mathcal{H}_1$ models the presence of active primary users. Above, B denotes the bandwidth of the system and therefore we have NB complex signal samples in the sensing duration of N seconds.

We further assume that $\{s_i\}$ is an independent and identically distributed (i.i.d.) sequence of circularly symmetric, complex Gaussian random variables with mean zero and

variance $\mathbb{E}\{|s_i|^2\} = \sigma_s^2$, i.e., $s \sim \mathcal{CN}(0, \sigma_s^2)$. The optimal Neyman-Pearson energy detector is employed for channel sensing, and under the above-mentioned statistical assumptions, the test statistic is the total energy gathered in N seconds, which is compared with a threshold λ:

$$T(y) = \frac{1}{NB} \sum_{i=1}^{NB} |y_i|^2 \gtrless_{\mathcal{H}_0}^{\mathcal{H}_1} \lambda. \tag{7.4}$$

Above, $T(y)$ is the sum of NB independent χ^2-distributed complex random variables and hence is itself χ^2-distributed with $2NB$ degrees of freedom. With this characterization, the false alarm and detection probabilities can be expressed as

$$\mathscr{P}_{\mathrm{f}} = \Pr\{T(y) > \lambda | \mathcal{H}_0\} = \Pr(\hat{\mathcal{H}}_1 | \mathcal{H}_0) = 1 - P\left(\frac{NB\lambda}{\sigma_n^2}, NB\right), \tag{7.5}$$

$$\mathscr{P}_{\mathrm{d}} = \Pr\{T(y) > \lambda | \mathcal{H}_1\} = \Pr(\hat{\mathcal{H}}_1 | \mathcal{H}_1) = 1 - P\left(\frac{NB\lambda}{\sigma_n^2 + \sigma_s^2}, NB\right) \tag{7.6}$$

where $P(s, x) = \frac{\gamma(s,x)}{\Gamma(s)}$ is the regularized Gamma function [62, eq. 6.5.1], $\gamma(s, x)$ is the lower incomplete Gamma function [62, eq. 6.5.2], and $\Gamma(s)$ is the Gamma function [62, eq. 6.1.1]. Additionally, $\hat{\mathcal{H}}_1$ and $\hat{\mathcal{H}}_0$ denote busy and idle sensing decisions, respectively. We further express the rest of the conditional probabilities of channel sensing decisions given channel true states, i.e., $\Pr(\hat{\mathcal{H}}_i | \mathcal{H}_j)$, in terms of $\mathscr{P}_{\mathrm{d}}$ and $\mathscr{P}_{\mathrm{f}}$, as follows:

$$\Pr(\hat{\mathcal{H}}_i | \mathcal{H}_j) = \begin{cases} 1 - \mathscr{P}_{\mathrm{d}} & \text{if } j = 1, i = 0 \\ 1 - \mathscr{P}_{\mathrm{f}} & \text{if } j = 0, i = 0 \end{cases}. \tag{7.7}$$

Combining (7.5) – (7.7) and applying the Bayes' rule, we can obtain the probabilities of channel being sensed to be busy and idle as

$$\Pr(\hat{\mathcal{H}}_1) = \frac{q}{q+s} \mathscr{P}_{\mathrm{d}} + \frac{s}{s+q} \mathscr{P}_{\mathrm{f}}, \tag{7.8}$$

$$\Pr(\hat{\mathcal{H}}_0) = \frac{q}{q+s} (1 - \mathscr{P}_{\mathrm{d}}) + \frac{s}{s+q} (1 - \mathscr{P}_{\mathrm{f}}). \tag{7.9}$$

Finally, we would like to note that channel sensing can be performed by either the secondary

receiver or transmitter, and we have implicitly assumed that the secondary receiver performs this task. In such a case, we further assume that the binary sensing decision made by the secondary receiver is reliably fed back to the secondary transmitter through a low-rate control channel.

7.1.3 Data Transmission Parameters, Interference Management, and Channel Model

Following channel sensing, secondary users initiate the data transmission phase in the remaining $T - N$ seconds. They adapt transmission rates and power levels depending on the channel sensing decision and availability of channel side information (CSI). More specifically, in the absence of CSI at the secondary transmitter, fixed-rate transmission is performed with constant power level while in the presence of perfect CSI, data is sent at a variable rate. Additionally, the average power is $\overline{P}_1$ and transmission rate is r_1 in the case of channel being sensed to be busy, and average power is $\overline{P}_2$ and transmission rate is r_2 in the case of channel being sensed to be idle.

The two-level transmission scheme described above is adopted to limit the interference inflicted on the primary users. Therefore, we in general have $\overline{P}_1 \leq \overline{P}_2$. If cognitive users are not allowed to transmit when the primary user activity is detected in the channel, then we set $\overline{P}_1 = 0$. In general, power $\overline{P}_1$ should be below a certain threshold in order to limit the interference inflicted on the primary users. Note that when the transmission power is $\overline{P}_1$, the average interference experienced by a primary user is $\overline{P}_1 \mathbb{E}\{|g_{sp}|^2\}$ where g_{sp} is the fading coefficient of the channel between the secondary transmitter and primary receiver. Then, an upper bound on the transmission power $\overline{P}_1$ can be expressed as

$$\overline{P}_1 \leq \frac{I_0}{\max_j \mathbb{E}\{|g_{sp,j}|^2\}} \tag{7.10}$$

where I_0 is the maximum average interference power that the primary users can tolerate and

$|g_{sp,j}|^2$ is the channel gain between the secondary transmitter the and j^{th} primary receiver. However, this may not provide sufficient protection in the presence of sensing errors since primary receivers are disturbed with average transmission power of $\overline{P}_2$ in the case of miss-detections. Therefore, as an additional mechanism to control the interference, an upper bound on the probability of miss detection or equivalently a lower bound on the detection probability should be imposed in cognitive radio systems so that miss-detections occur rarely.

Yet, another method to limit the average interference power experienced by the primary users is to impose the following constraint on the transmission powers:

$$\mathscr{P}_{\text{d}}\overline{P}_1 + (1-\mathscr{P}_{\text{d}})\overline{P}_2 \leq \frac{I_0}{\max_j \mathbb{E}\{|g_{sp,j}|^2\}} \tag{7.11}$$

together with possibly peak constraints $\overline{P}_1 \leq \overline{P}_{\text{peak},1}$ and $\overline{P}_2 \leq \overline{P}_{\text{peak},2}$. Above, $\mathscr{P}_{\text{d}}$ is the detection probability in channel sensing. Note that primary receiver is disturbed with transmissions of power $\overline{P}_1$ and $\overline{P}_2$ with probabilities $\mathscr{P}_{\text{d}}$ and $(1-\mathscr{P}_{\text{d}})$, respectively, which are the probabilities of correct detection and miss-detection events. Hence, average interference power is proportional to $\mathscr{P}_{\text{d}}\overline{P}_1 + (1-\mathscr{P}_{\text{d}})\overline{P}_2$. We note that such an average interference power constraint was, for instance, considered in [15].

Finally, we remark that the analysis in Section 7.3 is conducted for given average power constraints and given signal-to-noise ratios. Therefore, any of the interference constraints discussed above can be easily be accommodated in the subsequent throughput analysis.

Next, we describe the channel model. The channel between the secondary users is assumed to experience flat fading. We also consider the block-fading assumption in which the fading coefficients are constant within the frame of T seconds and change independently between the frames. Under these assumptions, the complex input-complex output relationship

is

$$\mathbf{y} = \begin{cases} h\mathbf{x} + \mathbf{n} & \text{in the absence of primary user activity,} \\ h\mathbf{x} + \mathbf{n} + \mathbf{s} & \text{in the presence of primary user activity.} \end{cases} \tag{7.12}$$

Above, h is the circularly-symmetric complex fading coefficient with a finite variance, i.e., $\mathbb{E}\{|h|^2\} < \infty$. $\mathbf{x}$ and $\mathbf{y}$ are the $(T-N)B$–dimensional complex channel input and output vectors, respectively. Since we assume that transmissions are power constrained by $\overline{P}_1$ or $\overline{P}_2$, the average energy available in the data transmission period of $(T-N)$ seconds is $(T-N)\overline{P}_i$ for $i = 1, 2$, and hence $\mathbb{E}\{\|\mathbf{x}\|^2\} = (T-N)\overline{P}_i$. With energy uniformly distributed across input symbols, the average energy per symbol becomes $\mathbb{E}\{|x_i|^2\} = \frac{\overline{P}_i}{B}$[1].

In (7.12), $\mathbf{n}$ denotes the vector of i.i.d. noise samples that are circularly symmetric, Gaussian random variables with mean zero and variance $E\{|n|^2\} = \sigma_n^2$, and $\mathbf{s}$ again represents the vector of active primary users' faded sum signal received at the secondary receiver similarly as in (7.3). We again assume that the components of $\mathbf{s}$ are i.i.d. Gaussian random variables with mean zero and variance $E\{|s|^2\} = \sigma_s^2$.

7.2 Transmission Rate in the Finite Blocklength Regime

In [87], Polyanskiy, Poor and Verdú studied the channel coding rate achieved with finite blocklength codes and identified a second-order expression for the channel capacity of the real additive white Gaussian noise (AWGN) channel in terms of the coding blocklength $(T-N)B$, error probability ϵ, and signal-to-noise ratio (SNR). As done in [88], this result can be slightly modified to obtain the following approximate expression for the instantaneous channel capacity of a flat-fading channel attained in the data transmission duration of $(T-$

[1]Alternatively, if an average energy constraint of $\mathbb{E}\{\|\mathbf{x}\|^2\} = \overline{P}_i T$ is imposed in the data transmission period rather than an average power constraint, the average energy per symbol becomes $\mathbb{E}\{|x_i|^2\} = \frac{T\overline{P}_i}{(T-N)B}$. This leads to the scaling of the signal-to-noise ratio by a factor of $\frac{T}{T-N}$. Since the analysis in Section 7.3 is conducted for given signal-to-noise ratio expressions, an average energy constraint given as above can be incorporated into the analysis easily.

$N)B$ symbols[2]:

$$r = \log_2(1+\text{SNR}|h|^2) - \sqrt{\frac{1}{(T-N)B}\left(1 - \frac{1}{(\text{SNR}|h|^2+1)^2}\right)}Q^{-1}(\epsilon)\log_2 e \tag{7.13}$$

where $Q(x) = \int_x^\infty \frac{1}{\sqrt{2\pi}} e^{-t^2/2} dt$ is the Gaussian Q-function and SNR denotes the signal-to-noise ratio which can be expressed as average energy per symbol normalized by the variance of the noise random variable. The above expression provides the rate that can be achieved with error probability ϵ for a given fading coefficient h and signal-to-noise ratio SNR. Note that as the blocklength $(T-N)B$ grows without bound, the second term on the right-hand side of (7.13) vanishes and transmission rate r approaches the instantaneous channel capacity $\log_2(1+\text{SNR}|h|^2)$ for any arbitrarily small $\epsilon > 0$.

Equivalently, we can also conclude from (7.13) that transmission with a given fixed rate r can be supported with error probability

$$\epsilon_{|h|^2} = Q\left(\frac{\log_2(1+\text{SNR}|h|^2) - r}{\sqrt{\frac{1}{(T-N)B}\left(1 - \frac{1}{(\text{SNR}|h|^2+1)^2}\right)}\log_2 e}\right) \tag{7.14}$$

where the dependence of the error probability on fading is made explicit by expressing ϵ with subscript $|h|^2$.

In order to observe the effect of finite-length codewords on the reliability of transmissions, in Fig. 7.2 we display the error probability vs. transmission rate when the transmitter is assumed to employ finite-length codewords together with the asymptotical behavior as the codeword length grows without bound. According to the Shannon capacity limit, when the codeword length increases without bound, we can achieve reliable transmission with no decoding errors (i.e., $\epsilon = 0$) for any transmission rate less than the instantaneous channel capacity, i.e., $r < C = \log_2(1+\text{SNR}|h|^2)$, whereas reliable communication is not possible when $r \geq C$. Indeed, as noted in [89], by the strong converse, when $r > C$, probability of error goes exponentially to 1 as the blocklength increases. Therefore, we have the sharp

[2]For (7.13) to hold, we assume that $(T-N)B$ is sufficiently large but finite.

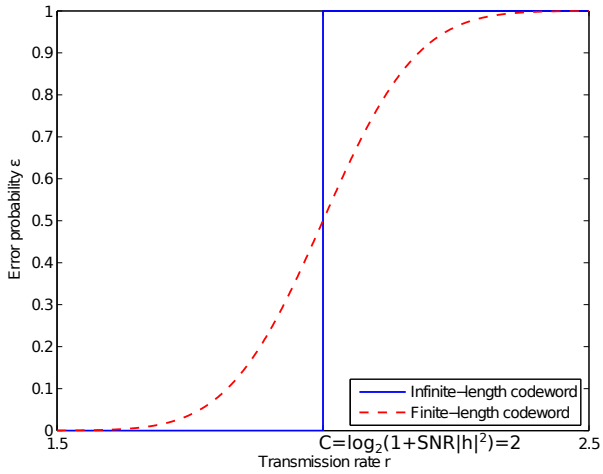

Figure 7.2: Error probability vs. transmission rate for infinite-length and finite-length codewords, $\text{SNR} = 3, |h|^2 = 1$, and $C = \log_2(1 + \text{SNR}|h|^2) = 2$.

cutoff at the instantaneous capacity in Fig. 7.2 for the asymptotic scenario of codewords of infinite length. Close inspection of (7.14) leads to the same conclusion as well. Let $r > \log_2(1 + \text{SNR}|h|^2)$. Then, as the blocklength $(T - N)B$ increases to infinity, the term $\sqrt{\frac{1}{(T-N)B}\left(1 - \frac{1}{(\text{SNR}|h|^2+1)^2}\right)}$ vanishes and in the limit, we have $\epsilon_{|h|^2} = Q(-\infty) = 1$. If $r < \log_2(1 + \text{SNR}|h|^2)$, we asymptotically have $\epsilon_{|h|^2} = Q(\infty) = 0$.

On the other hand, for finite-length codewords, when we plot (7.14), we see that we have a relatively smooth transition. This behavior indicates that for transmissions with rates less than the instantaneous capacity, we can still have errors, albeit with relatively small probabilities, while transmission rates above the instantaneous capacity can lead to successful transmissions but again only with small probability.

7.3 State Transition Model for the Cognitive Radio Channel and Effective Throughput

Before a detailed analysis, we first briefly describe the impact of considering finite-blocklength regime in the throughput analysis of cognitive radio channels in the presence of buffer con-

straints. The critical difference from the studies with infinite-blocklength codes is that we now have non-zero error probabilities even if the transmission rates are less than the instantaneous capacity. Moreover, we observe from (7.14) that error probabilities, for fixed-rate transmissions, fluctuate depending on the channel conditions. In general, such error events will be reflected in the subsequent analysis by the presence of OFF states in which reliable communication is not achieved due to errors and consequently retransmissions are required. This potentially has significant impact in buffer-limited systems as frequent communication failures and retransmission requests can easily lead to buffer overflows. Therefore, coding rates and error probabilities in the finite-blocklength regime should be judiciously analyzed and optimal transmission parameters should be identified. Situation is further exacerbated in cognitive radio systems in which channel sensing is performed imperfectly and interference constraints are imposed. Firstly, time allocated to channel sensing results in reduced transmission duration, leading to reduced codeword blocklength with consequences on both the rates and error probabilities. Additionally, false-alarms and miss-detections, experienced due to imperfect sensing, cause over- or underestimations of the channel, and resulting mismatches cause transmission rates and/or error probabilities to exceed or be lower than required or target levels.

In this section, we first construct an eight-state Markov chain in order to model the cognitive radio channel, and then derive the corresponding state transition probabilities when CSI is assumed to be perfectly known either at the receiver only or at both the receiver and transmitter. Subsequently, we analyze the throughput achieved with finite blocklength codes in the presence of buffer constraints under these two assumptions.

7.3.1 Perfect CSI at the Receiver Only

It is assumed that perfect knowledge of fading realizations is available at the secondary receiver, but not at the secondary transmitter. Therefore, the transmitter performs data transmission with constant rate of r_1 or r_2 based on the sensing decision about the channel

occupancy by the primary users.

7.3.1.1 State Transition Model

Before analyzing the throughput achieved by the secondary users with finite blocklength codes under buffer constraints, we construct a state transition model for the cognitive radio channel. First, we list the four possible scenarios, together with corresponding signal-to-noise ratio expressions, arising as a result of different channel sensing decisions and the true nature of primary users' activity:

- *Scenario I* (Correct-detection denoted by joint event $(\mathcal{H}_1, \hat{\mathcal{H}}_1)$):
  Busy channel is sensed as busy and $\text{SNR}_1 = \frac{\overline{P}_1}{B(\sigma_n^2+\sigma_s^2)}$.

- *Scenario II* (Miss-detection denoted by $(\mathcal{H}_1, \hat{\mathcal{H}}_0)$):
  Busy channel is sensed as idle and $\text{SNR}_2 = \frac{\overline{P}_2}{B(\sigma_n^2+\sigma_s^2)}$.

- *Scenario III* (False-alarm denoted by $(\mathcal{H}_0, \hat{\mathcal{H}}_1)$):
  Idle channel is sensed as busy and $\text{SNR}_3 = \frac{\overline{P}_1}{B\sigma_n^2}$.

- *Scenario IV* (Correct-detection denoted by $(\mathcal{H}_0, \hat{\mathcal{H}}_0)$):
  Idle channel is sensed as idle and $\text{SNR}_4 = \frac{\overline{P}_2}{B\sigma_n^2}$.

Additionally, transmission rate is r_1 bits/s/Hz in scenarios 1 and 3 above, and is r_2 bits/s/Hz in scenarios 2 and 4. When codewords of length $(T-N)B$ are used to send the data at these fixed rates, we know from the discussion in Section 7.2 that information is received reliably with probability $(1-\epsilon_{|h|^2})$ while errors occur and retransmission is needed with probability $\epsilon_{|h|^2}$ as formulated in (7.14). More specifically, the error probabilities in scenarios 1 and 3 are

$$\epsilon_d(|h|^2) = Q\left(\frac{\log_2(1+\text{SNR}_d|h|^2) - r_1}{\sqrt{\frac{1}{(T-N)B}\left(1-\frac{1}{(\text{SNR}_d|h|^2+1)^2}\right)}\log_2 e}\right) \tag{7.15}$$

for $d = 1$ and 3, respectively. Similarly, we have

$$\epsilon_l(|h|^2) = Q\left(\frac{\log_2(1+\text{SNR}_l|h|^2) - r_2}{\sqrt{\frac{1}{(T-N)B}\left(1-\frac{1}{(\text{SNR}_l|h|^2+1)^2}\right)}\log_2 e}\right) \tag{7.16}$$

in scenarios 2 and 4 for $l = 2$ and 4, respectively. Above, we see that error probability is a function of the fading coefficient $|h|$ and SNR. From this discussion, we conclude that the channel can be either in the ON state (in which information is reliably received) or the OFF state (in which erroneous reception occurs) in each scenario. Hence, we have eight states in total in the Markov model for the cognitive radio channel as depicted in Fig. 7.3. Note that

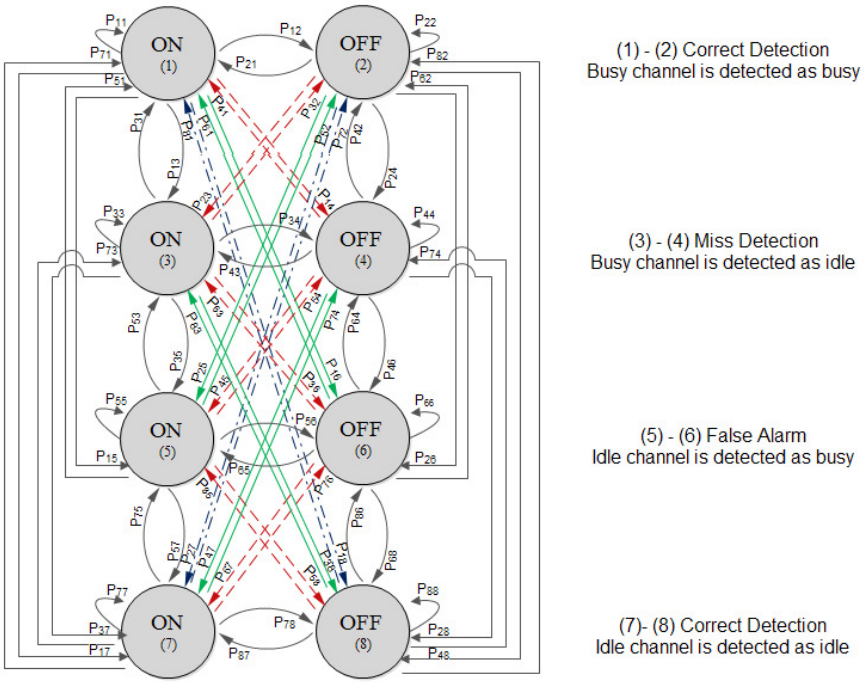

Figure 7.3: The state-transition model for the cognitive radio channel with eight possible states.

since reliable communication cannot be achieved in the OFF states, the transmission rate is effectively zero and the data has to be retransmitted in these states. Therefore, the service

rates (in bits/frame) in four scenarios can be expressed, respectively, as

$$R_d = \begin{cases} 0 & \text{with probability } \epsilon_d(|h|^2) \\ (T-N)Br_1 & \text{with probability } (1-\epsilon_d(|h|^2)) \end{cases} \tag{7.17}$$

$$R_l = \begin{cases} 0 & \text{with probability } \epsilon_l(|h|^2) \\ (T-N)Br_2 & \text{with probability } (1-\epsilon_l(|h|^2)) \end{cases} \tag{7.18}$$

for $d = 1, 3$ and $l = 2, 4$.

Next, we identify the transition probabilities from state i to state k denoted by p_{ik} in the eight state transition model of the cognitive radio channel. We initially analyze in detail p_{11}, the probability of staying in the topmost ON state.

We can first express p_{11} as follows:

$$p_{11} = \Pr\left\{ \begin{array}{c} \text{Channel is busy and detected as busy} \\ \text{and channel is ON in the } i^{th} \text{ frame} \end{array} \middle| \begin{array}{c} \text{Channel was busy and detected as busy} \\ \text{and channel was ON in the } (i-1)^{th} \text{ frame} \end{array} \right\} \tag{7.19}$$

$$= \Pr\left\{ \begin{array}{c} \text{Channel is busy} \\ \text{in the } i^{th} \text{ frame} \end{array} \middle| \begin{array}{c} \text{Channel was busy} \\ \text{in the } (i-1)^{th} \text{ frame} \end{array} \right\} \tag{7.20}$$

$$\times \Pr\left\{ \begin{array}{c} \text{Channel is detected as busy} \\ \text{in the } i^{th} \text{ frame} \end{array} \middle| \begin{array}{c} \text{Channel is busy} \\ \text{in the } i^{th} \text{ frame} \end{array} \right\}$$

$$\times \Pr(\text{Channel is ON in the } i^{th} \text{ frame}) \tag{7.21}$$

$$= (1-s)\mathscr{P}_{\mathrm{d}}(1-\epsilon_1(|h|^2). \tag{7.22}$$

Subsequently, we can write (7.20) by noting that channel being actually busy in the current frame depends on its state in the previous frame due to the two-state Markov chain, and channel being detected as busy in the i^{th} frame depends only on the true state of the channel

being busy or idle in the i^{th} frame and not on previous true states and sensing decisions since channel sensing is performed in each frame independently. Moreover, channel being ON does not depend on the sensing decisions and channel being ON or OFF in the previous frames due to the block-fading assumption. Finally, we have (7.22) by observing that the first probability in (7.20) is $P_{B,B} = 1 - s$ in the Markov chain, the second probability is the correct detection probability $\mathscr{P}_{\mathrm{d}}$ in channel sensing, and channel is ON with probability $(1 - \epsilon_1(|h|^2))$ as discussed above.

By following the same steps, transition probabilities from all eight states to state 1 can be found as

$$\begin{aligned} p_{i1} &= p_{11} = p_{21} = p_{31} = p_{41} = (1-s)\mathscr{P}_{\mathrm{d}}(1-\epsilon_1(|h|^2)), \\ p_{k1} &= p_{51} = p_{61} = p_{71} = p_{81} = q\mathscr{P}_{\mathrm{d}}(1-\epsilon_1(|h|^2)). \end{aligned} \tag{7.23}$$

The channel is busy in the first four states and we see that the transition probabilities from these four states to the first state are the same. The channel is idle in the last four states and similarly their transition probabilities are equal. Hence, (7.23) shows that we can group the transition probabilities into two with respect to the true nature of the channel, i.e., busy or idle. The rest of the transition probabilities between each state can be derived in a similar fashion and the overall result can be listed as follows for $i = 1, 2, 3, 4$ and $k = 5, 6, 7, 8$:

$$\begin{aligned} p_{i2} &= (1-s)\mathscr{P}_{\mathrm{d}}\epsilon_1(|h|^2) & p_{k2} &= q\mathscr{P}_{\mathrm{d}}\epsilon_1(|h|^2), \\ p_{i3} &= (1-s)(1-\mathscr{P}_{\mathrm{d}})(1-\epsilon_2(|h|^2)) & p_{k3} &= q(1-\mathscr{P}_{\mathrm{d}})(1-\epsilon_2(|h|^2)), \\ p_{i4} &= (1-s)(1-\mathscr{P}_{\mathrm{d}})\epsilon_2(|h|^2) & p_{k4} &= q(1-\mathscr{P}_{\mathrm{d}})\epsilon_2(|h|^2), \\ p_{i5} &= s\mathscr{P}_{\mathrm{f}}(1-\epsilon_3(|h|^2)) & p_{k5} &= (1-q)\mathscr{P}_{\mathrm{f}}(1-\epsilon_3(|h|^2)), \\ p_{i6} &= s\mathscr{P}_{\mathrm{f}}\epsilon_3(|h|^2) & p_{k6} &= (1-q)\mathscr{P}_{\mathrm{f}}\epsilon_3(|h|^2), \\ p_{i7} &= s(1-\mathscr{P}_{\mathrm{f}})(1-\epsilon_4(|h|^2)) & p_{k7} &= (1-q)(1-\mathscr{P}_{\mathrm{f}})(1-\epsilon_4(|h|^2)), \\ p_{i8} &= s(1-\mathscr{P}_{\mathrm{f}})\epsilon_4(|h|^2) & p_{k8} &= (1-q)(1-\mathscr{P}_{\mathrm{f}})\epsilon_4(|h|^2). \end{aligned} \tag{7.24}$$

The set of transition probabilities is expressed in an 8×8 state transition matrix given in (7.25) on the next page. Note that the rank of R is 2 since it has only two linearly

$$R = \begin{bmatrix} p_{1,1} & p_{1,2} & \cdots & p_{1,8} \\ . & . & \cdots & . \\ p_{4,1} & p_{4,2} & \cdots & p_{4,8} \\ p_{5,1} & p_{5,2} & \cdots & p_{5,8} \\ . & . & \cdots & . \\ p_{8,1} & p_{8,2} & \cdots & p_{8,8} \end{bmatrix} = \begin{bmatrix} p_{i1} & . & . & p_{i8} \\ . & . & . & . \\ p_{i1} & . & . & p_{i8} \\ p_{k1} & . & . & p_{k8} \\ . & . & . & . \\ p_{k1} & . & . & p_{k8} \end{bmatrix}. \tag{7.25}$$

independent column vectors.

7.3.1.2 Throughput Under Buffer Limitations

Now, we determine the throughput achieved with finite blocklength codes subject to buffer constraints by obtaining the effective rate of the cognitive radio channel with the state-transition model constructed in the case of perfect CSI at the receiver only. The approach and techniques in this section closely follow [86] with the difference that we now consider performance in the finite blocklength regime. In [90, Chap. 7, Example 7.2.7], it is shown for Markov modulated processes that

$$\frac{\Lambda(\theta)}{\theta} = \frac{1}{\theta} \log_e sp(\phi(\theta)R) \tag{7.26}$$

where $\Lambda(\theta)$ is defined underneath (2.19), $sp(\phi(\theta)R)$ is the spectral radius or the maximum of the absolute values of the eigenvalues of the matrix $\phi(\theta)R$, R is the transition matrix of the underlying Markov process, and $\phi(\theta) = \text{diag}(\phi_1(\theta), \ldots, \phi_M(\theta))$ is a diagonal matrix whose components are the moment generating functions of the processes in M states ($M = 8$ in our model). In our case, we have

$$\phi(\theta) = \text{diag}\{e^{\theta(T-N)Br_1}, 1, e^{\theta(T-N)Br_2}, 1, e^{\theta(T-N)Br_1}, 1, e^{\theta(T-N)Br_2}, 1\}, \text{ and} \tag{7.27}$$

$$\phi(\theta)R = \begin{bmatrix} e^{\theta(T-N)Br_1}p_{i1} & \dots & e^{\theta(T-N)Br_1}p_{i8} \\ p_{i1} & \dots & p_{i8} \\ e^{\theta(T-N)Br_2}p_{i1} & \dots & e^{\theta(T-N)Br_2}p_{i8} \\ p_{i1} & \dots & p_{i8} \\ e^{\theta(T-N)Br_1}p_{k1} & \dots & e^{\theta(T-N)Br_1}p_{k8} \\ p_{k1} & \dots & p_{k8} \\ e^{\theta(T-N)Br_2}p_{k1} & \dots & e^{\theta(T-N)Br_2}p_{k8} \\ p_{k1} & \dots & p_{k8} \end{bmatrix}. \tag{7.28}$$

Note that $\phi(\theta)R$ is a rank-2 matrix as well. As the n-rowed ($n \geq 3$) principal minors of $\phi(\theta)R$ are zero, the coefficients of the characteristic polynomial of the matrix $\phi(\theta)R$ can be found in terms of adding only the 1-rowed and 2-rowed principal minors, then the maximum root of this polynomial gives the spectral radius $sp(\phi(\theta)R)$, which is expressed in

$$\begin{aligned} sp(\phi(\theta)R) =& \frac{1}{2}\Big[\phi_1(\theta)p_{i1} + \cdots + \phi_4(\theta)p_{i4} + \phi_5(\theta)p_{k5} + \cdots + \phi_8(\theta)p_{k8}\Big] \\ &+ \frac{1}{2}\Bigg\{\Big[\phi_1(\theta)p_{i1} + \cdots + \phi_4(\theta)p_{i4} - \phi_5(\theta)p_{k5} - \cdots - \phi_8(\theta)p_{k8}\Big]^2 \\ &+ 4(\phi_1(\theta)p_{k1} + \cdots + \phi_4(\theta)p_{k4}) \times (\phi_5(\theta)p_{i5} + \cdots + \phi_8(\theta)p_{i8})\Bigg\}^{\frac{1}{2}}. \end{aligned} \tag{7.29}$$

Now, combining (2.19), (7.26), and (7.29), we can easily express the effective rate of the

cognitive channel in the following:

$$R_E(\mathrm{SNR},\theta) = \max_{r_1,r_2\geq 0} -\frac{1}{\theta TB}\log_e \mathbb{E}_{|h|^2}\Bigg(\frac{1}{2}\Big[(p_{i1}+p_{k5})e^{-\theta(T-N)Br_1} + (p_{i3}+p_{k7})e^{-\theta(T-N)Br_2} + p_{i2} + p_{i4} + p_{k6} + p_{k8}\Big] + \frac{1}{2}\Big\{\Big[(p_{i1}-p_{k5})e^{-\theta(T-N)Br_1} + (p_{i3}-p_{k7})e^{-\theta(T-N)Br_2} + p_{i2} + p_{i4} - p_{k6} - p_{k8}\Big]^2 + 4(p_{k1}e^{-\theta(T-N)Br_1} + p_{k2} + p_{k3}e^{-\theta(T-N)Br_2} + p_{k4}) \times (p_{i5}e^{-\theta(T-N)Br_1} + p_{i6} + p_{i7}e^{-\theta(T-N)Br_2} + p_{i8})\Big\}^{\frac{1}{2}}\Bigg). \tag{7.30}$$

Note that $R_E(\mathrm{SNR},\theta)$ in (7.30) characterizes the maximum constant arrival rates that the cognitive radio channel can support in the finite blocklength regime under buffer limitations characterized by the QoS exponent θ. Note that this throughput is maximized over transmission rates r_1 and r_2.

Throughput in the absence of any buffer constraints, which can be easily determined by letting $\theta \to 0$ in $R_E(\mathrm{SNR},\theta)$, is given by

$$\begin{aligned} R_E(\mathrm{SNR},0) = \max_{r_1,r_2\geq 0} &\frac{(T-N)r_1\mathscr{P}_{\mathrm{d}}}{2T(s+q)}\Big((1-s)(3q-s)+4sq\Big)(1-\mathbb{E}_{|h|^2}\{\epsilon_1(|h|^2)\}) \\ &+ \frac{(T-N)r_2(1-\mathscr{P}_{\mathrm{d}})}{2T(s+q)}\Big((1-s)(3q-s)+4sq\Big)(1-\mathbb{E}_{|h|^2}\{\epsilon_2(|h|^2)\}) \\ &+ \frac{(T-N)r_1\mathscr{P}_{\mathrm{f}}}{2T(s+q)}\Big((1-s)(3s-q)+4sq\Big)(1-\mathbb{E}_{|h|^2}\{\epsilon_3(|h|^2)\}) \\ &+ \frac{(T-N)r_2(1-\mathscr{P}_{\mathrm{f}})}{2T(s+q)}\Big((1-s)(3s-q)+4sq\Big)(1-\mathbb{E}_{|h|^2}\{\epsilon_4(|h|^2)\}) \end{aligned} \tag{7.31}$$

7.3.2 Perfect CSI at both the Receiver and Transmitter

Instead of CSI known by the receiver only, we in this subsection consider that both the secondary transmitter and receiver have access to perfect CSI. Therefore, the secondary

transmitter can adapt its transmission scheme by varying the rate depending on the instantaneous values of the fading coefficient $|h|$.

7.3.2.1 State Transition Model

Under the assumption of perfect CSI at the transmitter, the eight-state Markov model for the cognitive radio channel with four possible scenarios and ON/OFF states is unchanged as we defined in the case of perfect CSI at the receiver only. Additionally, the SNR expressions in each scenario are still the same. In contrast to fixed-rate transmission schemes, for a given fixed target error probability ϵ, the secondary transmitter now varies its transmission rate according to the channel conditions and channel sensing decision. More specifically, in the case of channel being sensed as busy, the secondary transmitter initiates data transmission with rate

$$r_1(\text{SNR}_1, |h|^2) = \log_2(1 + \text{SNR}_1|h|^2) - \sqrt{\frac{1}{(T-N)B}\left(1 - \frac{1}{(\text{SNR}_1|h|^2+1)^2}\right)}Q^{-1}(\epsilon)\log_2 e. \quad (7.32)$$

On the other hand, if no primary user activity is sensed in the channel, we have the following transmission rate

$$r_2(\text{SNR}_4, |h|^2) = \log_2(1 + \text{SNR}_4|h|^2) - \sqrt{\frac{1}{(T-N)B}\left(1 - \frac{1}{(\text{SNR}_4|h|^2+1)^2}\right)}Q^{-1}(\epsilon)\log_2 e. \quad (7.33)$$

Before specifying the transition probabilities of the cognitive radio channel, we initially determine the error probabilities in each scenario that are associated with the transmission rates $r_1(\text{SNR}_1, |h|^2)$ or $r_2(\text{SNR}_4, |h|^2)$:

- In scenario 1, the fixed target error probability ϵ is attained with the transmission rate $r_1(\text{SNR}_1, |h|^2)$ defined above.

- In scenario 2 (in which we have missed detection), due to the primary user activity and the resulting interference on secondary users, the actual channel rate associated with error probability ϵ is

$$\log_2(1 + \text{SNR}_2|h|^2) - \sqrt{\frac{1}{(T-N)B}\left(1 - \frac{1}{(\text{SNR}_2|h|^2+1)^2}\right)}Q^{-1}(\epsilon)\log_2 e. \quad (7.34)$$

However, the secondary users do not know the true state of the channel, and they only have the imperfect channel sensing result. In this case, the channel is detected as idle even if the primary users are active. Hence, for the given target error probability ϵ, the secondary users send data with rate $r_2(\text{SNR}_4, |h|^2)$, which is obviously higher than the actual rate in (7.34) that the channel actually supports with error probability ϵ.

As a result, we have in fact higher error probability $\epsilon''_{|h|^2}$ (compared to the given target error probability ϵ) when the transmission rate is $r_2(\text{SNR}_4, |h|^2)$. Equating the transmission rate $r_2(\text{SNR}_4, |h|^2)$ to that in (7.34), and rearraging the terms, the final expression of the actual error probability $\epsilon''_{|h|^2}$ can be found as

$$\epsilon''_{|h|^2} = Q\left(\frac{\log_2(\frac{1+\text{SNR}_2|h|^2}{1+\text{SNR}_4|h|^2}) + \sqrt{\frac{1}{(T-N)B}\left(1-\frac{1}{(\text{SNR}_4|h|^2+1)^2}\right)}Q^{-1}(\epsilon)\log_2 e}{\sqrt{\frac{1}{(T-N)B}\left(1-\frac{1}{(\text{SNR}_2|h|^2+1)^2}\right)}\log_2 e}\right). \quad (7.35)$$

In this case, due to the sensing error, we are subject to more transmission errors resulting in lower reliability in data transmission. We also see that error probability $\epsilon''_{|h|^2}$ in (7.35) that can be achieved with transmission rate $r_2(\text{SNR}_4, |h|^2)$ is a function of the fading coefficient $|h|$.

- In scenario 3 (in which we have false alarm), for a given error probability ϵ, the channel supports the rate

$$\log_2(1+\text{SNR}_3|h|^2) - \sqrt{\frac{1}{(T-N)B}\left(1-\frac{1}{(\text{SNR}_3|h|^2+1)^2}\right)}Q^{-1}(\epsilon)\log_2 e \quad (7.36)$$

which is higher than the rate $r_1(\text{SNR}_1, |h|^2)$ because there is actually no interference from the primary users, i.e, $\text{SNR}_1 < \text{SNR}_3$. Therefore, the error probability that can be attained with this transmission rate is less than the given fixed target error probability ϵ. Following the same approach adopted in scenario 2, the actual error probability $\epsilon'_{|h|^2}$

can be expressed as

$$\epsilon'_{|h|^2} = Q\left(\frac{\log_2\left(\frac{1+\mathrm{SNR}_3|h|^2}{1+\mathrm{SNR}_1|h|^2}\right) + \sqrt{\frac{1}{(T-N)B}\left(1-\frac{1}{(\mathrm{SNR}_1|h|^2+1)^2}\right)}Q^{-1}(\epsilon)\log_2 e}{\sqrt{\frac{1}{(T-N)B}\left(1-\frac{1}{(\mathrm{SNR}_3|h|^2+1)^2}\right)}\log_2 e}\right). \quad (7.37)$$

Note that, the error probability $\epsilon'_{|h|^2}$ again varies with the fading coefficient $|h|$.

- In scenario 4, the constant error probability ϵ is attained with rate $r_2(\mathrm{SNR}_4, |h|^2)$.

By combining the above error probability expressions, the average probability of error for variable-rate transmissions is given by

$$\epsilon_{avg} = \Pr(\mathcal{H}_1, \hat{\mathcal{H}}_1)\epsilon + \Pr(\mathcal{H}_1, \hat{\mathcal{H}}_0)\mathbb{E}_{|h|^2}\{\epsilon''_{|h|^2}\} + \Pr(\mathcal{H}_0, \hat{\mathcal{H}}_1)\mathbb{E}_{|h|^2}\{\epsilon'_{|h|^2}\} + \Pr(\mathcal{H}_0, \hat{\mathcal{H}}_0)\epsilon. \quad (7.38)$$

We can further express ϵ_{avg} by using the prior probabilities of the channel state given in (7.1) and the probabilities of channel sensing decisions in (7.5) – (7.7) as follows:

$$\begin{aligned}\epsilon_{avg} &= \Pr(\mathcal{H}_1)\Pr(\hat{\mathcal{H}}_1|\mathcal{H}_1)\epsilon + \Pr(\mathcal{H}_1)\Pr(\hat{\mathcal{H}}_0|\mathcal{H}_1)\mathbb{E}_{|h|^2}\{\epsilon''_{|h|^2}\} \\ &\quad + \Pr(\mathcal{H}_0)\Pr(\hat{\mathcal{H}}_1|\mathcal{H}_0)\mathbb{E}_{|h|^2}\{\epsilon'_{|h|^2}\} + \Pr(\mathcal{H}_0)\Pr(\hat{\mathcal{H}}_0|\mathcal{H}_0)\epsilon \\ &= \frac{q}{q+s}\mathscr{P}_{\mathrm{d}}\epsilon + \frac{q}{q+s}(1-\mathscr{P}_{\mathrm{d}})\mathbb{E}_{|h|^2}\{\epsilon''_{|h|^2}\} + \frac{s}{s+q}\mathscr{P}_{\mathrm{f}}\mathbb{E}_{|h|^2}\{\epsilon'_{|h|^2}\} + \frac{s}{s+q}(1-\mathscr{P}_{\mathrm{f}})\epsilon.\end{aligned} \quad (7.39)$$

Now we can obtain the transition probabilities for $i = 1, 2, 3, 4$ and $k = 5, 6, 7, 8$ in a similar fashion as in the case of perfect CSI only at the receiver

$$\begin{aligned}
p_{i1} &= (1-s)\mathscr{P}_{\mathrm{d}}(1-\epsilon) & p_{k1} &= q\mathscr{P}_{\mathrm{d}}(1-\epsilon),\\
p_{i2} &= (1-s)\mathscr{P}_{\mathrm{d}}\epsilon & p_{k2} &= q\mathscr{P}_{\mathrm{d}}\epsilon,\\
p_{i3} &= (1-s)(1-\mathscr{P}_{\mathrm{d}})(1-\epsilon''_{|h|^2}) & p_{k3} &= q(1-\mathscr{P}_{\mathrm{d}})(1-\epsilon''_{|h|^2}),\\
p_{i4} &= (1-s)(1-\mathscr{P}_{\mathrm{d}})\epsilon''_{|h|^2} & p_{k4} &= q(1-\mathscr{P}_{\mathrm{d}})\epsilon''_{|h|^2},\\
p_{i5} &= s\mathscr{P}_{\mathrm{f}}(1-\epsilon'_{|h|^2}) & p_{k5} &= (1-q)\mathscr{P}_{\mathrm{f}}(1-\epsilon'_{|h|^2}),\\
p_{i6} &= s\mathscr{P}_{\mathrm{f}}\epsilon'_{|h|^2} & p_{k6} &= (1-q)\mathscr{P}_{\mathrm{f}}\epsilon'_{|h|^2},\\
p_{i7} &= s(1-\mathscr{P}_{\mathrm{f}})(1-\epsilon) & p_{k7} &= (1-q)(1-\mathscr{P}_{\mathrm{f}})(1-\epsilon),\\
p_{i8} &= s(1-\mathscr{P}_{\mathrm{f}})\epsilon & p_{k8} &= (1-q)(1-\mathscr{P}_{\mathrm{f}})\epsilon,
\end{aligned} \tag{7.40}$$

where the transition probabilities to states 1, 2, 7 and 8 are constant while the rest of the transition probabilities depend on the fading coefficient $|h|$.

7.3.2.2 Throughput Under Buffer Limitations

We will use the same techniques described in the case of perfect CSI at the receiver only. Since service rates in ON states are functions of the fading coefficient in variable-rate transmission, the only difference comes from the moment generating functions of the processes in ON states as follows:

$$\begin{aligned}
\phi(\theta) = \mathrm{diag}\Big\{ &\mathbb{E}_{|h|^2}\{e^{\theta(T-N)Br_1(\mathrm{SNR}_1,|h|^2)}\}, 1, \mathbb{E}_{|h|^2}\{e^{-\theta(T-N)Br_2(\mathrm{SNR}_4,|h|^2)}\}, 1,\\
&\mathbb{E}_{|h|^2}\{e^{\theta(T-N)Br_1(\mathrm{SNR}_1,|h|^2)}\}, 1, \mathbb{E}_{|h|^2}\{e^{-\theta(T-N)Br_2(\mathrm{SNR}_4,|h|^2)}\}, 1\Big\}.
\end{aligned} \tag{7.41}$$

Then, the approach given in the case of perfect CSI only at the receiver, can be applied to obtain the effective rate under QoS constraints as

$$R_E(\mathrm{SNR},\theta) = \max_{\epsilon\geq 0} -\frac{1}{\theta TB}\log_e \mathbb{E}_{|h|^2}\Bigg(\frac{1}{2}\Big[(p_{i1}+p_{k5})\mathbb{E}_{|h|^2}\{e^{-\theta(T-N)Br_1(\mathrm{SNR}_1,|h|^2)}\}$$
$$+(p_{i3}+p_{k7})\mathbb{E}_{|h|^2}\{e^{-\theta(T-N)Br_2(\mathrm{SNR}_4,|h|^2)}\}+p_{i2}+p_{i4}+p_{k6}+p_{k8}\Big]$$
$$+\frac{1}{2}\Big\{\Big[(p_{i1}-p_{k5})\mathbb{E}_{|h|^2}\{e^{-\theta(T-N)Br_1(\mathrm{SNR}_1,|h|^2)}\}+(p_{i3}-p_{k7})\mathbb{E}_{|h|^2}\{e^{-\theta(T-N)Br_2(\mathrm{SNR}_4,|h|^2)}\}$$
$$+p_{i2}+p_{i4}-p_{k6}-p_{k8}\Big]^2+4(p_{k1}\mathbb{E}_{|h|^2}\{e^{-\theta(T-N)Br_1(\mathrm{SNR}_1,|h|^2)}\}+p_{k2}+p_{k3}\mathbb{E}_{|h|^2}\{e^{-\theta(T-N)Br_2(\mathrm{SNR}_4,|h|^2)}\}$$
$$+p_{k4})\times(p_{i5}\mathbb{E}_{|h|^2}\{e^{-\theta(T-N)Br_1(\mathrm{SNR}_1,|h|^2)}\}+p_{i6}+p_{i7}\mathbb{E}_{|h|^2}\{e^{-\theta(T-N)Br_2(\mathrm{SNR}_4,|h|^2)}\}+p_{i8})\Big\}^{\frac{1}{2}}\Bigg) \tag{7.42}$$

The target error probability ϵ can be optimized to maximize the effective throughput. When the cognitive radio channel is not subject to any buffer constraints, hence QoS exponent $\theta\to 0$, we have the effective rate expression given by

$$\begin{aligned}R_E(\mathrm{SNR},0) = \max_{\epsilon\geq 0}\ &\frac{(T-N)\mathbb{E}_{|h|^2}\{r_1(\mathrm{SNR}_1,|h|^2)\}\mathscr{P}_{\mathrm{d}}}{2T(s+q)}\Big((1-s)(3q-s)+4sq\Big)(1-\epsilon)\\
&+\frac{(T-N)\mathbb{E}_{|h|^2}\{r_2(\mathrm{SNR}_4,|h|^2)\}(1-\mathscr{P}_{\mathrm{d}})}{2T(s+q)}\Big((1-s)(3q-s)+4sq\Big)(1-\mathbb{E}_{|h|^2}\{\epsilon''_{|h|^2}\})\\
&+\frac{(T-N)\mathbb{E}_{|h|^2}\{r_1(\mathrm{SNR}_1,|h|^2)\}\mathscr{P}_{\mathrm{f}}}{2T(s+q)}\Big((1-s)(3s-q)+4sq\Big)(1-\mathbb{E}_{|h|^2}\{\epsilon'_{|h|^2}\})\\
&+\frac{(T-N)\mathbb{E}_{|h|^2}\{r_2(\mathrm{SNR}_4,|h|^2)\}(1-\mathscr{P}_{\mathrm{f}}}{2T(s+q)}\Big((1-s)(3s-q)+4sq\Big)(1-\epsilon)\end{aligned} \tag{7.43}$$

7.4 Numerical Results

In this section, the results of numerical computations are illustrated. More specifically, we numerically investigate optimal transmission parameters such as optimal fixed transmission rates and optimal target error probabilities in variable-rate transmissions. Furthermore, we analyze the impact sensing parameters and performance (e.g., sensing duration and threshold, and detection and false-alarm probabilities), different levels of QoS constraints, and codeword blocklengths on the throughput in cognitive radio systems. Numerically, we pro-

vide characterizations for key tradeoffs.

In the simulations, we consider Rayleigh fading channel with exponentially distributed fading power with unit mean, i.e., $f_{|h|^2}(|h|^2) = e^{-|h|^2}$. It is assumed that the channel bandwidth $B = 10$ kHz, noise power $\sigma_n^2 = 0.05$, interference power $\sigma_s^2 = 0.12$ and $\mathbb{E}\{|g_{sp,j}|^2\} = 1$. In the two state Markov model, the transition probabilities from busy to idle state $P_{B,I} = s$ and from idle to busy state $P_{I,B} = q$ are set to 0.6 and 0.2, respectively. The average power values are $\overline{P}_1 = 0$ dB and $\overline{P}_2 = 10$ dB in the cases of channel being sensed to be busy and idle, respectively. Sensing threshold λ is chosen as 0.1 in order to have reasonable probabilities of false alarm and detection. In this case, we have $\mathscr{P}_{\rm d} \approx 0.863$ and $\mathscr{P}_{\rm f} \approx 0.005$. Unless mentioned explicitly, frame duration T is 100 ms, sensing duration N is 1 ms, and hence data transmission is performed with $(T - N)B = 990$ complex signal samples.

7.4.1 Fixed-Rate Transmissions

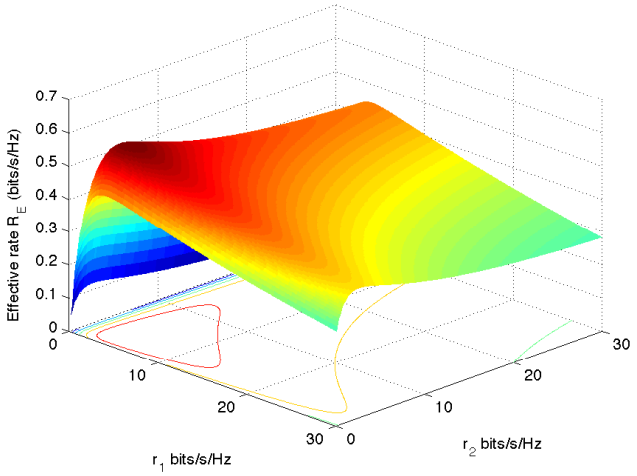

Figure 7.4: The effective rate R_E vs. fixed transmission rates r_1 and r_2 in the Rayleigh fading environment. The code blocklength is $(T - N)B = 990$.

In Fig. 7.4, the effective rate R_E is plotted as a function of fixed transmission rates r_1 and r_2. The QoS exponent θ is set to 0.001. We see that effective rate is maximized at unique r_1 and r_2 values.

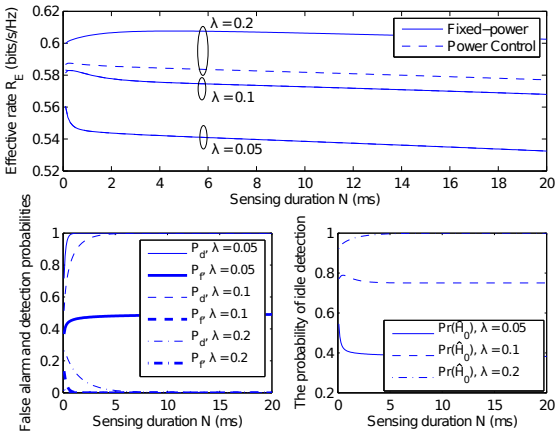

Figure 7.5: The effective rate R_E, the probabilities of false alarm $\mathscr{P}_{\rm f}$ and detection $\mathscr{P}_{\rm d}$, the probability of idle detection $\Pr(\hat{\mathcal{H}}_0)$ vs. sensing duration N in fixed-rate transmission.

We analyze the tradeoff between the sensing duration N and the effective rate R_E. Hence, in Fig. 7.5, we plot the effective rate, the probabilities of false alarm and detection, the probability of idle detection $\Pr(\hat{\mathcal{H}}_0)$ as a function of the channel sensing duration N for $\lambda = 0.05, 0.1$ and 0.2. The QoS exponent θ is set to 0.001. Again, fixed-rate transmissions are considered and the effective rate is maximized over transmission rates. For $\lambda = 0.05$, the false alarm and detection probabilities increase to 1 and approximately 0.5, respectively with increasing N. Since the false alarm probability is higher, we have lower probability of detecting channel as idle as seen in the lower right figure. Hence, the channel is not efficiently utilized by cognitive users due to imperfect channel sensing decisions. Therefore, the effective rate is small. On the other hand, when $\lambda = 0.2$, we have lower false alarm and detection probabilities since the threshold level in hypothesis testing is higher. The probabilities of false alarm and detection diminish to 0 as N increases. Thus, the secondary user senses the channel as idle more frequently and performs data transmission with higher average power level, which leads to higher effective rate. But, this comes at the expense of higher interference on the primary users, which may be prohibitive since primary users' transmission cannot be sufficiently protected. If we impose the average interference power constraint in (7.11) with $\frac{I_0}{\max_j \mathbb{E}\{|g_{sp,j}|^2\}} = 7$ dB, and peak transmission power constraints 0

dB and 10 dB for $\overline{P}_1$ and $\overline{P}_2$, respectively, the power level is limited by the interference constraint for lower values of detection probability. Hence, we have lower effective rate with power control imposed through the constraint in (7.11) when $\lambda = 0.2$. As a result, we provide effective protection for primary users. In the case of $\lambda = 0.1$, reliable channel sensing is achieved since the probabilities of false alarm and detection approach 0 and 1, respectively. The effective rate increases until a certain threshold due to reliable channel sensing. However, after that threshold, the effective rate decreases with increasing channel sensing duration. The reason is that as channel sensing takes more time, less time is available for data transmission. Additionally, shorter coding blocklength for data transmission further affects adversely, leading to lower effective throughput. Thus, there is a more intricate tradeoff between channel sensing duration and throughput in the finite blocklength regime.

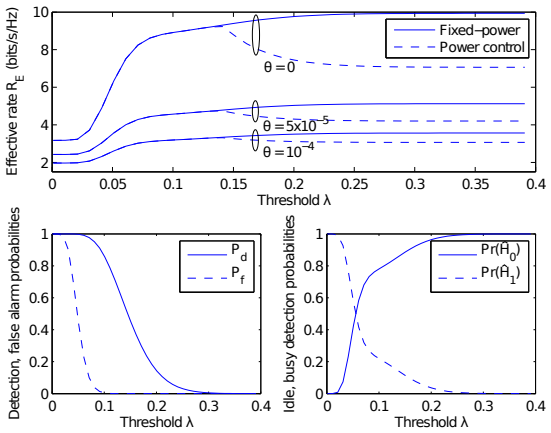

Figure 7.6: The effective rate R_E, the probabilities of detection and false alarm, probabilities of idle and busy detection vs. sensing threshold λ in fixed-rate transmissions.

In order to analyze the impact of the choice of the sensing threshold on the effective rate, in Fig. 7.6, we plot the effective rate, probabilities of false alarm and detection, probabilities of idle and busy detection vs. sensing threshold λ for the values of QoS exponent $\theta = 0$, 5×10^{-5} and 10^{-4} in the fixed-rate transmission case. Since the channel sensing method is independent of θ, we display the behavior of the above-mentioned probabilities without any buffer limitations in the lower subfigures. The effective rate is again maximized with

respect to transmission rates. Initially, as λ increases, the probability of false alarm starts to diminish. This improves the detection performance, and hence secondary users obtain more accurate channel sensing results. Therefore, the effective rate starts increasing. As λ continues to increase, the false alarm probability approaches 0 and the probability of detection starts to decrease as well. Hence, the cognitive users fail to detect the primary users' activity even if they are active in the channel (i.e., we have higher miss detection probability), and use the channel more frequently by transmitting data with higher average power level, which explains the second increase in the effective rate. However, experiencing significant interference can deteriorate the primary users' data transmission. To avoid this harmful interference caused by the secondary user, the lower bound on the detection probability can be imposed, i.e., $\mathscr{P}_{\mathrm{d}} \geq 0.6$. Also, the transmission power $\overline{P}_2$ can be limited by the average interference constraint in (7.11) with $\frac{I_0}{\max_j \mathbb{E}\{|g_{sp,j}|^2\}} = 7$ dB , which leads to decreasing effective rate as the secondary users fail to detect the primary users' activity. In the figure, we also see that effective rate decreases with increasing θ. Thus, the effective rate takes the highest values in the absence of QoS constraints, i.e., when $\theta = 0$.

7.4.2 Variable-Rate Transmissions

In Fig. 7.7, we consider variable-rate transmissions, and display numerical results for the effective rate as a function of the target error probability ϵ for $\theta = 0, 0.01$ and 0.1. As larger values of the error probability ϵ indicate that cognitive users' data transmission is subject to more errors, they enter into OFF states frequently, where rate of reliable transmission is effectively zero. Therefore, effective rate decreases as ϵ increases beyond a threshold. We also observe that effective rate is maximized at a unique optimal error probability ϵ. Moreover, effective rate decreases as QoS constraints become more stringent (i.e., for larger values of θ).

The tradeoff between the blocklength and effective rate in variable-rate transmission is analyzed. Hence, in Fig. 7.8, we display the behavior of the optimized error probability and

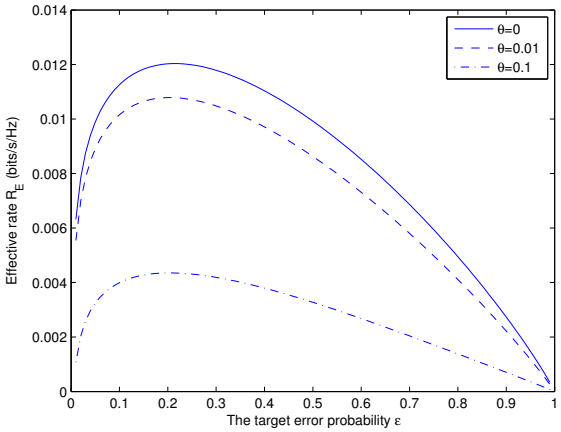

Figure 7.7: The effective rate R_E vs the probability of error ϵ for different values of QoS exponent θ in variable-rate transmission.

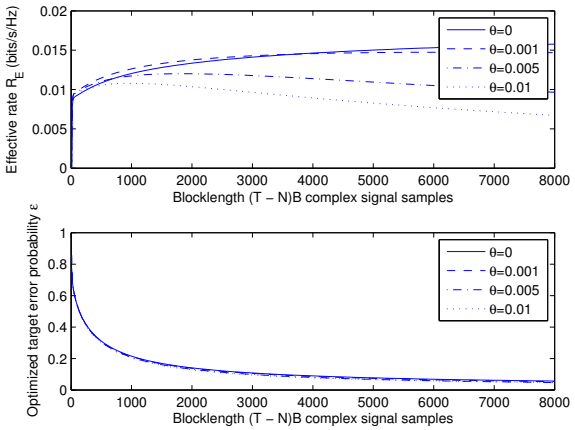

Figure 7.8: The effective rate R_E and the probability of error ϵ vs. blocklength $(T-N)B$ in variable-rate transmission.

effective rate as a function of the code blocklength $(T-N)B$ for $\theta = 0, 0.001, 0.005, 0.01$. In the lower subfigure we see that as the code blocklength increases, the optimal error probability, which maximizes the effective rate, decreases for given θ values. In the upper subfigure, we observe that if there is no such buffer limitation, effective rate increases with increasing blocklength. However, under buffer constraints with $\theta = 0.005$ and 0.01, as code blocklength increases until a certain threshold, data transmission is performed with decreasing error probability ϵ, which improves the system performance because longer codewords are transmitted more reliably. On the other hand, the effective rate starts to decrease after the

threshold. This is due to our assumption that fading stays constant over the frame of T seconds. As the blocklength and hence the value of T increase, cognitive users experience slower fading. Therefore, possible unfavorable deep fading lasts longer, leading to degradation in performance. In order to avoid buffer overflows, secondary transmitter becomes more conservative and supports only smaller arrival rates.

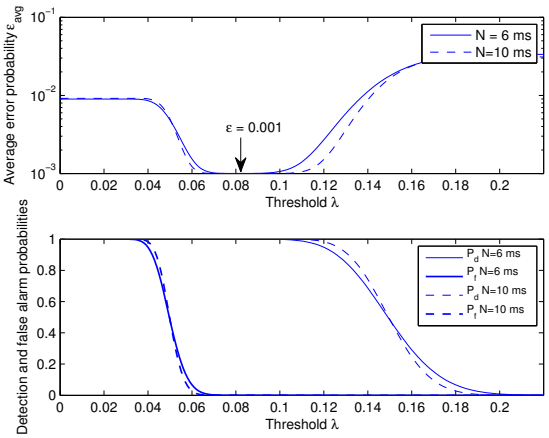

Figure 7.9: The average error probability ϵ_{avg} and probabilities of false-alarm, detection vs. sensing threshold λ.

In Fig. 7.9, we plot the average error probability ϵ_{avg}, which maximizes the effective rate in variable-rate transmission and the probabilities of detection and false alarm vs. sensing threshold λ for sensing duration of $N = 6$ ms and 10 ms. In the presence of CSI knowledge at the transmitter, secondary transmitter performs variable-rate data transmission with given fixed target error probability $\epsilon = 0.001$ and $\theta = 0.001$. As we know from the analysis in the case of perfect CSI at both the receiver and transmitter, error probability does not stay fixed at the target level of ϵ in scenarios 2, 3 where busy channel is sensed as idle and idle channel is sensed as busy, respectively. As λ increases, the probability of false alarm starts decreasing. Hence, average error probability decreases. When the probability of detection and the probability of false alarm approach 1 and 0, respectively (in the case of perfect channel sensing), the average error probability is equal to the fixed target error probability $\epsilon = 0.001$. As λ continues to increase, the detection probability diminishes and

miss detection (scenario 2) occurs more frequently, resulting in error probabilities greater than ϵ. Cognitive users can experience frequent errors in miss detections with variable error probability $\epsilon'_{|h|^2}$, which is larger than the fixed target error probability of ϵ. Therefore, we have higher average error probability. We can see that channel sensing plays a critical role on the average error probability in variable-rate transmissions. Finally we note that as sensing duration increases, the probabilities of false alarm and detection decrease with higher slopes as threshold increases. We also note that lower average error probability is achieved with larger N values when $0.05 < \lambda \leq 0.14$.

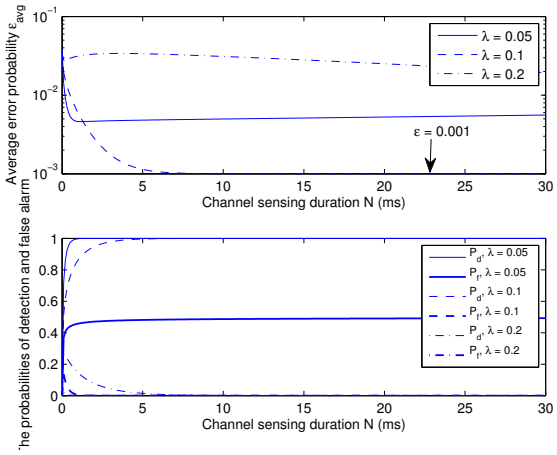

Figure 7.10: The average error probability ϵ_{avg} and probabilities of false-alarm, detection vs. channel sensing duration N.

Next, we analyze the tradeoff between the reliability of the variable-rate transmission and the sensing duration. In Fig. 7.10, the average probability of error ϵ_{avg}, which achieves the highest effective rate, the probabilities of detection and false alarm are given as a function of sensing duration N for $\lambda = 0.05, 0.1$ and 0.2. The target error probability ϵ is fixed to 0.001. When $\lambda = 0.05$, the detection probability approaches 1 and the false alarm probability approaches 0.5 as sensing duration increases. Thus, cognitive users detect the channel as busy more and transmit data with fixed error probability ϵ or variable error probability $\epsilon'_{|h|^2}$ (scenario 1 and scenario 3, respectively). The average error probability decreases when channel sensing takes more time and approaches approximately ϵ. For $\lambda = 0.1$, cognitive users almost

perfectly sense the channel with false alarm and detection probabilities approaching 0 and 1, respectively with increasing sensing duration. Thus, average error probability decreases and approaches $\epsilon = 0.001$. Therefore, data transmission is performed at the target error rate. If λ is chosen as 0.2, error probability increases until a certain threshold since we have lower false alarm and detection probabilities and the channel is detected as idle even though it is occupied by primary users, where cognitive users' transmission rate is achieved with error rate $\epsilon''_{|h|^2}$ that is much bigger than the target error probability ϵ. After that threshold, less time is allocated for data transmission. Therefore, lower transmission rates are supported, yielding more reliable data transmission, and hence decreasing the average error probability.

7.4.3 Fixed-Rate vs. Variable-Rate Transmissions

In this subsection, we compare the effective rate achieved under fixed-rate and variable-rate transmission schemes.

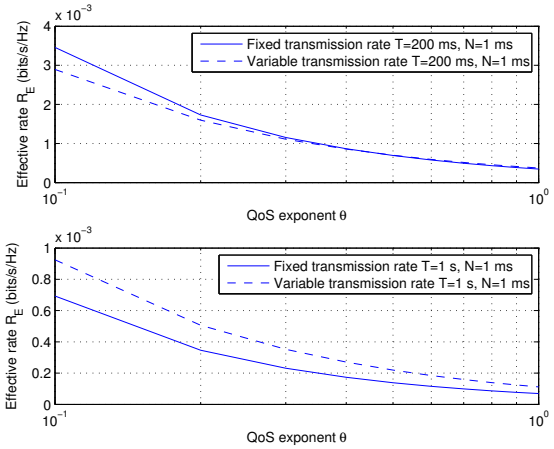

Figure 7.11: The effective rate R_E vs. QoS exponent θ for fixed-rate and variable-rate transmission for different T values.

In Fig. 7.11, we display numerical results for the effective rate vs. QoS exponent θ in fixed-rate and variable-rate transmissions for $T = 200$ ms, $N = 1$ ms and $T = 1$ s, $N = 1$ ms. Larger values of θ indicate that data transmission is performed under more strict QoS constraints. We see that increasing θ diminishes the effective rate R_E for both transmission

schemes. The variable-rate transmission achieves better performance when $T = 1$ s, $N = 1$ ms for all values of θ. On the other hand, fixed-rate transmission outperforms for low values of θ when $T = 200$ ms, $N = 1$ ms. Under more strict buffer limitations (higher values of θ), cognitive users send data with lower rates. Thus, the reliability of transmission becomes more important. Therefore, instead of sending data at constant rates, transmitter benefits more by varying the rate.

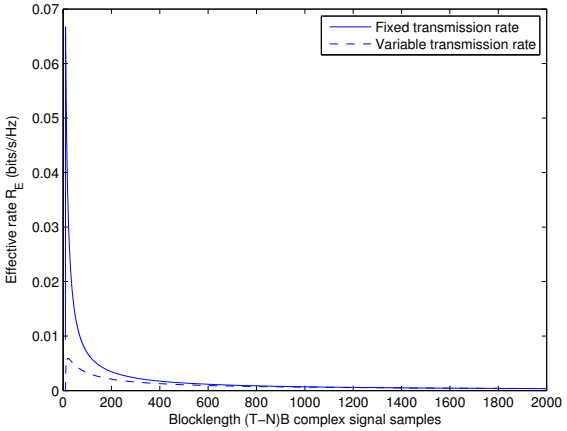

Figure 7.12: The effective rate R_E vs. blocklength $(T-N)B$ for fixed-rate and variable-rate transmission, $\theta = 1$.

Effective rate R_E is given as a function of blocklength $(T-N)B$ for fixed-rate and variable-rate transmissions in Fig. 7.12. We previously observed that effective rate increases until a certain threshold with increasing code blocklength. After that threshold, effective rate starts to diminish. The reason of this trend is explained in Fig. 7.8 for variable-rate transmission. In this figure, we also see that the same behavior is observed for fixed-rate transmission. We interestingly note that transmitting with constant rates leads to higher effective rate compared to varying the rate based on channel conditions when code blocklength is less than 1500 complex signal samples. When $(T - N)B$ is increased beyond 1500 complex signal samples, keeping the error probability constant and performing data transmission with variable rate result in better performance.

Chapter 8

Throughput and Energy Efficiency Optimization with QoS Constraints and Arbitrary Input Distributions

This chapter mainly studies energy-efficiency and throughput optimization in the presence of QoS constraints. The optimal power control policies maximizing the energy efficiency or maximizing the throughput with arbitrary input signaling for general fading distributions are obtained. Section 8.1 considers constant-rate arrivals while random arrivals are taken into account in Section 8.2.

8.1 QoS-Driven Power Control Schemes for a Constant-Rate Source

In this section, the optimal power control scheme that maximizes the effective capacity or energy efficiency for constant-rate sources and arbitrary input distributions subject to an average power constraint and QoS requirements are presented. The analysis leads to simplified expressions for the optimal power control strategies in two limiting cases, i.e.,

extremely stringent QoS constraints and looser QoS constraints. Also, tradeoff between the effective capacity and energy efficiency is studied.

Section 8.1.1 introduces the system model. In Section 8.1.2, the optimal power control policy maximizing the effective capacity achieved with arbitrary input distribtions is derived. In Section 8.1.3, the optimal power control in limiting cases is analyzed. Section 8.1.4 provides low power regime analysis of the effective capacity attained with constant power scheme and the optimal power control. Section 8.1.5 provides energy-efficient power control scheme with arbitrarily distributed signals. Two limiting cases of the corresponding power control scheme are analyzed in Section 8.1.6. Before presenting the numerical results in Section 8.1.8, the optimal power control that maximizes the effective capacity subject to a minimum energy efficiency constraint is obtained in Section 8.1.7.

8.1.1 System Model

We consider a point-to-point wireless communication link between the transmitter and the receiver over a flat fading channel. Hence, the received signal is given by

$$y[i] = h[i]x[i] + n[i] \quad i = 1, 2, \dots \tag{8.1}$$

where $x[i]$ and $y[i]$ denote the transmitted and received signals, respectively, and $n[i]$ is a zero-mean, circularly symmetric, complex Gaussian random variable with variance N_0. It is assumed that noise samples $\{n[i]\}$ form an independent and identically distributed (i.i.d.) sequence. Also, $h[i]$ represents the channel fading coefficient, and the channel power gain is denoted by $z[i] = |h[i]|^2$.

If the transmitter perfectly knows the instantaneous values of $\{h[i]\}$, it can adapt its transmission power according to the channel conditions. Let $P[i]$ denote the power allocated in the i^{th} symbol duration. Then, the instantenous received signal-to-noise ratio, SNR can be expressed as $\gamma = \frac{P[i]z[i]}{N_0 B}$ where B is the system total bandwidth. The transmission

power is constrained by $\bar{P}$, i.e., $\mathbb{E}\{P[i]\} \leq \bar{P}$, which is equivalent to $\mathbb{E}\{\mu[i]\} \leq \text{SNR}$, where $\mu[i] = \frac{P[i]}{N_0 B}$ and $\text{SNR} = \frac{\bar{P}}{N_0 B}$. In the rest of the analysis, we omit the time index i for notational brevity. We express the transmitted signal x in terms of a normalized unit-power arbitrarily distributed input signal s. Now, the received signal can be expressed as

$$\hat{y} = \sqrt{\rho} s + \hat{n}, \tag{8.2}$$

where $\rho = \mu z$, jointly representing the channel gain and transmission and noise powers, and $\hat{n}$ is the normalized Gaussian noise with unit variance. In this setting, the delay-bound violation probability is characterized to decay exponentially and can be approximated as [91]

$$\Pr\{D \geq D_{\text{th}}\} \approx \varphi \mathrm{e}^{-\theta C_E(\text{SNR}) D_{\text{th}}}, \tag{8.3}$$

where D denotes the steady state queueing delay, D_{th} represents the delay threshold, $\varphi = \Pr\{Q > 0\}$ is the probability that the buffer is nonempty, which can be approximated by the ratio of the average arrival rate to the average service rate [56].

When the service process $\{R[j]\}$ is i.i.d., the effective capacity simplifies to

$$C_E(\text{SNR}) = -\frac{1}{\theta} \log_e(\mathbb{E}\{e^{\theta R[j]}\}). \tag{8.4}$$

8.1.2 Throughput-Efficient Optimal Power Control

Our goal is to derive the optimal power control policy that maximizes the effective capacity achieved with an arbitrary input distribution, which can be found by solving the following optimization problem

$$C_E^{\text{opt}}(\text{SNR}) = \max_{\mu(\theta,z)} -\frac{1}{\theta T B} \log(\mathbb{E}\{\mathrm{e}^{-\theta T B \mathcal{I}(\mu(\theta,z)z)}\}) \tag{8.5}$$

$$\text{subject to } \mathbb{E}\{\mu(\theta,z)\} \leq \text{SNR}, \tag{8.6}$$

where the expectation $\mathbb{E}\{.\}$ is taken with respect to the channel power gain z. Above, $C_E^{\text{opt}}(\text{SNR})$ denotes the maximum effective capacity attained with the optimal power control scheme and $\mu(\theta, z)$ represents the instantaneous transmission power as a function of both the QoS exponent θ and channel power gain z. We first have the following characterization.

Theorem 8.1.1 *The optimal power control, denoted by $\mu_{opt}(\theta, z)$, which maximizes the effective capacity in (8.5), is given by*

$$\mu_{opt}(\theta, z) = \begin{cases} 0, & z \leq \alpha, \\ \mu^*(\theta, z), & z > \alpha, \end{cases} \tag{8.7}$$

where $\mu^*(\theta, z)$ is solution to

$$\mathrm{e}^{-\theta TB\mathcal{I}(\mu^*(\theta,z)z)} MMSE(\mu^*(\theta, z)z)z = \alpha \tag{8.8}$$

and α satisfies

$$\int_{\alpha}^{\infty} \mu^*(\theta, z) f(z) dz = SNR. \tag{8.9}$$

Above, $f(z)$ is the probability density function (PDF) of the channel power gain z.

Proof: See Appendix M.

Solving the equation in (8.8) does not result in a closed form expression for $\mu^*(\theta, z)$. We next show that the equation in (8.8) has at most one solution, denoted by $\mu^*(\theta, z)$. Hence numerical root finding methods, e.g., bisection method, can efficiently determine $\mu^*(\theta, z)$ [92].

Proposition 8.1.1 *The optimization problem in (8.5) has at most one solution.*

Proof: See Appendix N.

Table 8.1

Algorithm 7 Proposed power control algorithm for the effective capacity maximization with arbitrarily distributed inputs under an average power constraint

Initialization: $\mu_h(\theta,z)=\mu_{h,\text{init}}$, $\mu_l(\theta,z)=\mu_{l,\text{init}}$, $\varepsilon>0$, $\delta>0$, $t>0$, $\alpha^{(0)}=\alpha_{\text{init}}$
repeat
  $n \leftarrow 0$
  repeat
    update $\mu^*(\theta,z)=\frac{1}{2}(\mu_h(\theta,z)+\mu_l(\theta,z))$
    if $g(\mu^*(\theta,z))g(\mu_h(\theta,z))<0$ (where $g(.)$ is defined in (N.1)), then
      $\mu_l(\theta,z) \leftarrow \mu^*(\theta,z)$
    else if $g(\mu^*(\theta,z))g(\mu_l(\theta,z))<0$, then
      $\mu_h(\theta,z) \leftarrow \mu^*(\theta,z)$
    end if
  until $|g(\mu^*(\theta,z))|<\varepsilon$
  update α using the projection subgradient method as follows
  $\alpha^{(n+1)}=\left[\alpha^{(n)}-t(\text{SNR}-\mathbb{E}\{\mu^*(\theta,z)\})\right]^+$
  $n \leftarrow n+1$
until $|\alpha^{(n)}(\text{SNR}-\mathbb{E}\{\mu^*(\theta,z)\})|\leq\delta$

In Table 8.1, the proposed power control algorithm that maximizes the effective capacity with an arbitrary input distribution subject to an average power constraint is summarized, where α in (8.8) is determined by using the projected subgradient method. In this method, α is updated iteratively according to the subgradient direction until convergence as follows:

$$\alpha^{(n+1)}=\Big[\alpha^{(n)}-t\big(\text{SNR}-\mathbb{E}\{\mu^*(\theta,z)\}\big)\Big]^+ \tag{8.10}$$

where $[x]^+=\max\{0,x\}$, n is the iteration index and t is the step size. When t is chosen to be constant, it was shown that the subgradient method is guaranteed to converge to the optimal value within a small range [60].

Remark 8.1.1 *When the input signal is Gaussian, we have MMSE*$(\rho)=\frac{1}{1+\rho}$ *and* $\mathcal{I}(\rho)=\log_2(1+\rho)$. *Substituting these expressions into (8.8), we can see that the optimal power*

control policy reduces to

$$\mu_{opt}(\theta, z) = \begin{cases} 0 & z \leq \alpha, \\ \frac{1}{\alpha^{\frac{1}{\beta+1}} z^{\frac{\beta}{\beta+1}}} - \frac{1}{z} & z > \alpha, \end{cases} \tag{8.11}$$

which has exactly the same structure as given in [41].

8.1.3 Throughput-Efficient Optimal Power Control in Limiting Cases

In this section, we analyze two limiting cases of the proposed optimal power control, in particular, when the system is subject to extremely stringent QoS constraints (i.e., as $\theta \to \infty$) and looser QoS constraints (i.e., as $\theta \to 0$), respectively.

8.1.3.1 Optimal Power Control under Extremely Stringent QoS Constraints

Asymptotically, when $\theta \to \infty$, the system is subject to increasingly stringent QoS constraints and hence it cannot tolerate any delay. In this case, the transmitter maintains a fixed transmission rate and the optimal power control converges to total channel inversion scheme as follows:

$$\mu_{\text{opt}}(z) = \frac{\mathcal{C}}{z}, \tag{8.12}$$

where the constant $\mathcal{C}$ can be found by satisfying the average transmit power constraint with equality. In particular,

$$\int_0^\infty \frac{\mathcal{C}}{z} f(z) dz = \text{SNR}.$$

In Nakagami-m fading channel, the channel power gain is distributed according to the Gamma distribution

$$f(z) = \frac{z^{m-1}}{\Gamma(m)}\left(\frac{m}{\Omega}\right)^{m} \mathrm{e}^{-\frac{m}{\Omega}z} \text{ for } m \geq 0.5, \tag{8.13}$$

where m is the fading parameter, Ω is the average fading power and $\Gamma(x)$ is the Gamma function [85, eq. 8.310.1]. In this case, $\mathcal{C}$ is given by

$$\mathcal{C} = \mathrm{SNR}\mathbb{E}\left\{\frac{1}{z}\right\} = \begin{cases} \frac{\mathrm{SNR}m}{\Omega(m-1)} & m > 1 \\ 0 & m \leq 1 \end{cases}. \tag{8.14}$$

It should be noted that Nakagami-m fading can model different fading conditions, e.g. including Rayleigh fading (i.e., $m = 1$) and one-sided Gaussian fading (i.e., $m = 0.5$) as special cases. Also, Nakagami-m fading distribution is commonly used to characterize the received signal in urban radio [93] and indoor-mobile multipath propagation environments [94].

Remark 8.1.2 *The power control policy under very stringent QoS constraints in (8.12) is the same regardless of the signaling distribution while the effective capacity depends on the input distribution through mutual information expression in (8.4).*

8.1.3.2 Optimal Power Control under Loose QoS Constraints

As $\theta \to 0$, QoS constraints become looser and eventually vanish, and hence the system can tolerate arbitrarily long delays. In this case, the effective capacity is equivalent to the achievable (mutual information) rate with finite discrete inputs. Subsequently, the optimization problem is expressed as

$$\min_{\mu(z)} \mathbb{E}\{\mathcal{I}(\mu(\theta, z))\} \tag{8.15}$$

$$\text{subject to } \mathbb{E}\{\mu(\theta, z)\} \leq \mathrm{SNR}. \tag{8.16}$$

By following similar steps as in the proof of Theorem 8.1.1, the optimal power control policy is given by

$$\mu_{\text{opt}}(z) = \frac{1}{z}\text{MMSE}^{-1}\Big(\min\Big\{1, \frac{\eta}{\log_2(e)z}\Big\}\Big). \tag{8.17}$$

Above, $\text{MMSE}^{-1}(.) \in [0, \infty)$ denotes the inverse MMSE function and the Lagrange multiplier, η can be found by inserting the proposed power control into the power constraint in (8.16) and satisfying this constraint with equality as follows:

$$\int_{\frac{\eta}{\log_2(e)}}^{\infty} \mu_{\text{opt}}(z) f(z) dz = \text{SNR}. \tag{8.18}$$

Remark 8.1.3 *The power control policy in the absence of QoS constraints in (8.42) has the same structure of mercury/water-filling [52]. It is seen that the power level depends on the input distribution through the expression of inverse MMSE.*

8.1.4 Low-Power Regime Analysis

In this section, we study, in the low-power regime, the effective capacity achieved with arbitrary input distributions depending on the availability of CSI at the transmitter. In particular, we study constant-power transmission in addition to the analysis of the optimal power control in this regime.

8.1.4.1 Constant Power

Here, we assume that only the receiver has perfect CSI, and hence the signal is sent with constant power. In the low-power regime, EE can be characterized by the minimum energy

per bit $\frac{E_b}{N_0}_{\min}$ and wideband slope S_0 [95]. First, energy per bit is defined as

$$\frac{E_b}{N_0} = \frac{\mathrm{SNR}}{C_E(\mathrm{SNR})}. \tag{8.19}$$

Consequently, the minimum energy per bit required for reliable communication under QoS constraints is obtained from

$$\frac{E_b}{N_{0\,\min}} = \lim_{\mathrm{SNR}\to 0} \frac{\mathrm{SNR}}{C_E(\mathrm{SNR})} = \frac{1}{\dot{C}_E(0)}, \tag{8.20}$$

where $\dot{C}_E(0)$ denotes the first derivative of the effective capacity $C_E(\mathrm{SNR})$ with respect to SNR in the limit as SNR vanishes. Correspondingly, at $\frac{E_b}{N_0}_{\min}$, S_0 represents the growth of the spectral efficiency with respect to $\frac{E_b}{N_0}$ (in dB), which is obtained from

$$S_0 = \frac{-2(\dot{C}_E(0))^2}{\ddot{C}_E(0)} \log_e 2. \tag{8.21}$$

Above, $\ddot{C}_E(0)$ denotes the second derivative of $C_E(\mathrm{SNR})$ with respect to SNR in the limit as SNR approaches zero. By using the minimum energy per bit in (8.20) and wideband slope expression in (8.21), throughput can be approximated as a linear function of the energy per bit (in dB) as follows:

$$R = \frac{S_0}{10\log_{10}(2)}\left(\frac{E_b}{N_{0\,\mathrm{dB}}} - \frac{E_b}{N_{0\,\min,\mathrm{dB}}}\right) + o\left(\frac{E_b}{N_{0\,\mathrm{dB}}} - \frac{E_b}{N_{0\,\min,\mathrm{dB}}}\right), \tag{8.22}$$

where $\frac{E_b}{N_{0\,\mathrm{dB}}} = 10\log_{10}\frac{E_b}{N_0}$ which denotes the energy per bit in dB. We provide the following characterization.

Theorem 8.1.2 *The minimum energy per bit and wideband slope with arbitrary input distributions under QoS constraints for general fading distributions are given, respectively, by*

$$\frac{E_b}{N_{0\,\min}} = \frac{\log 2}{\mathbb{E}\{z\}} \text{ and } S_0 = \frac{2}{(-\ddot{\mathcal{I}}(0)+\beta)\frac{\mathbb{E}\{z^2\}}{(\mathbb{E}\{z\})^2} - \beta}, \tag{8.23}$$

where $\ddot{\mathcal{I}}(0)$ *denotes the second derivative of mutual information evaluated at* $SNR = 0$.

Proof: See Appendix O.

From the above result, we immediately see that the same minimum energy per bit is achieved regardless of the signaling distribution and QoS constraints. On the other hand, the wideband slope depends on both the input distribution through $\ddot{\mathcal{I}}(0)$, and the QoS exponent, θ. More speficially, for quadrature symmetric constellations such as QPSK, 8-PSK or 16-QAM, we have $\ddot{\mathcal{I}}(0) = -1$ while real valued constellations such as BPSK and m-PAM have $\ddot{\mathcal{I}}(0) = -2$ [52]. Hence, even though they have the same minimum energy per bit, quadrature symmetric constellations have higher wideband slopes compared to real valued constellations, yielding higher EE.

It should also be noted that we obtain the low power behavior of the mutual information exhibited by the Gaussian input by setting $\ddot{\mathcal{I}}(0) = -1$ in (O.1). Hence, substituting $\ddot{\mathcal{I}}(0) = -1$ in (8.23), the minimum energy per bit and wideband slope expressions can be specialized to the case of Gaussian input, which leads the same formulations as in [46] under the assumption of perfect CSI only at the receiver.

Remark 8.1.4 *For a Nakagami-m fading channel,* $\mathbb{E}\{z\} = \Omega$ *and* $\mathbb{E}\{z^2\} = \Omega^2\big(1 + \frac{1}{m}\big)$. *Inserting these expressions into (8.23), the minimum energy per bit and wideband slope for a Nakagami-m fading channel can be found, respectively, as*

$$\frac{E_b}{N_{0\,\min}} = \frac{\log_e(2)}{\Omega}, \text{ and } S_0 = \frac{2}{-\big(1 + \frac{1}{m}\big)\ddot{\mathcal{I}}(0) + \frac{\beta}{m}}. \tag{8.24}$$

We note that while the minimum bit energy depends only on the average fading power, Ω*, the wideband slope is a function of Nakagami-m fading parameter, input distribution and QoS exponent,* θ.

When there exists a dominant line of sight component along the propagation path, the Rician fading channel is an accurate model. This type of fading typically occurs in microcellular (e.g., suburban land-mobile radio communication) [96] and picocellular environments

(e.g., indoor communication) [97]. In this case, the pdf of the channel power gain is given by

$$f(z) = \frac{(1+K)\mathrm{e}^{-K}}{\Omega}\mathrm{e}^{-\frac{(K+1)z}{\Omega}} I_0\left(2\sqrt{\frac{K(K+1)z}{\Omega}}\right) \text{ for } K, \Omega \geq 0, \tag{8.25}$$

where K denotes the Rician K-factor and $I_0(x)$ represents the zero-th order modified Bessel function of the first kind [85, eq. 8.405.1].

Remark 8.1.5 *By substituting* $E\{z\} = \Omega$ *and* $\mathbb{E}\{z^2\} = \frac{(2+4K+K^2)\Omega}{(K+1)^2}$ *into (8.23), we obtain the minimum energy per bit and wideband slope for Rician fading channel as follows:*

$$\frac{E_b}{N_0}_{\min} = \frac{\log_e(2)}{\Omega} \text{ and } S_0 = \frac{2(K+1)^2}{-(2+4K+K^2)\ddot{\mathcal{I}}(0) + (2K+1)\beta}. \tag{8.26}$$

It can be easily verified that the wideband slope is an increasing function of the Rician K*-factor. Also, similar to Nakagami-m fading channel, the minimum energy per bit for Rician fading channel depends only on the average fading power,* Ω*.*

8.1.4.2 Optimal Power Control

Now, we assume that both the transmitter and receiver have perfect CSI. Below, we identify the optimal power control policy in the low-power regime.

Theorem 8.1.3 *he optimal power policy that maximizes the effective capacity with arbitrary input distributions in the low power regime is given by*

$$\mu^*_{opt}(\theta, z) = \frac{z - \alpha}{\big(\beta - \ddot{\mathcal{I}}(0)\big)z^2}. \tag{8.27}$$

Proof: See Appendix P.

For Nakagami-m fading channel, α can be determined as the solution of

$$\frac{-m^2\alpha\Gamma(m-2,\frac{m\alpha}{\Omega})+\Omega m\Gamma(m-1,\frac{m\alpha}{\Omega})}{\Omega^2\Gamma(m)}=\big(\beta-\ddot{\mathcal{I}}(0)\big)\mathrm{SNR}, \tag{8.28}$$

where $\Gamma(a,x)$ denotes the upper incomplete gamma function [85, eq. 8.350.2].

8.1.5 Energy-Efficient Optimal Power Control

In this subsection, we derive the optimal power control scheme that maximizes the energy efficiency achieved with finite discrete inputs, which is defined as the ratio of the effective capacity to the total power consumption, i.e.,

$$\mathrm{EE}(\theta)=\frac{C_E(\mathrm{SNR})}{P_c+\frac{1}{\epsilon}\mathbb{E}\{P(\theta,z)\}}. \tag{8.29}$$

Above, the total power consumption includes average transmission power and circuit power denoted by P_c, which corresponds to the average power consumption of the transmitter circuitry (i.e., by filters, mixers, frequency synthesizers, etc.). Also, ϵ denotes the power amplifier efficiency, i.e., $\epsilon\in[0,1]$ and $E\{.\}$ represents the expectation operator with respect to the channel power gain, z.

By using the effective capacity expression in (8.4) and normalizing the system performance with respect to TB, the optimization problem can now be formulated as

$$\mathrm{EE}^{\mathrm{opt}}(\theta)=\max_{P_n(\theta,z)\geq 0}\frac{-\frac{1}{\theta TB}\log\Big(\mathbb{E}\{\mathrm{e}^{-\theta TB\mathcal{I}(P_n(\theta,z)z)}\}\Big)}{N_0B(P_{c_n}+\frac{1}{\epsilon}\mathbb{E}\{P_n(\theta,z)\})} \tag{8.30}$$

Above, $P_{c_n}=\frac{P_c}{N_0B}$ is the scaled circuit power, $\mathrm{EE}^{\mathrm{opt}}(\theta)$ represents the maximum energy efficiency attained with the optimal power control scheme, and $P_n(\theta,z)=\frac{P(\theta,z)}{N_0B}$. Respectively, the optimal power control strategy is determined in the following result.

Theorem 8.1.4 *The optimal power control policy, denoted by $P_n^{opt}(\theta,z)$, which maximizes*

energy efficiency for finite discrete inputs under QoS constraints, is given by

$$P_n^{opt}(\theta, z) = \begin{cases} 0, & z \leq \gamma_1, \\ P^*(\theta, z), & z > \gamma_1 \end{cases} \tag{8.31}$$

where $P^*(\theta, z)$ *is solution to*

$$\mathrm{e}^{-\theta TB\mathcal{I}(P^*(\theta,z)z)} MMSE(P^*(\theta, z)z)z = \gamma_1 \tag{8.32}$$

with

$$\gamma_1 = \frac{\lambda \mathbb{E}\{\mathrm{e}^{-\theta TB\mathcal{I}(P^*(\theta,z)z)}\}}{\epsilon\theta TB\log_2(e)}. \tag{8.33}$$

The optimal value of λ *can be found by solving the equation below:*

$$\log\Big(\mathbb{E}\big\{\mathrm{e}^{-\theta TB\mathcal{I}(P_n^{opt}(\theta,z)z)}\big\}\Big) + \lambda\Big(P_{c_n} + \frac{1}{\epsilon}\mathbb{E}\big\{P_n^{opt}(\theta, z)\big\}\Big) = 0. \tag{8.34}$$

Proof: See Appendix Q.

It should be noted that Theorem 8.1.4 does not address any average power constraints. If an average power constraint, $\mathbb{E}\{P(\theta, z)\} \leq P_{\text{avg}}$, where P_{avg} denotes the average transmit power limit at the transmitter, is imposed and the optimal power constraint in (8.31) satisfies this constraint, then the average transmit power constraint does not have any effect on the maximum energy efficiency. On the other hand, when $\mathbb{E}\{P(\theta, z)\} > P_{\text{avg}}$, in which the average transmit power constraint is violated, the optimal power control that maximizes energy efficiency is no longer valid. In such a case, the energy efficiency maximization problem reduces to effective capacity maximization for finite discrete inputs subject to an average transmit power constraint, and the optimal power control strategy is given by [98].

Remark 8.1.6 *For Gaussian input signal, we have* $MMSE(\rho) = \frac{1}{1+\rho}$ *and* $\mathcal{I}(\rho) = \log_2(1+\rho)$.

Inserting these expressions into (8.32), the optimal power control policy becomes

$$P_n^{opt}(\theta, z) = \begin{cases} 0 & z \leq \frac{\gamma_2}{\alpha}, \\ \frac{\alpha^{\frac{1}{1+\alpha}}}{\gamma_2^{\frac{1}{1+\alpha}} z^{\frac{\alpha}{1+\alpha}}} - \frac{1}{z} & z > \frac{\gamma_2}{\alpha} \end{cases} \tag{8.35}$$

which has the same structure as given in [41]. Above, $\alpha = \theta TB \log_2(e)$ *is the normalized QoS exponent and* $\gamma_2 = \frac{\lambda}{\epsilon}\mathbb{E}\{(1 + P_n^{opt}(\theta_z)z)^{-\alpha}\}$ *where the optimal value of* λ *is determined by solving the following equation:*

$$\log\left(\mathbb{E}\left\{(1 + P_n^{opt}(\theta, z)z)^{-\alpha}\right\}\right) + \lambda\left(P_{c_n} + \frac{1}{\epsilon}\mathbb{E}\left\{P_n^{opt}(\theta, z)\right\}\right) = 0 \tag{8.36}$$

8.1.6 Energy-Efficient Optimal Power Control in Limiting Cases

In this subsection, we analyze the optimal power control strategies which maximize the energy efficiency for finite discrete inputs in two limiting cases, which are that the system is operating under extremely stringent QoS constraints (i.e., $\theta \to \infty$) and looser QoS constraints (i.e., $\theta \to 0$), respectively.

8.1.6.1 Optimal Power Control under Extremely Stringent QoS Constraints

When QoS constraints become stringent, i.e., $\theta \to \infty$, the optimal power control policy converges to the total channel inversion as follows:

$$\mu_{\text{opt}}(z) = \frac{\mathcal{C}}{z}, \tag{8.37}$$

where the constant $\mathcal{C}$ can be found by maximizing the energy efficiency, which can be expressed as

$$\text{EE}^{\text{opt}}(\theta) = \frac{\mathcal{I}(\mathcal{C})}{N_0 B(P_{c_n} + \frac{1}{\epsilon}\mathcal{C}\mathbb{E}\{\frac{1}{z}\})}. \tag{8.38}$$

The above energy efficiency is strictly quasi-concave function in $\mathcal{C}$ since the mutual information is strictly concave in $\mathcal{C}$ [99] and the denominator is both affine and positive, and hence the level sets $S_\beta = \{\mathcal{C} : \mathrm{EE}^{\mathrm{opt}}(\theta) \geq \beta\} = \{\beta(N_0 B(P_{c_n} + \frac{1}{\epsilon}\mathcal{C}\mathbb{E}\{\frac{1}{z}\})) - \mathcal{I}(\mathcal{C}) \leq 0\}$ are strictly convex for any $\beta \in \mathbb{R}$. Therefore, the energy efficiency in (8.38) has a unique global maximum, which can be found by solving the equation below:

$$\frac{d\mathrm{EE}^{\mathrm{opt}}(\theta)}{d\mathcal{C}} = 0 \Rightarrow \tag{8.39}$$

$$\frac{\mathrm{MMSE}(\mathcal{C})\log_2(e)(P_{c_n} + \frac{1}{\epsilon}\mathcal{C}\mathbb{E}\{\frac{1}{z}\}) - \mathcal{I}(\mathcal{C})\frac{1}{\epsilon}\mathbb{E}\{\frac{1}{z}\}}{N_0 B(P_{c_n} + \frac{1}{\epsilon}\mathcal{C}\mathbb{E}\{\frac{1}{z}\})^2} = 0, \tag{8.40}$$

where the optimal value of $\mathcal{C}$ can be found numerically using a bisection method.

Remark 8.1.7 *From the above result, it is seen that the power control scheme under stringent QoS constraints is the total channel inversion regardless of the signaling distribution. On the other hand, the value of $\mathcal{C}$ depends on the input distribution through MMSE and mutual information expressions in (8.40).*

8.1.6.2 Optimal Power Control under Looser QoS Constraints

Here, we analyze the power control scheme maximizing the energy efficiency in the presence of looser QoS constraints, which correspond to $\theta \to 0$. In this case, the effective capacity is equivalent to the achievable rate with finite discrete inputs. Specifically, the energy efficiency now becomes

$$\mathrm{EE}(\theta) = \frac{\mathbb{E}\{\mathcal{I}(P_n(\theta, z)z)\}}{N_0 B\big(P_{c_n} + \frac{1}{\epsilon}\mathbb{E}\{P_n(\theta, z)\}\big)}. \tag{8.41}$$

By following similar steps as in the proof of Theorem 8.1.4, the optimal power control policy is obtained as

$$P_n^{\mathrm{opt}}(\theta, z) = \frac{1}{z}\mathrm{MMSE}^{-1}\Big(\min\Big\{1, \frac{\lambda_1}{\epsilon \log_2(e) z}\Big\}\Big), \tag{8.42}$$

where $\text{MMSE}^{-1}(.) \in [0, \infty)$ indicates the inverse MMSE function and the Lagrange multiplier, λ_1 can be determined by solving the following equation:

$$\mathbb{E}\{\mathcal{I}(P_n^{\text{opt}}(\theta, z)z)\} - \lambda_1 \Big(P_{c_n} + \frac{1}{\epsilon} \mathbb{E}\{P_n^{\text{opt}}(\theta, z)\} \Big) = 0. \tag{8.43}$$

Remark 8.1.8 *The power control policy in (8.42) has the structure of mercury/water-filling [52]. However, the water level in this policy is determined to maximize the energy efficiency, and average power constraint is not necessarily satisfied with equality in contrast to the case of achievable rate maximization.*

8.1.7 Optimal Power Control under a Minimum Energy Efficiency Constraint

In this section, we analyze the tradeoff between the EE and the effective capacity achieved with finite discrete inputs by formulating the optimization problem to maximize the effective capacity subject to minimum EE and average transmit power constraints. More specifically, the optimization problem is expressed as

$$C_E^{\text{opt}}(\text{SNR}) = \max_{\mu(\theta,z)} -\frac{1}{\theta TB} \log \mathbb{E}\big\{ \mathrm{e}^{-\theta TB\mathcal{I}(\mu(\theta,z)z)} \big\} \tag{8.44}$$

$$\text{subject to} \quad \frac{-\frac{1}{\theta TB} \log \mathbb{E}\big\{ \mathrm{e}^{-\theta TB\mathcal{I}(\mu(\theta,z)z)} \big\}}{N_0 B(\frac{1}{\epsilon}\mathbb{E}\{\mu(\theta, z)\} + P_{c_n})} \geq \text{EE}_{\min} \tag{8.45}$$

$$\mathbb{E}\{\mu(\theta, z)\} \leq \text{SNR}, \tag{8.46}$$

where P_{c_n} represents the normalized circuit power, $\text{EE}_{\min}$ denotes the minimum required EE. In the following, we first derive the optimal power control subject to a minimum EE constraint in (8.45) and then address the average power constraint given in (8.46).

Theorem 8.1.5 *The optimal power control policy maximizing the effective capacity with finite discrete inputs subject to a minimum EE constraint is obtained as*

$$\mu_{opt}(\theta, z) = \mu^*(\theta, z), \tag{8.47}$$

where $\mu^*(\theta, z)$ *is solution to the equation below:*

$$\mathrm{e}^{-\theta TB\mathcal{I}(\mu^*(\theta,z)z)} MMSE(\mu^*(\theta, z)z)z = \frac{\nu EE_{min} N_0 B \mathbb{E}\{\mathrm{e}^{-\theta TB\mathcal{I}(\mu(\theta,z)z)}\}}{\epsilon(1+\nu)\log_2(e)}. \tag{8.48}$$

Above, the Lagrange multiplier, ν *can be found by solving the equation below:*

$$-\frac{1}{\theta TB}\log \mathbb{E}\{\mathrm{e}^{-\theta TB\mathcal{I}(\mu_{opt}(\theta,z)z)}\} - EE_{min} N_0 B\Big(\frac{1}{\epsilon}\mathbb{E}\{\mu_{opt}(\theta, z)\} + P_{c_n}\Big) = 0. \tag{8.49}$$

Consequently, the average transmit power that satisfies the required minimum EE is calculated as

$$\bar{P}^* = N_0 B \mathbb{E}\{\mu_{opt}(\theta, z)\}. \tag{8.50}$$

Proof: See Appendix R.

Now, we incorporate the average transmit power constraint in (8.46) into the proposed power control in (8.47). More specifically, if $\bar{P} < \bar{P}^*$ and the maximum EE subject to average power constraint, $\bar{P}$ is less than $\mathrm{EE}_{\min}$, then the optimization problem is not feasible and the the power level is set to zero, i.e., $\mu^*(\theta, z) = 0$. Otherwise the optimal power control is found considering the following two cases:

- if $\bar{P} \geq \bar{P}^*$, average transmit power constraint is loose. In this case, the optimal power control is given by (8.47) where the minimum EE constraint is satisfied with equality.
- if $\bar{P} < \bar{P}^*$ and the maximum EE subject to average power constraint, $\bar{P}$ is greater than $\mathrm{EE}_{\min}$, the minimum EE constraint does not have any effect on the maximum effective

capacity. In this case, the optimal power control is determined by (8.31) where the average transmit power constraint, $\bar{P}$ is satisfied with equality.

Remark 8.1.9 *Inserting MMSE*$(\rho) = \frac{1}{1+\rho}$ *and* $\mathcal{I}(\rho) = \log_2(1+\rho)$ *into (8.48), the optimal power control scheme for Gaussian distributed signal becomes*

$$\mu^*(\theta, z) = \begin{cases} 0 & z \leq \gamma_1 \\ \frac{1}{\gamma_1^{\frac{1}{1+\beta}} z^{\frac{\beta}{1+\beta}}} - \frac{1}{z} & z > \gamma_1 \end{cases}, \tag{8.51}$$

which is in agreement with the result obtained in [45]. Above, $\gamma_1 = \frac{\nu E E_{min} N_0 B \mathbb{E}\{\mathrm{e}^{-\theta T B \mathcal{I}(\mu(\theta,z)z)}\}}{\epsilon(1+\nu)\log_2(e)}$ *is the scaled Lagrange multiplier, which can be found by inserting the above power control into (8.48) and solving the corresponding equation for* γ_1.

8.1.8 Numerical Results

In this section, we present numerical results to illustrate the proposed optimal power control policies and the corresponding performance levels. Unless mentioned explicitly, we consider Nakagami-m fading channel with $m = 1$ (which corresponds to Rayleigh fading) in the simulations, and it is assumed that $N_0 B = 1$, $TB = 1$, $\Omega = 1$ and average transmit power constraint, $\bar{P} = 0$ dB. In the iterations, t is chosen as 0.1, ε and δ are set to 10^{-5}.

In Fig. 8.1, we plot the instaneous power level as a function of the channel power gain z and the QoS exponent θ for both Gaussian and BPSK signals. As θ decreases, QoS constraint becomes looser. In this case, the power control for BPSK input has the structure of mercury/water-filling policy. In particular, the power is allocated to the better channel up to capacity saturation and then extra power is assigned to the worse channel. When the input is Gaussian, the power adaptation policy becomes the water-filling scheme, with which more power is assigned to the better channel opportunistically, deviating from the mercury/water-filling policy. When θ increases and hence stricter QoS constraints are imposed, the optimal power control policy becomes channel inversion for both inputs.

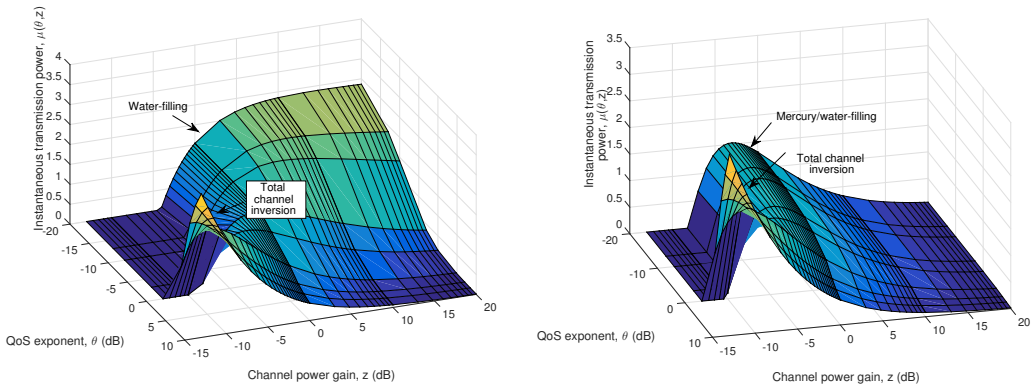

(a) (b)

Figure 8.1: The instantaneous transmission power as a function of channel power gain, z and QoS exponent, θ for (a) Gaussian input; (b) BPSK input .

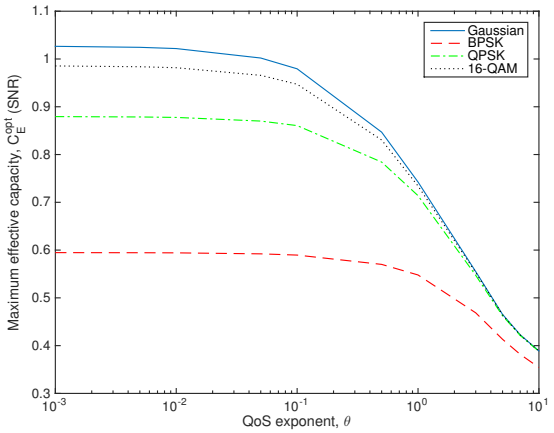

Figure 8.2: Maximum effective capacity $C_E^{\text{opt}}(\text{SNR})$ vs. QoS exponent θ for Gaussian, BPSK, QPSK and 16-QAM inputs.

In Fig. 8.2, we display the effective capacity $C_E^{\text{opt}}(\text{SNR})$ as a function of the QoS exponent θ for Gaussian, BPSK, QPSK and 16-QAM inputs. It is observed that as θ increases, the effective capacity for all inputs decreases since the transmitter is subject to more stringent QoS constraints, which results in lower arrival rates hence lower effective capacity. It is also seen that Gaussian inputs always achieve higher effective capacity. For large θ values, Gaussian input and QPSK exhibit nearly the same performance. Therefore, under strict QoS constraints, QPSK can be efficiently used in practical systems rather than the Gaussian input which is difficult to implement.

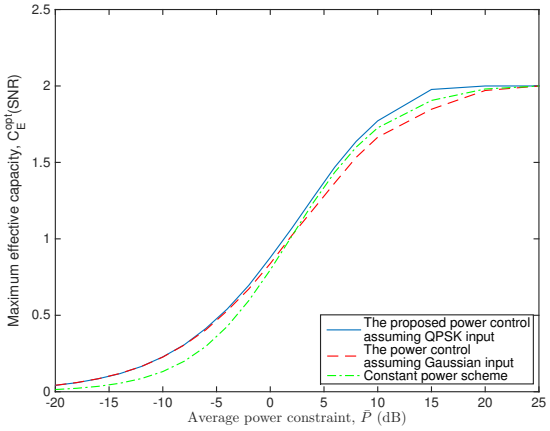

Figure 8.3: Maximum effective capacity $C_E^{\text{opt}}(\text{SNR})$ vs. average transmit power constraint, $\bar{P}$ for QPSK input.

In Fig. 8.3, we plot maximum effective capacity $C_E^{\text{opt}}(\text{SNR})$ as a function of average transmit power constraint, $\bar{P}$ for QPSK input. QoS exponent, θ is set to 0.1. We compare the performances of the constant-power scheme, power control assuming Gaussian input and power control assuming QPSK input. It is observed that as $\bar{P}$ increases, the effective capacity increases and then saturates due to being fact that the input is generated from a finite discrete modulation. It is seen that the power control considering the true input distribution, in this case QPSK, achieves the highest effective capacity since the power control assuming Gaussian input is not the optimal policy for the QPSK input and constant-power transmission strategy does not take advantage of favorable channel conditions. In addition, the performance gap between the optimal power control considering the discrete constallation and power control assuming Gaussian input increases at moderate SNR levels.

In Fig. 8.4, maximum effective capacity $C_E^{\text{opt}}(\text{SNR})$ as a function of QoS exponent, θ for QPSK input is illustrated. We again consider the constant-power scheme, power control assuming Gaussian input and power control assuming QPSK input. The constant-power scheme has the worst performance with the lowest effective capacity for all values of θ. It is also interesting to note that the performance gap between the power control policies assuming Gaussian input and QPSK input decreases as θ increases. This is mainly due to

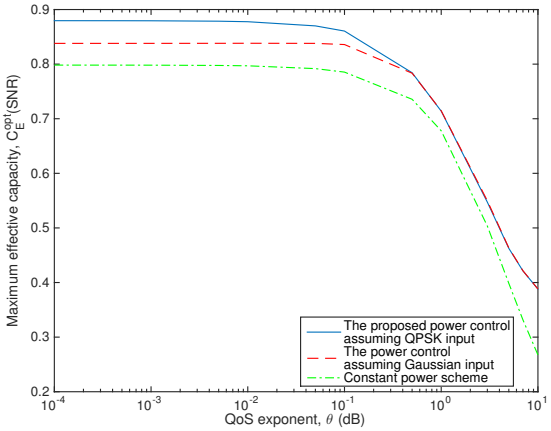

Figure 8.4: Maximum effective capacity $C_E^{\text{opt}}(\text{SNR})$ vs. QoS exponent, θ for QPSK input.

the fact that for higher values of θ, the power control scheme does not depend on the input distribution and becomes total channel inversion.

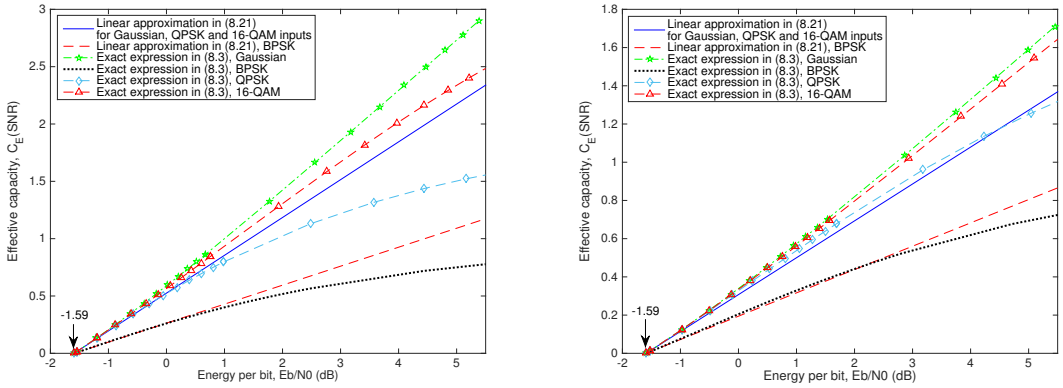

(a) (b)

Figure 8.5: Effective capacity vs. energy per bit, $\frac{E_b}{N_0}_{\text{dB}}$ for Gaussian, BPSK, QPSK and 16-QAM inputs (a) $\theta = 0.01$ and (b) $\theta = 1$.

In Fig. 8.5, we plot the effective capacity as a function of energy per bit, $\frac{E_b}{N_0}_{\text{dB}}$ for constant-power transmission when $\theta = 0.01$ and $\theta = 1$. We compare the performances of Gaussian, BPSK, QPSK and 16-QAM inputs in the low power regime by analyzing the minimum energy per bit and wideband slope values. It is observed that all inputs achieve the same minimum energy per bit of -1.59 dB while the wideband slope for BPSK is smaller than those of Gaussian, QPSK and 16-QAM inputs, which indicates lower EE for BPSK. Gaussian input

achieves the highest EE among the inputs. We also consider the linear approximation for the effective capacity in the low power regime given in (8.22) and the exact analytical effective capacity expression in (8.4). It is seen that the linear approximation for all inputs is tight at low SNR values or equivalently low values of E_b/N_0 (dB). Additionally, when we compare Fig. 5a with Fig.5b, we readily observe that the minimum energy per bit remains the same as QoS exponent, θ changes from 0.01 to 1. On the other hand, wideband slope decreases with increasing θ, which confirms the result in (8.24).

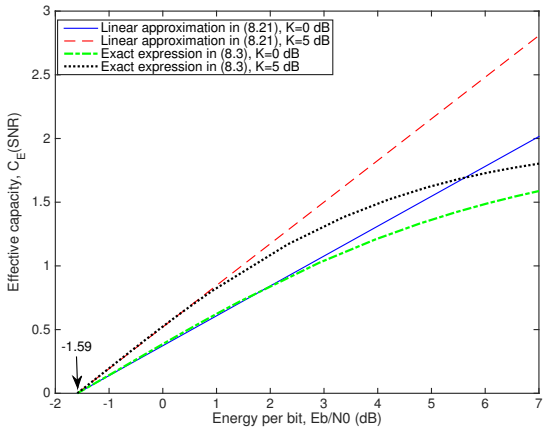

Figure 8.6: Effective capacity vs. energy per bit, $\frac{E_b}{N_0}_{\text{dB}}$ for QPSK input in Rician fading channel.

In Fig. 8.6, we display effective capacity as a function of energy per bit, $\frac{E_b}{N_0}_{\text{dB}}$ for QPSK input. We consider Rician fading channel with different values of Rician K-factor (i.e., $K = 0$ dB and $K = 5$ dB). It is again observed that the linear approximation for the effective capacity in (8.22) and the exact analytical effective capacity expression in (8.4) matches well at low SNR values. Minimum energy per bit does not get affected by the Rician K-factor. However, as K increases, EE increases as evidenced by the increased wideband slope. This observation is in agreement with the minimum energy per bit and wideband slope expressions in (8.26).

In Fig. 8.7, we plot effective capacity as a function of average transmit power constraint, $\bar{P}$ for Gaussian, BPSK, QPSK and 16-QAM inputs. We consider the proposed power control

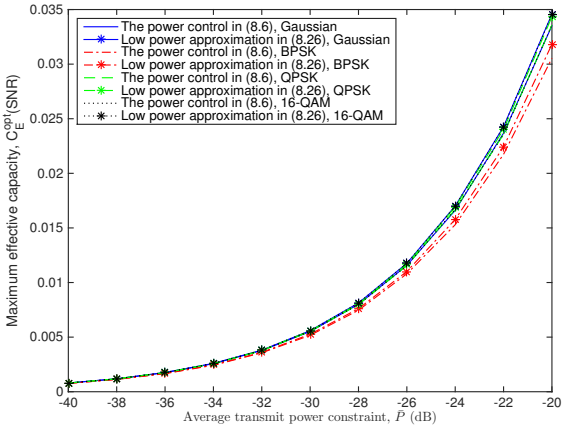

Figure 8.7: Effective capacity vs. average transmit power constraint, $\bar{P}$ for Gaussian, BPSK, QPSK and 16-QAM inputs.

in (8.31) and low-power approximation for the power control in (8.27). The figure validates the accuracy of the approximation at low power levels. Also, decreasing $\bar{P}$ leads to lower effective capacity for all inputs.

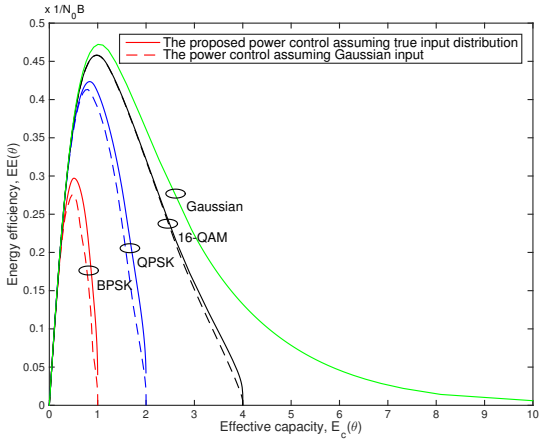

Figure 8.8: The energy efficiency vs the effective capacity for Gaussian, BPSK, QPSK and 16-QAM inputs.

In Fig. 8.8, we display the energy efficiency as a function of the effective capacity for Gaussian, BPSK, QPSK and 16-QAM inputs. QoS exponent, θ is set to 0.001. It is seen that the energy efficiency vs. effective capacity relation has a bell-shaped curve due to accounting for circuit power consumption in the total power expenditure. Also, Gaussian inputs always have higher energy efficiency compared to BPSK, QPSK and 16-QAM inputs. It is

observed from the figure that if the signal constellation size is small, there is a considerable performance gap in terms of energy efficiency achieved with the proposed optimal power control assuming the true distribution of the input and that with the power control assuming Gaussian distributed input. The reason is that the power control assuming Gaussian input signaling is suboptimal for finite discrete inputs (i.e., BPSK, QPSK and 16-QAM inputs). On the other hand, the performance gap decreases for larger constellation size, i.e., when we have 16-QAM.

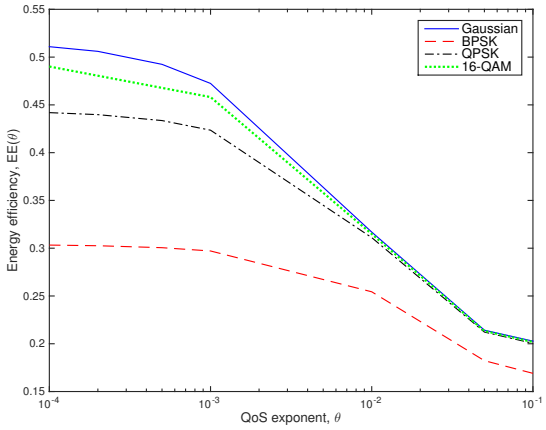

Figure 8.9: The maximum achievable energy efficiency vs. QoS exponent, θ.

In Fig. 8.9, we plot the maximum achievable energy efficiency as a function of QoS exponent, θ for Gaussian, BPSK, QPSK and 16-QAM inputs. We observe that the energy efficiency for all inputs decreases and energy efficiencies get closer to each other as θ increases because QoS requirement becomes more stringent. In the limiting case in which θ grows, the transmitter adopts the total channel inversion scheme and supports lower transmission rates. On the other hand, the maximum achievable energy efficiency of Gaussian, BPSK, QPSK and 16-QAM inputs increases when QoS constraints get looser, and the performance gap among the inputs is pronounced at low values of θ.

We analyze the tradeoff between effective capacity and EE. In particular, we display effective capacity as a function of EE gain (%) for Gaussian, BPSK, QPSK and 16-QAM inputs in Fig. 8.10. We assume that QoS exponent, $\theta = 0.1$ and average transmit power

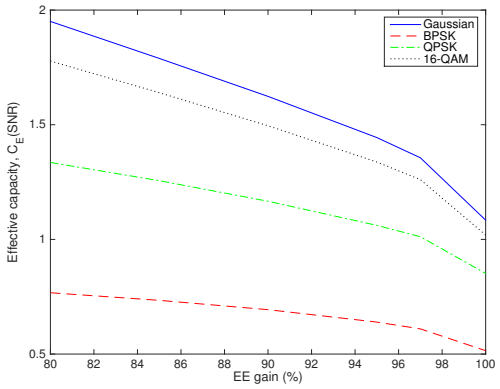

Figure 8.10: Effective capacity gain vs. EE gain for Gaussian, BPSK, QPSK and 16-QAM inputs.

constraint, $\bar{P} = 6$ dB. The EE gain is determined as the ratio of the minimum required EE denoted by EE_{min} to the maximum achievable EE. It is seen that the effective capacity decreases with increasing EE gain for all inputs. Again, Gaussian input achieves the highest effective capacity.

8.2 QoS-Driven Power Control Schemes for Random Sources

In the previous section, we consider constant-rate arrivals. However, other types of traffic such as video or voice can be modeled using Markovian process. Therefore, proper choice of source traffic models should be taken into account for effective QoS provisioning. To address this issue, we incorporate more general random arrival models (e.g., discrete-time Markov and Markov fluid sources, and discrete-time and continuous-time Markov modulated Poisson (MMP) sources) and analyze the optimal power control policies that maximize the energy efficiency and throughput with arbitrary input signaling under QoS constraints accordingly.

Section 8.2.1 introduces the channel model. In Section 8.2.2, we present effective bandwidth of Markovian arrivals. In Section 8.2.3, throughput of wireless fading channels for Markovian arrival models is provided. In Section 8.2.4, we derive the optimal power adap-

tation policy maximizing the energy efficiency with arbitrary input signaling. Section 8.2.5 determines the optimal power control scheme that maximizes the throughput subject to a constraint on the minimum required energy efficiency. In Section 8.2.6, numerical results are illustrated.

8.2.1 Channel Model

We consider a wireless communication link in which a transmitter is sending data to a receiver over a flat fading channel. Thus, the channel input-output relation can be expressed as

$$y_i = h_i x_i + n_i \text{ for } i = 1, 2, \ldots \tag{8.52}$$

where x_i and y_i are the transmitted and received signals, respectively, and h_i denotes the channel fading coefficient and the channel power gain is represented by $z_i = |h_i|^2$. Also, n_i denotes the zero-mean, circularly-symmetric, complex Gaussian noise with variance $\mathbb{E}\{|n_i|^2\} = N_0$.

We assume that the transmitter is equipped with perfect channel side information (CSI) and hence performs power control. Let $\mathrm{P}(\theta, z_i)$ denote the transmission power as a function of z_i and θ, which is the QoS exponent described in the following section. We consider a block-fading model and assume that the realizations of the fading coefficients stay fixed for a block of symbols and change independently for the next block. Also, fading coefficients are assumed to be identically distributed having arbitrary marginal distributions with finite variances.

The time index i is omitted in the sequel for notational brevity. We express the transmitted signal x in terms of a normalized unit-power arbitrarily distributed input signal s. Hence, the normalized received signal can be written as

$$\hat{y} = \sqrt{\rho} s + \hat{n}, \tag{8.53}$$

where $\rho = \frac{\mathrm{P}(\theta,z)}{N_0} z$ including both the channel gain, transmission and noise powers, and $\hat{n}$ is the normalized Gaussian noise with unit variance.

8.2.2 Effective Bandwidth of Markov Arrivals

We assume that the data to be sent is generated by Markovian sources and is initially stored in a buffer prior to transmission. Statistical QoS constraints are imposed in the form of limitations on the buffer overflow probability. We mainly focus on Markovian sources with two states (ON-OFF), namely discrete-time Markov and Markov fluid sources, and discrete-time and continuous-time MMP sources. For these sources, we briefly describe below the effective bandwidth, which characterizes the minimum constant transmission (or service) rate required to support the given time-varying data arrivals while satisfying the statistical QoS guarantees described in (2.17).

8.2.2.1 Discrete-time Markov Source

In this case, data arrivals are modeled as a discrete-time Markov process having a transition probability matrix $\mathbf{J}$ with two states: an ON state in which r bits arrive (i.e., the arrival rate is r bits/block), and an OFF state in which there are no arrivals. For this model, the state transition probability matrix is

$$\mathbf{J} = \begin{bmatrix} p_{11} & p_{12} \\ p_{21} & p_{22} \end{bmatrix}. \tag{8.54}$$

Consequently, the effective bandwidth of this ON-OFF Markov model with transition probability $\mathbf{J}$ can be found as [100]

$$a(\theta) = \frac{1}{\theta} \log \left(\frac{p_{11} + p_{22}\mathrm{e}^{r\theta} + \sqrt{(p_{11} + p_{22}\mathrm{e}^{r\theta})^2 - 4(p_{11} + p_{22} - 1)\mathrm{e}^{r\theta}}}{2} \right). \tag{8.55}$$

Above p_{11} and p_{22} denote the probabilities of staying in the OFF state and ON state, respectively. Hence, the transition probabilities from one state to a different one are denoted by $p_{21} = 1 - p_{22}$ and $p_{12} = 1 - p_{11}$.

8.2.2.2 Markov Fluid Source

In this case, data arrivals are modeled as a continuous-time Markov process with a generating matrix $\mathbf{G}$, which is defined for two states (ON-OFF) as follows:

$$\mathbf{G} = \begin{bmatrix} -\alpha & \alpha \\ \beta & -\beta \end{bmatrix} \tag{8.56}$$

where α and β are the transition rates from OFF state to ON state and vice-versa, respectively. In particular, there is no arrival in the OFF state while the arrival rate is r bits/block in the ON state. Given the above generating matrix, the effective bandwidth of this ON-OFF Markov model is expressed as [101]

$$a(\theta) = \frac{1}{2\theta}\left[\theta r - (\alpha + \beta) + \sqrt{(\theta r - (\alpha + \beta))^2 + 4\alpha\theta r}\right]. \tag{8.57}$$

8.2.2.3 Discrete-time Markov Modulated Poisson (MMP) Source

In this case, the data source is modeled as a Poisson process whose intensity varies according to a discrete-time Markov chain. For the two-state model, the intensity of the Poisson arrival process is r bits/block in the ON state whereas the intensity is 0 in the OFF state. Let the Markov chain have the transition probability matrix $\mathbf{J}$ given in (8.54). Then, the effective bandwidth is given by [56]

$$a(\theta) = \frac{1}{\theta}\log\left(\frac{p_{11} + p_{22}\mathrm{e}^{r(\mathrm{e}^{\theta}-1)} + \sqrt{[p_{11} + p_{22}\mathrm{e}^{r(\mathrm{e}^{\theta}-1)}]^2 - 4(p_{11} + p_{22} - 1)\mathrm{e}^{r(\mathrm{e}^{\theta}-1)}}}{2}\right). \tag{8.58}$$

8.2.2.4 Continuous-time Markov Modulated Poisson (MMP) Source

In this case, the data arrival is again modeled as a Poisson process but now the Poisson arrival intensity is controlled by a continuous-time Markov chain. As in the previous subsubsection, we consider that the intensities of the Poisson arrival process are r bits/block and 0 in the ON and OFF states, respectively. Given the generating matrix $\mathbf{G}$ as in (8.56), the effective bandwidth of this source is written as [101]

$$a(\theta) = \frac{1}{2\theta}[(\mathrm{e}^{\theta} - 1)r - (\alpha + \beta)] + \frac{1}{2\theta}\sqrt{[(\mathrm{e}^{\theta} - 1)r - (\alpha + \beta)]^2 + 4\alpha(\mathrm{e}^{\theta} - 1)r}. \tag{8.59}$$

8.2.2.5 Effective Capacity in Fading Channels

Effective capacity, as a dual concept to effective bandwidth, identifies the maximum constant arrival rate that can be supported by a given time-varying service process while satisfying (2.17). Under the block-fading assumption, the effective capacity can be expressed as [102]

$$C_E(\theta, z) = -\frac{1}{\theta}\log \mathbb{E}\left\{\mathrm{e}^{-\theta\mathcal{I}(\rho)}\right\}, \tag{8.60}$$

where $\mathcal{I}(\rho)$ indicates the input-output mutual information.

8.2.3 Throughput with Markovian Source Models

In this subsection, we seek to formulate the throughput of wireless fading channels for Markovian arrival models by incorporating the effective bandwidth expressions and the notion of effective capacity introduced in Section 8.2.2. Since we consider two-state Markov arrival models with arrival rates r and 0 in the ON and OFF states, respectively, the average arrival rate simply becomes

$$r_{\text{avg}} = P_{\text{ON}} r, \tag{8.61}$$

which is equal to the average departure rate when the queue is in steady state [103]. Above, P_{ON} denotes the probability of source being in the ON state.

Now, the throughput can be determined by identifying the maximum average arrival rate that can be supported by the fading channel while satisfying the statistical QoS limitations given in the form in (2.17). As shown in [103, Theorem 2.1], (2.17) is satisfied, i.e., buffer overflow probability decays exponentially fast with rate controlled by the QoS exponent θ, if the effective bandwidth of the arrival process is equal to the effective capacity of the service process, i.e.,

$$a(\theta) = C_E(\theta). \tag{8.62}$$

By solving the above equation in (8.62), we obtain closed-form expressions of the maximum average arrival rates $r^*_{\mathrm{avg}}(\theta)$ for discrete-time Markov and Markov fluid sources, and discrete-time and continuous-time MMP sources with ON-OFF states in the following subsubsections. The derivations below are similar to that in [104] and are provided here as well briefly for the sake of completeness.

8.2.3.1 Discrete-time Markov Source

Inserting the effective bandwidth expression of the discrete-time Markov source in (8.55) into (8.62), we can further simplify and express (8.62) in the following equivalent form:

$$\left(p_{11}+p_{22}\mathrm{e}^{r\theta}-2\mathrm{e}^{\theta C_E}\right)^2 = (p_{11}+p_{22}\mathrm{e}^{r\theta})^2 - 4(p_{11}+p_{22}-1)\mathrm{e}^{r\theta}. \tag{8.63}$$

After solving the equation for r, we obtain the maximum ON-state arrival rate as

$$r^*(\theta) = \frac{1}{\theta}\log_e\left(\frac{\mathrm{e}^{2\theta C_E(\theta)} - p_{11}\mathrm{e}^{\theta C_E(\theta)}}{(1-p_{11}-p_{22})+p_{22}\mathrm{e}^{\theta C_E(\theta)}}\right) \tag{8.64}$$

and hence, the maximum average arrival rate can be expressed in terms of $C_E(\theta)$ as

$$r^*_{\text{avg}}(\theta) = \frac{P_{\text{ON}}}{\theta} \log_e \left(\frac{\mathrm{e}^{2\theta C_E(\theta)} - p_{11}\mathrm{e}^{\theta C_E(\theta)}}{(1-p_{11}-p_{22}) + p_{22}\mathrm{e}^{\theta C_E(\theta)}} \right), \tag{8.65}$$

where the probability of being in the ON state, P_{ON}, is given by

$$P_{\text{ON}} = \frac{1-p_{11}}{2-p_{11}-p_{22}}. \tag{8.66}$$

8.2.3.2 Markov Fluid Source

Incorporating the effective bandwidth expression of Markov fluid source in (8.57) into (8.62) and performing straightforward simplifications, we can rewrite (8.62) in the form of

$$(\theta r - (\alpha+\beta) - 2\theta C_E)^2 = (\theta r - (\alpha+\beta))^2 + 4\alpha\theta r. \tag{8.67}$$

Solving the above equation yields the maximum average arrival rate in terms of $C_E(\theta)$ as

$$r^*_{\text{avg}}(\text{SNR}, \theta) = P_{\text{ON}} \frac{\theta C_E(\theta) + \alpha + \beta}{\theta C_E(\theta) + \alpha} C_E(\theta). \tag{8.68}$$

Above, P_{ON} is given by

$$P_{\text{ON}} = \frac{\alpha}{\alpha+\beta}. \tag{8.69}$$

8.2.3.3 Discrete-time Markov Modulated Poisson (MMP) Source

We first combine the effective bandwidth expression in (8.58) with (8.62) and express (8.62) in the following simplified form:

$$\left(p_{11} + p_{22}\mathrm{e}^{r(\mathrm{e}^{\theta}-1)} - 2\mathrm{e}^{\theta C_E(\theta)}\right)^2 = \left(p_{11} + p_{22}\mathrm{e}^{r(\mathrm{e}^{\theta}-1)}\right)^2 - 4(p_{11}+p_{22}-1)\mathrm{e}^{r(\mathrm{e}^{\theta}-1)}. \tag{8.70}$$

Then, we solve for the maximum ON-state Poisson arrival intensity, r. Following this characterization, the maximum average arrival rate for the two-state discrete-time MMP source model is obtained in terms of $C_E(\theta)$ as follows:

$$r^*_{\text{avg}}(\text{SNR},\theta) = \frac{P_{\text{ON}}}{(\mathrm{e}^{\theta}-1)}\left[\log\left(\frac{\mathrm{e}^{2\theta C_E(\theta)} - p_{11}\mathrm{e}^{\theta C_E(\theta)}}{(1-p_{11}-p_{22}) + p_{22}\mathrm{e}^{\theta C_E(\theta)}}\right)\right]. \tag{8.71}$$

8.2.3.4 Continuous-time Markov Modulated Poisson (MMP) Source

Following similar steps as in the previous subsubsection, we simplify and express the equality in (8.62) by incorporating (8.59) as

$$[(\mathrm{e}^{\theta}-1)r - (\alpha+\beta) - 2\theta C_E(\theta)]^2 = [(\mathrm{e}^{\theta}-1)r - (\alpha+\beta)]^2 + 4\alpha(\mathrm{e}^{\theta}-1)r. \tag{8.72}$$

After solving for r, the maximum average arrival rate for the two-state continuous-time MMP source model can be found as

$$r^*_{\text{avg}}(\text{SNR},\theta) = P_{\text{ON}}\Big(\frac{\theta}{\mathrm{e}^{\theta}-1}\Big)\frac{\theta C_E(\theta)+\alpha+\beta}{\theta C_E(\theta)+\alpha}\, C_E(\theta). \tag{8.73}$$

8.2.4 Energy-Efficient Power Adaptation

In this subsection, we characterize and determine the optimal power control policy that maximizes the energy efficiency, which is defined as the ratio of the maximum average arrival rate to the total power. The optimization problem can be formulated as

$$\text{EE}_{\text{opt}}(\theta) = \max_{\text{P}(\theta,z)\geq 0} \frac{r^*_{\text{avg}}(\theta)}{\frac{1}{\epsilon}\mathbb{E}\left\{\text{P}(\theta,z)\right\} + \text{P}_c}, \tag{8.74}$$

where the expectation $\mathbb{E}\{\cdot\}$ is taken with respect to the channel power gain z. Above, P_c denotes the average power consumption of the electronic circuits such as amplifiers, mixers, filters, and ϵ represents the power amplifier efficiency. In addition, $\text{EE}_{\text{opt}}(\theta)$ represents the maximum energy efficiency achieved with the optimal power control. In the following

subsections, we derive the optimal power control policies for different Markovian arrival models.

8.2.4.1 Discrete-Time Markov Source

First, we consider discrete-time Markov sources. Inserting the maximum average rate expression in (8.65) into (8.74), the optimization problem in (8.74) becomes

$$\mathrm{EE}_{\mathrm{opt}}(\theta) = \max_{\mathrm{P}(\theta,z)\geq 0} \frac{\frac{P_{\mathrm{ON}}}{\theta}\log\left(\frac{\mathrm{e}^{2\theta C_E(\theta)}-p_{11}\mathrm{e}^{\theta C_E(\theta)}}{(1-p_{11}-p_{22})+p_{22}\mathrm{e}^{\theta C_E(\theta)}}\right)}{\frac{1}{\epsilon}\mathbb{E}\left\{\mathrm{P}(\theta,z)\right\}+\mathrm{P}_c}. \tag{8.75}$$

In the following result, we identify the optimal power control strategy for this case.

Proposition 8.2.1 *The optimal power control policy, denoted by $P_{opt}(\theta,z)$, which maximizes the energy efficiency for discrete-time Markov sources with arbitrary input signaling, is given by*

$$P_{opt}(\theta,z) = \begin{cases} 0 & z \leq \gamma, \\ P^*(\theta,z) & z > \gamma \end{cases}. \tag{8.76}$$

Above, $P^*(\theta,z)$ is solution to

$$\mathrm{e}^{-\theta\mathcal{I}(P^*(\theta,z)z)}MMSE\big(P^*(\theta,z)z\big)z = \gamma \tag{8.77}$$

where

$$\gamma = \frac{\lambda((1-p_{11}-p_{22})\mathrm{e}^{-\theta C_E(\theta)}+p_{22})(1-p_{11}\mathrm{e}^{-\theta C_E(\theta)})}{\epsilon\log_2(e)\theta\big(\big(2-p_{11}\mathrm{e}^{-\theta C_E(\theta)}\big)(1-p_{11}-p_{22})+p_{22}\mathrm{e}^{\theta C_E(\theta)}\big)}. \tag{8.78}$$

The optimal value of λ can be found by solving the equation below:

$$-\log\left(\frac{\mathrm{e}^{2\theta C_E(\theta)}-p_{11}\mathrm{e}^{\theta C_E(\theta)}}{(1-p_{11}-p_{22})+p_{22}\mathrm{e}^{\theta C_E(\theta)}}\right)+\lambda\Big(\frac{1}{\epsilon}\mathbb{E}\left\{P(\theta,z)\right\}+P_c\Big)=0. \tag{8.79}$$

Proof: See Appendix S.

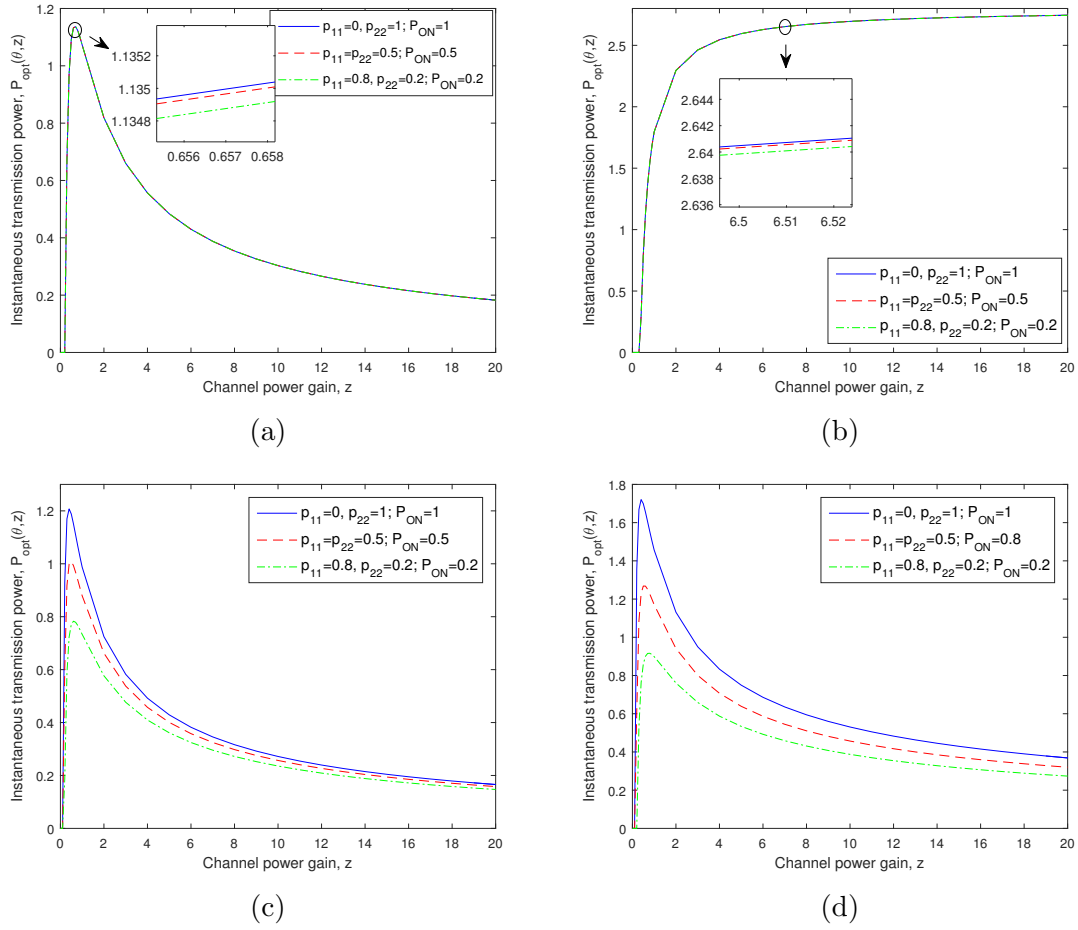

Figure 8.11: $\mathrm{P}_{\mathrm{opt}}(\theta, z)$ vs. channel power gain, z for (a) BPSK, $\theta = 0.0001$; (b) Gaussian, $\theta = 0.0001$, (c) BPSK, $\theta = 1$, (d) Gaussian, $\theta = 1$.

In Fig. 8.11, we plot the instantaneous transmission power levels, $\mathrm{P}_{\mathrm{opt}}(\theta, z)$, as a function of channel power gain, z, for BPSK and Gaussian inputs under different QoS constraints, e.g., $\theta = 0.0001$ and $\theta = 1$. We consider discrete-time Markov source with different transition probabilities. It is observed that transmission power level depends on the QoS exponent, θ and the source burstiness. In particular, when the system is subject to looser QoS constraints, e.g., $\theta = 0.0001$, the power control policy follows the water-filling scheme for Gaussian inputs, i.e., more power is assigned as the channel power gain increases. However, for BPSK inputs, the power is distributed according to the mercury/water-filling policy, i.e., the power is allocated to better channel up to capacity saturation and then extra power is assigned

to weaker channel. When $\theta = 1$ corresponding the system is operating under strict QoS constraints, the transmission power first increases and then diminishes as the channel power gain increases for both inputs. It is also seen that less power is allocated for a given channel power gain z as $P_{\rm ON}$ decreases and hence the source burstiness increases. Conversely, highest instantaneous transmission power levels are achieved with the constant-rate source (with $p_{22} = 1$ and $p_{11} = 0$, and hence $P_{\rm ON} = 1$), which does not exhibit any burstiness. We also notice from the upper figures that the impact of the source burstiness diminishes at low values of θ as reflected by all curves being very close. In summary, source characteristics, input types, and QoS requirements are critical factors affecting the optimal power control policies.

Remark 8.2.1 *When the input signal is Gaussian, we have* $MMSE(\rho) = \frac{1}{1+\rho}$ *and* $\mathcal{I}(\rho) = \log_2(1+\rho)$. *Inserting these expressions in (8.76), the optimal power control policy reduces to*

$$P_{opt}(\theta, z) = \begin{cases} 0 & z \leq \gamma \\ \frac{1}{\gamma^{\frac{1}{\eta+1}} z^{\frac{\eta}{\eta+1}}} - \frac{1}{z} & z > \gamma \end{cases}, \tag{8.80}$$

where $\eta = \theta \log_2(e)$ *and* γ *is again defined in (8.78), which is a function of the Lagrange multiplier* λ.

In the case of Rayleigh fading, a closed-form expression for finding λ *is obtained by evaluating the integrals in (8.79) as follows:*

$$-\log\Big(\frac{g(\theta)^2 - p_{11}g(\theta)}{(1-p_{11}-p_{22}) + p_{22}g(\theta)}\Big) + \lambda\Big[\frac{1}{\epsilon}\Big(\Big(\frac{1}{\gamma}\Big)^{\frac{1}{1+\eta}}\Gamma\Big(\frac{1}{1+\eta}, \gamma\Big) + Ei(-\gamma)\Big) + P_c\Big] = 0,$$

where

$$g(\theta) = \frac{1}{\gamma^{\frac{\eta}{\eta+1}}\Gamma\Big(\frac{1}{1+\eta}, \gamma\Big) + 1 - \mathrm{e}^{-\gamma}}. \tag{8.81}$$

Above, $\Gamma(s,w)$ *denotes the upper incomplete gamma function [54, eq. 6.5.3], and* $Ei(w)$ *represents the exponential integral [85, eq. 8.211.1].*

8.2.4.2 Markov Fluid Source

Now, we consider Markov fluid sources. Incorporating the maximum average rate expression in (8.68), the objective function in (8.74) can be written as

$$\mathrm{EE}_{\mathrm{opt}}(\theta) = \max_{\mathrm{P}(\theta,z)\geq 0} \frac{P_{\mathrm{ON}} \frac{\theta C_E(\theta)+\alpha+\beta}{\theta C_E(\theta)+\alpha} C_E(\theta)}{\frac{1}{\epsilon}\mathbb{E}\left\{\mathrm{P}(\theta,z)\right\} + \mathrm{P}_c}. \tag{8.82}$$

In this case, the optimal power control policy is determined in the following result.

Proposition 8.2.2 *The optimal power control policy that maximizes the energy efficiency for Markov fluid sources with arbitrary input signaling is obtained as*

$$P_{opt}(\theta,z) = \begin{cases} 0 & z \leq \gamma \\ P^*(\theta,z) & z > \gamma \end{cases}. \tag{8.83}$$

Above, $P^*(\theta,z)$ *is solution to*

$$\mathrm{e}^{-\theta \mathcal{I}(P^*(\theta,z)z)} MMSE\big(P^*(\theta,z)z\big) z = \gamma, \tag{8.84}$$

where

$$\gamma = \frac{\lambda \mathrm{e}^{-\theta C_E(\theta)}}{\epsilon \log_2(e)\big(\frac{\alpha\beta}{(\theta C_E(\theta)+\alpha)^2}+1\big)}. \tag{8.85}$$

The optimal value of λ *can be calculated by solving the following equation:*

$$-\frac{\theta C_E(\theta)+\alpha+\beta}{\theta C_E(\theta)+\alpha} C_E(\theta) + \lambda\Big(\frac{1}{\epsilon}\mathbb{E}\left\{P(\theta,z)\right\} + P_c\Big) = 0. \tag{8.86}$$

Proof: See Appendix T.

Remark 8.2.2 *We note that the optimal power control policy in (8.83) depends on statistical queueing constraints through the QoS exponent, θ, and on the Markov source characteristics through the transition rates α and β. Similar conclusions also apply for the discrete-time Markov source. Hence,subject to a minimum energy efficiency constraint is given by in general, the optimal energy-efficient power adaptation varies for different sources and different QoS requirements.*

Remark 8.2.3 *Optimal power control also varies with the input distribution as seen from its dependence on the mutual information and MMSE in (8.84). For Gaussian distributed input signal, we have the closed-form expression below:*

$$P_{opt}(\theta, z) = \begin{cases} 0 & z \leq \gamma \\ \frac{1}{\gamma^{\frac{1}{\eta+1}} z^{\frac{\eta}{\eta+1}}} - \frac{1}{z} & z > \gamma \end{cases}, \tag{8.87}$$

where γ is defined in (8.85) and is a function of the Lagrange multiplier λ.

8.2.4.3 Discrete-time and Continuous-time Markov Modulated Poisson (MMP) Sources

The throughput expressions of discrete-time Markov and Markov fluid sources have similarities to discrete-time and continuous-time MMP sources, respectively. More specifically, there is an additional multiplicative factor $\frac{\theta}{e^{\theta}-1}$ for discrete-time and continuous-time MMP sources. The presence of this factor does not affect the solution of the optimization problem since it is only a function of θ and it does not depend on power levels, and hence it can be omitted during optimization. Therefore, the optimal power control policies for discrete-time and continuous-time MMP sources are the same as in the cases of discrete-time Markov and Markov fluid sources.

8.2.5 Power Adaptation with a Minimum Energy Efficiency Constraint

In this subsection, we identify the optimal power control policy that maximizes the throughput in the presence of random arrivals under a constraint on the minimum required energy efficiency. In this regard, the optimization problem can be written as

$$r^*_{\text{avg,opt}}(\theta) = \max_{\text{P}(\theta,z)\geq 0} r^*_{\text{avg}}(\theta) \tag{8.88}$$

subject to

$$\frac{r^*_{\text{avg}}(\theta)}{\frac{1}{\epsilon}\mathbb{E}\left\{\text{P}(\theta,z)\right\} + \text{P}_c} \geq \text{EE}_{\min}(\theta), \tag{8.89}$$

where $\text{EE}_{\min}(\theta)$ denotes the minimum required energy efficiency. In the following subsections, we identify the optimal power control policies for Markovian arrival models, i.e., for discrete-time Markov and Markov fluid sources, and discrete-time and continuous-time MMP sources.

8.2.5.1 Discrete-Time Markov Source

The main characterization for the optimal power control with the discrete-time Markov source is given as follows:

Proposition 8.2.3 *The optimal power control policy that maximizes the throughput achieved with arbitrary input signaling in the presence of discrete-time Markov source subject to a minimum energy efficiency constraint is given by*

$$P_{opt}(\theta,z) = \max\{0, P^*(\theta,z)\}, \tag{8.90}$$

where $P^*(\theta,z)$ is obtained by solving

$$\text{e}^{-\theta\mathcal{I}(P^*(\theta,z)z)}MMSE\big(P^*(\theta,z)z\big)z = \mu. \tag{8.91}$$

Above, μ is a function of the Lagrange multiplier, λ, and is given by

$$\mu = \frac{\lambda EE_{min}(\theta)}{(1+\lambda)P_{ON}\log_2(e)\epsilon}\left[\frac{(1-p_{11}\mathrm{e}^{-\theta C_E(\theta)})((1-p_{11}-p_{22})\mathrm{e}^{-\theta C_E(\theta)}+p_{22})}{(2-p_{11}\mathrm{e}^{-\theta C_E(\theta)})((1-p_{11}-p_{22})+p_{22}\mathrm{e}^{\theta C_E(\theta)})}\right]. \tag{8.92}$$

Consequently, the optimal value of λ can be found by solving the following equation:

$$\frac{P_{ON}}{\theta}\log\left(\frac{\mathrm{e}^{2\theta C_E(\theta)}-p_{11}\mathrm{e}^{\theta C_E(\theta)}}{(1-p_{11}-p_{22})+p_{22}\mathrm{e}^{\theta C_E(\theta)}}\right) - EE_{min}\Big(\frac{1}{\epsilon}\mathbb{E}\left\{P^*(\theta,z)\right\}+P_c\Big) = 0. \tag{8.93}$$

Proof: See Appendix U.

Remark 8.2.4 *The optimal power control scheme in (8.90) depends on the state transition probabilities, QoS exponent θ and the minimum energy efficiency requirement. In particular, the optimal average transmission power in this policy satisfies the minimum energy efficiency with equality.*

Remark 8.2.5 *When the input signal is Gaussian distributed, the optimal power control specializes to*

$$P_{opt}(\theta,z) = \max\left\{0, \frac{1}{\mu^{\frac{1}{\eta+1}}z^{\frac{\eta}{\eta+1}}} - \frac{1}{z}\right\}, \tag{8.94}$$

where μ is defined in (8.92).

8.2.5.2 Markov Fluid Source

The optimal power control scheme for the Markov fluid source is determined in the following result:

Proposition 8.2.4 *The optimal power control policy that maximizes the throughput with arbitrary input signaling and Markov fluid source subject to a minimum energy efficiency*

constraint is

$$P_{opt}(\theta, z) = \max\{0, P^*(\theta, z)\}, \tag{8.95}$$

where $P^*(\theta, z)$ *is obtained by solving*

$$\mathrm{e}^{-\theta \mathcal{I}(P^*(\theta,z)z)} MMSE\big(P^*(\theta, z)z\big)z = \mu. \tag{8.96}$$

Above, μ *is given by*

$$\mu = \frac{\lambda EE_{min}(\theta)}{(1+\lambda)P_{ON}\log_2(e)\epsilon}\left[\frac{\mathrm{e}^{-\theta C_E(\theta)}}{\big(\frac{\alpha\beta}{(\theta C_E(\theta)+\alpha)^2}+1\big)}\right], \tag{8.97}$$

and the optimal value of λ *can be found by solving the following equation:*

$$P_{ON}\frac{\theta C_E(\theta)+\alpha+\beta}{\theta C_E(\theta)+\alpha}C_E(\theta) - EE_{min}\Big(\frac{1}{\epsilon}\mathbb{E}\left\{P^*(\theta, z)\right\} + P_c\Big) = 0.$$

Since similar steps as in the proof of Proposition 8.2.3 are followed, the proof is omitted for brevity.

Remark 8.2.6 *Generally, we do not have closed-form expressions for the optimal power control policies due to not having simple expressions for the mutual information and MMSE for any given input distribution. The exception is again the case of the Gaussian input. Substituting the expressions* $MMSE(\rho) = \frac{1}{1+\rho}$ *and* $\mathcal{I}(\rho) = \log_2(1+\rho)$ *into the general characterization in (8.95), we can obtain, as a special case, the optimal power control for Gaussian signaling as*

$$P_{opt}(\theta, z) = \max\left\{0, \frac{1}{\mu^{\frac{1}{\eta+1}} z^{\frac{\eta}{\eta+1}}} - \frac{1}{z}\right\}, \tag{8.98}$$

where μ *is given in (8.97).*

8.2.5.3 Discrete-time Markov Modulated Poisson (MMP) Source

The optimal power control that maximizes the throughput in the presence of discrete-time MMP source has the same formulation as that obtained for the discrete-time Markov source in (8.90). The only modifications are in μ and λ. In particular, multiplying the expression in (8.92) with the term $\frac{\mathrm{e}^{\theta}-1}{\theta}$ yields μ as

$$\mu = \frac{\lambda \mathrm{EE}_{\min}(\theta)(\mathrm{e}^{\theta}-1)}{(1+\lambda)\theta P_{\mathrm{ON}} \log_2(e)\epsilon}\left[\frac{(1-p_{11}\mathrm{e}^{-\theta C_E(\theta)})((1-p_{11}-p_{22})\mathrm{e}^{-\theta C_E(\theta)}+p_{22})}{(2-p_{11}\mathrm{e}^{-\theta C_E(\theta)})((1-p_{11}-p_{22})+p_{22}\mathrm{e}^{\theta C_E(\theta)})}\right]. \tag{8.99}$$

Also, the optimal value of λ can be found by solving

$$\frac{P_{\mathrm{ON}}}{\mathrm{e}^{\theta}-1}\log\left(\frac{\mathrm{e}^{2\theta C_E(\theta)}-p_{11}\mathrm{e}^{\theta C_E(\theta)}}{(1-p_{11}-p_{22})+p_{22}\mathrm{e}^{\theta C_E(\theta)}}\right) - \mathrm{EE}_{\min}\Big(\frac{1}{\epsilon}\mathbb{E}\left\{\mathrm{P}^*(\theta,z)\right\}+\mathrm{P}_c\Big)=0. \tag{8.100}$$

8.2.5.4 Continuous-time Markov Modulated Poisson (MMP) Source

Similarly, the optimal power control scheme for the continuous-time MMP source is the same as that obtained for the Markov fluid source in (8.95) but with slightly modified μ and λ. More specifically, multiplying the expression in (8.97) with $\frac{\mathrm{e}^{\theta}-1}{\theta}$, we get

$$\mu = \frac{\lambda \mathrm{EE}_{\min}(\theta)(\mathrm{e}^{\theta}-1)}{(1+\lambda)\theta P_{\mathrm{ON}} \log_2(e)\epsilon}\left[\frac{\mathrm{e}^{-\theta C_E(\theta)}}{(\frac{\alpha\beta}{(\theta C_E(\theta)+\alpha)^2}+1)}\right], \tag{8.101}$$

which is a function of λ. Subsequently, the optimal value of λ can be obtained from

$$P_{\mathrm{ON}}\Big(\frac{\theta}{\mathrm{e}^{\theta}-1}\Big)\frac{\theta C_E(\theta)+\alpha+\beta}{\theta C_E(\theta)+\alpha}C_E(\theta) - \mathrm{EE}_{\min}\Big(\frac{1}{\epsilon}\mathbb{E}\left\{\mathrm{P}^*(\theta,z)\right\}+\mathrm{P}_c\Big)=0. \tag{8.102}$$

8.2.6 Numerical Results

In this subsection, we present more detailed numerical results to analyze the impact of input distributions, source burstiness and QoS constraints on the maximum energy efficiency and maximum throughput achieved with the obtained optimal power control schemes. Unless

mentioned explicitly, we assume that the channel power gain $z = |h|^2$ follows an exponential distribution with unit mean and ϵ is set to 1.

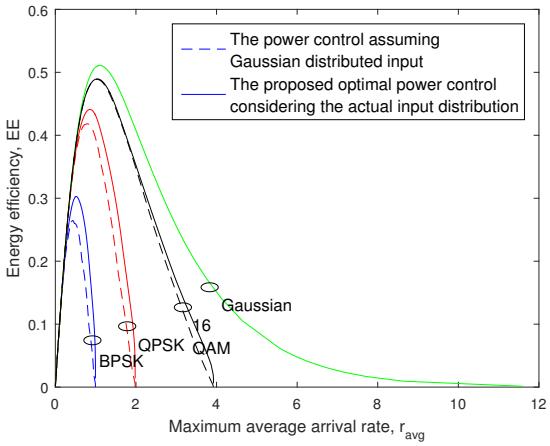

Figure 8.12: Energy efficiency vs. the maximum average arrival rate r_{avg} for Gaussian, BPSK, QPSK and 16-QAM.

In Fig. 8.12, we plot the energy efficiency as a function of the maximum average arrival rate, r_{avg} for Gaussian, BPSK, QPSK and 16-QAM. Discrete-time Markov source with transition probabilities $p_{11} = p_{22} = 0.5$ is considered. θ is set to 0.01. Since the circuit power is taken into account, energy efficiency vs. maximum average arrival rate is a bell shaped curve. We consider the energy efficiency of non-Gaussian inputs (i.e., 16-QAM, QPSK, BPSK) attained with the power control optimized under the assumption of Gaussian distributed input and also with the optimal power control, which takes into account the true distribution of the input. It is seen from the figure that the energy efficiencies of 16-QAM, QPSK and BPSK achieved with the power control designed for a Gaussian input are lower than those achieved with the optimal power control considering the discrete constellations and distributions, since the power control obtained under the assumption of Gaussian input is suboptimal for these non-Gaussian inputs. Therefore, it is concluded that if the power control is optimized under the assumption of Gaussian distributed input and the inputs are chosen from discrete constellations in actual applications, considerable performance degradation in terms of energy efficiency would occur especially if the constellation size is small. On the other hand, we

notice that the gap is smaller for 16-QAM, which has more signals. Hence, constellations with relatively large number of signals may experience less severe degradations.

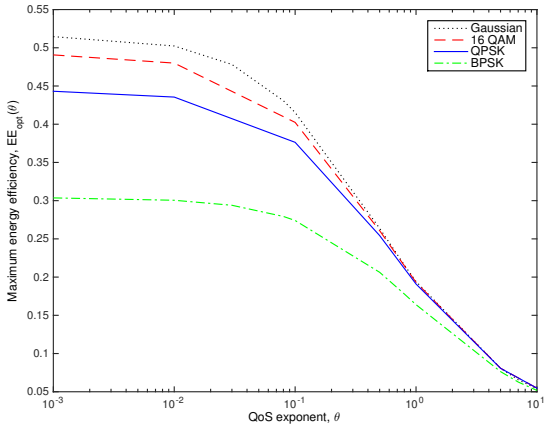

Figure 8.13: Maximum energy efficiency attained under the proposed power control vs. QoS exponent θ for Gaussian, BPSK, QPSK and 16-QAM inputs.

In Fig. 8.13, we display the maximum energy efficiency achieved with the optimal power control as a function of the QoS exponent θ for Gaussian, BPSK, QPSK and 16-QAM. We again consider a discrete-time Markov source but with transition probabilities $p_{11} = 0.8$ and $p_{22} = 0.2$. It is observed that the energy efficiency for all inputs decreases as θ increases since the transmitter is subject to more stringent QoS constraints, which result in lower transmission rates at given power levels and hence lower energy efficiency. It is seen that Gaussian signaling always achieves higher energy efficiency compared to BPSK, QPSK and 16-QAM. At low θ values, there is a performance gap in terms of energy efficiency between Gaussian, BPSK, QPSK and 16-QAM. On the other hand, at high θ values, the performances of Gaussian, BPSK, QPSK and 16-QAM inputs converge, indicating the near-optimality of even simple modulation schemes under stringent QoS constraints.

In Fig. 8.14, we plot the energy efficiency achieved with different power control schemes as a function of the QoS exponent θ for QPSK in the presence of a discrete-time Markov source with transition probabilities $p_{11} = 0.8$ and $p_{22} = 0.2$. We compare the energy efficiencies attained with the optimal power control considering the actual signal distribution, power

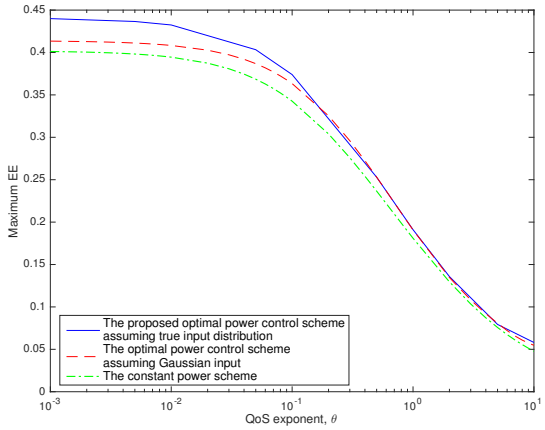

Figure 8.14: Maximum energy efficiency vs. QoS exponent θ for QPSK with different power control schemes.

control assuming Gaussian input, and the constant-power scheme. It is observed that the optimal power control outperforms both the power control strategy assuming Gaussian input and the constant-power scheme.

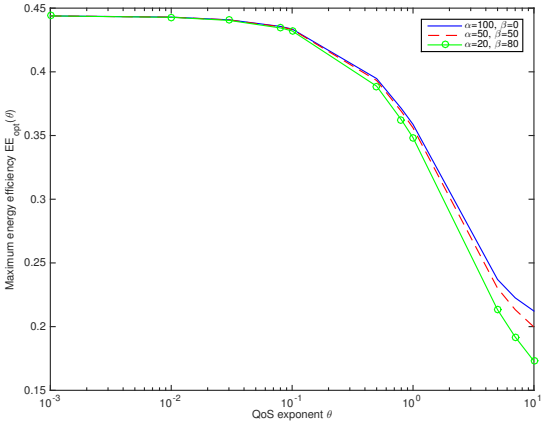

Figure 8.15: Maximum energy efficiency vs. QoS exponent θ for QPSK with different source burstiness.

In Fig. 8.15, we display the energy efficiency attained with the optimal power control as a function of the QoS exponent θ for QPSK when the source has different levels of burstiness. We consider a Markov fluid source with transition rates $\alpha = 20$, $\beta = 80$, and $\alpha = \beta = 50$ (for which $P_{\text{ON}} = \frac{\alpha}{\alpha+\beta} = 0.2$ and $P_{\text{ON}} = 0.5$, respectively), and also $\alpha = 100, \beta = 0$ (for which $P_{\text{ON}} = 1$, indicating essentially a constant-rate source). We set the sum of α and β to 100 as

shown in the figure. Hence, the burstiness of the source depends on the probability of being in the ON state, $P_{\text{ON}} = \frac{\alpha}{\alpha+\beta}$. More specifically, lower values of ON state probability, P_{ON}, correspond to a more bursty source. It is seen that the burstiness of the source has negligible impact on the energy efficiency for looser QoS constraints, i.e., for lower values of θ. On the other hand, energy efficiency decreases with decreasing P_{ON} when the QoS constraints become more stringent, i.e., as θ increases.

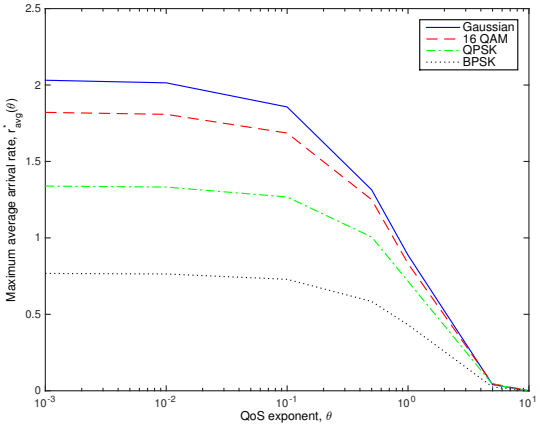

Figure 8.16: Maximum average arrival vs. QoS exponent θ for Gaussian, BPSK, QPSK and 16-QAM signaling, considering MMP sources.

In Fig. 8.16, we plot the maximum average arrival rate obtained with the optimal power control as a function of the QoS exponent θ for Gaussian, BPSK, QPSK and 16-QAM inputs. We consider continuous-time MMP source with transition rates $\alpha = 50$ and $\beta = 50$. We set $\text{EE}_{\min}(\theta) = 0.8 \times \text{EE}_{\max}(\theta)$. It is seen that there is again a performance gap in terms of the maximum throughput supported by Gaussian, BPSK, QPSK and 16 QAM signaling for lower θ values, and Gaussian input always achieves the best performance. Also, high values of θ yield lower arrival rates under all signaling schemes.

In Fig 8.17, we plot the maximum average arrival rate gain in percentage vs. the energy efficiency gain in percentage for QPSK in the presence of a Markov fluid source with different transition rates. We set $\theta = 10$. The energy efficiency gain is calculated as the ratio of the minimum required energy efficiency, denoted by $\text{EE}_{\min}(\theta)$ to the maximum energy efficiency

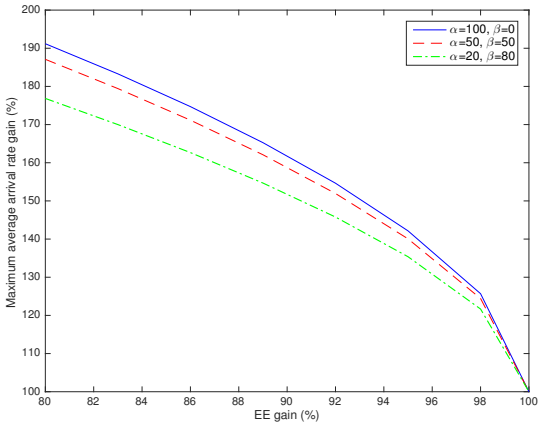

Figure 8.17: The maximum average arrival rate gain in percentage vs. the energy efficiency gain in percentage for QPSK, considering a Markov fluid source.

obtained with the proposed power control in (8.83). Similarly, the maximum average arrival rate gain is determined as the ratio of $r^*_{\text{avg}}(\theta)$ attained under a constraint on the minimum required energy efficiency to the corresponding $r^*_{\text{avg}}(\theta)$ achieved with the power control in (8.83). It is seen that the maximum average arrival rate gain increases as energy efficiency gain decreases. More specifically, a small reduction in energy efficiency gain leads to a significant gain in the maximum average arrival rate. For instance, when the energy efficiency gain is reduced from 100% to 85%, the maximum average arrival rate gain increases by 71% when $\alpha = 20$ and $\beta = 80$ (for which $P_{\text{ON}} = 0.2$). It is also observed that the maximum average arrival rate gain decreases with increasing source burstiness (i.e., with smaller value of P_{ON}).

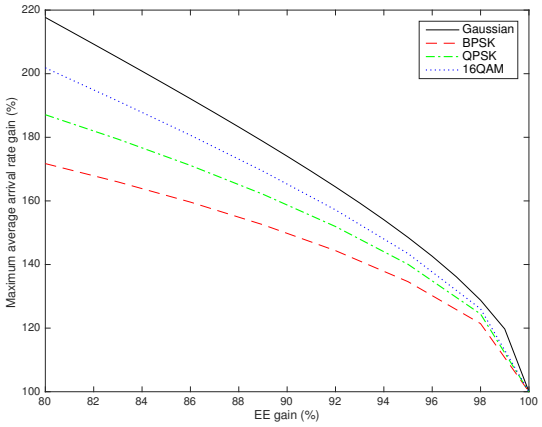

Figure 8.18: The maximum average arrival rate gain in percentage vs. the energy efficiency gain in percentage for Gaussian, BPSK, QPSK and 16-QAM, considering a Markov fluid source.

In Fig 8.18, we display the maximum average arrival rate gain in percentage vs. the energy efficiency gain in percentage for Gaussian, BPSK, QPSK, 16-QAM signaling. We consider a Markov fluid source with transition rates $\alpha = \beta = 50$. It is assumed that $\theta = 10$. We observe that Gaussian distributed input achieves higher maximum average arrival rate gain compared to non-Gaussian inputs (i.e.,16-QAM, QPSK and BPSK inputs). In addition, there is considerable difference in terms of the maximum average arrival rate gain between the input distributions as the energy efficiency gain decreases.

Chapter 9

Conclusion

9.1 Summary

In this thesis, performance of cognitive radio systems has been studied in terms of throughput, error rate and energy efficiency, and throughput- and energy-efficient optimal resource allocation schemes for both cognitive radio systems and general wireless systems operating subject to statistical QoS constraints have been determined. Specifically, the contributions of this thesis are summarized below.

In Chapter 3, we obtained the optimal power control policies for underlay cognitive radio systems with arbitrary input signaling subject to peak/average transmit power and peak/average interference power constraints for general fading distributions. We provided low-complexity power control algorithms. In addition, we analyzed the optimal power control policy in the low-power regime. Numerical results reveal that Gaussian input expectedly results in higher achievable rates at high power levels while Gaussian inputs and QPSK provide nearly the same performance in the low-power regime. Therefore, QPSK input can be efficiently used in practical systems rather than the Gaussian input which is not easy to realize. It is also shown that there can be considerable performance degradation if the system is designed under the assumption of Gaussian input and the inputs are chosen from discrete

constellations at moderate and high power levels. We observed that power control provides significant improvements in performance when compared with that achieved with constant power transmissions. We demonstrated that simpler low-power approximations of the power control strategies and achievable rates provide very accurate results when compared to exact expressions.

In Chapter 4, we determined the energy-efficient power allocation schemes for cognitive radio systems subject to peak/average transmit power constraints and peak/average interference power constraint in the presence of sensing errors and different levels of CSI regarding the transmission and interference links. It is assumed that the primary user transmits in a time-slotted fashion (i.e., the activity of the primary user remains the same during the transmission phase of secondary users). A low-complexity algorithm based on Dinkelbach's method was proposed to iteratively solve the power allocation that maximizes energy efficiency. It was shown that power allocation schemes depend on sensing performance through detection and false alarm probabilities, transmission link between secondary transmitter and secondary receiver, and interference link between the secondary transmitter and the primary receiver. Throughput numerical results, it was shown that maximum achievable energy efficiency increases with increasing detection probability and decreases with increasing false alarm probability. Imperfect CSI of the transmission and interference links significantly degrades the performance of secondary users in terms of energy efficiency. Therefore, accurate estimation of the transmission and interference links is of great importance in order to obtain higher energy efficiency. Moreover, under the same average interference constraint, secondary users' transmission subject to peak transmit constraint achieves smaller achievable energy efficiency than that under average transmit power constraint.

In Chapter 5, we obtained the optimal power control policies that maximize the energy efficiency or maximize the average throughput of the secondary users while satisfying a minimum required energy efficiency level, operating with unslotted primary users subject to peak/average transmit power, average interference power and collision constraints in the

presence of sensing errors. We provided low-complexity algorithms to jointly optimize the transmission power and frame duration. Numerical results reveal important relations and tradeoffs between the energy efficiency and throughput performance of the secondary users. We have addressed how secondary user's energy efficiency, collisions with the primary user transmissions, and the optimal frame duration vary as a function of the probabilities of detection and false alarm. It was also shown that optimal power control policy significantly enhances the system performance compared to constant power scheme. The impact of the primary traffic on the system performance was analyzed. In particular, we observed that secondary users achieve smaller throughput when the primary user has a heavy traffic load.

In Chapter 6, we studied the error rate performance of cognitive radio transmissions in both sensing based spectrum sharing and opportunistic access schemes in the presence of transmit and interference power constraints, sensing uncertainty, and Gaussian mixture distributed interference from primary user transmissions. In this setting, we proved that the midpoints between the signals are optimal thresholds for the detection of equiprobable rectangular QAM signals. We have first obtained exact symbol error probability expressions for given fading realizations and then derived closed-form average symbol error probability expressions for the Rayleigh fading channel. We provided upper bounds on the error probabilities averaged over the fading between the secondary transmitter and primary receiver under the peak interference constraint. In the numerical results, we have had several interesting observations. We have seen that, when compared to sensing based spectrum sharing, lower error rates are generally attained in the opportunistic spectrum access scheme. Also, better error performance is achieved in the presence of Gaussian-mixture distributed primary user signal in comparison to that achieved when it is Gaussian distributed with the same variance. We demonstrated that symbol error probabilities are in general dependent on sensing performance through the detection and false alarm probabilities. For instance, we have observed that as the detection probability increases, the error rate performance under both schemes improves in interference-limited environments. Similarly, symbol error

probability is shown to decrease with decreasing false-alarm probability. Hence, we conclude that sensing performance is tightly linked to error performance and improved sensing leads to lower error rates.

In Chapter 7, we analyzed the throughput of cognitive radio systems in the finite block-length regime under buffer constraints. We first focused on the scenario in which the CSI of the secondary link is assumed to be perfectly known at the secondary receiver only. In this case, the secondary transmitter sends the data at two different constant rate levels, which depend on the channel sensing decision, and error rates vary with the channel conditions. In the second scenario, perfect CSI is available at both the secondary transmitter and receiver. Under this assumption, the secondary transmitter, considering a target error rate level, varies its transmission rate according to the time-varying channel conditions. For both scenarios, we determined the throughput as a function of state transition probabilities of the cognitive radio channel, prior probabilities of idle/busy state of primary users, sensing decisions and reliability, the block error probability, QoS exponent, frame and sensing durations. Through the numerical results, we observed that highly inaccurate sensing can either lead to inefficient use of resources and low throughput or cause possibly high interference on the primary users. We also noted that sensing-throughput tradeoff is more involved since increasing the sensing duration for improved sensing performance not only decreases the time allocated to data transmission but also results in shorter codewords being sent, lowering the transmission reliability. Additionally, we observed in the case of variable transmission-rate that average error probability can deviate significantly from the target error rate due to imperfect sensing. Moreover, we remarked that throughput generally decreases as the QoS exponent θ increases (i.e., as QoS constraints become more stringent), and variable-rate transmissions have better performance under more strict QoS restrictions while fixed-rate transmissions lead to higher throughput under looser QoS constraints.

In Chapter 8, we derived the optimal power control policies, maximizing the energy efficiency of wireless transmissions with arbitrary input signaling under QoS constraints when

the data arrival is constant or random modeled by Markovian processes, or more specifically by discrete-time Markov and Markov fluid processes, and discrete-time and continuous-time MMP processes. Also, we determined the optimal power adaptation scheme that maximizes the average arrival rate (or equivalently throughput) under a minimum energy efficiency constraint in this setting. We analyzed two limiting cases of the optimal power control for constant sources. In particular, when QoS constraints are looser, the optimal power allocation strategy converges to mercury/water-filling for finite discrete inputs and water-filling for Gaussian input, respectively. When QoS constraints are extremely stringent, the power control becomes the total channel inversion and no longer depends on the input distribution. We determined the optimal power control policy in the low-power regime and analyzed the performance with arbitrary signal constellations at low spectral efficiencies by characterizing the minimum energy per bit and wideband slope for general fading distributions and constant arrivals. We showed that while the minimum energy per bit does not get affected by the input distribution, the wideband slope depends on both the QoS exponent, the input distribution and the fading parameter. Through numerical results, we observed that there is a significant performance gap in terms of energy efficiency and throughput attained with Gaussian, 16-QAM, QPSK and BPSK signaling when QoS constraints are relatively loose. On the other hand, Gaussian input and QPSK achieve nearly the same energy efficiency and throughput under strict QoS constraints. Moreover, energy efficiency decreases with increasing source burstiness, especially under strict QoS constraints in the case of random arrivals.

9.2 Future Research Directions

9.2.1 Resource Allocation in Cognitive Radio Systems with Unslotted Primary Users under QoS Constaints

In Chapter 5, we studied throughput-efficient power control schemes for cognitive users in the presence of unslotted primary users. We assumed the data traffic of the secondary users as delay insensitive, and hence considered ergodic capacity as the performance metric. It is of interest to determine the corresponding power allocation scheme, optimal frame duration for delay-sensitive data traffic and to analyze the interactions among the primary user activity patterns, sensing performance and the resulting collisions with the primary user.

9.2.2 Cognitive Radio for 5G Networks

Cognitive radio technology has high degree of potential to improve the performance and address the key tradeoffs among interference management, resource allocation, spectral efficiency, and energy efficiency. Therefore, adaptive and intelligent transmission strategies using cognitive radio techniques can be developed to enhance the overall efficiency of Machine-to-Machine (M2M) and Device-to-Device (D2D) communication systems and heterogeneous networks (HetNets) by allowing opportunistic and shared spectrum access.

Appendix A

Proof of Theorem 3.2.1

The objective function in (3.5) is strictly concave since it follows from the relation in (2.9) that the first derivative of the mutual information is MMSE, which is a strictly decreasing function [52] . Also, the optimization problem is subject to affine inequality constraints given in (3.10) and (3.11). Hence, the optimal power can be obtained by using the Lagrangian optimization approach as follows:

$$L(P(z_s, z_{sp}), \lambda) = \mathbb{E}\{\mathcal{I}(P(z_s, z_{sp})z_s)\} + \lambda(Q_{\text{avg}} - \mathbb{E}\{P(z_s, z_{sp})z_{sp}\}) \tag{A.1}$$

$$= \mathbb{E}\{\mathcal{I}(P(z_s, z_{sp})z_s) - \lambda P(z_s, z_{sp})z_{sp}\} + \lambda Q_{\text{avg}}. \tag{A.2}$$

Above, λ denotes the nonnegative Lagrange multiplier. The Lagrange dual problem is defined as

$$\min_{\lambda \geq 0} \max_{0 \leq P(z_s, z_{sp}) \leq P_{\text{pk}}} L(P(z_s, z_{sp}), \lambda). \tag{A.3}$$

For a fixed λ and each fading state, the subproblem is expressed, by applying the Lagrange dual decomposition method [105], as

$$\max_{0 \leq P(z_s, z_{sp}) \leq P_{\text{pk}}} \mathcal{I}(P(z_s, z_{sp})z_s) - \lambda P(z_s, z_{sp})z_{sp}. \tag{A.4}$$

According to the Karush-Kuhn-Tucker (KKT) conditions, the optimal power control $P^*(z_s, z_{sp})$ must satisfy the following:

$$g(P(z_s, z_{sp})) = \text{MMSE}(P(z_s, z_{sp})z_s)z_s \log_2 \text{e} - \lambda z_{sp} = 0, \tag{A.5}$$

$$\lambda(\mathbb{E}\{P(z_s, z_{sp})z_{sp}\} - Q_{\text{avg}}) = 0, \tag{A.6}$$

$$\lambda \geq 0, \tag{A.7}$$

$$\mathbb{E}\{P(z_s, z_{sp})z_{sp}\} - Q_{\text{avg}} \leq 0. \tag{A.8}$$

In (A.5), we have used the relation between the mutual information and MMSE given in (2.9). It is observed from the constraint in (3.10), and the conditions in (A.6), (A.7), (A.8) that if $\mathbb{E}\{z_{sp}\} \leq \frac{Q_{\text{avg}}}{P_{\text{pk}}}$, then the average interference power constraint in (3.11) is loose. Therefore, $\lambda = 0$ and $P^*(z_{sp}, z_s) = P_{\text{pk}}$. If $\mathbb{E}\{z_{sp}\} > \frac{Q_{\text{avg}}}{P_{\text{pk}}}$, then $\lambda > 0$. Hence, by solving (A.5), the optimal transmit power can be obtained as

$$P^*(z_{sp}, z_s) = \frac{1}{z_s}\text{MMSE}^{-1}\Big(\frac{\lambda z_{sp}}{\log_2 \text{e}\ z_s}\Big). \tag{A.9}$$

Incorporating the nonnegativity of the transmit power, noting that $\text{MMSE}^{-1}(1) = 0$, and combining (A.9) with (3.10) yield the desired result in (3.12). □

Appendix B

Proof of Theorem 3.2.2

It is easy to show that the optimization problem is a concave maximization problem. Hence, following the same approach adopted in the proof of Theorem 1, the original problem reduces to solving a series of subproblems one for each fading state as follows:

$$\max_{0 \leq P(z_s, z_{sp}) \leq \frac{Q_{\text{pk}}}{z_{sp}}} \mathcal{I}(P(z_s, z_{sp}) z_s) - \mu P(z_s, z_{sp}). \tag{B.1}$$

Applying the KKT conditions leads to the following set of equations and inequalities:

$$h(P(z_s, z_{sp})) = \text{MMSE}(P(z_s, z_{sp}) z_s \log_2 \text{e} - \mu = 0, \tag{B.2}$$

$$\mu(\mathbb{E}\{P(z_s, z_{sp})\} - P_{\text{avg}}) = 0, \tag{B.3}$$

$$\mu \geq 0, \tag{B.4}$$

$$\mathbb{E}\{P(z_s, z_{sp})\} - P_{\text{avg}} \leq 0 \tag{B.5}$$

It is observed from the constraint in (3.16), and the conditions in (B.3), (B.4), and (B.5) that if $\mathbb{E}\{\frac{Q_{\text{pk}}}{z_{sp}}\} \leq P_{\text{pk}}$, then the average power constraint in (3.15) is loose. Therefore, $\mu = 0$ and $P^*(z_{sp}, z_s) = \frac{Q_{\text{pk}}}{z_{sp}}$. If $\mathbb{E}\{\frac{Q_{\text{pk}}}{z_{sp}}\} > P_{\text{pk}}$, then $\mu > 0$. Hence, the optimal transmit power can

be obtained as follows by solving (B.2):

$$P^*(z_{sp}, z_s) = \frac{1}{z_s}\mathrm{MMSE}^{-1}\Big(\frac{\mu}{\log_2 \mathrm{e}\ z_s}\Big). \tag{B.6}$$

Hence, we can obtain the closed-form optimal power policy in (3.17) by combining (B.6), (3.16) and the nonnegativity of the transmit power. □

Appendix C

Proof of Theorem 3.2.3

The Lagrangian is expressed as

$$L(P(z_s, z_{sp}), \lambda, \mu) = \mathbb{E}\{\mathcal{I}(P(z_s, z_{sp})z_s)\} - \mu(\mathbb{E}\{P(z_s, z_{sp})\} - P_{\text{avg}}) - \lambda(\mathbb{E}\{P(z_s, z_{sp})z_{sp}\} - Q_{\text{avg}}). \tag{C.1}$$

Applying the KKT conditions results in the following equation, we have

$$\eta(P(z_s, z_{sp})) = \text{MMSE}(P(z_s, z_{sp})z_s)z_s \log_2 \text{e} - \mu - \lambda z_{sp} = 0. \tag{C.2}$$

Solving the above equation gives the desired result in (3.21).

Appendix D

Proof of Theorem 3.3.1

In the low power regime, MMSE behaves as [52]

$$\mathrm{MMSE}(\rho) = \dot{\mathcal{I}}(0) + \ddot{\mathcal{I}}(0)\rho + o(\rho^2) \tag{D.1}$$

where $\dot{\mathcal{I}}(0) = 1$ [52]. Incorporating the above second-order approximation into (A.5), we obtain

$$\big(1 + \ddot{\mathcal{I}}(0)P(z_s, z_{sp})z_s\big)z_s \log_2 \mathrm{e} - \lambda z_{sp} = 0. \tag{D.2}$$

Solving the above equation, and then combining the corresponding result with the peak transmit power constraint in (3.10) and the nonnegativity of the transmission power provides the optimal power policy in (3.32). □

Appendix E

Proof of Proposition 4.1.1

We first write the achievable rate of secondary users in terms of mutual information between the received and transmitted signals given the sensing decision in the following:

$$R_{GM} = \frac{T-\tau}{T} I(x; y|h, \hat{\mathcal{H}}) = \frac{T-\tau}{T} \Bigg[\Pr\{\hat{\mathcal{H}}_0\} I(x_0; y|h, \hat{\mathcal{H}}_0) + \Pr\{\hat{\mathcal{H}}_1\} I(x_1; y|h, \hat{\mathcal{H}}_1) \Bigg], \quad \text{(E.1)}$$

where $I(x_k; y|h, \hat{\mathcal{H}}_k)$ for $k \in \{0, 1\}$ can be further expressed as

$$I(x_k; y|h, \hat{\mathcal{H}}_k) = \mathbb{E}_{x_k, y, g, h} \Bigg\{ \log \left(\frac{f(y|x_k, h, \hat{\mathcal{H}}_k)}{f(y|h, \hat{\mathcal{H}}_k)} \right) \Bigg\}. \quad \text{(E.2)}$$

The above conditional distribution, $f(y|x_k, h, \hat{\mathcal{H}}_k)$, is determined through the input-output relation in (4.1) as follows:

$$f(y|x_k, h, \hat{\mathcal{H}}_k) = \frac{\Pr\{\mathcal{H}_0|\hat{\mathcal{H}}_k\}}{\pi N_0} \mathrm{e}^{-\frac{|y-hx_k|^2}{N_0}} + \frac{\Pr\{\mathcal{H}_1|\hat{\mathcal{H}}_k\}}{\pi(N_0+\sigma_s^2)} \mathrm{e}^{-\frac{|y-hx_k|^2}{N_0+\sigma_s^2}} \quad \text{(E.3)}$$

with variance

$$\mathbb{E}\{|y|^2|x_k, h, \hat{\mathcal{H}}_k\} = N_0 + \Pr\{\mathcal{H}_1|\hat{\mathcal{H}}_k\}\sigma_s^2. \quad \text{(E.4)}$$

Also, the conditional distribution, $f(y|h,\hat{\mathcal{H}}_k)$ in (E.2) is given by

$$f(y|h,\hat{\mathcal{H}}_k) = \frac{\Pr\{\mathcal{H}_0|\hat{\mathcal{H}}_k\}}{\pi(N_0+P_k(g,h)|h|^2)}\mathrm{e}^{-\frac{|y|^2}{N_0+P_k(g,h)|h|^2}} + \quad \frac{\Pr\{\mathcal{H}_1|\hat{\mathcal{H}}_k\}}{\pi(N_0+P_k(g,h)|h|^2+\sigma_s^2)}\mathrm{e}^{-\frac{|y|^2}{N_0+P_k(g,h)|h|^2+\sigma_s^2}} \tag{E.5}$$

with variance

$$\mathbb{E}\{|y|^2|h,\hat{\mathcal{H}}_k\} = N_0 + P_k(g,h)|h|^2 + \Pr\{\mathcal{H}_1|\hat{\mathcal{H}}_k\}\sigma_s^2. \tag{E.6}$$

Above, it is seen that the conditional distributions of the received signal y given sensing decisions become a mixture of Gaussian distributions due to channel sensing errors. Therefore, there is no closed form expression for mutual information in (E.2). However, we can still find a closed-form lower bound for the achievable rate expression by following the steps in [106, pp. 938-939] and replacing the additive disturbance w in (4.2) with the worst-case Gaussian noise with the same variance as follows:

$$I(x_k;y|h,\hat{\mathcal{H}}_k) \geq \mathbb{E}_{g,h}\left\{\log\left(1+\frac{P_k(g,h)|h|^2}{E\{|w|^2|\hat{\mathcal{H}}_k\}}\right)\right\} \tag{E.7}$$

where

$$E\{|w|^2|\hat{\mathcal{H}}_k\} = N_0 + \Pr\{\mathcal{H}_1|\hat{\mathcal{H}}_k\}\sigma_s^2. \tag{E.8}$$

Inserting these lower bounds into (E.1), we have obtained the achievable rate expression in (4.3). □

Appendix F

Proof of Theorem 4.1.1

We first express $I_0(x_0; y|h, \hat{\mathcal{H}}_0)$ as follows:

$$I_0(x_0; y|h, \hat{\mathcal{H}}_0) = \Big(\frac{T-\tau}{T}\Big)\Bigg[\int_h \Big(\int_{-\infty}^{\infty} \sum_{i=1}^{2} \frac{\Pr(\mathcal{H}_i|\hat{\mathcal{H}}_0)}{\pi c_i} \mathrm{e}^{-\frac{|y-x_0h|^2}{c_i}} \log\Big(\sum_{i=1}^{2} \frac{\Pr(\mathcal{H}_i|\hat{\mathcal{H}}_0)}{\pi c_i} \mathrm{e}^{-\frac{|y-x_0h|^2}{c_i}}\Big) dy\Big) f_h(h) dh$$
$$- \int_g \Big(\int_h \Big(\int_{-\infty}^{\infty} \sum_{i=1}^{2} \frac{\Pr(\mathcal{H}_i|\hat{\mathcal{H}}_0)}{\pi(c_i + |h|^2 P_0(g,h))} \mathrm{e}^{-\frac{|y|^2}{c_i+|h|^2P_0(g,h)}} \log\Big(\sum_{i=1}^{2} \frac{\Pr(\mathcal{H}_i|\hat{\mathcal{H}}_0)}{\pi(c_i + |h|^2 P_0(g,h))} \mathrm{e}^{-\frac{|y|^2}{c_i+|h|^2P_0(g,h)}}\Big) dy\Big)$$
$$\times f_h(h) dh\Big) f_g(g) dg\Bigg], \tag{F.1}$$

where $c_1 = N_0 + \sigma_s^2$ and $c_2 = N_0$. Then, we obtain the upper bound below by using the inequalities in (F.3) and (F.4) as follows:

$$I_0(x_0; y|h, \hat{\mathcal{H}}_0) \leq \Big(\frac{T-\tau}{T}\Big)\Bigg[\int_h \Big(\int_{-\infty}^{\infty} \sum_{i=1}^{2} \frac{\Pr(\mathcal{H}_i|\hat{\mathcal{H}}_0)}{\pi c_i} \mathrm{e}^{-\frac{|y-x_0h|^2}{c_i}} \log\Big(\sum_{i=1}^{2} \frac{\Pr(\mathcal{H}_i|\hat{\mathcal{H}}_0)}{\pi c_i} \mathrm{e}^{-\frac{|y-x_0h|^2}{c_1}}\Big) dy\Big) f_h(h) dh$$
$$- \int_g \Big(\int_h \Big(\int_{-\infty}^{\infty} \sum_{i=1}^{2} \frac{\Pr(\mathcal{H}_i|\hat{\mathcal{H}}_0)}{\pi(c_i + |h|^2 P_0(g,h))} \mathrm{e}^{-\frac{|y|^2}{c_i+|h|^2P_0(g,h)}} \log\Big(\sum_{i=1}^{2} \frac{\Pr(\mathcal{H}_i|\hat{\mathcal{H}}_0)}{\pi(c_i + |h|^2 P_0(g,h))} \mathrm{e}^{-\frac{|y|^2}{c_2+|h|^2P_0(g,h)}}\Big) dy\Big)$$
$$\times f_h(h) dh\Big) f_g(g) dg\Bigg] \tag{F.2}$$

$$\mathrm{e}^{-\frac{|y|^2}{c_1+|h|^2P_0(g,h)}} \geq \mathrm{e}^{-\frac{|y|^2}{c_i+|h|^2P_0(g,h)}} \geq \mathrm{e}^{-\frac{|y|^2}{c_2+|h|^2P_0(g,h)}} \tag{F.3}$$

$$\mathrm{e}^{-\frac{|y-hx_0|^2}{c_1}} \geq \mathrm{e}^{-\frac{|y-hx_0|^2}{c_i}} \geq \mathrm{e}^{-\frac{|y-hx_0|^2}{c_2}} \tag{F.4}$$

Evaluating the integrals in (F.2) yields the following upper bound:

$$I_0(x_0;y|h,\hat{\mathcal{H}}_0) \leq \left(\frac{T-\tau}{T}\right)\left[\mathbb{E}_{g,h}\left\{\sum_{k=1}^{2}\log\left(\frac{\sum_{i=1}^{2}\frac{\Pr(\mathcal{H}_i|\hat{\mathcal{H}}_0)}{c_i}}{\sum_{i=1}^{2}\frac{\Pr(\mathcal{H}_i|\hat{\mathcal{H}}_0)}{c_i+|h|^2P_0(g,h)}}\right)\right\} - \left(\frac{N_0+\Pr(H_1|\hat{\mathcal{H}}_0)\sigma_s^2}{N_0+\sigma_s^2}\right) + \mathbb{E}_{g,h}\left\{1+\frac{\Pr(H_1|\hat{\mathcal{H}}_0)\sigma_s^2}{N_0+|h|^2P_0(g,h)}\right\}\right] \tag{F.5}$$

Following the similar steps, we obtain the upper bound for $I_1(x_1;y|h,\hat{\mathcal{H}}_1)$ as follows:

$$I_1(x_1;y|h,\hat{\mathcal{H}}_1) \leq \left(\frac{T-\tau}{T}\right)\left[\mathbb{E}_{g,h}\left\{\sum_{k=1}^{2}\log\left(\frac{\sum_{i=1}^{2}\frac{\Pr(\mathcal{H}_i|\hat{\mathcal{H}}_1)}{c_i}}{\sum_{i=1}^{2}\frac{\Pr(\mathcal{H}_i|\hat{\mathcal{H}}_1)}{c_i+|h|^2P_1(g,h)}}\right)\right\} - \left(\frac{N_0+\Pr(H_1|\hat{\mathcal{H}}_1)\sigma_s^2}{N_0+\sigma_s^2}\right) + \mathbb{E}_{g,h}\left\{1+\frac{\Pr(H_1|\hat{\mathcal{H}}_1)\sigma_s^2}{N_0+|h|^2P_1(g,h)}\right\}\right] \tag{F.6}$$

Inserting the inequalities in (F.5) and (F.6) into (E.1) and subtracting from R_a in (4.3) gives the desired result in (4.6). □

Appendix G

Proof of Theorem 4.2.1

The optimization problem is quasiconcave since achievable rate R_a is concave in transmission powers and total power consumption $P_{\text{tot}}(P_0, P_1)$ is both affine and positive, and hence the level sets $S_\alpha = \{(P_0, P_1) : \eta_{\text{EE}} \geq \alpha\} = \{\alpha P_{\text{tot}}(P_0, P_1) - R_a \leq 0\}$ are convex for any $\alpha \in \mathbb{R}$. Since quasiconcave functions have more than one local maximum, local maximum does not always guarantee the global maximum. Therefore, standard convex optimization algorithms cannot be directly used. Hence, iterative power allocation algorithm based on Dinkelbach's method [107] is employed to solve the quasiconcave EE maximization problem by formulating the equivalent parameterized concave problem as follows:

$$\max_{\substack{P_0(g,h)\\P_1(g,h)}} \Big\{ \mathbb{E}_{g,h}\big\{ R\big(P_0(g,h), P_1(g,h)\big)\big\} - \alpha(\mathbb{E}_{g,h}\{\Pr\{\hat{\mathcal{H}}_0\}P_0(g,h) + \Pr\{\hat{\mathcal{H}}_1\}P_1(g,h)\} + P_{\text{c}}) \Big\} \tag{G.1}$$

$$\text{subject to} \quad \mathbb{E}_{g,h}\{\Pr\{\hat{\mathcal{H}}_0\}\, P_0(g,h) + \Pr\{\hat{\mathcal{H}}_1\}\, P_1(g,h)\} \leq P_{\text{avg}} \tag{G.2}$$

$$\mathbb{E}_{g,h}\{\big[(1 - \mathscr{P}_{\text{d}})\, P_0(g,h) + \mathscr{P}_{\text{d}}\, P_1(g,h)\big]|g|^2\} \leq Q_{\text{avg}} \tag{G.3}$$

$$P_0(g,h) \geq 0, P_1(g,h) \geq 0, \tag{G.4}$$

where α is a nonnegative parameter. At the optimal value of α^*, solving the EE maximization problem in (4.8) is equivalent to solving the above parametrized concave problem if and only if the following condition is satisfied

$$F(\alpha^*) = \mathbb{E}_{g,h}\big\{R\big(P_0(g,h), P_1(g,h)\big)\big\} - \alpha^*\Big(\mathbb{E}_{g,h}\{\Pr\{\hat{\mathcal{H}}_0\}P_0(g,h) + \Pr\{\hat{\mathcal{H}}_1\}P_1(g,h)\} + P_{\rm c}\Big) = 0. \tag{G.5}$$

The detailed proof of the above condition is available in [107]. Since the problem in (G.1) is concave, the optimal power values are obtained by forming the Lagrangian as follows:

$$\begin{aligned} L(P_0, P_1, \lambda_1, \nu_1, \alpha) &= \mathbb{E}_{g,h}\big\{R\big(P_0(g,h), P_1(g,h)\big)\big\} - \alpha(\mathbb{E}_{g,h}\{\Pr\{\hat{\mathcal{H}}_0\}P_0(g,h) + \Pr\{\hat{\mathcal{H}}_1\}P_1(g,h)\} + P_{\rm c}) \\ &- \lambda_1(\mathbb{E}_{g,h}\{\Pr\{\hat{\mathcal{H}}_0\}\, P_0(g,h) + \Pr\{\hat{\mathcal{H}}_1\}\, P_1(g,h)\} - P_{\rm avg}) - \nu_1(\mathbb{E}_{g,h}\{\big[(1-\mathscr{P}_{\rm d})\, P_0(g,h) + \mathscr{P}_{\rm d}\, P_1(g,h)\big]|g|^2\} \\ &- Q_{\rm avg}), \end{aligned} \tag{G.6}$$

where λ_1 and ν_1 are nonnegative Lagrange multipliers. According to the Karush-Kuhn-Tucker (KKT) conditions, the optimal values of $P_0^*(g,h)$ and $P_1^*(g,h)$ satisfy the following equations:

$$\frac{\frac{T-\tau}{T}\Pr\{\hat{\mathcal{H}}_0\}|h|^2\log_2 e}{N_0 + \Pr(\mathcal{H}_1|\hat{\mathcal{H}}_0)\sigma_s^2 + P_0^*(g,h)|h|^2} - (\lambda_1+\alpha)\Pr\{\hat{\mathcal{H}}_0\} - \nu_1|g|^2(1-\mathscr{P}_{\rm d}) = 0 \tag{G.7}$$

$$\frac{\frac{T-\tau}{T}\Pr\{\hat{\mathcal{H}}_1\}|h|^2\log_2 e}{N_0 + \Pr(\mathcal{H}_1|\hat{\mathcal{H}}_1)\sigma_s^2 + P_1^*(g,h)|h|^2} - (\lambda_1+\alpha)\Pr\{\hat{\mathcal{H}}_1\} - \nu_1|g|^2\mathscr{P}_{\rm d} = 0 \tag{G.8}$$

$$\lambda_1(\mathbb{E}\{\Pr\{\hat{\mathcal{H}}_0\}\, P_0^*(g,h) + \Pr\{\hat{\mathcal{H}}_1\}\, P_1^*(g,h)\} - P_{\rm avg}) = 0 \tag{G.9}$$

$$\nu_1(\mathbb{E}\{[(1-\mathscr{P}_{\rm d})\, P_0^*(g,h) + \mathscr{P}_{\rm d}\, P_1^*(g,h)]|g|^2\} - Q_{\rm avg}) = 0 \tag{G.10}$$

$$\lambda_1 \geq 0, \nu_1 \geq 0. \tag{G.11}$$

Solving equations (G.7) and (G.8), yield the optimal power values in (4.12) and (4.13), respectively. □

Appendix H

Proof of Proposition 5.1.1

The first derivative of $\mathscr{P}_c$ with respect to frame duration T_f is

$$\begin{aligned}\frac{\partial \mathscr{P}_c}{\partial T_\mathrm{f}} = &\Big(\Pr\{\mathcal{H}_0|\hat{\mathcal{H}}_0\}\lambda_0 \Pr\{\mathcal{H}_1\}^2 - \Pr\{\mathcal{H}_1|\hat{\mathcal{H}}_0\}\lambda_1 \Pr\{\mathcal{H}_0\}^2\Big) \\ &\times \left(\frac{1-\mathrm{e}^{-\frac{T_\mathrm{f}-\tau}{\lambda_0 \Pr\{\mathcal{H}_1\}}}}{(T_\mathrm{f}-\tau)^2} - \frac{1}{\lambda_0 \Pr\{\mathcal{H}_1\}(T_\mathrm{f}-\tau)}\mathrm{e}^{-\frac{T_\mathrm{f}-\tau}{\lambda_0 \Pr\{\mathcal{H}_1\}}}\right).\end{aligned} \tag{H.1}$$

The expression inside the first parenthesis can easily be seen to be greater than zero if $P_\mathrm{f} < P_\mathrm{d}$ and less than zero if $P_\mathrm{f} > P_\mathrm{d}$ by using the formulations in (7.1), (5.9) and (5.10). In order to show that the expression inside the second parenthesis is always nonnegative, we compare it with zero as follows:

$$\frac{1-\mathrm{e}^{-\frac{T_\mathrm{f}-\tau}{\lambda_0 \Pr\{\mathcal{H}_1\}}}}{(T_\mathrm{f}-\tau)^2} - \frac{1}{\lambda_0 \Pr\{\mathcal{H}_1\}(T_\mathrm{f}-\tau)}\mathrm{e}^{-\frac{T_\mathrm{f}-\tau}{\lambda_0 \Pr\{\mathcal{H}_1\}}} > 0. \tag{H.2}$$

Above inequality can be rewritten as

$$\left(1+\frac{T_\mathrm{f}-\tau}{\lambda_0 \Pr\{\mathcal{H}_1\}}\right)\mathrm{e}^{-\frac{T_\mathrm{f}-\tau}{\lambda_0 \Pr\{\mathcal{H}_1\}}} < 1. \tag{H.3}$$

Left-hand side of (H.3) is a decreasing function since its first derivative with respect to frame duration T_f is $-\frac{T_\mathrm{f}-\tau}{(\lambda_0 \Pr\{\mathcal{H}_1\})^2}\mathrm{e}^{-\frac{T_\mathrm{f}-\tau}{\lambda_0 \Pr\{\mathcal{H}_1\}}} \leq 0$. Since it is a decreasing function and it takes

values between $(0,1)$ for $T_{\mathrm{f}} > \tau$, the inequality in (H.3) and hence the inequality in (H.2) hold. With this, we have shown that the expression inside the second parenthesis in (H.1) is nonnegative, and therefore the first derivative of $\mathscr{P}_c$ is greater than zero if $P_{\mathrm{f}} < P_{\mathrm{d}}$ and less than zero if $P_{\mathrm{f}} > P_{\mathrm{d}}$, proving the property that $\mathscr{P}_c$ is increasing with T_{f} if $P_{\mathrm{f}} < P_{\mathrm{d}}$ and decreasing with T_{f} if $P_{\mathrm{f}} > P_{\mathrm{d}}$.

Also, it can be easily verified that $\mathscr{P}_c$ takes values between $\Pr\{\mathcal{H}_1|\hat{\mathcal{H}}_0\}$ and $\Pr\{\mathcal{H}_1\}$. In particular, we examine the limit of $\mathscr{P}_c$ as T_{f} approaches τ and ∞ as follows:

$$\begin{aligned}\lim_{T_{\mathrm{f}}\to\tau} \mathscr{P}_c &= \Pr\{\mathcal{H}_0|\hat{\mathcal{H}}_0\}\left(\Pr\{\mathcal{H}_1\} - \frac{\lambda_0 \Pr\{\mathcal{H}_1\}^2}{\lambda_0 \Pr\{\mathcal{H}_1\}}\right) + \Pr\{\mathcal{H}_1|\hat{\mathcal{H}}_0\}\left(\Pr\{\mathcal{H}_1\} + \frac{\lambda_1 \Pr\{\mathcal{H}_0\}^2}{\lambda_0 \Pr\{\mathcal{H}_1\}}\right) \\ &= \Pr\{\mathcal{H}_1|\hat{\mathcal{H}}_0\} \qquad \text{(H.4)}\end{aligned}$$

$$\lim_{T_{\mathrm{f}}\to\infty} \mathscr{P}_c = \Pr\{\mathcal{H}_0|\hat{\mathcal{H}}_0\}\Pr\{\mathcal{H}_1\} + \Pr\{\mathcal{H}_1|\hat{\mathcal{H}}_0\}\Pr\{\mathcal{H}_1\} = \Pr\{\mathcal{H}_1\}. \qquad \text{(H.5)}$$

□

Appendix I

Proof of Theorem 5.2.1

The objective function in (5.11) is quasiconcave since the average throughput in the numerator is composed of positive weighted sum of logarithms which are strictly concave and the power consumption in the denominator is both affine and positive. Therefore, the optimal power value can be found iterativaly by using Dinkelbach's method [107]. The optimization problem is first transformed into the equivalent parameterized concave problem as follows:

$$\max_{P(g,h)\geq 0} \left\{ R_{\text{avg}} - \alpha \left(\left(\frac{T_{\text{f}} - \tau}{T_{\text{f}}} \right) \Pr\{\hat{\mathcal{H}}_0\} \mathbb{E}\{P(g,h)\} + P_{c_r} \right) \right\} \tag{I.1}$$

$$\text{subject to } \left(\frac{T_{\text{f}} - \tau}{T_{\text{f}}} \right) \Pr\{\hat{\mathcal{H}}_0\} \mathbb{E}\big\{P(g,h)\big\} \leq P_{\text{avg}} \tag{I.2}$$

$$\left(\frac{T_{\text{f}} - \tau}{T_{\text{f}}} \right) \mathscr{P}_c \Pr\{\hat{\mathcal{H}}_0\} \mathbb{E}\big\{P(g,h)|g|^2\big\} \leq Q_{\text{avg}}, \tag{I.3}$$

where α is a nonnegative parameter. At the optimal value of α^*, the following condition is satisfied

$$F(\alpha^*) = R_{\text{avg}} - \alpha^* \left(\left(\frac{T_{\text{f}} - \tau}{T_{\text{f}}} \right) \Pr\{\hat{\mathcal{H}}_0\} \mathbb{E}\{P(g,h)\} + P_{c_r} \right) = 0. \tag{I.4}$$

Explicitly, the solution of $F(\alpha^*)$ is equivalent to the solution of the EE maximization problem in (5.11). It is shown that Dinkelbach's method converges to the optimal solution at a

superlinear convergence rate. The detailed proof of convergence and further details can be found in [69]. Since the parameterized problem in (I.1) is concave for a given α, the optimal power levels can be obtained by using the Lagrangian optimization approach as follows:

$$\mathcal{L}(P(g,h),\lambda,\nu,\alpha) = R_{\text{avg}} - \alpha\Big(\Big(\frac{T_{\text{f}}-\tau}{T_{\text{f}}}\Big)\Pr\{\hat{\mathcal{H}}_0\}\mathbb{E}\{P(g,h)\}+P_{c_r}\Big) - \lambda\Big(\Big(\frac{T_{\text{f}}-\tau}{T_{\text{f}}}\Big)\Pr\{\mathcal{H}_0\}\mathbb{E}\{P(g,h)\} - P_{\text{avg}}\Big) - \nu\Big(\Big(\frac{T_{\text{f}}-\tau}{T_{\text{f}}}\Big)\mathscr{P}_c\Pr\{\hat{\mathcal{H}}_0\}\mathbb{E}\big\{P(g,h)|g|^2\big\} - Q_{\text{avg}}\Big), \tag{I.5}$$

where λ and ν are the nonnegative Lagrange multipliers. The Lagrange dual problem is defined as

$$\min_{\lambda,\nu\geq 0}\max_{P(g,h)\geq 0}\mathcal{L}(P(g,h),\lambda,\nu,\alpha). \tag{I.6}$$

For fixed λ and ν values, and each fading state, we express the subproblem using the Lagrange dual decomposition method [105]. According to the Karush-Kuhn-Tucker (KKT) conditions, the optimal power control $P_{\text{opt}}(g,h)$ must satisfy the set of equations and inequalities below:

$$\frac{\Pr\{\hat{\mathcal{H}}_0\}}{\log_e(2)}\Big(\frac{T_{\text{f}}-\tau}{T_{\text{f}}}\Big)\left[\left(\frac{(1-\mathscr{P}_c)|h|^2}{N_0+P_{\text{opt}}(g,h)|h|^2}\right)+\left(\frac{\mathscr{P}_c|h|^2}{N_0+\sigma_s^2+P_{\text{opt}}(g,h)|h|^2}\right)\right] - (\alpha+\lambda)\Big(\frac{T_{\text{f}}-\tau}{T_{\text{f}}}\Big)\Pr\{\hat{\mathcal{H}}_0\} - \nu\Big(\frac{T_{\text{f}}-\tau}{T_{\text{f}}}\Big)\Pr\{\hat{\mathcal{H}}_0\}\mathscr{P}_c|g|^2 = 0 \tag{I.7}$$

$$\lambda\Big(\Big(\frac{T_{\text{f}}-\tau}{T_{\text{f}}}\Big)\Pr\{\hat{\mathcal{H}}_0\}\mathbb{E}\{P_{\text{opt}}(g,h)\} - P_{\text{avg}}\Big) = 0, \tag{I.8}$$

$$\nu\Big(\Big(\frac{T_{\text{f}}-\tau}{T_{\text{f}}}\Big)\mathscr{P}_c\Pr\{\hat{\mathcal{H}}_0\}\mathbb{E}\big\{P_{\text{opt}}(g,h)|g|^2\big\} - Q_{\text{avg}}\Big) = 0, \tag{I.9}$$

$$\lambda\geq 0,\nu\geq 0. \tag{I.10}$$

Solving (I.7) and incorporating the nonnegativity of the transmit power yield the desired result in (8.31). □

Appendix J

Proof of Proposition 5.3.1

In order to find the operating power level, which satisfies the minimum required EE, we consider that the objective function in (5.34) is subject to only a minimum EE constraint in (5.36). Since R_{avg} is a concave function of the transmission power and the feasible set defined by the minimum EE constraint is a convex set, KKT conditions are both sufficient and necessary for the optimal solution. The constraint in (5.36) can be rewritten as follows

$$R_{\text{avg}} - \text{EE}_{\min}\Big(\big(\frac{T_{\text{f}} - \tau}{T_{\text{f}}}\big) \Pr\{\hat{\mathcal{H}}_0\}\mathbb{E}\{P(g,h)\} + P_{c_r}\Big) \geq 0. \tag{J.1}$$

By defining η as the Lagrange multiplier associated with the above constraint, the Lagrangian function is expressed as

$$\mathcal{L}(P(g,h),\eta) = (1+\eta)R_{\text{avg}} - \eta\text{EE}_{\min}\Big(\big(\frac{T_{\text{f}} - \tau}{T_{\text{f}}}\big) \Pr\{\hat{\mathcal{H}}_0\}\mathbb{E}\{P(g,h)\} + P_{c_r}\Big). \tag{J.2}$$

By setting the derivative of the above function with respect to $P(g,h)$ equal to zero at the optimal power level, we obtain the equation below:

$$\left.\frac{\partial \mathcal{L}(P(g,h),\eta)}{\partial P(g,h)}\right|_{P(g,h)=P^*(g,h)} = (1+\eta)\frac{\Pr\{\hat{\mathcal{H}}_0\}}{\log_e(2)}\Big(\frac{T_\mathrm{f}-\tau}{T_\mathrm{f}}\Big)\Bigg[\Bigg(\frac{(1-\mathscr{P}_c)|h|^2}{N_0+P^*(g,h)|h|^2}\Bigg) + \Bigg(\frac{\mathscr{P}_c|h|^2}{N_0+\sigma_s^2+P^*(g,h)|h|^2}\Bigg)\Bigg] - \eta \mathrm{EE}_{\min}\Big(\frac{T_\mathrm{f}-\tau}{T_\mathrm{f}}\Big)\Pr\{\hat{\mathcal{H}}_0\} = 0. \tag{J.3}$$

Solving the above equation leads to the desired characterization in (5.40) and the Lagrange multiplier, η can be determined by satisfying the minimum EE constraint with equality or solving (5.43). Consequently, the average transmission power is obtained by inserting (5.40) into (8.50). □

Appendix K

Proof of Theorem 5.3.1

The Lagrangian function is expressed as

$$\begin{aligned}\mathcal{L}(P(g,h),\vartheta,\varphi) = R_{\text{avg}} - \vartheta\Big(\Big(\frac{T_{\text{f}}-\tau}{T_{\text{f}}}\Big)P(\hat{\mathcal{H}}_0)\mathbb{E}\{P(g,h)\} - \min(P_{\text{avg}}, P^*_{\text{avg}})\Big) \\ - \varphi\Big(\Big(\frac{T_{\text{f}}-\tau}{T_{\text{f}}}\Big)\mathscr{P}_c \Pr\{\hat{\mathcal{H}}_0\}\mathbb{E}\{P(g,h)|g|^2\} - Q_{\text{avg}})\Big).\end{aligned} \tag{K.1}$$

Setting the derivative of the above function with respect to transmission power, $P(g,h)$, to zero and arranging the terms give the desired optimal power control in (5.45). □

Appendix L

Proof of Proposition 6.3.1

Since the signals are *equiprobable*, the maximum likelihood (ML) decision rule is optimal in the sense that it minimizes the average probability of error [108]. Since cognitive transmission is allowed only when the channel is sensed as idle under OSA scheme, it is enough to evaluate the ML decision rule under sensing decision $\hat{\mathcal{H}}_0$, which can be expressed as

$$\hat{m} = \underset{0 \leq m \leq M-1}{\arg\max}\ f(\bar{y}|s_{n,q}, h, \hat{\mathcal{H}}_0). \tag{L.1}$$

The above decision rule can further be expressed as

$$\hat{m} = \underset{0 \leq m \leq M-1}{\arg\max} \Big(\Pr\{\mathcal{H}_0|\hat{\mathcal{H}}_0\} f(\bar{y}|s_{n,q}, h, \hat{\mathcal{H}}_0, \mathcal{H}_0) + \Pr\{\mathcal{H}_1|\hat{\mathcal{H}}_0\} f(\bar{y}|s_{n,q}, h, \hat{\mathcal{H}}_0, \mathcal{H}_1) \Big). \tag{L.2}$$

Above maximization simply becomes the comparison of the likelihood functions of the received signals given the transmitted signals $s_{n,q}$. Without loss of generality, we consider the signal constellation point $s_{n,q}$. Then, the decision region for the in-phase component of this signal constellation point is given by (L.3). The right-side boundary of the corresponding decision region, which can be found by equating the likelihood functions in (L.3)–(L.4) shown at the top of next page. Gathering the common terms together, the expression in (L.3) can further be written as in (L.5) given on the next page.

$$\sum_{j=0}^{1} \Pr\{\mathcal{H}_j|\hat{\mathcal{H}}_0\} f(\bar{y}|s_{n,q}, h, \hat{\mathcal{H}}_0, \mathcal{H}_j) \geq \sum_{j=0}^{1} \Pr\{\mathcal{H}_j|\hat{\mathcal{H}}_0\} f(\bar{y}|s_{n+1,q}, h, \hat{\mathcal{H}}_0, \mathcal{H}_j) \tag{L.3}$$

$$\sum_{j=0}^{1} \Pr\{\mathcal{H}_j|\hat{\mathcal{H}}_0\} f(\bar{y}|s_{n,q}, h, \hat{\mathcal{H}}_0, \mathcal{H}_j) \geq \sum_{j=0}^{1} \Pr\{\mathcal{H}_j|\hat{\mathcal{H}}_0\} f(\bar{y}|s_{n-1,q}, h, \hat{\mathcal{H}}_0, \mathcal{H}_j) \tag{L.4}$$

$$\frac{\Pr\{\mathcal{H}_0|\hat{\mathcal{H}}_0\}}{2\pi\sigma_n^2} \mathrm{e}^{-\frac{(\bar{y}_r - s_n|h|)^2 + (\bar{y}_i - s_q|h|)^2}{2\sigma_n^2}} \left(1 - \mathrm{e}^{\frac{2d_{min,0}|h|(\bar{y}_r - s_n|h|) - d_{min,0}^2|h|^2}{2\sigma_n^2}}\right)$$
$$+ \Pr\{\mathcal{H}_1|\hat{\mathcal{H}}_0\} \sum_{l=1}^{p} \frac{\lambda_l}{2\pi(\sigma_l^2 + \sigma_n^2)} \mathrm{e}^{-\frac{(\bar{y}_r - s_n|h|)^2 + (\bar{y}_i - s_q|h|)^2}{2(\sigma_l^2 + \sigma_n^2)}} \left(1 - \mathrm{e}^{\frac{2d_{min,0}|h|(\bar{y}_r - s_n|h|) - d_{min,0}^2|h|^2}{2(\sigma_l^2 + \sigma_n^2)}}\right) \geq 0. \tag{L.5}$$

We note that all the terms on the left-hand side of (L.5) other than the terms inside the parentheses are nonnegative. Let us now consider these difference terms. Inside the first set of parentheses, we have

$$1 - \mathrm{e}^{\left(\frac{2(\bar{y}_r - s_n|h|)d_{min,0}|h| - d_{min,0}^2|h|^2}{2\sigma_n^2}\right)} \tag{L.6}$$

which can easily be seen to be greater than zero if $\bar{y}_r - s_n|h| < \frac{d_{min,0}|h|}{2}$ and is zero if $\bar{y}_r - s_n|h| = \frac{d_{min,0}|h|}{2}$. The same is also true for the term inside the second set of parentheses given by

$$1 - \mathrm{e}^{\left(\frac{2(\bar{y}_r - s_n|h|)d_{min,0}|h| - d_{min,0}^2|h|^2}{2(\sigma_l^2 + \sigma_n^2)}\right)}. \tag{L.7}$$

Therefore, the inequality in (L.5) can be reduced to

$$\bar{y}_r - s_n|h| \leq \frac{d_{min,0}|h|}{2}. \tag{L.8}$$

$$\sum_{j=0}^{1} \Pr\{\mathcal{H}_j|\hat{\mathcal{H}}_0\} f(\bar{y}|s_{n,q}, h, \hat{\mathcal{H}}_0, \mathcal{H}_j) \geq \sum_{j=0}^{1} \Pr\{\mathcal{H}_j|\hat{\mathcal{H}}_0\} f(\bar{y}|s_{n,q+1}, h, \hat{\mathcal{H}}_0, \mathcal{H}_j) \tag{L.10}$$

$$\sum_{j=0}^{1} \Pr\{\mathcal{H}_j|\hat{\mathcal{H}}_0\} f(\bar{y}|s_{n,q}, h, \hat{\mathcal{H}}_0, \mathcal{H}_j) \geq \sum_{j=0}^{1} \Pr\{\mathcal{H}_j|\hat{\mathcal{H}}_0\} f(\bar{y}|s_{n,q-1}, h, \hat{\mathcal{H}}_0, \mathcal{H}_j). \tag{L.11}$$

Similarly, (L.4) simplifies to

$$\bar{y}_r - s_n|h| \geq -\frac{d_{min,0}|h|}{2}. \tag{L.9}$$

From these observations, we immediately conclude that the decision rule to detect s_n involves comparing $\bar{y}_r$ with thresholds located at midpoints between the received neighboring signals.

Following the same approach, we can determine the decision region for the quadrature component of the signal constellation point $s_{n,q}$ by comparing the likelihood functions in (L.10) – (L.11) shown on the next page, which similarly reduce to $\bar{y}_i - s_q|h| \leq \frac{d_{min,0}|h|}{2}$ and $\bar{y}_i - s_q|h| \geq -\frac{d_{min,0}|h|}{2}$, respectively. Hence, we again have the thresholds at midpoints between the neighboring received signals.

Under the SSS scheme, the secondary users are allowed to transmit in busy-sensed channel (i.e., under sensing decision $\hat{\mathcal{H}}_1$) as well. Since the simplified decision rules in (L.8) and (L.9) do not depend on the sensing decision $\hat{\mathcal{H}}_i$, the same set of inequalities are obtained for the ML detection rule under sensing decision $\hat{\mathcal{H}}_1$, leading to the same conclusion regarding the decision rule and thresholds. □

Appendix M

Proof of Theorem 8.1.1

The mutual information $\mathcal{I}(\rho)$ is a concave function since its second derivative is negative, i.e., $\ddot{\mathcal{I}}(\rho) = -\mathbb{E}\{(\mathbb{E}\{|s[i] - \hat{s}[i]|^2 \big| \hat{y}[i]\})^2 + |\mathbb{E}\{(s[i] - \hat{s}[i])^2 \big| \hat{y}[i]\}|^2\} < 0$ [99]. Subsequently, $-\theta T B \mathcal{I}(\rho)$ is a convex function for given values of θ, T, B, and $\mathrm{e}^{-\theta T B \mathcal{I}(\mu(\theta,z)z)}$ is a log-convex function, which takes non-negative values. Since expectation preserves log-convexity, $\mathbb{E}\big\{\mathrm{e}^{-\theta T B \mathcal{I}(\mu(\theta,z)z)}\big\}$ is also log-convex [92]. This implies that $\log(\mathbb{E}\big\{\mathrm{e}^{-\theta T B \mathcal{I}(\mu(\theta,z)z)}\big\})$ is a convex function of ρ. Since the negative of a convex function is concave, it follows that the objective function in (8.5) is concave. Since logarithm is a monotonic increasing function, the optimal power control policy can be found by solving the following minimization problem:

$$\min_{\mu(\theta,z)} \mathbb{E}\big\{\mathrm{e}^{-\theta T B \mathcal{I}(\mu(\theta,z)z)}\big\} \tag{M.1}$$

$$\text{subject to} \quad \mathbb{E}\{\mu(\theta,z)\} \leq \text{SNR}. \tag{M.2}$$

The mutual information $\mathcal{I}(\rho)$ is a concave function since its second derivative is negative, i.e., $\ddot{\mathcal{I}}(\rho) = -\mathbb{E}\{(\mathbb{E}\{|s[i] - \hat{s}[i]|^2 \big| y[i]\})^2 + |\mathbb{E}\{(s[i] - \hat{s}[i])^2 \big| y[i]\}|^2\} < 0$ [99] . Hence, the above objective function is strictly convex and the constraint in (M.2) is linear, which implies that the optimization problem is convex. Therefore, the optimal power control can be obtained by first writing the expectations in (M.1) and (M.2) as integrals and then forming the

Lagrangian as follows:

$$\mathcal{L}(\theta, z) = \int_0^\infty \mathrm{e}^{-\theta TB\mathcal{I}(\mu(\theta,z)z)} f(z)dz + \lambda\Big(\int_0^\infty \mu(\theta, z)f(z)dz - \mathrm{SNR}\Big). \tag{M.3}$$

Above, λ denotes the Lagrange multiplier. Setting the derivative of the Lagrangian with respect to $\mu(\theta, z)$ equal to zero, we obtain

$$\frac{\partial\mathcal{L}(\mu(\theta,z),\lambda)}{\partial\mu(\theta,z)}\bigg|_{\mu(\theta,z)=\mu^*(\theta,z)} = 0 \Longrightarrow \Big(\lambda - \beta\mathrm{e}^{-\theta TB\mathcal{I}(\mu^*(\theta,z)z)}\mathrm{MMSE}(\mu^*(\theta,z)z)z\Big)f(z) = 0. \tag{M.4}$$

Above, we have used the relation between the mutual information and MMSE given in (2.9) and defined $\beta = \theta TB\log_2\mathrm{e}$. Let $\alpha = \frac{\lambda}{\beta}$. Rearranging the above expression inside the parentheses, we obtain the equation in (8.8) where α can found from the average power constraint given in (8.9). □

Appendix N

Proof of Proposition 8.1.1

We first rewrite the equation in (8.8) by using the relation in (2.9) as follows:

$$g\big((\mu(\theta,z)z)\big) = \mathrm{e}^{-\theta TB\mathcal{I}(\mu(\theta,z)z)}\dot{\mathcal{I}}(\mu(\theta,z)z)z\log 2 - \alpha. \tag{N.1}$$

Then, differentiating $g\big((\mu(\theta,z)z)\big)$ with respect to $(\mu(\theta,z)z)$ results in

$$\dot{g}\big((\mu(\theta,z)z)\big) = \mathrm{e}^{-\theta TB\mathcal{I}(\mu(\theta,z)z)}z^2\Big(-\theta TB(\dot{\mathcal{I}}(\mu(\theta,z)z))^2 + \ddot{\mathcal{I}}(\mu(\theta,z)z)(\log 2)^2\Big). \tag{N.2}$$

Since $\ddot{\mathcal{I}}(\rho) < 0$, the first derivative of $g\big((\mu(\theta,z)z)\big)$ is always negative, i.e., $\dot{g}\big((\mu(\theta,z)z)\big) < 0$. Hence, using Rolle's theorem [109], the equation in (8.8) cannot have more than one root, implying the uniqueness of the optimal power policy. □

Appendix O

Proof of Theorem 8.1.2

We first express the mutual information achieved with arbitrary input distributions in the low-power regime as follows:

$$\mathcal{I}(\mathrm{SNR}z) = \mathrm{SNR}z + \frac{\ddot{\mathcal{I}}(0)}{2}\mathrm{SNR}^2 z^2 + o(\mathrm{SNR}^2). \tag{O.1}$$

Inserting the above expression into the effective capacity formulation, $C_E(\mathrm{SNR})$, given in (8.5) and evaluating the first and second derivatives of $C_E(\mathrm{SNR})$ with respect to SNR at $\mathrm{SNR} = 0$ results in

$$\dot{C}_E(0) = \frac{\mathbb{E}\{z\}}{\log 2} \tag{O.2}$$

$$\ddot{C}_E(0) = (\ddot{\mathcal{I}}(0) - \beta \log_2 \mathrm{e})\mathbb{E}\{z^2\} \log_2 \mathrm{e} + \beta \log_2 \mathrm{e}(\mathbb{E}\{z\})^2. \tag{O.3}$$

Further inserting the above expressions into those in (8.20) and (8.21), the minimum energy per bit and wideband slope expressions in (8.23) are readily obtained. □

Appendix P

Proof of Theorem 8.1.3

In the low power regime, MMSE behaves as [52]

$$\mathrm{MMSE}(\rho) = 1 + \ddot{\mathcal{I}}(0)\rho + o(\rho^2). \tag{P.1}$$

Incorporating the above approximation into (8.8), we have

$$\mathrm{e}^{-\beta \int_0^{\mu(\theta,z)z} (1+\ddot{\mathcal{I}}(0)\rho + o(\rho^2))d\rho} \Big(1 + \ddot{\mathcal{I}}(0)\mu(\theta,z)z + o\big((\mu(\theta,z)z)^2\big)\Big)z = \alpha. \tag{P.2}$$

Via the first-order Taylor expansion of the above equation, we obtain

$$\Big(1 - \big(\beta - \ddot{\mathcal{I}}(0)\big)\mu(\theta,z)z + o\big((\mu(\theta,z)z)^2\big)\Big)z = \alpha. \tag{P.3}$$

Solving the above equation provides the optimal power policy in (8.27) where α is again found by satisfying the average power constraint as in (8.9). □

Appendix Q

Proof of Theorem 8.1.4

The objective function is quasiconcave since the effective capacity is a concave function of transmission power and the total consumed power in the denominator is affine and positive. Therefore, the optimal power policy can be found through fractional programming [69]. By using the variable transformation $\psi = \frac{1}{P_{c_n}+\frac{1}{\epsilon}\mathbb{E}\{P_n(\theta,z)\}}$, the problem can be converted to a minimization problem as follows:

$$\min_{P_n(\theta,z)\geq 0} \psi \log\left(\mathbb{E}\{\mathrm{e}^{-\theta TB\mathcal{I}(P_n(\theta,z)z)}\}\right) \tag{Q.1}$$

$$\text{subject to} \quad \psi(P_{c_n} + \frac{1}{\epsilon}\mathbb{E}\{P_n(\theta,z)\}) \leq 1. \tag{Q.2}$$

Since the objective function in (Q.1) is convex subject to an affine constraint, the optimal power control policy can be obtained through the Lagrangian optimization approach as follows:

$$\begin{aligned} L(P_n(\theta,z),\psi,\lambda) = \psi \log\left(\mathbb{E}\{\mathrm{e}^{-\theta TB\mathcal{I}(P_n(\theta,z)z)}\}\right) \\ + \lambda\Big[\psi\Big(P_{c_n} + \frac{1}{\epsilon}\mathbb{E}\{P_n(\theta,z)\}\Big) - 1\Big]. \end{aligned} \tag{Q.3}$$

Above, λ denotes the Lagrange multiplier. Applying the Karush-Kuhn-Tucker (KKT) conditions yields the set of following equations:

$$\psi(P_{c_n} + \frac{1}{\epsilon}\mathbb{E}\{P_n(\theta, z)\}) = 1 \tag{Q.4}$$

$$\frac{dL(P_n(\theta, z), \psi, \lambda)}{dP_n(\theta, z)} = -\frac{\psi\theta TB\mathrm{e}^{-\theta TB\mathcal{I}(P_n(\theta,z)z)}\mathrm{MMSE}(P_n(\theta, z))z\log_2(e)}{\mathbb{E}\{\mathrm{e}^{-\theta TB\mathcal{I}(P_n(\theta,z)z)}\}}f(z) + \frac{\lambda\psi}{\epsilon}f(z) = 0 \tag{Q.5}$$

$$\log\Big(\mathbb{E}\big\{\mathrm{e}^{-\theta TB\mathcal{I}(P_n(\theta,z)z)}\big\}\Big) + \lambda\Big(P_{c_n} + \frac{1}{\epsilon}\mathbb{E}\big\{P_n(\theta, z)\big\}\Big) = 0. \tag{Q.6}$$

Rearranging the terms in (Q.5) leads to the desired result in (8.31) where λ can be found by inserting the optimal power control in (8.31) into (Q.6) and solving the resulting equation in (8.34). $\square$

Appendix R

Proof of Theorem 8.1.5

The objective function is concave in transmission power and the feasible set defined by (8.45) is a convex set. Therefore, the Karush-Kush-Tucker conditions are sufficient and necessary to find the optimal solution. First, the EE min constraint in (8.45) can be rewritten as

$$-\frac{1}{\theta TB}\log\mathbb{E}\{\mathrm{e}^{-\theta TB\mathcal{I}(\mu(\theta,z)z)}\}-\mathrm{EE}_{\min}N_0B\Big(\frac{1}{\epsilon}\mathbb{E}\{\mu(\theta,z)\}+P_{c_n}\Big)\geq 0. \tag{R.1}$$

Let us define ν as the Lagrange multiplier associated with the min EE constraint. Then, the Lagrangian function is given by

$$\mathcal{L}(P(g,h),\nu)=(1+\nu)\Big(-\frac{1}{\theta TB}\log\mathbb{E}\{\mathrm{e}^{-\theta TB\mathcal{I}(\mu(\theta,z)z)}\}\Big)-\nu\mathrm{EE}_{\min}N_0B\Big(\frac{1}{\epsilon}\mathbb{E}\{\mu(\theta,z)\}+P_{c_n}\Big). \tag{R.2}$$

Differentiating the above Lagrangian function with respect to $\mu(\theta,z)$ and and setting the derivative equal to zero, we obtain the following equation:

$$\frac{\partial\mathcal{L}(\mu(\theta,z),\nu)}{\partial\mu(\theta,z)}\bigg|_{\mu(\theta,z)=\mu^*(\theta,z)}=(1+\nu)\frac{\log_2(e)\mathrm{MMSE}(\mu^*(\theta,z)z)z\mathrm{e}^{-\theta TB\mathcal{I}(\mu^*(\theta,z)z)}}{\mathbb{E}\{\mathrm{e}^{-\theta TB\mathcal{I}(\mu^*(\theta,z)z)}\}}-\nu\frac{\mathrm{EE}_{\min}}{\epsilon}N_0B=0. \tag{R.3}$$

Rearranging the terms in (R.3) leads to the desired result in (8.48) and the Lagrange multiplier, ν can be found by inserting the optimal power control in (8.47) into the minimum EE constraint and solving the equation in (8.48). Consequently, the average transmission power is determined by substituting the optimal power control in (8.47) into (8.50). $\square$

Appendix S

Proof of Proposition 8.2.1

The optimization problem is quasiconcave since the effective capacity, $C_E(\theta)$, is a concave function of the transmission power [46] and the logarithm in (8.65) is strictly monotonically increasing function of $C_E(\theta)$. Hence, the maximum average arrival rate in the numerator in (8.75) is a concave function of the transmission power and the power consumption in the denominator is both affine and positive. Therefore, the optimal power value can be found by using fractional programming [69]. By introducing an additional variable $\psi = \frac{1}{\frac{1}{\epsilon}\mathbb{E}\{\mathrm{P}(\theta,z)\}+\mathrm{P}_c}$, the problem can be transformed into

$$\min_{\mathrm{P}(\theta,z)\geq 0} -\psi \log\Big(\frac{\mathrm{e}^{2\theta C_E(\theta)} - p_{11}\mathrm{e}^{\theta C_E(\theta)}}{(1-p_{11}-p_{22}) + p_{22}\mathrm{e}^{\theta C_E(\theta)}}\Big) \tag{S.1}$$

$$\text{subject to } \psi\Big(\frac{1}{\epsilon}\mathbb{E}\left\{\mathrm{P}(\theta,z)\right\} + \mathrm{P}_c\Big) \leq 1. \tag{S.2}$$

Since the total consumed power in the denominator of the objective function in (8.75) is an affine function, the above inequality can be changed to equality. Consequently, the optimal power values are obtained by forming the Lagrangian function as follows:

$$\mathcal{L}(\mathrm{P}(\theta,z),\psi,\lambda) = -\psi \log\left(\frac{\mathrm{e}^{2\theta C_E(\theta)} - p_{11}\mathrm{e}^{\theta C_E(\theta)}}{(1-p_{11}-p_{22}) + p_{22}\mathrm{e}^{\theta C_E(\theta)}}\right) + \lambda\Big[\psi\Big(\frac{1}{\epsilon}\mathbb{E}\left\{\mathrm{P}(\theta,z)\right\} + \mathrm{P}_c\Big) - 1\Big], \tag{S.3}$$

where λ is the Lagrange multiplier. According to the Karush-Kuhn-Tucker (KKT) conditions, the optimal power control must satisfy the following set of equations:

$$\psi\Big(\frac{1}{\epsilon}\mathbb{E}\left\{\mathrm{P}(\theta,z)\right\}+\mathrm{P}_c\Big)=1 \tag{S.4}$$

$$-\psi\theta\mathrm{e}^{-\theta\mathcal{I}(\mathrm{P}^*(\theta,z)z)}\mathrm{MMSE}\big(\mathrm{P}^*(\theta,z)z\big)z\log_2(e)\left[\frac{(2-p_{11}\mathrm{e}^{-\theta C_E(\theta)})(1-p_{11}-p_{22})+p_{22}\mathrm{e}^{\theta C_E(\theta)}}{((1-p_{11}-p_{22})\mathrm{e}^{-\theta C_E(\theta)}+p_{22})(1-p_{11}\mathrm{e}^{-\theta C_E(\theta)})}\right]f(z)$$
$$+\frac{\lambda\psi}{\epsilon}f(z)=0 \tag{S.5}$$

$$-\log\left(\frac{\mathrm{e}^{2\theta C_E(\theta)}-p_{11}\mathrm{e}^{\theta C_E(\theta)}}{(1-p_{11}-p_{22})+p_{22}\mathrm{e}^{\theta C_E(\theta)}}\right)+\lambda\Big(\frac{1}{\epsilon}\mathbb{E}\left\{\mathrm{P}(\theta,z)\right\}+\mathrm{P}_c\Big)=0. \tag{S.6}$$

In (S.5), we have used the relation between MMSE and the mutual information given in (2.9). Rearranging the terms in (S.5) yields the desired result in (8.77) where λ is obtained by solving the equation in (S.6). $\square$

Appendix T

Proof of Proposition 8.2.2

The optimization problem is again quasiconcave due to the same reasoning explained in the proof of Proposition 8.2.1. Hence, fractional programming can be employed to find the optimal power control. Let us define $\psi = \frac{1}{\frac{1}{\epsilon}\mathbb{E}\{\mathrm{P}(\theta,z)\}+\mathrm{P}_c}$. Then the problem can be converted to

$$\min_{\mathrm{P}(\theta,z)\geq 0} -\psi \frac{\theta C_E(\theta)+\alpha+\beta}{\theta C_E(\theta)+\alpha} C_E(\theta) \tag{T.1}$$

$$\text{subject to } \psi\Big(\frac{1}{\epsilon}\mathbb{E}\left\{\mathrm{P}(\theta,z)\right\}+\mathrm{P}_c\Big) \leq 1. \tag{T.2}$$

The above inequality can be changed to equality since the total power in the denominator is an affine function. Hence, we can write the Lagrangian function to find the optimal power control as follows:

$$\mathcal{L}(\mathrm{P}(\theta,z),\psi,\lambda) = -\psi \frac{\theta C_E(\theta)+\alpha+\beta}{\theta C_E(\theta)+\alpha} C_E(\theta) + \lambda\Big[\psi\Big(\frac{1}{\epsilon}\mathbb{E}\left\{\mathrm{P}(\theta,z)\right\}+\mathrm{P}_c\Big)-1\Big], \tag{T.3}$$

where λ is the Lagrange multiplier. The optimal power control must satisfy the KKT conditions listed below:

$$\psi\Big(\frac{1}{\epsilon}\mathbb{E}\left\{\mathrm{P}(\theta,z)\right\}+\mathrm{P}_c\Big)=1 \tag{T.4}$$

$$-\psi \mathrm{e}^{-\theta\mathcal{I}(\mathrm{P}^*(\theta,z)z)}\mathrm{MMSE}\big(\mathrm{P}^*(\theta,z)z\big)z\log_2(e)\left[\Big(\frac{\alpha\beta}{(\theta C_E(\theta)+\alpha)^2}+1\Big)\frac{1}{\mathrm{e}^{-\theta C_E(\theta)}}\right]f(z)+\frac{\lambda\psi}{\epsilon}f(z)=0 \tag{T.5}$$

$$-\frac{\theta C_E(\theta)+\alpha+\beta}{\theta C_E(\theta)+\alpha}C_E(\theta)+\lambda\Big(\frac{1}{\epsilon}\mathbb{E}\left\{\mathrm{P}(\theta,z)\right\}+\mathrm{P}_c\Big)=0. \tag{T.6}$$

After further rearrangements in (T.5), we derive the equation in (8.84) and the optimal value of λ can be determined by solving the equation in (T.6). □

Appendix U

Proof of Proposition 8.2.3

The objective function in (8.88) is concave in the transmission power and the feasible set defined by the minimum EE constraint is a convex set. Hence, the optimal power can be found by using the Lagrangian optimization approach as in the following:

$$\mathcal{L}(\mathrm{P}(\theta,z),\lambda)=(1+\lambda)\frac{P_{\mathrm{ON}}}{\theta}\log\left(\frac{\mathrm{e}^{2\theta C_E(\theta)}-p_{11}\mathrm{e}^{\theta C_E(\theta)}}{(1-p_{11}-p_{22})+p_{22}\mathrm{e}^{\theta C_E(\theta)}}\right)-\lambda\mathrm{EE}_{\min}\Big(\frac{1}{\epsilon}\mathbb{E}\left\{\mathrm{P}(\theta,z)\right\}+\mathrm{P}_c\Big). \tag{U.1}$$

Setting the derivative of the Lagrangian function with respect to $\mathrm{P}(\theta,z)$ equal to zero at the optimal power level, we obtain the following equation:

$$\begin{aligned}\frac{\partial\mathcal{L}(\mathrm{P}(\theta,z),\lambda)}{\partial\mathrm{P}(\theta,z)}\bigg|_{\mathrm{P}(\theta,z)=\mathrm{P}^*(\theta,z)} &= (1+\lambda)P_{\mathrm{ON}}\mathrm{e}^{-\theta\mathcal{I}(\mathrm{P}^*(\theta,z)z)}\mathrm{MMSE}\big(\mathrm{P}^*(\theta,z)z\big)z\log_2(e)\\ &\quad\times\left[\frac{(2-p_{11}\mathrm{e}^{-\theta C_E(\theta)})(1-p_{11}-p_{22})+p_{22}\mathrm{e}^{\theta C_E(\theta)}}{(1-p_{11}\mathrm{e}^{\theta C_E(\theta)})((1-p_{11}-p_{22})\mathrm{e}^{-\theta C_E(\theta)}+p_{22})}\right]-\frac{\lambda}{\epsilon}\mathrm{EE}_{\min}(\theta)=0.\end{aligned} \tag{U.2}$$

Rearranging the terms in the expression in (U.2) results in the desired characterization in (8.90) where Lagrange multiplier λ can be found by satisfying the minimum EE constraint with equality or equivalently by solving (8.93) [45]. □

Bibliography

[1] P. Steenkiste, D. Sicker, G. Minden, and D. Raychaudhuri, "Future directions in cognitive radio network research," NSF Workshop Report, Tech. Rep., 2009.

[2] "Federal communications commission spectrum policy task force," FCC Report of the Spectrum Efficiency Working Group, Tech. Rep., Nov. 2002.

[3] R. J. Mitola, "Cognitive radio: An integrated agent architecture for software defined radio," Ph.D. dissertation, Royal Inst. Technol. (KTH), Sweden, 2000.

[4] C. Stevenson, G. Chouinard, Z. Lei, W. Hu, S. Shellhammer, and W. Caldwell, "IEEE 802.22: the first cognitive radio wireless regional area network standard," *IEEE Commun. Mag.*, vol. 47, no. 1, pp. 130–138, Jan. 2009.

[5] A. Flores, R. Guerra, E. Knightly, P. Ecclesine, and S. Pandey, "IEEE 802.11af: A standard for TV white space spectrum sharing," *IEEE Commun. Mag.*, vol. 51, no. 10, pp. 92–100, Oct. 2013.

[6] F. Granelli, P. Pawelczak, R. V. Prasad, K. P. Subbalakshmi, R. Chandramouli, J. A. Hoffmeyer, and H. S. Berger, "Standardization and research in cognitive and dynamic spectrum access networks: IEEE SCC41 efforts and other activities," *IEEE Commun. Mag.*, vol. 48, no. 1, pp. 71–79, Jan. 2010.

[7] "Second report and order and memorandum opinion and order," Federal Communications Commission, Tech. Rep. ET Docket No. 08-260, Nov. 2008.

[8] E. Biglieri, A. J. Goldsmith, L. J. Greenstein, N. B. Mandayam, and H. V. Poor, *Principles of Cognitive Radio*. Cambridge University Press, 2013.

[9] E. Hossain, D. Niyato, and Z. Han, *Dynamic Spectrum Access and Management in Cognitive Radio Networks*. Cambridge University Press, 2009.

[10] A. Goldsmith, S. Jafar, I. Maric, and S. Srinivasa, "Breaking spectrum gridlock with cognitive radios: An information theoretic perspective," in *Proc. of the IEEE*, vol. 97, no. 5, May 2009, pp. 894–914.

[11] I. F. Akyildiz, W.-Y. Lee, M. C. Vuran, and S. Mohanty, "NeXt generation/dynamic spectrum access/cognitive radio wireless networks: A survey," *Int. Journal of Computer and Telecomm. Networking*, vol. 50, no. 13, pp. 2127–2159, Sep. 2006.

[12] X. Kang, Y.-C. Liang, H. K. Garg, and L. Zhang, "Sensing-based spectrum sharing in cognitive radio networks," *IEEE Trans. Veh. Technol.*, vol. 58, no. 8, pp. 4649–4654, Oct. 2009.

[13] L. Musavian and S. Aissa, "Outage-constrained capacity of spectrum-sharing channels in fading environments," *IET Communications*, vol. 2, no. 6, pp. 724–732, July 2008.

[14] X. Kang, R. Zhang, Y.-C. Liang, and H. K. Garg, "Optimal power allocation strategies for fading cognitive radio channels with primary user outage constraint," *IEEE J. Sel. Areas Commun.*, vol. 29, no. 2, pp. 374–383, Feb. 2011.

[15] ——, "Optimal power allocation for cognitive radio under primary user outage capacity constraint," in *Proc. IEEE Int. Conf. Commun. (ICC)*, June 2009.

[16] X. Kang, H. K. Garg, Y.-C. Liang, and R. Zhang, "Optimal power allocation for OFDM-based cognitive radio with new primary transmission protection criteria," *IEEE Trans. Wireless Commun.*, vol. 9, no. 6, pp. 2066–2075, June 2010.

[17] L. Musavian and S. Aissa, "Capacity and power allocation for spectrum-sharing communications in fading channels," *IEEE Trans. Wireless Commun.*, vol. 8, no. 1, pp. 148–156, Jan. 2009.

[18] X. Kang, Y.-C. Liang, A. Nallanathan, H. K. Garg, and R. Zhang, "Optimal power allocation for fading channels in cognitive radio networks: ergodic capacity and outage capacity," *IEEE Trans. Wireless Commun.*, vol. 8, no. 2, pp. 940–950, Feb. 2009.

[19] X. Hong, J. Wang, C.-X. Wang, and J. Shi, "Cognitive radio in 5G: a perspective on energy-spectral efficiency trade-off," *IEEE Commun. Mag.*, vol. 52, no. 7, pp. 32–39, July 2014.

[20] F. Gabry, A. Zappone, R. Thobaben, E. A. Jorswieck, and M. Skoglung, "Energy efficiency analysis of cooperative jamming in cognitive radio networks with secrecy constraints," *IEEE Commun. Letters*, vol. 4, no. 4, pp. 437–440, Aug. 2015.

[21] Y. Pei, Y. C. Liang, K. C. Teh, , and K. H. Li, "Energy-efficient design of sequential channel sensing in cognitive radio networks: Optimal sensing strategy, power allocation, and sensing order," *IEEE J. Sel. Areas Commun.*, vol. 29, no. 8, pp. 1648–1659, Sep. 2011.

[22] Z. Shi, K. C. Teh, and K. H. Li, "Energy-efficient joint design of sensing and transmission durations for protection of primary user in cognitive radio systems," *IEEE Commun. Letters*, vol. 17, no. 3, pp. 565–568, Mar. 2013.

[23] C. Xiong, L. Lu, and G. Y. Li, "Energy-efficient spectrum access in cognitive radios," *IEEE J. Sel. Areas Commun.*, vol. 32, no. 3, pp. 550–562, Mar. 2014.

[24] E. Bedeer, O. Amin, O. A. Dobre, M. H. Ahmed, and K. E. Baddour, "Energy-efficient power loading for ofdm-based cognitive radio systems with channel uncertainties," *IEEE Trans. Veh. Technol.*, vol. 64, 2015, pages =.

[25] S. Wang, M. Ge, and W. Zhao, "Energy-efficient resource allocation for OFDM-based cognitive radio networks," *IEEE Trans. Commun.*, vol. 61, no. 8, pp. 3181–3191, Aug. 2013.

[26] J. Mao, G. Xie, J. Gao, and Y. Liu, "Energy efficiency optimization for cognitive radio MIMO broadcast channels," *IEEE Commun. Letters*, vol. 17, no. 2, pp. 337–340, Feb. 2013.

[27] R. Ramamonjison and V. K. Bhargava, "Energy efficiency maximization framework in cognitive downlink two-tier networks," *IEEE Trans. Wireless Commun.*, vol. 14, no. 3, pp. 1468–1479, Mar. 2015.

[28] H. Hu, H. Zhang, and Y.-C. Liang, "On the spectrum- and energy-efficiency tradeoff in cognitive radio networks," *IEEE Trans. Commun.*, vol. 64, no. 2, pp. 490–501, Feb. 2016.

[29] J. Zhang, F.-C. Zheng, X.-Q. Gao, and H.-B. Zhu, "Sensing-energy efficiency tradeoff for cognitive radio networks," *IET Commun.*, vol. 8, no. 18, pp. 3414–3423, Dec. 2014.

[30] H. Park and T. Hwang, "Energy-efficient power control of cognitive femto users for 5G communications," *IEEE J. Sel. Areas Commun.*, vol. 34, no. 4, Apr. 2016.

[31] V. Asghari and S. Aissa, "Adaptive rate and power transmission in spectrum-sharing systems," *IEEE Trans. on Wireless Commun.*, vol. 9, no. 10, pp. 3272–3280, Oct. 2010.

[32] L. Li, P. I. Derwin, and M. Pesavento, "Symbol error rate analysis in multiuser underlay cognitive radio systems," in *Proc. IEEE Personal Indoor and Mobile Radio Commun. (PIMRC)*, Sept. 2011, pp. 681–684.

[33] M. H. Islam, Y. C. Liang, and A. T. Hoang, "Combining eigen-beamforming and orthogonal space-time block coding for secondary usage of spectrum," in *Proc. IEEE Int. Conf. Commun. (ICC)*, May 2008, pp. 830–834.

[34] T. Do and B. L. Mark, "Exploiting multichannel diversity in cognitive radio networks," in *Proc. IEEE Int. Conf. Computer Commun. and Networks (ICCCN)*, Aug. 2010, pp. 1–6.

[35] R. Sarvendranath and N. B. Mehta, "Antenna selection in interference-constrained underlay cognitive radios: SEP-optimal rule and performance benchmarking," *IEEE Trans. on Commun.*, vol. 61, no. 2, pp. 496–506, Feb. 2013.

[36] Y. Wang and J. Coon, "BER minimization for cognitive radio systems with difference antenna selection," in *Proc. IEEE Pacific Rim Conf. Commun., Computer and Signal Process. (PacRim)*, Aug. 2011, pp. 304–309.

[37] H. Suraweera, J. P. Smith, and M. Shafi, "Capacity limits and performance analysis of cognitive radio with imperfect channel knowledge," *IEEE Trans. Veh. Technol.*, vol. 59, no. 4, pp. 1811–1822, May 2010.

[38] D. Xu, Z. Feng, and P. Zhang, "Minimum average BER power allocation for fading channels in cognitive radio networks," in *Proc. IEEE Wireless Commun. and Networking Conf. (WCNC)*, Mar. 2011, pp. 78–83.

[39] L. Musavian and S. Aissa, "Effective capacity of delay-constrained cognitive radio in Nakagami fading channels," *IEEE Trans. Wireless Commun.*, vol. 9, no. 3, pp. 1054–1062, Mar. 2010.

[40] L. Musavian, S. Aissa, and S. Lambotharan, "Adaptive modulation in spectrum-sharing channels under delay quality-of-service constraints," *IEEE Trans. Veh. Technol.*, vol. 60, no. 3, pp. 901–911, Mar. 2011.

[41] J. Tang and X. Zhang, "Quality-of-service driven power and rate adaptation over wireless links," *IEEE Trans. Wireless Commun.*, vol. 6, no. 12, pp. 4349–4360, Dec. 2007.

[42] ——, "Quality-of-service driven power and rate adaptation for multichannel communications over wireless links," *IEEE Trans. Wireless Commun.*, vol. 6, pp. 3058–3068, 2007.

[43] A. Helmy, L. Musavian, and T. Le-Ngoc, "Energy-efficient power adaptation over a frequency-selective fading channel with delay and power constraints," *IEEE Trans. Wireless Commun.*, vol. 12, no. 9, pp. 4529–4541, Sep. 2013.

[44] L. Liu, Y. Yang, J. F. Chamberland, and J. Zhang, "Energy-efficient power allocation for delay-sensitive multimedia traffic over wireless systems," *IEEE Trans. Veh. Techn.*, vol. 63, no. 5, pp. 2038–2047, June 2014.

[45] L. Musavian and Q. Ni, "Effective capacity maximization with statistical delay and effective energy efficiency requirements," *IEEE Trans. Wireless Commun.*, vol. 14, no. 7, pp. 3824–3835, July 2015.

[46] M. C. Gursoy, D. Qiao, and S. Velipasalar, "Analysis of energy efficiency in fading channels under QoS constraints," *IEEE Trans. Wireless Commun.*, vol. 8, no. 8, pp. 4252–4263, Aug. 2009.

[47] G. Ru, H. Li, L. Liu, Z. Hu, and Y. Gan, "Energy efficiency of hybrid cellular with heterogeneous QoS provisions," *IEEE Commun. Letters*, vol. 18, no. 6, pp. 1003–1006, June 2014.

[48] C. Zhong, T. Ratnarajah, K.-K. Wong, and M.-S. Alouini, "Effective capacity of correlated MISO channels," in *Proc. IEEE Int. Conf. Commun. (ICC)*, June 2011.

[49] F. Benkhelifa, Z. Rezki, and M.-S. Alouini, "Effective capacity of Nakagami-m fading channels with full channel state information in the low power regime," in *Proc. of IEEE Personal Indoor and Mobile Radio Communications (PIMRC)*, Sept. 2014, pp. 1883–1887.

[50] A. Ghasemi and E. S. Sousa, "Spectrum sensing in cognitive radio networks: requirements, challenges and design trade-offs," *IEEE Comm. Mag.*, vol. 46, no. 4, pp. 32–39, Apr. 2008.

[51] E. Axell, G. Leus, E. G. Larsson, and H. V. Poor, "Spectrum sensing for cognitive radio: State-of-the-art and recent advances," *IEEE Signal Process. Mag.*, vol. 29, no. 3, pp. 101–116, May 2012.

[52] A. Lozano, A. M. Tulino, and S. Verdú, "Optimum power allocation for parallel Gaussian channels with arbitrary input distributions," *IEEE Trans. Inform. Theory*, vol. 52, no. 7, pp. 3033–3051, July 2006.

[53] D. Guo, S. Shamai, and S. Verdú, "Mutual information and minimum mean-square error in Gaussian channels," *IEEE Trans. Inform. Theory*, vol. 51, no. 4, pp. 1261–1283, April 2005.

[54] M. Abramovitz and I. A. Stegun, *Handbook of Mathematical Functions*, ser. ser. Applied Mathematics Series. National Bureau of Standards, 1965.

[55] D. Wu and R. Negi, "Effective capacity: A wireless link model for support of quality of service," *IEEE Trans. Wireless Commun.*, vol. 2, no. 4, pp. 630–643, July 2003.

[56] C.-S. Chang, "Stability, queue length, and delay of deterministic and stochastic queuing networks," *IEEE Trans. Auto. Control*, vol. 39, no. 5, pp. 913–931, May 1994.

[57] M. S. Alouini and A. J. Goldsmith, "Capacity of rayleigh fading channels under different adaptive transmission and diversity-combining techniques," *IEEE Trans. Veh. Tech.*, vol. 48, no. 4, pp. 1165–1181, July 1999.

[58] J. M. Peha, "Approaches to spectrum sharing," *IEEE Commun. Mag.*, vol. 43, pp. 10–12, Feb. 2005.

[59] Q. Zhao, S. Geirhofer, L. Tong, and B. M. Sadler, "Opportunistic spectrum access via periodic channel sensing," *IEEE Trans. Signal Process.*, vol. 56, no. 2, pp. 785–796, Feb. 2008.

[60] S. Boyd, L. Xiao, and A. Mutapcic, *Subgradient methods*, ser. Lecture Notes of EE392o, Standford University, Autumn Quarter 2003-2004.

[61] K. D. Nguyen, A. G. i Fabregas, and L. K. Rasmussen, "Power allocation for block-fading channels with arbitrary input constellations," *IEEE Trans. Wireless Commun.*, vol. 8, no. 5, pp. 2514–2523, May 2009.

[62] M. Abramovitz and I. A. Stegun, *Handbook of Mathematical Functions with Formulas, Graphs, and Mathematical Tables*, 9th ed., NewYork: Dover, 1970.

[63] R. M. Corless, G. H. Gonnet, D. E. G. Hare, D. J. Jeffrey, and D. E. Knuth, "On the lambertW function," *Adv. in Comput. Math.*, vol. 5, pp. 329–359, 1996.

[64] Z. Rezki and M.-S. Alouini, "On the capacity of Nakagami-m fading channels with full channel state information at low SNR," *IEEE Wireless Commun. Letters*, vol. 1, no. 3, pp. 253–256, June 2012.

[65] A. Y. Wang, S. Chao, C. G. Sodini, and A. P. Chandrakasan, "Energy efficient modulation and mac for asymmetric rf microsensor system," in *Proc. Int. Symp. Low Power Electronics Design*, 2001, pp. 106–111.

[66] S. Cui, A. Goldsmith, and A. Bahai, "Energy-efficiency of mimo and cooperative mimo techniques in sensor networks," *IEEE J. Sel. Areas Commun.*, vol. 22, no. 6, pp. 1089–1098, Aug. 2004.

[67] B. Sadhu and R. Harjani, *Cognitive Radio Receiver Front-Ends: RF/Analog Circuit Techniques*. Springer, 2013.

[68] G. W. Miao, N. Himayat, and Y. Li, "Energy-efficient link adaptation in frequency-selective channels," *IEEE Trans. Commun.*, vol. 58, no. 2, pp. 545–554, Feb. 2010.

[69] S. Schaible, "Fractional programming. ii, on dinkelbach's algorithm," *Management Science*, vol. 22, no. 8, pp. 868–873, Mar. 1976.

[70] Z. Wang, I. Stupia, and L. Vandendorpe, "Energy efficient precoder design for mimo-ofdm with rate-dependent circuit power," in *Proc. of IEEE Inter. Conf. Commun. (ICC)*, 2015, pp. 1897–1902.

[71] L. Sboui, Z. Rezki, and M. Alouini, "A unified framework for the ergodic capacity of spectrum sharing cognitive radio systems," *IEEE Trans. on Commun.*, vol. 12, no. 2, pp. 877–887, Feb. 2013.

[72] J. Riihijärvi, J. Nasreddine, and P. Mähönen, "Impact of primary user activity patterns on spatial spectrum reuse opportunities," in *Proc. of IEEE Wireless Conference (EW)*, Apr. 2010, pp. 962–968.

[73] M. Wellens, J. Riihijärvi, and P. Mähönen, "Empirical time and frequency domain models for spectrum use," *Phys. Commun.*, vol. 2, no. 1-2, pp. 10–32, 2009.

[74] C. Jiang, Y. Chen, K. J. R. Liu, and Y. Ren, "Renewal-theoretical dynamic spectrum access in cognitive radio network with unknown primary behavior," *IEEE J. Sel. Areas Commun.*, vol. 31, no. 3, pp. 406–416, Mar. 2013.

[75] S. Stotas and A. Nallanathan, "Optimal sensing time and power allocation in multiband cognitive radio networks," *IEEE Trans. on Commun.*, vol. 59, no. 1, pp. 226–235, Jan. 2011.

[76] G. Ozcan, M. C. Gursoy, and J. Tang, "Power control for cognitive radio systems with unslotted primary users under sensing uncertainty," in *Proc. IEEE Int. Conf. Commun. (ICC)*, June 2015.

[77] Y. Y. Pei, A. T. Hoang, and Y. C. Liang, "Sensing-throughput tradeoff in cognitive radio network: how frequently should spectrum sensing be carried out?" in *Proc. of 18th Annual Inter. Symposium on Personal, Indoor and Mobile Radio Commun.*, 2007, pp. 1–5.

[78] Y. Xu, J. Wang, and Q. Wu, "Interference-throughput tradeoff in dynamic spectrum access: Analysis based on discrete-time queuing subjected to bursty preemption," in *Proc. of IEEE Inter. Conf. on Cognitive Radio Oriented Wireless Networks and Commun. (CROWNCOM)*, 2009, pp. 1–6.

[79] R. Tandra and A. Sahai, "Snr walls for signal detection," *IEEE J. on Sel. Topics Signal Process.*, vol. 2, no. 1, pp. 4–17, Feb. 2008.

[80] S. Stergiopoulos, *Advanced Signal Processing Handbook*. CRC Press, 2001.

[81] S. Pulkkinen, M. Mäkelä, and N. Karmitsa, "A continuation approach to mode-finding of multivariate Gaussian mixtures and kernel density estimates," *Journal on Global Optimization*, pp. 1–29, 2011.

[82] M. S. Alouini and A. J. Goldsmith, "A unified approach for calculating the error rates of linearly modulated signals over generalized fading channels," *IEEE Trans. Commun.*, vol. 47, pp. 1324–1334, 1999.

[83] J. W. Craig, "A new, simple, and exact result for calculating the probability of error for two-dimensional signal constellations," in *Military Commun. Conf. (MILCOM)*, McLean, VA, Oct. 1991, pp. 571–575.

[84] M. K. Simon and D. Divsalar, "Some new twists to problems involving the Gaussian probability integral," *IEEE Trans. Commun.*, vol. 46, pp. 200–210, Feb. 1998.

[85] I. S. Gradshteyn and I. Ryzhik, *Table of Integrals, Series, and Products*, 7th ed. Academic Press, 2007.

[86] S. Akin and M. C. Gursoy, "Performance analysis of cognitive radio systems under QoS constraints and channel uncertainty," *IEEE Trans. Wireless Commun.*, vol. 10, no. 9, pp. 2883–2895, Sept. 2011.

[87] Y. Polyanskiy, H. V. Poor, and S. Verdú, "Channel coding rate in the finite blocklength regime," *IEEE Trans. Inform. Theory*, vol. 56, no. 5, pp. 2307–2359, May 2010.

[88] M. C. Gursoy, "Throughput analysis of buffer-constrained wireless systems in the finite blocklength regime," in *Proc. IEEE Int. Conf. Commun. (ICC)*, Kyoto, Japan, June 2011.

[89] T. M. Cover and J. A. Thomas, *Elements of Information Theory*, 2nd ed. Springer, 2006.

[90] C.-S. Chang, *Performance Guarantees in Communication Networks*. NewYork: Springer, 1995.

[91] Q. Du and X. Zhang, "Statistical qos provisioning for wireless unicast/multicast of multi-layer video streams," *IEEE J. Sel. Areas Commun.*, vol. 28, no. 3, pp. 420–433, Apr. 2010.

[92] S. Boyd and L. Vandenberghe, *Convex optimization*. Cambridge, UK: Cambridge University Press, 2004.

[93] H. Suzuki, "A statistical model for urban radio propagation," *IEEE Trans. Wireless Commun.*, vol. 25, no. 7, pp. 673–680, May 1974.

[94] A. U. Sheikh, M. Handforth, and M. Abdi, "Indoor mobile radio channel at 946 MHz: Measurements and modeling," in *Proc. of IEEE Veh. Technol. Conf. (VTC)*, May 1993, pp. 73–76.

[95] S. Verdú, "Spectral efficiency in the wideband regime," *IEEE Trans. Inform. Theory*, vol. 48, no. 6, pp. 1319–1343, June 2002.

[96] K. A. Stewart, G. P. Labedz, and K. Sohrabi, "Wideband channel measurements at 900 MHz," in *Proc. IEEE Veh. Technol. Conf. (VTC)*, July 1995, pp. 236–240.

[97] R. Bultitude, S. A. Mahmoud, and W. A. Sullivan, "A comparison of indoor radio propagation characteristics at 910 MHz and 1.75 GHz," *IEEE J. Sel. Areas Commun.*, vol. 7, no. 1, pp. 20–30, Jan. 1989.

[98] G. Ozcan and M. C. Gursoy, "QoS-driven power control for fading channels with arbitrary input distributions," in *Proc. of the IEEE Int. Symp. on Inf. Theory (ISIT)*, July 2014, pp. 1381–1385.

[99] M. Payaró and D. P. Palomar, "Hessian and concavity of mutual information, differential entropy,and entropy power in linear vector Gassign channels," *IEEE Trans. Inform. Theory*, vol. 55, no. 8, pp. 3613–3628, Aug. 2009.

[100] C. Courcoubetis and R. Weber, "Effective bandwidth for stationary sources," *Prob. Eng. Inf. Sci.*, vol. 9, pp. 285–296, 1995.

[101] G. Kesidis, J.Walrand, and C.-S. Chang, "Effective bandwidths for multiclass Markov fluids and other ATM sources," *IEEE/ACM Trans. Netw.*, vol. 1, no. 4, pp. 424–428, Aug. 1993.

[102] D. Qiao and M. C. Gursoy, "Transmission strategies in multiple-access fading channels with statistical QoS constraints," *IEEE Trans. Inform. Theory*, vol. 58, no. 3, pp. 1578–1593, Mar. 2012.

[103] C.-S. Chang and T. Zajic, "Energy-efficient power adaptation for cognitive radio systems under imperfect channel sensing," in *Proc. of the IEEE Inter. Conf. on Computer Commun. (INFOCOM)*, 1995.

[104] M. Ozmen and M. C. Gursoy, "Wireless throughput and energy efficiency with random arrivals and statistical queueing constraints," *IEEE Trans. Inform. Theory*, vol. 62, no. 3, pp. 1375–1395, Mar. 2016.

[105] D. Palomar and M. Chiang, "A tutorial on decomposition methods for network utility maximization," *IEEE J. on Sel. Areas in Commun.*, vol. 24, no. 8, pp. 1439 –1451, Aug. 2006.

[106] M. Medard, "The effect upon channel capacity in wireless communications of perfect and imperfect knowledge of the channel," *IEEE Trans. Inform. Theory*, vol. 46, no. 3, pp. 933–946, May 2000.

[107] W. Dinkelbach, "On nonlinear fractional programming," *Management Science*, vol. 13, pp. 492–498, Mar. 1967.

[108] H. V. Poor, *An Introduction to Signal Detection and Estimation*. New York: Springer-Verlag, 1994.

[109] G. Strang, *Calculus*. Wellesley-Cambridge Press, 2008.

VITA

GOZDE OZCAN: She received the B.S. degree in Electrical and Electronics Engineering from Bilkent University, Ankara, Turkey in 2011. She has been a Ph.D. student at Syracuse University since 2011. She was TPC member of VTC'2014-Fall. She was a research intern with Mitsubishi Electric Research Laboratories, Cambridge, MA, USA, in 2015. Her research interests include wireless communications, radio resource management, energy-efficient transmission techniques, statistical signal processing, machine learning and cognitive radio systems.